Role of surfactin from Bacillus subtilis *in protection against antimicrobial peptides produced by* Bacillus *species*

by

Hans André Eyéghé-Bickong
BSc. Honours (Biochemistry)

February 2011

Dissertation approved for the degree
Doctor of Philosophy (Biochemistry)
in the
Faculty of Science
at the
University of Stellenbosch

Promoter: Prof. Marina Rautenbach
Department of Biochemistry
University of Stellenbosch

Declaration

By submitting this dissertation electronically, I declare that the entirety of the work contained therein is my own, original work, that I am the sole author thereof (save to the extent explicitly otherwise stated), that reproduction and publication thereof by Stellenbosch University will not infringe any third party rights and that I have not previously in its entirety or in part submitted it for obtaining any qualification.

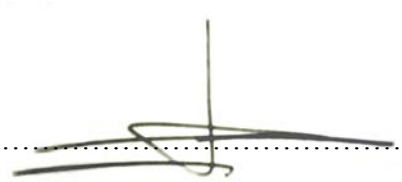

……. ……28/02/2011..……

Hans André Eyéghé-Bickong Date

Summary

Antagonism of antimicrobial action represents an alternative survival strategy for cohabiting soil organisms. Under competitive conditions, our group previously showed that surfactin (Srf) produced by *Bacillus subtilis* acts antagonistically toward gramicidin S (GS) from a cohabiting bacillus, *Aneurinibacillus migulanus*, causing the loss the antimicrobial activity of GS. This antagonism appeared to be caused by inactive complex formation. This study aimed to elucidate whether the previously observed antagonism of GS activity by Srf is a general resistance mechanism that also extends to related peptides such as the tyrocidines (Trcs) and linear gramicidins (Grcs) from *Bacillus aneurinolyticus*. Molecular interaction between the antagonistic peptide pairs was investigated using biophysical analytical methods such as electrospray mass spectrometry (ESMS), circular dichroism (CD), fluorescence spectroscopy (FS) and nuclear magnetic resonance (NMR).

Results from this study corroborated the previous findings, namely that Srf antagonised the activity of GS towards Gram positive bacteria. However, for *Micrococcus luteus* synergism of GS action was observed at low Srf concentrations, while antagonism only occurred at Srf concentrations above the critical micelle concentration (CMC) of Srf when the bacteria were pre-incubated with Srf. This result and an ultra-performance liquid chromatography mass-spectrometry (UPLC-MS) study indicated that Srf pre-absorbed to cells, as well as Srf micelles interacted with GS, preventing GS from reaching the membrane target. Antagonism of GS action by Srf was also observed towards the Srf producer *B. subtilis* ATCC21332 and *B. subtilis* OKB120, a non-producer. The Srf producer was less sensitive than the non-producer towards GS, possibly due to Srf production. Pre-incubation of Srf at different concentrations caused a dose-dependent antagonism, from as low as 0.9 μM Srf of GS activity towards *B. subtilis* OKB120. This antagonism at the low Srf concentration may be related to the induction of more resistant biofilms by Srf in *B. subtilis*. It was also found that Srf significantly improved the survival of *B. subtilis* OKB120 above that of *M luteus* in a

mixed culture. In addition, the Srf producer *B. subtilis* ATCC21332 grew in the inhibition zone of the GS producer *A. migulanus* ATCC9999 during co-culturing, while *B. subtilis* OKB120 growth was inhibited.

Srf induced biofilm formation in *B. subtilis* may be important in protecting the bacteria in solution, but not on solid phase such as on or in agar plates. Also, the protection of various cell types (previous studies by our group) by Srf from GS indicated a directed antagonistic Srf mode of action. Srf formed complexes that are visible and stable under ESMS conditions with GS, with the peptide bonds in the Val-Orn-Leu-D-Phe moiety of GS and the Val-Asp-D-Leu-Leu moiety of Srf protected from fragmentation. ^{1}H-NMR titration studies strongly indicated that the molecular interaction of Srf and GS involved the re-orientation of the D-Phe^{4,9} and Orn^{2,7} residues in GS. From CD spectra it was observed that Srf induced a concentration dependent decrease in the β-turn component and increase in β-sheet structures of the GS-Srf mixture. Diffusion orientated NMR (DOSY) indicated that Srf and GS formed homo-oligomers with the Srf-GS mixture having a slightly higher diffusion coefficient indicating the formation of smaller homo-oligomers or more compact hetero-oligomers. These hetero-oligomers involve intermolecular interaction at <5Å between the Orn^{2,7} residue of GS with Asp residue of Srf, as observed with ROESY-NMR. These results strongly indicate that inactive complex formation between Srf and GS is part of the antagonistic mechanism of action of Srf towards GS.

Two high performance liquid chromatography (HPLC) methods was developed to purify peptides from the tyrothricin complex, namely the Trcs (contains one GS Val-Orn-Leu-D-Phe-Pro moiety) and Grcs. These peptides were used to assess if Srf has an antagonistic activity beyond that of GS. Srf indeed showed antagonistic action against the antimicrobial activity of Trcs towards *B. subtilis* ATCC21332 and OKB120, with the tyrocidine C (TrcC) being more sensitive to antagonism than tyrocidine B (TrcB). Srf had an ambiguous effect on the linear gramicidin A (GA) that is co-produced with Trcs in tyrothricin. GA acted

synergistically with Srf at low GA concentrations, but slight antagonism was observed at high GA concentrations. In contrast, GA showed pronounced synergism with TrcB towards the *M. luteus*. However, Srf at 30 μM, antagonised the synergistic action of a lethal mixture of 25 μM GA and TrcB. The Srf producer was also able to withstand and grow in the presence of the tyrothricin producer *B. aneurinolyticus* ATCC10068, indicating that antagonism of peptide action may allow different organisms to cohabit. Basic NMR and ESMS studies failed to show complex formation between Srf and the Trcs. However, CD presented clear evidence of Srf induced changes in secondary structures and/or higher order self-assembled structures of the Trcs-Srf mixture. FS also provided evidence of the reorientation/exposure of the Trp^6 residue of the Trcs in the presence of Srf. These results corroborated the previous findings that complexation between Srf and GS or peptides analogous to GS may be part of the mechanism of Srf antagonistic action.

In conclusion, this study showed that the antagonism of GS activity by Srf, conferred in part by inactive complex formation, is a putative resistance mechanism that also extends to other peptides containing the Val-Orn-Leu-D-Phe-Pro moiety such as the Trcs from *B. aneurinolyticus*.

Opsomming

Antagonisme van antimikrobiese aksie verteenwoordig ’n alternatiewe oorlewingstrategie vir grondorganismes wat in dieselfde habitat gevestig is. Ons groep het gewys dat surfaktien (Srf), geproduseer deur *Bacillus subtilis*, antagonistiese werking teenoor gramisidien S (GS) vanaf die bacillus *Aneurinibacillus migulanus*, onder kompeterende kondisies, toon. Die antagonistiese werking, wat moontlik veroorsaak word deur vorming van onaktiewe komplekse, lei tot die verlies van die antimikrobiese aktiwiteit van GS. Hierdie studie se doel was die ontrafeling van die moontlikheid dat die antagonisme van GS aktiwiteit deur Srf, soos deur vorige studies uitgewys, ’n algemene weerstandsmeganisme is wat moontlik ook verwante peptiede soos die tirosidiene (Trcs) en lineêre gramisidiene (Grcs), afkomstig vanaf *Bacillus aneurinolyticus*, insluit. In hierdie studie is die molekulêre interaksie tussen antagonistiese peptiedpare ondersoek met biofisiese analitiese metodes wat elektrosproei-massaspektroskopie (ESMS), sirkulêre dichroïsme (SD), fluoressensie-spektroskopie (FS) en kernmagnetiese resonansspektroskopie (KMR) insluit.

Die resultate wat tydens hierdie studie verkry is, het gewys dat Srf die werking van GS teenoor Gram-positiewe bakterie teenwerk, en het die vorige waarnemings ondersteun. Daar is egter sinergisme tussen Srf en GS werking by lae Srf-konsentrasies teenoor *Micrococcus luteus* waargeneem, terwyl antagonisme slegs waargeneem is by Srf-konsentrasies hoër as die kritiese miselêre Srf konsentrasie wanneer bakterieë vooraf met Srf met inkubeer is. Hierdie resultaat, tesame met ’n ultra-hoë verrigting vloeistofchromatografie gekoppelde massaspektroskopie (UPLC-MS) studie, het daarop gedui dat Srf wat voorheen op selle geabsorbeer het, sowel as Srf-miselle in die media, met GS interaksie het en sodanig kan voorkom dat GS die membraanteiken bereik. Antagonisme deur Srf op die GS aktiwiteit is ook waargeneem teenoor die Srf-produseerder *B. subtilis* ATCC21332 en *B. subtilis* OKB120, ’n nie-produseerder. Hierdie tipe antagonisme by ’n lae konsentrasie van Srf mag

verwant wees aan die induksie van meer weerstandige biofilms deur Srf in *B. subtilis*. Dit is ook gevind dat Srf die oorlewing van *B. subtilis* OKB120 aansienlik verhoog teenoor dié van *M luteus* in 'n gemengde kultuur. Daar is verder bevind dat die Srf-produseerder, *B. subtilis* ATCC21332, in die inhibisiesone van die GS-produseerder, *A. migulanus ATCC9999*, gegroei het tydens kokultivering, terwyl die groei van *B. subtilis* OKB120 geïnhibeer is.

Srf induseer biofilm-vorming in *B. subtilis* wat moontlik belangrik kan wees om die bakterieë in suspensie te beskerm, maar nie op soliede fase soos byvoorbeeld agar plate nie. Verder dui die beskerming van 'n verskeidenheid sel-tipes (vorige studies deur ons groep) deur Srf teen GS, 'n direkte antagonistiese aksie van Srf. Sigbare en stabiele komplekse tussen Srf en GS is waargeneem onder ESMS kondisies, waar die peptiedbindings in die Val-Orn-Leu-D-Phe-Pro eenheid van GS en die Val-Asp-Leu-D-Leu eenheid van Srf beskerm is teen fragmentering in die komplese. ^{1}H-KMR titrasiestudies het duidelik aangetoon dat die molekulêre interaksie van Srf en GS die D-Phe^{4,9} en Om^{2,7} residue in GS heroriënteer. SD-spektra van GS-Srf mengsels het daarop gedui dat Srf 'n konsentrasie-afhanklike vermindering in die β-draai komponente van die mengsel veroorsaak, maar dat β-plaat komponent van die mengsel vermeerder. Diffusie-georiënteerde KMR spektrometrie (DOSY) toon dat Srf en GS homo-oligomere vorm, maar 'n hoër diffusie koeffisiënt vir die mengsel het aangedui dat die Srf-GS mengsel kleiner of meer kompakte hetero-oligomere. ROESY-KMR toon dat hierdie oligomere intermolekulêre interaksie(s) van <5Å tussen die Om^{2,7} residue van GS en die Asp residu van Srf het. Die resultate gee 'n sterk aanduiding dat die onaktiewe kompleks-vorming tussen Srf en GS deelneem in die antagonistiese werking van Srf teenoor GS.

Twee hoë verrigting vloeistofchromatografie metodes is ontwikkel om peptiede uit die tirotrisienkompleks, naamlik die Trcs (bevat een GS Val-Om-Leu-D-Phe-Pro eenheid) en die gramisidiene (Grcs), te suiwer. Hierdie peptiede is gebruik om te bepaal of Srf antagonistiese aktiwiteit het wat verder strek as net dié van GS. Dit was inderdaad die geval en daar is

gevind dat Srf antagonisties is teenoor die antimikrobiese aktiwiteit van Trcs met *B. subtilis* ATCC21332 en OKB120 as teikens, met tirosidien C (TrcC) wat meer sensitief vir antagonistiese werking van Srf was as tyrosidien B (TrcB). Srf het ’n gemengde effek getoon teenoor lineêre gramisidien A (GA) wat saam met die Trcs in tirotrisien gekoproduseer word. GA het sinergisties met Srf gewerk by lae GA konsentrasies, maar milde antagonistiese werking getoon by hoë GA konsentrasies. Daarteenoor het GA en TrcB uitgesproke sinergisme getoon teenoor *M. luteus*. In teenstelling het Srf by 30 μM die sinergistiese aksie van die dodelike mengsel van 25 μM GA en TrcB elk geantagoniseer. Die Srf produseerder was ook bestand en kon in die teenwoordigheid van die tirotrisien produseerder *B. aneurinolyticus* ATCC10068 groei wat aangedui het dat die antagonisme van antibiotiese peptiedaktiwiteit die kohabitasie van organismes toelaat. Basiese KMR en ESMS studies kon nie kompleksvorming tussen Srf en die Trcs aantoon nie, terwyl SD duidelike bewyse gelewer het dat Srf verandering geïnduseer het in die sekondêre strukture en/of hoër orde/self-geassosieerde strukture van die Trc-Srf mengsel. FS het ook bewyse gelewer van die reoriëntasie/blootstelling van die Trp^6 residu in die Trcs in die teenwoordigheid van Srf. Hierdie resultate ondersteun die vorige bevindinge dat kompleksvorming tussen Srf en GS of GS-peptiedanaloë deel van die meganisme van Srf se antagonistiese aksie uitmaak.

Samevattend het hierdie studie getoon dat die antagonisme van GS aktiwiteit deur Srf deels toegeken kan word aan onaktiewe kompleksvorming tussen die twee peptiede en dat die voorgestelde weerstandsmeganisme ook ander peptiede wat die Val-Orn-Leu-D-Phe-Pro eenheid, soos die Trcs van *B. aneurinolyticus*, insluit.

Même si le chemin semble étroit et interminable, m'abandonnes jamais tes rêves et ne décline pas tes responsabilités, il y a toujours une récompense au bout de l'effort!

Even if the road seems narrow and unending, you shall not let go of your dreams and do not back out your commitments, there is always a price at the finish line!

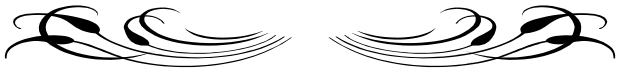

Acknowledgements

I would like to express my thanks and gratitude to the following persons:

- Prof. Marina Rautenbach, my supervisor for all the good challenges that she put me through to enhance my ability as a scientist; for her critical evaluation, motivation and excellent guidance in my study and in the preparation of this manuscript;

- Dr Maré Vlok, for the training he gave me during the honours program at the Biochemistry Department, for his help, guidance and inspiration;

- Dr Raymond Sparrow, CSIR Biosciences, for the use of the circular dichroism facility;

- Dr Marietjie Stander, CAF ESMS Unit, Stellenbosch University, for the help in optimizing the ultra-performance liquid chromatography mass spectrometry and all the electrospray mass spectrometry work;

- Dr Jaco Brand, CAF NMR Unit, University of Stellenbosch, for training me in NMR and his help and assistance with the NMR analysis.

- Dr Katalin E Kövér and Prof Laszlo Szilagyi, Department of Chemistry, University of Debrecen, Hungary, for training me in advanced NMR and guidance with the non-sequential assignment NMR;

- Prof. Pieter Swart, Head of the Biochemistry Department, “the professor” for his assistance with the high performance liquid chromatography;

- Ms. Gertrude Gerstner, BIOPEP Peptide Group laboratory manager and the BIOPEP research group, for their friendship and for the good research (and social) atmosphere that they maintain;

- my colleagues, professors and all personnel in the department of Biochemistry, for all the help and support throughout the years;

- my many friends, who remained my friends in spite of my pre-occupation with my work and research;

- the Gabonese community of South Africa, especially “l’association des étudiants Gabonais a l’Université de Stellenbosch” (AEGUS) for helping making my long stay in South Africa as enjoyable as being home;

- my family back home, my mother Ngwé-Bilong épouse Eyéghé Marcelline, my sisters Josiane Mindze mi-Eyéghé and Blanche Delicat, my brothers Loic N’nah Eyéghé and Wilfride Nzeng-Eyéghé, my father Marcel Francis Eyéghé-Bickong, and all my family members for their support, absolute believe in my abilities and constant love;

- Last, but certainly not the least to my loved ones, my life partner Sarah and our baby girl Andrée Marcie, for their presence, love and help everyday of these past years. Thank you for being there for me and thank you for believing in me always. I love you*!*

Table of Contents

CHAPTER 6: Summary, general conclusions and future prospects

List of Abbreviations and Acronyms

1D	One-dimensional
^{1}H-NMR	One dimension nuclear magnetic resonance
2D	two-dimension
3D	three-dimensional
α	selectivity factor
A-domain	adenylation domain
Amp(s)	antimicrobial peptide(s)
ATCC	American type culture collection
A. migulanus	*Aneurinibacillus migulanus*
B. subtilis	*Bacillus subtilis*
B. aneurinolyticus	*Bacillus aneurinolyticus*
C	condensation
CD	circular dichroism
CD_3CN	deuterated acetonitrile
CFU	central facility unit
CH_3CN	acetonitrile
CID	collision induced dissociation/decomposition
CMC	critical micelle concentration
COSY	correlation spectroscopy
CV	cone voltage
Da	Dalton
DIPEA	N-ethyldiisoprolamine
DMF	N, N'-dimethylformamide
DMSO	dimethysulphoxide
DOSY	diffusion orientated spectroscopy
DPC	diphosphatidylcholine
E	epimerisation
E. coli	*Escherichia coli*
ESMS	electrospray mass spectrometry
FAB	fast atom bombardment
FHC	fractional hemolytic concentration
FIC	fractional inhibition concentration

FS	fluorescence spectroscopy
GA	gramicidin A
GB	gramicidin B
GC	gramicidin C
GD	gramicidin D
GS	gramicidin S
Grc(s)	gramicidin(s)
HC_{50}	peptide concentration leading to 50 % haemolysis
HIV	human immunodeficient virus
HPLC	high performance liquid chromatography
HSV	herpes simplex viruses
IC_{50}	peptide concentration leading to 50 % bacterial growth inhibition
IGA	isoleucyl-gramicidin A
IGB	isoleucyl-gramicidin B
IGC	isoleucyl-gramicidin C
k’	HPLC capacity factor
K	temperature in Kelvin
LB	Luria Bertani
LC	liquid chromatography
LCMS	liquid chromatography mass spectrometry
[M]	molecular ion
M	molar
MALDI	matrix-assisted laser desorption/ionization
MDR-pump	multi-drug resistant efflux pumps
M. luteus	*Micrococcus luteus*
MprF	multi-peptide resistance factor
Mr	molar weight
MS	mass spectrometry
m/z	mass over charge ratio
NAC	N-acetylcysteamine
NMR	nuclear magnetic resonance
NOESY	nuclear Overhauser effect spectroscopy
NRPSs	non-ribosomal peptide synthethases
ORF	open reading frame
PBS	phosphate buffered saline

PCP-domain	peptydyl carrier protein domain
P. falciparum	*Plasmodium falciparum*
PGPR	plant-growth-promoting rhizobacteria
Phcs	phenycidines
POPC	palmitoyloleylphosphatidylcholine
ppb	parts per billion
ppm	parts per million
PSD	peptide sensing and detoxification
R_t	retention time of analyte in column chromatography
R_s	resolution
ROESY	rotating-frame Overhauser effect spectroscopy
RP-HPLC	reverse phase high performance liquid chromatography
SDS	sodium dodecyl sulphate
SEM	standard error of the mean
Srf	surfactin
TCS	two components system
TE	thioestherase
TFA	trifluoroacetic acid
TFE	2,2,2-trifluoroethanol
TLC	thin layer chromatography
TOCSY	total correlation spectrometry
Tpcs	tryptocidines
Trc(s)	tyrocidine(s)
TrcA	tyrocidine A
TrcB	tyrocidine B
TrcC	tyrocidine C
TSB	tryptone soy broth
UV	ultraviolet
VGA	valyl-gramicidin A
VGB	valyl-gramicidin B
VGC	valyl-gramicidin C

Preface

Antimicrobial peptides (Amps) are the most abundant antimicrobial agent in the world since they are produced by all living organisms. They can play an important role as antibiotics in the pharmaceutical industry but also as bio-control agents in the agricultural industry. They are produced under nutritional stress conditions in order for the producing organism to survive by killing interfering organisms. However, many organisms producing Amps are able to cohabit possibly due to various resistance or defence mechanisms. These resistance mechanisms can include drug efflux, hydrolysis, modification, trapping, neutralization or binding, change in cell envelope, mutation/modification of protein targets and/or vital processes of the host cell, biofilm formation and sporulation.

We have hypothesised that a putative resistance mechanism namely antagonism between bacterially produced Amps may affect the soil microbial ecosystems. This occurs between two peptides from cohabiting bacteria, namely GS from *A. migulanus* and Srf from *B. subtilis*. Investigations showed that this takes place via formation of strong solution phase complexes between GS and Srf. It has also been hypothesised that similar antagonistic behaviour may also occur among other peptides analogues to GS such as the Trcs and linear Grcs from *B. aneurinolyticus*. Therefore, this study aims to elucidate the influence among different peptides from the soil bacteria *A. migulanus*, *B. aneurinolyticus* and *B. subtilis* on the activity of one another and attempts to clarify its underlying molecular mechanism and specificity.

This thesis describes how the hypothesis was explored in term of the microbiological and chemical nature of Srf derived antagonism. A short overview of the peptides in this study, namely GS, Srf and peptides from the tyrothricin complex (Trcs and Grcs) is given in Chapter 1. The following four chapters (Chapters 2-5) describe the experimental results obtained in this study. In the final chapter (Chapter 6) the results of this study are summarised and related to Srf antagonistic mechanism of action. To ease future publication, each of these chapters was written with an article format in mind and form, to a degree, independent units. Although some repetition is unavoidable, it has been kept to a minimum.

The major goal of this PhD was to test the hypothesis: “Resistance of the cohabiting organisms, *B. subtilis* and *A. migulanus* toward each others antibiotic peptides are the consequence of antagonistic peptide action”. To reach the research goal, the aims of this investigation were as follows:

- Determine the influence of the *B. subtilis* peptide Srf on GS antibacterial activity using broth based dose-response assays and agar based antimicrobial assays (Chapter 2).
- Elucidate the biophysical character of the antagonism of GS by Srf using biophysical analytical methods such as ESMS, CD, and advanced NMR (Chapter 3).
- Develop HPLC purification protocols, purify and chemically characterise selected peptides from the tyrothricin complex (Chapter 4).
- Determine the influence of GA and Srf on the activity of the purified Trcs to identify possible antagonistic/synergistic peptide pairs using broth based dose-response assays and agar based antimicrobial assays (Chapter 5).
- Characterisation of the possible molecular interactions of the antagonistic/synergestic peptide pairs using biophysical analytical methods such as ESMS, CD, FS and basic NMR (Chapter 5).

Although our research group and department have the facilities to achieve some of the most important goals of this study, partnerships and collaboration with researchers and groups elsewhere were crucial to meet the aims, in particular those concerned with biophysical analyses.

Chapter 1

Antimicrobial peptides from *Bacillus* species

Introduction

Soil bacteria such as plant-growth-promoting rhizobacteria (PGPR) live in symbiosis with plants with which they interact at the plant roots in the rhizosphere [1]. In this partisanship, the two organisms communicate with one another to meet each other's needs. PGPR produce nutrients, enzymes, small antibiotics, peptides and other metabolites that are beneficial for the plant nutritionally as well as providing protection against pathogenic microorganisms and parasites [1]. The plant offers the optimal conditions for bacterium growth and development. One of the most well-studied PGPR groups is the *Bacillus* species [2-4].

Bacillus bacteria are Gram-positive, aerobic or facultative anaerobic spore-forming soil-borne bacteria. Because of their ability to produce enzymes, metabolites and antibiotics, in addition to their physiological properties, they found application in many processes, such as the medical, agricultural, pharmaceutical and food industries [5-7]. The ability to activate specific mechanisms enables *Bacillus* species to adapt for survival during starvation [3]. *Bacillus subtilis,* for example, uses complex motility and chemotaxis systems to search for nutrients in the environment [8-10]. The production of antibiotics, such as antimicrobial peptides (Amps) and degrading enzymes, are the most common adaptations following food

depravation of *Bacillus* species [3]. The synthesis of these stress induced compounds requires the activation of certain genes during the transition from exponential to stationary phase [3]. These genes include operons that encode for the synthesis of enzymes responsible for the non-ribosomal assembly of specific Amps in *Bacillus* species [3]. Amps act as the first defence, which not only helps the bacterium to kill competitor organisms but also prevents intrusion of unwanted microbes in the growth environment [7]. They generally operate as components of the innate immunity and are widely distributed in other species [11]. Prolonged nutritional stress also results in sporulation, which provides the bacterium with a way to survive extended harsh environmental conditions [8]. The production of lipopeptides allows certain *B. subtilis* strain to modify their outer surface which permits them to regroup together in a biofilm in order to proliferate and spread in the territory (review in [5]). Biofilm formation also contributes to the defence and resistance mechanism of *B. subtilis* species towards other peptide or antibiotic producing organisms [12, 13].

The discussion in this chapter will be limited to the three groups of Amps, produced by selected *Bacillus* species used in our study: the linear gramicidins (Grcs), gramicidin S (GS) and the analogous tyrocidines (Trcs), and the surfactins (Srfs) produced by three different bacilli. *Bacillus brevis* reclassified as *Bacillus aneurinolyticus* [14], produces the tyrothricin peptide complex that contains the neutral linear Grc and the basic cyclic Trc fractions [15]. *Aneurinibacillus migulanus* (previously known as the Nagano strain of *B. brevis* [14, 16, 17]), produces GS which is also a basic cyclic peptide related to Trcs [18]. *B. subtilis* strains produce two groups of cyclic lipopeptides, Srfs and iturins [19, 20].

Peptide structures

Peptides from soil bacteria are cyclic or linear, cationic or non-charged peptides which contain two or more moieties derived from amino acids [21]. Their structures have an amphipathic character and they can form different types of β-sheet or helical structures reinforced by intramolecular hydrogen bonds.

Linear gramicidins

The gramicidin D (GD) fraction of the tyrothricin complex are all linear, neutral pentadecapeptides formylated on the N-terminus end, with an alkanolamide on the C-terminus [18] and a sequence in which L- and D-amino acid residues alternate [22]. There are ten known Grcs which differ from each other in three different residues. The first amino acid residue at the N-terminus end can either be a valyl (Val) or an isoleucyl (Ile). This creates two groups of Grcs (Val-Grc and Ile-Grc) [18]. Within each group, gramicidin A (GA), gramicidin B (GB) and gramicidin C (GC) can be distinguished by the nature of the eleventh amino acid residue. This amino acid residue is tryptophanyl (Trp), phenylalanyl (Phe) or tyrosyl (Tyr), respectively in GA, GB and GC (Table 1.1) [18]. A third replacement occurs at the C-terminus end of Val-GA (VGA) and Ile-GA (IGA) where the ethanolamide ($HN(CH_2)_2OH$) group is replaced by a propanolamide ($NH(CH_2)_3OH$) group [23]. Tang *et al.* [18], proposed a variant at the C-terminus end of all three Ile-Grcs where the C_2H_4 moiety of ethanolamide is branched rather than linear, whilst, Orwa *et al.* [23], reported another two methionine (Met) variants of GA at position 4 and 10 (4-Met-VGA and 10-Met-VGA) (Table 1.1).

Grcs can form dimers that exist as β-sheets like secondary structures, folded to form a helix [24]. The dimers self-associate in organic solvents of low dielectric constant and their assembly number increases inversely with the polarity of the solvent [22].

Table 1.1. Summary of the different naturally occurring Grcs with native structure CHO-AA^1-Gly^2-Ala^3-AA^4-Ala^5-Val^6-Val^7-Val^8-Trp^9-AA^{10}-AA^{11}-Leu^{12}-Trp^{13}-Leu^{14}-Trp^{15}-Z, showing the different substitution at positions 1, 4, 10, 11 and Z (Amino acids are denoted using the three-letter abbreviation).

Grcs	AA^1	AA^4	AA^{10}	AA^{11}	**Z**	**Mr**	**References**
VGA	L-Val	D-Leu	D-Leu	L-Trp	$NH(CH_2)_2OH$	1881.1	[18]
IGA	L-Ile	D-Leu	D-Leu	L-Trp	$NH(CH_2)_2OH$*	1895.1	[18]
VGB	L-Val	D-Leu	D-Leu	L-Phe	$NH(CH_2)_2OH$	1842.1	[18]
IGB	L-Ile	D-Leu	D-Leu	L-Phe	$NH(CH_2)_2OH$*	1856.1	[18]
VGC	L-Val	D-Leu	D-Leu	L-Tyr	$NH(CH_2)_2OH$	1858.1	[18]
IGC	L-Ile	D-Leu	D-Leu	L-Tyr	$NH(CH_2)_2OH$*	1872.1	[18]
4-Met-VGA	L-Val	Met	D-Leu	L-Trp	$NH(CH_2)_2OH$	1899.1	[23]
10-Met-VGA	L-Val	D-Leu	Met	L-Trp	$NH(CH_2)_2OH$	1875.1	[23]
VGA-propanolamide	L-Val	D-Leu	D-Leu	L-Trp	$NH(CH_2)_3OH$	1895.1	[23]
IGA-propanolamide	L-Ile	D-Leu	D-Leu	L-Trp	$NH(CH_2)_3OH$	1909.1	[23]

*The $-CH_2$ of the $-NH(CH_2)_2OH$ groups can either be linear or branched isoform [18].

In this project optimised HPLC methods for the analysis and purification of a number of Grcs were developed and utilised and their identity and primary structures were confirmed with electrospray mass spectrometry (reported in Chapter 4).

Normally, and depending on both the solvent and their amino acid sequences, Grcs are either monomers or double stranded dimers, and once integrated into the membrane lipid they adopt a single type of structure, namely a right-handed single-stranded $\beta^{6.3}$-helical dimer [25-30]. This structural conformation only occurs in double-layer membranes or micelles, and has been proven to be insensitive to the lipid environment, in several experiments, using different lipid membranes [26, 28, 31]. However, Grcs have also been reported to form double-stranded $\beta^{6.3}$-helical dimers in membranes containing unsaturated lipids [29, 32].

According to tandem mass spectrometry result metal ions bind inside the Grc dimers causing them to weaken, [22]. This effect increases with increasing metal ion size [22]. Grcs can also form dimers in phospholipid membranes, in which the conformation has been proven to be an amino terminal-to-amino terminal helix [24]. The common sequence for VGA, as a dimer is shown in Figure 1.1 with the different possible substitutions at specific sites indicated.

The low temperature crystal structure of the GD-RbCl complex has been determined at 14 Å resolution [33]. The crystal unit is asymmetric with two right-handed antiparallel double stranded dimers formed by four different Grc molecules [33]. Each dimer forms a symmetric channel that contains seven distinct Rb binding domains [33]. The Grc channel is thus formed by the peptide backbone and three to five carbonyl groups through which Rb^+ ions, coordinated by delocalized π-electrons, pass [33].

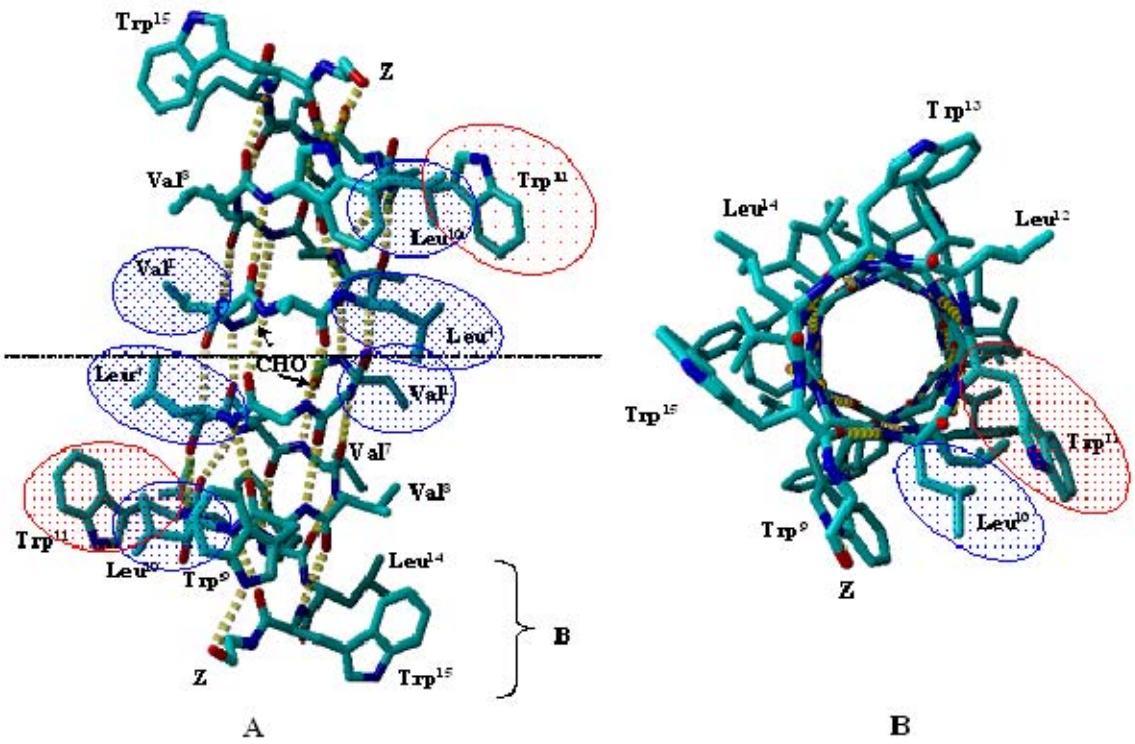

Figure 1.1. Schematic representations of VGA dimer (A) and of its channel structure (B) [adapted from Townsley *et al*. [34]]. Substituted amino acid residues are indicated with blue (non-aromatic hydrophobic amino acids) and red (aromatic amino acids).The 3-letter abbreviations of the amino acid residues are also given. The structure was drawn using the Yasara® version 8.6.29 for Windows [35, 36].

Gramicidin S

GS is a basic cyclic decapeptide consisting of a pentapeptide repeat of an L-valyl-L-ornityl-L-leucyl-D-phenylananyl-L-prolyl unit (L-Val^1-L-Orn^2-L-Leu^3-D-Phe^4-L-Pro^5), which is also conserved in the analogous Trcs [18]. The ring structure is linked between Val and Pro, forming an antiparallel β-sheet terminated in two type II β-turns, defined by D-Phe-Pro residues [37]. It adopts this three-dimensional arrangement in various solutions of different polarity and in the crystalline form [37]. Apart from that, GS structure is reinforced by four hydrogen bonds: two between Leu^3 and Val^6 residues and two

between Leu[8] and Val[1] (Figure 1.2) [38]. GS also adopts a geometrical arrangement, leading to an amphipathic structure that is ideal for interaction with biological membranes. The hydrophobic side chains on one side interacts with the non-polar lipid tails and the hydrophilic groups and cationic ornithines on the other side with the polar lipid/water interface [39]. According to NMR experiments, GS shows limited conformational flexibility because of its two rigid type II' β-turns and its antiparallel β-sheet conformation [37, 39]. The antiparallel β-sheet conformation of GS is presented in Figure 1.2.

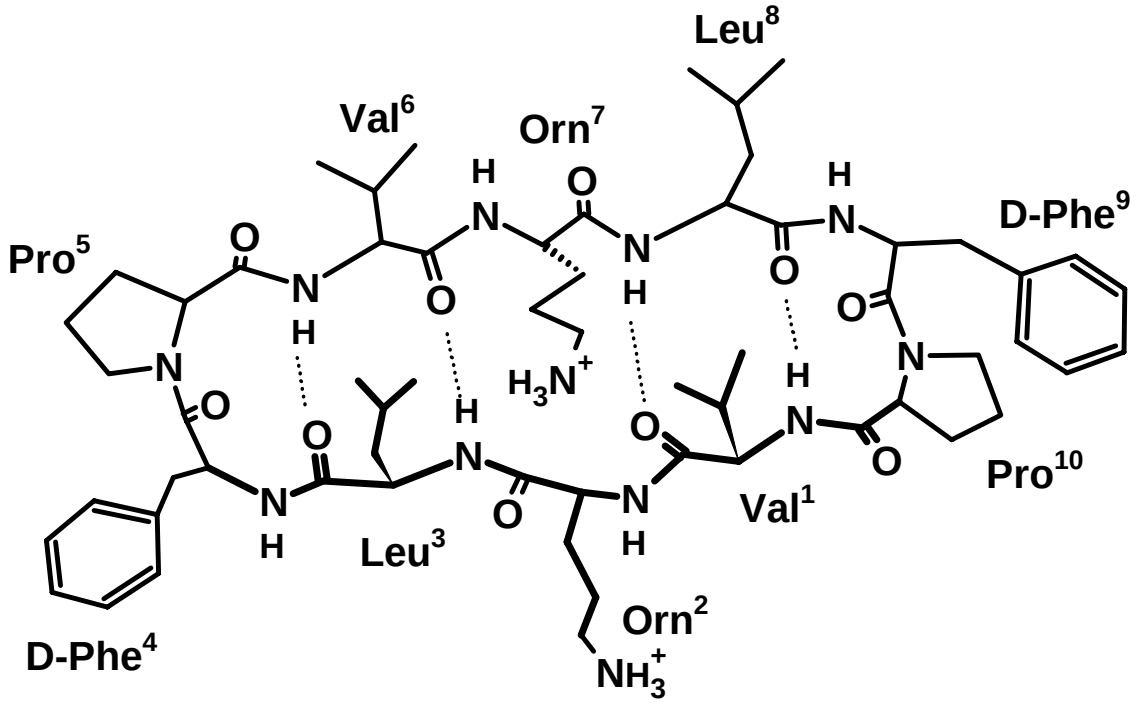

Figure 1.2. A structural model of GS depicting its proposed antiparallel β-sheet conformation (adapted from Kawai *et al.* [40]). The two Orn and two Phe residues are oriented in one plane forming the hydrophilic side of the molecule. The hydrophobic side formed by the two Leu and two Val residues is directed to the opposite plane of the molecule [41]. The structure is reinforced by four hydrogen bonds: two between Val_1 and Leu_8 and two between Leu_3 and Val_6 [38]. The structure was drawn using ACD/ChemSketch software (ACDLABS 12.0 software, [42, 43])

Tyrocidines

The Trcs are basic cyclic decapeptide analogues of GS, since they share the same pentapeptide unit Val[1]-Orn[2]-Leu[3]-Phe[4]-Pro[5]. However, the second pentapeptide unit of the Trcs and analogues have a variable sequence namely L-(Phe/Trp/Tyr)[6]-D-(Phe/Trp/Tyr)[7]-L-Asn[8]-L-Gln[9]-L-(Phe/Trp/Tyr)[10] [18]. Tang *et al.* [18] identified 28 Trcs which differ from one another in residue positions 1, 2, 6, 7 and 10, occupied by a combinations of Leu/Ile, Lys, Phe, Tyr or Trp. The substitutions occur only between amino acids belonging to the same groups: aliphatic for aliphatic, aromatic for aromatic (Table 1.2 and Figure 1.3) [18]. There are also two groups of Trcs that differ in terms of the nature of the cationic residue, which can either be an Orn or a Lys. Each group A/A_1, B/B_1 and C/C_1 can be distinguished from each other by their dipeptide units: L-Phe-D-Phe, L-Trp-D-Phe and L-Trp-D-Trp at positions 6 and 7.

Table 1.2. Summary of the most common Trcs in the tyrothricin complex with the native structure cyclo-(L-Val[1]-L-AA[2]-L-Leu[3]-D-Phe[4]-L-Pro[5]-L-AA[6]-D-AA[7]-L-Asn[8]-L-Gln[9]-L-AA[10]) showing the different substitution at positions 2, 6 and 7.

Trcs/ Tryptocidines	L-AA[2]	L-AA[6]	D-AA[7]	**Mr**
TrcA	Orn	Phe	Phe	1279.7
TrcA_1	Lys	Phe	Phe	1283.7
TrcB	Orn	Phe	Trp	1308.7
TrcB_1	Lys	Phe	Trp	1322.7
TrcC	Orn	Trp	Trp	1347.7
TrcC_1	Lys	Trp	Trp	1361.7

Amino acids are denoted using the three-letter abbreviation. This table was adapted from Tang *et al.* [18].

The tryptocidines (Tpcs) and phenycidines (Phcs) are Trc analogues also found in the tyrothricin peptide complex, with respectively a Trp and Phe residue at position 10 rather than a Tyr. It has been proposed that the Trcs, similar to GS, form a rigid antiparallel β-plated sheet structure maintained by four intrastrand hydrogen bonds that are not sensitive to side chain variation [44]. Figure 1.3 shows the structure of cyclic TrcA taken as model structure of the Trcs.

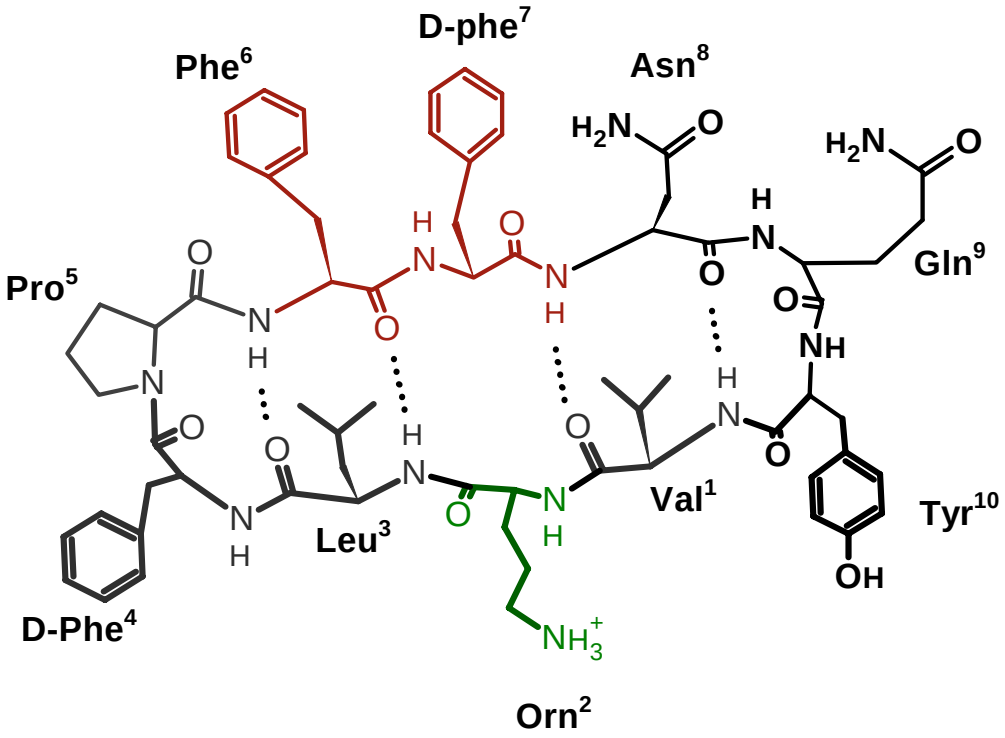

Figure 1.3. A structural model of the proposed antiparallel β-pleated sheet structure of TrcA [18], adapted from Qin *et al.* [44]. The variable amino acids of the Trcs are indicated in red (aromatic residues) and green (cationic residue). The conserved hydrophobic residues are shown in grey and the polar amino acids are shown in black. The structure was drawn using ACD/ChemSketch software (ACDLABS 12.0, [42, 43])

In this project optimised HPLC methods for the analysis and purification of a number of Trcs and analogues were developed and utilised and their identity and primary structures were confirmed with electrospray mass spectrometry (reported in Chapter 4).

Surfactins

The Srfs are acidic cyclic lipopeptides consisting of seven amino acids with the cyclic peptide sequence L-glutamyl-L-leucyl-D-leucyl-L-valyl-L-aspartyl-D-leucyl-L-leucyl (L-Glu^1-L-Leu^2-D-Leu^3-L-(Val/Ala)^4-L-Asp^5-D-Leu^6-L-(Leu/Val/Ile)^7) interlinked with a long hydrophobic alkyl chain (fatty acid residue) via a lactone bond (β-hydroxy fatty acid bond) between Leu^7 and Glu^1 (Table 1.3 and Figure 1.4) [45].

Table 1.3. Summary of the most common surfactins in the commercial peptide extract with native structure X-cyclo-(Glu^1-Leu^2-D-leu^3-AA^4-Asp^5-D-leu^6-AA^7) showing the different substitution at positions X, 4 and 7 [45].

Srfs	**X**	**AA^4**	**AA^7**	**M_r**
Srf_1	C_{15}	Ala	Val	994.7
Srf_2	C_{13}	Val	Leu	1008.7
Srf_3	C_{14}	Val	Leu	1022.7
Srf_4	C_{15}	Val	Leu	1036.7

Several Srf variants that coexist in the same extract, differing at either residues 4 and 7 or the fatty acid tail length (Table 1.3) [45]. The fatty acyl chain generally contains between 13 and 15 carbon atoms in the n, iso and ante-iso configurations [45]. Srf also has an amphipathic character with a hydrophobic side composed of the fatty acyl tail and non-polar non-hydrophilic amino acid residues located in positions 2, 3, 4 and 7, while Glu^1 and Asp^5 form the hydrophilic side of the molecule (Figure 1.4) [45].

Srf has a limited aqueous solubility and forms aggregates in solution. Aggregation is the consequence of Srf's very strong surface tension activity resulting from its tendency to

absorb at a hydrophilic/hydrophobic interface [46]. This strong interface absorption is dependent on the balance between its minor polar and major hydrophobic domains [47].

The three-dimensional structure of Srf has been determined from two dimensional ^{1}H-NMR in $^{2}H_6$-dimethylsulfoxide by Bonmatin *et al.* [47]. Two possible conformations of Srf (S1 and S2), characterised by a "horse saddle" ring atom on which the two polar Glu^{1} and Asp^{5} are attached, are proposed [47] (Figure 1.4).

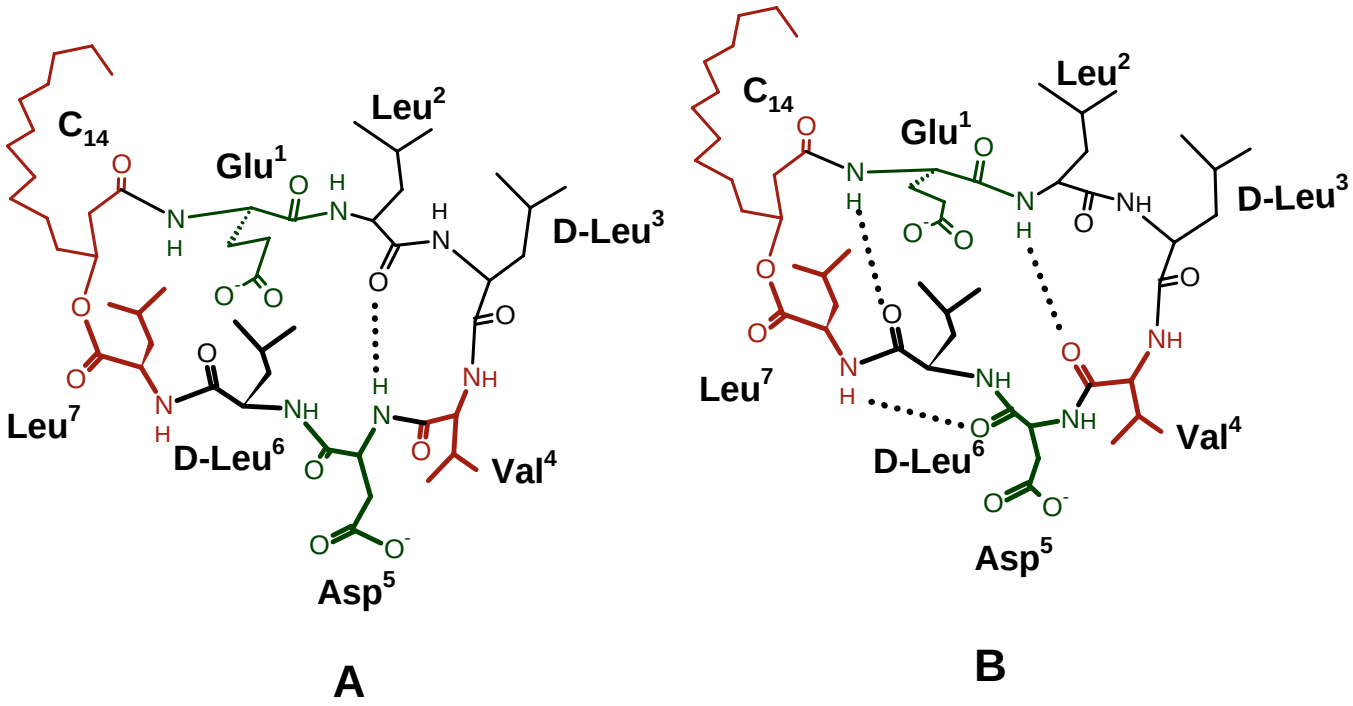

Figure 1.4. Structural representation of the two models S1 (A) and S2 (B) of Srf_3 structure (adapted from Tsan *et al*. [48]). In both models, the two acidic amino acid residues Glu^{1} and Asp^{5} together with Val_4 form the hydrophilic plane of the molecule, whereas the four hydrophobic Leu residues are oriented in the other side of the peptide forming the hydrophobic plane. The variable amino acids of the Srfs are indicated in red (including the fatty acid chain) and the acidic amino acid in green. ACD/ChemSketch software (ACDLABS 12.0, [42, 43]) was used to draw these structures.

Polar and hydrophobic side chains are directed in opposite directions in the two models [47]. However, the two models differ in terms of the hydrogen bonds; there is only one hydrogen bond between the NH of Asp^5 and the C=O of Leu^2 in the S1 model (Figure 1.4 A), whereas in the S2 model there are three hydrogen bonds (Figure 1.4 B) [47]. The two acidic groups in the S1 model are close together on the same side and form a "claw", which can interact with divalent ions such as Ca^{2+} [47]. Thus, the conformation of S2 might correspond to a calcium-bound Srf whereas S1 might correspond to the cation-free lipopeptide [49]. Gallet *et al.* [46] modelled Srf at the hydrophobic/hydrophilic interface and found that the S2 conformation was the one that gave the most consistent interfacial characteristic, compared to experimental data obtained by a Langmuir film balance with S1 conformation. According to Deleu *et al.* [49] S1 and S2 interact differently with membranes. Whether the membrane is charged or not, both acidic residues in the S2 structure are situated in the polar region of the membrane, while in the S1 structure the two polar groups appear in different locations [49]. Asp^5 is found in charged membranes in aqueous solution whereas Glu^1 appears in the hydrophobic core in uncharged membranes [49]. However, when Tsan *et al.* [48] modelled the structure of Srf in sodium dodecyl sulphate (SDS) micelles they only found a single family of low energy structures, whereas in organic solvent the two families (S1 and S2) of similar energy minima were found. They hypothesized that SDS might stabilize the structure of Srf by "solvating" it [48]. No match could be made between the structure of Srf in SDS with either of the S1 or S2 structures obtained in organic solvent [48]. Only the "saddle-shaped" conformation with the two polar residues on the same side of the molecule was conserved [48]. There were no qualitative

differences in the dynamic properties of Srf in negatively charged micelles (SDS) and in uncharged micelles (dodecylphosphocholine, DPC) [48].

Bioactivity and structure-activity relationships

All the above peptides are membrane active and have a broad spectrum of activity against Gram-positive and Gram-negative bacteria [50-52], as well as against fungi and yeast. However, they also have lytic effects against human red blood cells at low concentrations, limiting their medical application [53-55]. The activity of this class of antimicrobial peptides is mediated not only by their amphipathic character, but also by key side chain groups in their amino acid sequences.

Linear gramicidins

The linear Grcs are active against Gram-positive bacteria as a defence mechanism of its producer [56]. They have potential as antibiotics agents in topical ophthalmic preparations and antibiotic preparations used to treat patients with burns [52, 57]. Their antibiotic activity is mediated by an increase cation permeability in biological membranes of the competitor organisms through ion channel formation which causes membrane lysis and cell death [58, 59]. Chapter 5 describes the action of linear Grcs alone and in combination with selected Trcs and GS.

Apart from their potent antibacterial activity, linear Grcs also have exceptional antiviral activity, indicating their potential activity as prophylactic agents against sexually transmitted diseases such as HIV and herpes simplex viruses (HSV) type 1 and 2 [60].

Nanomole concentrations in the order of 10 ng/mL are required for complete and effective HIV inactivation under *in vitro* conditions (10 ρg/mL leads to 50% inhibition of HIV infection) [61]. According to Bourinbaiar *et al.* [61] Grcs have an IC_{50} of 0.3 μg/mL against the type 1 and 2 HSV isolates and their efficacy is comparable to the anti-HSV agent acyclovir. The Grcs also has a suppressive effect on the replication of acyclovir-resistant thymidine kinase and DNA polymerase HSV mutants at the same effective dosage than against acyclovir-sensitive strains. The linear antibiotics also have antagonistic actions on the inhibitory effects of Trc on RNA synthesis in *B. brevis* [62, 63]. Grc have been assessed to have potential as immunosuppressants for organ transplantation [64]. Grcs also have lytic activity on normal erythrocytes, with a high selectivity for erythrocytes infected with malaria [65-67]. The activity of linear Grcs towards one of the major human pathogens leading to malaria, *Plasmodium falciparum*, was observed [53, 65-67]. According to Gumila *et al*. [68], GD has a 50% inhibitory concentration of 0.035 ng/mL against *P. falciparum in vitro*. Divo *et al.* [65] reported the IC_{50} value of Grcs toward the malaria parasite to be <0.02 ng/mL.

Linear Grcs generally interact with lipid membranes and affect the membrane stability by forming monovalent cation selective ion pores (see [69] for detailed review). Trp residues have been found to play a very important role in the ion channel forming property of Grcs. Jordan *et al.* [70], examined the effect of substituting Trp residues on GA structure and function. They synthesized Grc analogues with Trp at positions 9, 11, 13 and 15 substituted by Gly. Two-dimensional NMR and distance geometry-simulated annealing structure calculations were used to determine the three-dimensional structure of analogues and

correlated with subsequent functional changes [70]. The Gly for Trp substitutions had little effect on the $\beta^{6.3}$-helical structure in the peptide channel, however, it caused large changes in channel function since it altered the ion-dipole interactions that modulate ion movement [70]. According to Seoh and Busath [71], replacement of the four Trp residues with Phe disturbs the stability of the ion channels formed by Grc since the Trp residues mediate channel stability. The GA analogue, in which all four Trp residues were substituted with Phe, still undergoes a conformational change from β-helical monomer to stable double stranded dimer once inserted into the lipid membrane [72]. Only negligible effects were observed when the Trp at position 11 was replaced by Phe, compared to at the other positions [71]. Deletion or addition (Tyr or hexafluorovaline at position 1) of a single amino acid residue, in only one of the two subunits of the dimer channel near the point where the two Grc molecules meet in the membrane centre, caused a mismatch between the subunits and can lead to voltage-dependent Grc channels [29, 73]. Replacement of Trp^{11} with a Phe or Tyr as in GB and GC respectively, affects the binding enthalpies of monovalent cations to the Grc channel and the transport properties of Grc analogues.

Gramicidin S

GS has applications as a broad spectrum antibiotic because of its antibacterial, antifungal and haemolytic activity. According to Kondejewski *et al.* [50], the minimum inhibitory concentration (MIC) of GS ranges between 3 and 12.5 μg/mL for Gram-negative bacteria and is 3 μg/mL for Gram-positive bacteria. GS has inhibitory actions on active transport of [^{3}H]-alanine and [^{3}H]-uridine in membrane vesicles isolated from *B. brevis* and *B. subtilis*

at concentrations of 2 to 4 μmol/mg of membrane protein [74]. GS also exhibits activity against several pathogenic fungi [75, 76]. GS also has lytic activity on eukaryotic cells such as human red blood cells *in vivo* and *in vitro* and against malarial infected erythrocytes [75, 77]. According to Rautenbach *et al.* [54], GS is substantially less active than Trcs toward the growth of *P. falciparum* infected erythrocytes with an IC_{50} of about 1.3 μM. This antiplasmodial activity is the result of selective lysis of the more fragile infected erythrocytes. The investigations of the influence of Srf and GA on the *B. subtilis*, *Micrococcus luteus* and *haemolytic* activity of GS are reported in Chapters 2 and 5.

The amphipathic balance of GS plays a crucial role in its antimicrobial and anti-fungal activity. Its amphipathicity is characterised by the existence of both a major hydrophobic side, composed of all its hydrophobic residues, and its minor polar side, composed of the two cationic Orn residues. These two Orn residues are important for ionic interactions of the peptide with the negatively charged phospholipids in membranes. Acylation of the amino groups in Orn residues was found to cause a drastic decrease in GS antibacterial activity (98% loss) and inhibition of active transport in membrane vesicles in *vitro* [74]. Nagamurthi and Rambhav [78] also investigated the importance of the two Orn groups of GS on the antimicrobial and haemolytic activity of this molecule by chemically modifying it through acetylation, formylation, carbamylation, deamination, trimethylation, succinylation and maleylation. More than 95% of the antimicrobial activity of the antibiotic was lost after these modifications, however, about 70-88% of the haemolytic activity of the drug was retained [78]. Modification or blockage of one of the two amino groups caused

only a 50% loss of the antimicrobial activity showing the equal contribution of the two Orn groups to GS activity [78].

The ring size of GS also plays a crucial role in its antimicrobial activity. Kirisci *et al.* [79], studied the effects of ring size analogues of GS, having 10, 12 and 14 amino acids in sequence (GS10, GS12 and GS14 respectively), on the thermotropic phase behaviour and permeability of a phospholipid model membrane, as well as on the growth of *Acholeplasma laidlawii.* A correlation was found between the relative potencies of GS and the ring-size with GS14 > GS10 > GS12 in terms of inhibition of *A. laidlawii* growth and membrane perturbation [79]. They also hypothesised that the primary target of gramicidin S is the bacteria bilayer membrane [79].

Tyrocidines

As with GS, the analogous Trcs are membrane-active peptides that have a broad spectrum of activity towards a number of pathogens, including fungi, Gram-negative and Gram-positive bacteria [52, 80]. According to Spathelf and Rautenbach [81], Trcs have lytic and growth inhibitory activity toward Gram-positive *B. subtilis, M. luteus* and *Listeria monocytogenes* and Gram-negative *Escherichia coli*. The IC_{50} value of the Trc mixture was 3.9 ± 0.04 μg/mL against *M. luteus* [81]. The activity of cyclic Trcs towards *B. subtilis* and *M. luteus* and the influence by both Srf and GA on their activity is reported in Chapters 5.

They also exhibit lytic activity against erythrocytes and malaria infected erythrocytes [54]. The IC_{50} values of Trcs were found to be in the nanomolar range with, TrcA, as the most

active, having an IC_{50} of 580 pM against *in vitro P. falciparum* [54]. The 50% lethal concentration (LC_{50}) of the Trcs is ranged between 9 and 28 μM towards Hela and A549 cells [54].

In *B. aneurinolyticus*, the Trcs regulate the RNA transcription during sporulation by forming a complex with the DNA [62, 63, 82]. This complexation with GC rich DNA sequences [63] induces conformational changes in the DNA structure [82] and results in an inhibition of RNA synthesis [62]. The presence of linear Grcs reverses the effect of Trcs on RNA synthesis since it weakens the Trc-DNA complex and causes its dissociation [63]. An increase in temperature also causes the dissociation of the Trc-DNA complex [63]. Trcs have been observed to inhibit active transport of [^{3}H]alanine and [^{3}H]uridine in membrane vesicles isolated from *B. aneurinolyticus* and *B. subtilis* at concentrations of about 2-4 μg/mL [74].

Several features are essential in the structure of Trcs to exert their function. The L-Phe^6 residue is important for bacterial activity and the ability of TrcA to inhibit both active transport *in vitro* and RNA synthesis [74]. The replacement of this amino acid with a Val residue reduces these effects *in vitro* [74]. The topology of Trc, with its hydrophobic region composed of all hydrophobic residues and its hydrophilic side consisting of the sequence Asn^8-Gln^9-Tyr^{10}, also contributes to the antimicrobial action of the drug [83]. Consequently, replacing for example D-Phe^7 with an D-Orn residue, to match the structure of its analogue GS, caused a large reduction in the antibacterial and inhibitory action of TrcA since it disturbs the hydrophobic-hydrophilic topology of the molecule [74, 83].

However, replacing the Gln^8 in TrcA with a cationic residue, such as Lys, increases the antibacterial activity [83].

Rautenbach *et al.* [54] investigated the structure-activity relationships of the naturally occurring Trcs on the growth of the malaria parasite *in vitro*. Activity against *P. falciparum in vitro* was closely related to the apparent hydrophobicity of the peptide, which increases with the Phe content, and inversely correlated to the side chain surface area of the major tyrocidines [54]. These correlations possibly explain why the antiplasmodial activity of $TrcC_1$ was much lower than that of TrcA, the most potent Trc investigated in that study [54]. In general, the Orn analogues were also found to be more active than the Lys analogues in terms of their antiplasmodial activity. In addition to its importance in active transport and RNA inhibition [74], the Phe dipeptide unit is also an important determinant of antiplasmodial effects of Trcs [54]. Substituting these amino acids with two Trp, as is the case of the naturally occurring $TrcC_1$, greatly reduced the selective activity of the Trc *in vitro* [54].

Spathelf and Rautenbach [81] found that the more polar TrcB/B_1 and TrcC/C^1 groups were substantially more active against Gram-positive bacteria than the TrcA/A_1 group. However, several authors also investigated the effect of substituting other groups, which are not naturally alternated, on the antimicrobial and haemolytic action of Trcs. Qin *et al.* [44] synthesised TrcA analogues having a number of different amino acid residues at position 8 (Gln) and tested their antibacterial and haemolytic activity. They found that substituting Gln^8 from the TrcA sequence with basic amino acids significantly reduces the undesired haemolytic activity of the peptide and simultaneously increases its potency toward

microorganisms [44]. This result, in addition to the activity differences between structural variants at the aromatic dipeptide unit (positions 6 and 7), constitutes that it is possible to develop novel synthetic analogues of the Trcs with improved activity, and reduced antimicrobial resistance and haemolytic activity [44].

Surfactins

Srf has good antifungal activity and moderate antibacterial activity. It has been proposed that Srf can act synergistically with its analogue iturin A as bio-control agents to inhibit the growth of certain plant pathogenic fungi at low concentrations [84-86]. After they are excreted in extracellular medium, both iturin A and Srf can absorb to *B. subtilis* surface and induce changes in its hydrophobicity [87]. This is to allow the producer to adhere to plant and fruit surface which is essential for its survival and its biological control of plant diseases [87]. Vlok [88] has shown that Srf antagonises the antimicrobial activity of GS by forming stable complexes in the solution phase and possibly in the cell membrane. This was further investigated and is reported in Chapters 2 and 3. In Chapters 5 we report the effect of Srf on the activity of GS analogous Trcs.

Srf also has antitumoral, antiviral [40] , as well as antimycoplasma activity [89, 90]. It disrupts the membranes of several viruses such as herpes viruses, retroviruses and other enveloped RNA and DNA viruses by interacting with the virus lipid membrane or envelope [91]. However, it also exhibits haemolytic properties that make it an unsuitable compound for medical applications [92]. Dufour *et al.* [55] found the IC_{50} of Srf against red blood cells to be 300 μM.

Srf also have activities not related to its lytic activity, for example some inhibitory effects on fibrin clot formation [93], cyclic adenosine monophosphate (cAMP) formation [93] and on platelet and spleen cytosolic phospholipase A_2 [89]. The binding of Srf to bivalent cations such as calcium ions explains its inhibitory action upon enzymes that need bivalent ions for their activity, such as cAMP phosphodiesterase and alkaline phosphatise [92, 94].

Biosurfactants such as Srf must first adhere to their microbial target surface, which predominantly takes place through hydrophobic interactions, in order to exert activity [95]. Its membrane activity arises from the amphipathic three-dimensional topology of Srf, which comprises a hydrophobic face made up of all the hydrophobic amino acids and the fatty acid chain and a hydrophilic face with the two carboxylic groups of Glu_1 and Asp_5. The length of the lipid chain and the cyclic polar head of Srf promotes its insertion and penetration into the membrane layer, and the longer the lipid chain the deeper the penetration into the membrane lipid [95]. The activity of Srf is improved when its two acidic groups, protruding in the same side, are ionised and form a complex with a calcium ion [45]. Calcium ions induce changes in the binding of Srf to the membrane at the air-water interface [45]. According to Gallet *et al.* [46], in the S2 structure the peptide ring of Srf adopts a flat orientation irrespectively to the fatty acid length, allowing similar interfacial areas of the folded and extended conformation of the peptide.

Mode of action of the selected *Bacillus* antimicrobial peptides

In order to study resistance or defence mechanisms toward antimicrobial peptides, the major goal of this project, it is necessary to have knowledge about their target(s) and mode

of action. Although the mode of action of some of these Amps has not yet been fully elucidated, studies have proven that they generally bind to the cell membranes of bacteria (or target cells) causing cell death by lysis. This lysis is possibly mediated by the formation of pores that induce ion leakage and general disruption of the membrane function and integrity [96]. Apart from the membrane target, these Amps under discussion also have several other targets which can be intracellular or nuclear [62, 82, 89, 94].

Linear gramicidins

The linear gramicidins have both membrane and intracellular targets. Because of their hydrophobicity linear Grcs generally interact with lipid membranes where they induce cation-selective ion channels/pores that allow the passive transport of ions (monovalent cations) across the membranes and cause an inhibition of cellular processes and cell death [97, 98]. The Grc channel occurs by dimerisation of transmembrane monomers through the formation of six hydrogen bonds [99, 100]. The formation of the Grc channel induces membrane deformation and is influenced by the membrane thickness [101]. Cholesterol increases the membrane thickness [102, 103] and therefore reduces the channel activity of Grc [104, 105].

Selectivity of the Grc channel for monovalent cations (such as K^+, Na^+, Li^+, Ti^+, NH_4^+ and H^+) and impermeability of multivalent cations and anions have been observed [98]. The binding of a cation to the Grc channel constitutes the first step in this free energy transport process. The order of Grc selectivity for monovalent cations is $Cs^+ > Rb^+ > K^+ > Na^+ > Li^+$ [106, 107]. The ions inside the channel are coordinated by four alpha-carbonyl groups from

the four Trp residues in GA, and two water molecules that also contribute to the free energy barrier of the channel [108]. These Trp residues play a very important role in the ion channel forming property of GA [70, 71].

Grcs have the ability to convert the micellar organisation of lysophosphosphatidylcholine to a bilayer type of organisation depending on the type of solvent [109, 110]. Additionally, hexagonal H_{II} phases have been demonstrated to occur when Grcs are present in high concentrations in natural and bilayer-forming lipids [111, 112]. The thickness of the acyl chain of the membrane has an influence on the concentration of Grc required to induce H_{II} phases [113, 114]. The latter is known to decrease with an increase in membrane thickness [113, 114]. The cyclic Trcs reverse the H_{II} phase, induced by a high concentration of Grc, in dioleoylphosphatidylcholine model membranes [115].

It has been suggested that Grcs, together with Trcs, act as gene regulators (interaction with RNA-polymerase and DNA) in the producer *B. aneurinolyticus* [62, 63, 116]. Linear Grcs inhibit RNA polymerase in a nonspecific way by interfering with the formation of a stable initiation complex between RNA polymerase and DNA [116]. Depending on the presence of RNA polymerase from *B. aneurinolyticus*, linear Grcs also antagonise the Trc-DNA complex responsible for the inhibition of the RNA synthesis by dissociating the tyrocidine-DNA complex [116] similar to the way in which it antagonises the effect of tyrocidine on membrane permeability in model membranes [115].

Otten-Kuipers *et al.* [66] studied the mechanism of the lytic action of Grc and tryptophan-N-formylated Grc by looking at their ability to change the potassium and sodium

composition of normal human and malaria infected erythrocytes. Both peptides cause potassium efflux and sodium influx in erythrocytes with Grc being ten times more effective than its analogue [66, 67]. It was hypothesised that *P. falciparum* death is caused by potassium leakage from infected erythrocytes, induced by the peptide application [66, 67]. Even though more than 50% of the erythrocyte potassium content can be lost upon the treatment with Grcs and analogues, erythrocytes are still able to restore their normal ion content since Grcs do not cause irreversible damage to them [66].

Recent studies have shown that linear Grcs have effects on viral replication, such as HIV and HSV [60]. However, the mechanism of this action can only be inferred due to lack of experimental evidence. Viruses cause an increase in the cytosolic K^+ content in order to force the host cell to produce their own proteins and multiply [60]. It has been proposed that linear Grcs may reverse this process by expelling K^+ from the cell and re-establishing the normal cell polarity [60]. Depletion of the cytosolic K^+ content is detrimental to the survival of the virus in the host system and will cause the virus to die. A perturbation of the ionic gradient across the cell membrane by the ionophore action of the Grcs may also be a possible way to inactivate viruses, for instance retroviruses [60].

According to Hirano *et al.* [64] Grcs suppress the proliferation and differentiation of cytotoxic T cells or B cells by altering the membrane composition of blastomers, which results in the disturbance of membrane fluidity of target immune cells. A modulation of the intracellular Ca^{2+} levels by the action of Grcs may also account for the mechanism of lymphocyte suppression since increased intracellular Ca^{2+} concentrations are important for nitrogen stimulation of lymphocytes proliferation [64]. Hirano *et al.* [64] also showed that

linear Grcs suppress allograft rejection *in vitro*, in a manner similar to that of cyclosporine at 4-8 mg/kg/day, in a heterotopic heart transplantation rat model.

Gramicidin S

The antibiotic GS targets both the cell membrane and intracellular targets [20-27]. The mechanism by which GS kills bacterial cells and lyses erythrocytes appears to be through permeabilisation and disruption of the lipid bilayer of their biological membrane (outer membrane) [117, 118]. GS acts by changing the ion permeability of the lipid membrane because of its amphiphatic character and its rigid β-turns structure which it adopts in membrane environments [37, 39]. As shown by Jelokhani-Niaraki *et al.* [75], the first step in the mode of action of gramicidin S is its absorption into the membrane and its stabilization in a β-turn/sheet secondary structure. In the second step, the interaction of the peptide with membrane lipids and/or other GS molecules brings about changes in the morphology of the lipid bilayer, which causes a deterioration in the membrane structure [75]. According to Staudegger *et al.* [119], GS disrupts lipid membranes by increasing the negative curvature stress, causing the formation of bi-continuous inverted cubic phases at a lipid-to-membrane ratio of 25. This loss of the non-lamellar phase, essential for normal membrane function promotes the permeabilisation and/or disruption of the lipid bilayers [120]. Mihailescou and Smith [39] found that GS had little effect on the membrane potential and water permeability of the membrane. However, GS orders lipids which is not directly interacting with it and disorders neighbouring lipids, rendering certain areas of the membrane more crystalline and other more fluid [39].

The mechanism of GS action on bacterial and fungal targets has also been reported. It has been demonstrated that GS can absorb to the outer membrane of Gram-negative bacteria such as *E. coli* and disrupt its permeability barrier and/or stimulate the efflux of K^+ ions through the outer membrane [117]. GS may compete with divalent cations such as Mg^{2+} and Ca^{2+} which help to stabilize the lipopolysaccharide moiety of the *E. coli* outer membrane [117]. GS also proved to be potent against mollicutes at a MIC of 2 to 50 nM [120]. These actions are most probably due to a change in the membrane potential of spiroplasmas, which is partly responsible for their motility and shape [120].

In erythrocytes, GS molecules embed in the lipid membrane from its hydrophobic side, with the two cationic Orn residues oriented in the hydrophilic interface preventing further penetration of the peptide deeper into the bilayer [77]. GS accumulation in the membrane leads to a deformation in the erythrocyte as the membrane structure becomes more and more unstable [121]. Instability is subsequently due to membrane phospholipids being released, which leads to an increase in permeability and lysis through small lesions [118, 121]. Our group demonstrated multiple small associated vesicles that trails the GS affected erythrocyte, a result that substantiates the curvature stress hypotheses [122]. The susceptibility of prokaryotic, rather than eukaryotic organisms to GS is due the presence of cholesterol in eukaryotic membranes which attenuates but does not abolish the interactions of GS with phospholipids bilayer membranes [123].

Apart from the primary membrane target GS also has several other possible targets, such as certain proteins embedded in the cytoplasmic membrane that are involved in ion transport and respiratory processes of the producer organism [74]. Since GS inhibits the active

transport of [^{3}H]-alanine and [^{3}H]-uridine across membranes, these effects are proposed to be mediated by hydrophobic and hydrophilic interactions with the cytoplasmic membrane [74]. GS was also determined to cause inhibition of the *in vitro* DNA transcription by forming a complex with *A. migulanus* DNA [16]. However, no inhibition was recorded during growth and sporulation of the producer by the antibiotic *in vitro* [16]. It was suggested that GS may not affect sporulation directly, but play an inhibitory role in DNA transcription during germination and outgrowth [16, 124, 125]. According to Bentzen and Demain [126], GS causes delay in germination outgrowth of its producer strain either by killing cells or decreasing their metabolism.

Tyrocidines

The mode of action of the Trcs upon membrane disruption has not yet been fully elucidated although they were one of the first membrane active agents discovered [127, 128]. However, they are known to act on both membranes and intracellular targets, with a more pronounced activity against Gram-positive targets [128]. Both lytic activity and an influence on intracellular processes, such as the inhibition of certain enzymes and DNA transcription in its producer have been proposed [62, 63, 82]. Studies of the kinetics of TrcB on phospholipid bilayers have shown that the peptide absorbs into the bilayer prior to act through bimolecular transmembrane structures [129]. On the membrane, Trcs are proposed to act as ion-carriers for monovalent cations such as Na^+ and K^+ [130]. The ion kinetic rates of TrcB increase in the order $K^+ < Na^+ < NH_4^+$ [131]. Studies by Spathelf [132]

indicated the divalents ions, in particular Ca^{2+}, may be an important mediator in the activity of the Trcs.

Cyclic Trcs can interact with different lipid membrane systems since they have the ability to perturb the gel state of these membranes [115]. A lower gel to liquid-crystalline transition temperature was induced by interaction of the peptide with dielaidoylphosphatidylethanolamine model membranes, with a maximum decrease for phosphatidylcholines [115]. The interaction of the peptide was stronger with phosphatidylcholine acyl chains, showing a strong fluidizing effect on these chains [115]. Furthermore, cyclic tyrocidines were shown to reverse the H_{II} phase transition promoted by linear gramicidins [115].

The antibacterial and antifungal activities of Trcs have also been described. Trcs are active against Neurospora *in vitro* [133]. It has been reported that the peptide interacts primarily with the Neurospora cell membrane, causing membrane damage and ion release [133].

Trcs also exhibit inhibitory effects not related to its lytic activity. According to Changeux *et al.* [134], the peptide inhibits acetylcholinesterase from the electroplax membrane causing the enzyme to form aggregates through interaction with it. The antibiotic-enzyme complex may cause structural modification of the enzyme, which could be responsible for the reduction of the accessibility of the enzymes catalytic site to its substrate [134]. Trcs were also found to inhibit yeast hexokinase activity responsible for the anaerobic fermentation and respiration of the organism at very low concentrations. Furthermore, an inhibition of anaerobic glycolysis of tumor slices in mice by the peptide (at high concentrations) was

also reported in the same study [135]. According to Rautenbach *et al.* [54], naturally occurring TrcA have a highly selective non-lytic activity on the erythrocytic stages *P. falciparum,* halting the parasite in the trophozoite stage.

Results of several studies have also suggested the extension of the biological activity of Trcs to the producer organism, *B. aneurinolyticus,* as gene regulator during sporogenesis [62, 63, 82]. Trcs were determined to bind by interchelation onto the G+C rich region of DNA causing an inhibition of the transcription of the double-stranded DNA [63]. According to Bohg and Ristow [82], under conditions of saturation one Trc molecule interacts within ten base pairs, with a preference for G+C base pairs. At low Trc:DNA ratios, Trcs induce changes in the super-helical secondary structure of plasmids by reducing the number of their β-helical turns, which causes relaxation of plasmids [62]. Grcs weaken this complex by reducing the Trc:DNA dissociation energy [116].

Surfactins

The biosurfactant peptide Srf possesses both membrane targets and some non-membrane targets. The primary step in Srf's mechanism of membrane disturbance is the insertion of the peptide into the lipid bilayers [136]. This action depends on the nature of the phospholipid bilayers since penetration is better in the case of phospholipids, such as myristoyl acyl containing phospholipids, with hydrocarbon chains of similar lengths as its fatty acid tail (which contains about 13 to 16 carbon atoms). Srf spontaneously interacts with the lipid membrane by means of hydrophobic interactions [137]. Electrostatic interactions and increased phospholipid acyl chain length reduce the penetration of Srf,

whereas the presence of bivalent ions such as Ca^{2+}, which neutralize the charge of the peptide, leads to changes in the penetration process [137]. Srf aligns itself so that its fatty acid tail interacts with the phospholipids and faces toward the phospholipid acyl chains and its ring alongside the phospholipid head groups. Once inserted into the membrane, Srf molecules aggregate and cause the formation of pores that break down the underlying structure of the lipid bilayer [136]. According to Heerklotz *et al.* [138] Srf tilts the acyl chain of lipid membranes and causes the lipid head groups to re-orientate towards the membrane interior upon insertion of the peptide deep inside the hydrophobic-hydrophilic interface of the membrane. Because Srf forms an inverted cone-like structure, the Srf aggregates lead to a positive curvature in the membrane, which is responsible for the destabilisation of the lipid bilayer [138]. The incorporation of the peptide is accompanied by a strong dehydration of the phospholipid carbonyl groups, which is caused by a decrease in the hydrogen bonding of water to these group [139]. The decrease in hydrogen bonding with water reduces the water penetration into the polar head groups of the membrane and causes vesicle/membrane fusion [139]. These effects, combined with the interaction of surfactin with phospholipid acyl chains explain the destabilisation of lipid packing by the lipopeptide and the loss of vesicular content that is observed [139]. The prevalence of hydrophobic residues also facilitates the insertion of Srf into the membrane [138]. The Srf-active properties of Srf increase with the length of the aliphatic chain of Srf, which is crucial in penetration ability [95]. Cholesterol and palmitoyloleylphosphatidylcholine (POPC) modify the membrane curvature and thus reduce the effects of Srf, presumably by counteracting its inverted cone shape that is responsible for the introduction of curvature stress in the lipid bilayer [139].

Srf and iturin A, another co-produced lipopeptide in some *B. subtilis* strains, were shown to have synergistic antifungal and antibacterial activity [84-86]. Furthermore, it has been demonstrated that Srf and iturin A can absorb to the *B. subtilis* surface and modify its hydrophobicity [87]. Once secreted by its producer, Srf readily absorbs to the bacterium surface and may increase or decrease its hydrophobicity (depending to the *B. subtilis* strain). With hydrophobic strains the absorption will result in a decrease in hydrophobicity and with hydrophilic strains there will be an increase in hydrophobicity [87]. The increase in *B. subtilis* surface hydrophobicity by Srf has been determined to enhance the motility and chemotaxis system of the bacterium during nutritional depravation to search for nutrients [8, 10, 140]. Swarming motility is only possible in an undomesticated *B. subtilis* strain capable of producing Srf [10]. This can only occur with a minimum potassium ion concentration, since K^+ stimulates Srf production [140]. Motility appears to be a crucial stage before the differentiation of bacteria into complex structures such as biofilm [141] and it has been shown that Srf encourage the formation of biofilm in *B. subtilis* strains [5, 142].

Srf also has antiviral activity, and several studies have been conducted to investigate the mechanism by which it inactivates enveloped viruses [91]. Interaction of the lipopeptide with a virus lipid membrane appears to be the mode of action by which Srf neutralise viruses [91]. Ion leakage occurs at high Srf concentrations (higher than 50 μM which is well above its critical micellular concentration of about 7 μM) by a complete disintegration of the envelope and the capsid of the virus particles, probably as a consequence of the detergent-like effect of Srf [91].

Biosynthesis

All the antimicrobial peptides described here are secondary metabolites that are synthesised non-ribosomally on multifunctional enzyme complexes during periods of nutritional depletion or environmental stress [21, 143]. This synthesis is not sensitive to protein synthesis inhibitors, it can occur in particle-free RNAase-treated bacterial extracts [144] and is not restricted to the 20 natural occurring amino acids [145]. Unnatural amino acids (D-amino acids, L-α-amino butyric acid, hydroxy-amino acids and, D- and N-methylated amino acids) and other groups such as fatty acid moieties can also be included in these Amp structures [145].

The synthesis of non-ribosomal peptides takes place on multiple-carrier thioesterase templates through a series of ordered and arranged processes facilitated by each module [145, 146]. Each peptide synthetase can contain four to six modules capable of recognizing, activating, modifying and adding a residue to the growing peptide chain [21, 147]. Each module has a specialised function in the non-ribosomal peptide synthetases (NRPSs) and is responsible for the incorporation of a single amino acid to the peptide chain [145, 148]. Modules comprise enzymatic units, called domains, that catalyse amino acid activation, binds covalently to the activated amino acid substrate and facilitates peptide bond formation [145]. Related amino or carboxy acid substrate are activated to aminoacyl adenylate on the adenylation domain (A-domain) of NRPSs using ATP [145, 149]. A peptidyl carrier protein (PCP-domain) then transfers the activated substrate to the condensation domain, which helps in elongating the peptide chain by catalysing the

condensation of the thioester-bound intermediates [145, 149]. The termination of the synthesis is catalysed by the thioesterase-domain, the terminal enzyme of the last module which can achieve the incorporation of groups such as N-terminal β-hydroxy fatty acyls (Srf and iturins) or the formation of cyclic structures (Trcs and GS) to the peptide [145]. Secondary modifications such as acylation, glycosylation and methylation (to form linear Grcs) may follow this process [21].

Linear gramicidins

Grcs are produced by a nonribosomal multi-enzyme thiotemplate mechanism. Kessler *et al.* [149] studied and characterised the new reductase domain of the linear Grcs biosynthetic genes cluster through cloning, sequencing and biochemical analysis using a DNA locus of *B. aneurinolyticus* ATCC 8185. They identified four genes; *lgrA, lgrB, lgrC* and *lgrD* (with the respective molecular masses of 6.8 kbps, 15.5 kbps, 23.3 kbps and 15.3 kbps) coding for the NRPSs (LgrA, LgrB, LgrC and LgrD respectively) having two, four, six and four modules, respectively [149]. There are seven epimeration domains, which alternate in position within the 16 modules: a formylation domain linked to the first module LgrA and a reductase domain attached to the C-terminal module LgrD [149]. The 16 modules catalyse the biosynthesis of a 16 amino acid peptide, which comprises a C-terminal N-formylated glycine residue bound to PCP-domain of module 16 via a thioester bond to its carboxyl group [149, 150]. This glycine terminal attached to the PCP-domain is then reduced to the corresponding aldehyde intermediate by an adjacent reductase through a process that is dependent on NAD(P)H [149, 150]. A second reductase, the aldoreductase LgrE, catalyses

the NADPH-dependent reduction of the aldehyde intermediate to an alcohol releasing the N-formyl-pentadecapeptide-ethanolamine product [149, 150]. LgrE is an aldo/keto reductase family protein encoded by an open reading frame (ORF) of 1692 base pairs upstream of *lgrA* responsible of post-NRPS assembly steps of Grc synthesis [149, 150].

Gramicidin S

The synthesis of GS is catalysed by two enzymes, gramicidin synthetase 1 (G1) and gramicidin synthetase 2 (G2) that form a multifunctional enzyme complex [4] (Figure 1.5]. The DNA sequence of the GS biosynthetic operon (*grs*) contains three ORFs corresponding to the genes *grsA, grsB* and *grsT,* organised in one transcriptional unit [151]. The *grsA* structural gene is located 3 kb from the 5' end of *grsB* and both genes are transcribed in opposite directions [152]. The genes *grsA* and *grsB* encode for G1 (126.661 Da) and G2, each containing one and four modules respectively [152, 153].

G2, the C-terminal domain of each reaction centre, has an active serine involved in covalent binding to the substrate amino acids [153]. The peptide chain is formed via the multiple peripheral 4'-phosphopantetheine carrier attached to an active serine at the reaction centres in GS synthesis [153] . First, a Phe residue is activated and racemised to D-Phe in G1, where after it is transferred to G2 which catalyses the elongation of the additional four amino acids (Pro, Val, Orn and Leu) forming a pentapeptide.

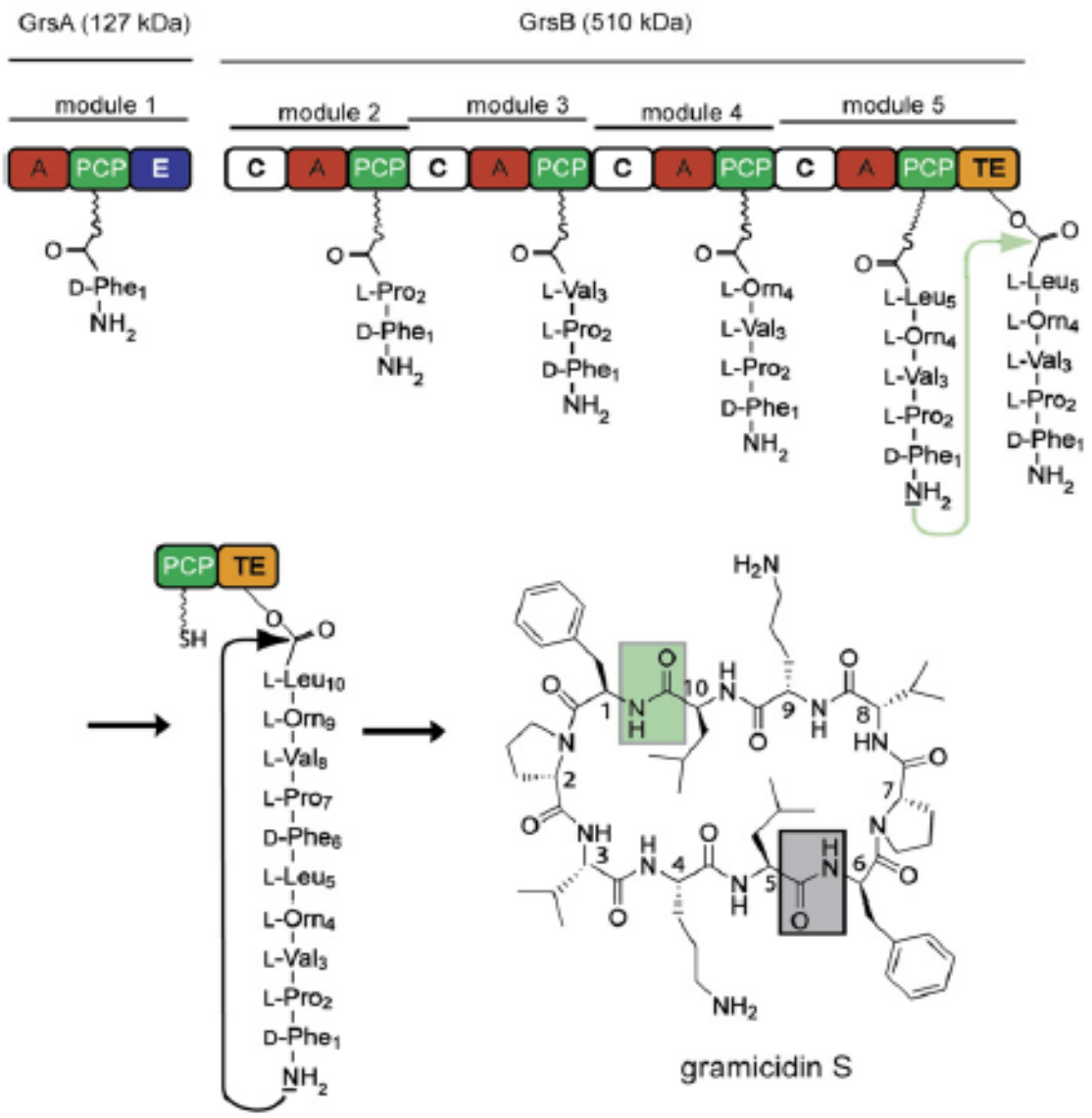

Figure 1.5. Schematic representation of the biosynthetic machinery, consisting of two NRPSs, G1 (module 1) and G2 (modules 2-5), responsible for the enzymatic assembly of GS. Abbreviations for the different domains: A, adenylation; PCP, peptidyl carrier protein; E, epimerisation; C, condensation; TE, thioesterase ([154]).

Two assembled pentapeptides are dimerised on the thioesterase domain of G2 (TE domain) which subsequently catalyses the cyclisation of the decapeptide, resulting in the cyclic GS (Figure 1.5) [155]. A 4'-phosphopantetheine moiety participates in the growing of the

peptide chain as a carrier in the enzyme complex [153]. In *A. migulanus* strains, the amino acid L-Orn is formed from arginine by a highly specific enzyme, namely arginase [17]. GS production is accelerated by an increase in L-Orn formation by arginase [17].

Tyrocidines

The synthesis of the Trcs are similar to the GS synthesis [149, 154]. The entire Trc biosynthesis operon (39.5 kb) containing the genes *tycA, tycB* and *tycC* of the DNA locus of *B. aneurinolyticus* ATCC 8185, has been cloned and sequenced by Mootz *et al.* [148] (Figure 1.6). It encodes three multifunctional Trc synthetases TycA, TycB and TycC (also called TY1, TY2 and TY3 by certain authors, [154]) that consist of one, three and six modules, respectively [148]. The first gene *tycA* encodes for only one module with a 123kDa gene product, TycA. Downstream of this gene are two large ORFs that are transcribed in the same direction. The first ORF *tycB* (735 bp) encodes for 404. 6 kDa gene product, TycB consisting of three modules, each containing a putative condensation domain, an adenylation domain and a thiolation domain [148]. The C-terminal end of the last module of TycB contains the epimerization domain [148]. The second ORF, *tycC* (19461 bp) encodes for a 723.6 kDa gene product TycC containing six modules [148]. The C-terminal end of the sixth module contains a putative thioesterase domain [148]. It catalyses the incorporation six amino acids Asn, Gln, Tyr, Val, Orn and Leu into the peptide product, taking TrcA as the reference peptide of the Trc fraction of tyrothricin (Figure 1.6).

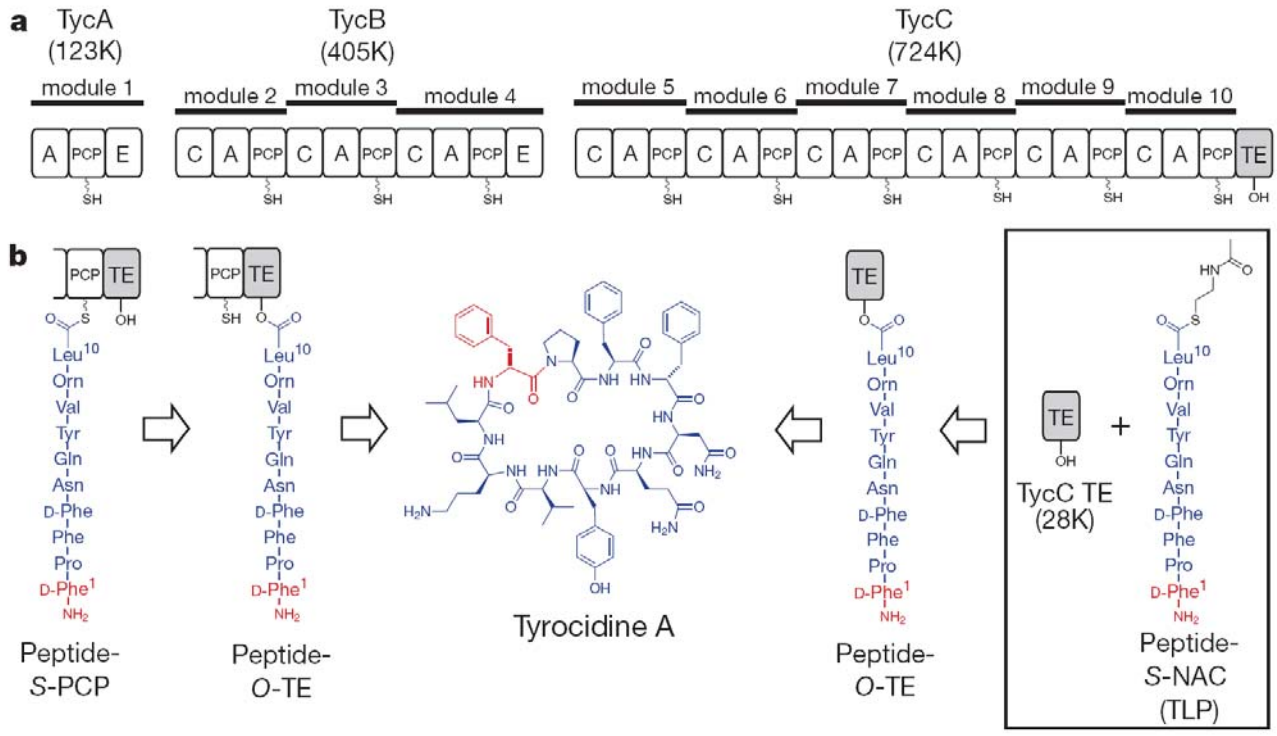

Figure 1.6. Schematic representation of the Trc biosynthetic machinery, consisting of two NRPSs, TycA (module 1), TycB (modules 2-4) and TycC (modules 5-10), responsible for the enzymatic assembly of Trcs. The linear N-acetylcysteamine (S-NAC) TrcA derivative in the box represents a synthetic precursor the can be cyclisized using TycC-TE. Abbreviations for the different domains: A, adenylation; PCP, peptidyl carrier protein; E, epimerisation; C, condensation; TE, thioesterase ([154]).

The sequence comparison of the gene product of the Trc biosynthesis operon shows high sequence similarity between the modules of the Trc synthetases with each other (34% to 60% identity) and the GS synthetases (adenylation domains of TycB and TycC with G2 have between 63% to 68% identity) [148]. Since GS shares the sequence unit Val-Orn-Leu-D-Phe-Pro with the Trc fraction of tyrothricin similarities in modules between GS and Trc synthetases also occur [148]. The Trc synthetase may have evolved by insertion of the five modules from the GS synthetases since the last two domains of TycB and the first three

domains of TycC correspond to G1 and G2 (consisting of five modules each) [148]. However, the *tyc* operon has a higher G+C content compared to the *grs* operon (45% compared 36%, respectively).

Mootz and Marahiel [148] detected three additional ORFs, *tycD, tycE* and *tycF*, downstream of the *tyc* gene which encode for the gene products tycD, TycE and TycF (66 kDa, 64 kDa and 28 kDa, respectively) [148]. TycD and TycE show good similarities to members of the ABC transporter family since they present six trans-membranes helices in their N-terminal part and the ATP-binding cassette at their C-terminal [148]. These transporters may be involved in conferring resistance against Trcs in its producer and the gene product TycF may be a putative thioesterase [148].

Surfactins

The NRPS mechanism of Srf synthesis differs from that of the three described above in that all amino acids are activated by an ATP-P_i exchange reaction during the biosynthesis [4]. Four enzymes E1A, E1B, E2 and E3 form the Srf multi-enzyme template system. These enzymes are encoded in the *srfA* operon of *B. subtilis* and catalyse the incorporation of the substrate amino acids of the Srfs. The first and second ORFs of *srfA*, *srfAA* and *srfAB* encode for the NRPS E1A and E1B which are composed of three domains each [156]. E1A is responsible for the incorporation of the residues Glu^1, Leu^2 and D-Leu^3 while E1B incorporates the residues Val^4, Asp^5 and D-Leu^6. The third ORF of *srfAC* encodes for the NRPS E2, which is responsible for the incorporation of Leu^7 into the peptide sequence [156]. Another ORF within the *srfA* operon, *srfAD*, encodes for an acyltransferase E3

which catalyses the binding and transfer of the β-hydroxy fatty acid substrate to E1A thus initiating the synthesis of the Srfs [156]. Figure 1.7 gives a schematic representation of the biosynthetic machinery of assembly line of Srf_3 (also referred as SrfA [157]); E1A (SrfA-A), E1B (SrfA-B) composed of three modules each and E2 (SrfA-C) composed of one module [157].

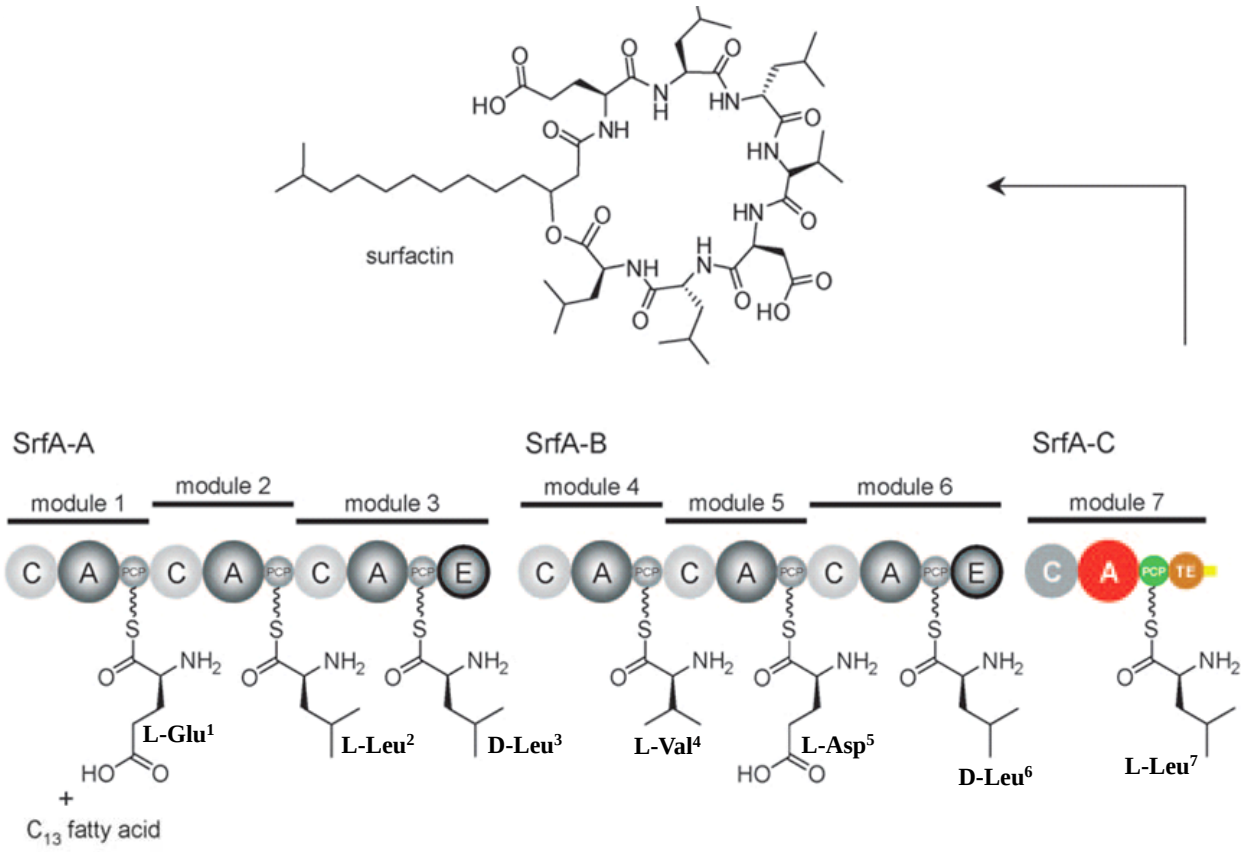

Figure 1.7. Schematic representation of the biosynthetic machinery of assembly line of Srf_3 taken as the reference Srf from *Bacillus subtilis* ([157]). The building blocks incorporated by each module are indicated (three modules for both SrfA-A and SrfA-B; one for SrfA-C). Abbreviations for the different domains: A, adenylation; E, epimerisation; C, condensation; TE, thioesterase. Amino acids are denoted by the three letters abbreviation.

Vollenbroich *et al.* [156] proposed that the Srf synthesis takes place as follows: the acyltransferase E3 first transfers the hydroxy fatty acid moiety to E1A to form hydroxy fatty acylglutamate. Thus E3, which functions as a thioesterase/acyltransferase, initiates Srf formation by transferring the β-hydroxy fatty acid from β-hydroxymyristoyl-coenzyme A to E1A to form the β-hydroxymyristoyl-glutamate [158]. E1A then elongates the peptide to a lipotripeptide, which is transferred to E1B [156]. E1B adds the three amino acids Val^4, Asp^5 and D-Leu^6 to the lipotripeptide to form a lipohexapeptide that is transferred to E2 [156]. E2 catalyses the incorporation of the last amino acid, Leu^7, into the lipopeptide [156]. The mechanism of cyclisation of the lipopeptide chain by lactone bond formation between Leu^7 and the hydroxyl group of the hydroxy fatty acid is unknown [156].

Antimicrobial resistance

The first site of action of Amps including *Bacillus* peptides, to kill microbial targets, is to reach their cytoplasmic membranes [159, 160] generally through electrostatic interactions (reviewed in [161, 162]). Amps are able to distinguish between microbial targets and normal host cells because of the differences in their membrane composition, hydrophobicity, charge, asymmetry and affinity [161, 163]. Once reaching the cytoplasmic membrane, they generally act upon it (reviewed in [161]) or pass through to reach interior targets [164]. Although Amps have diverse structures and sizes, most Amps are small and share an amphiphilic membrane active character, they are more effective in killing and present little or no resistance as compared to classical antibiotics (reviewed in [162, 163]). However, general mechanisms of resistance could be adapted to render resistance to Amps.

These resistance mechanisms can be regrouped into four general mechanisms; i) modification of the target; ii) protection or masking of target; iii) modification or destruction of Amp/antibiotic and iv) modification or transport of Amp/antibiotic.

The first mode of antibiotic resistance includes target modification, namely cell surface modification to avoid binding [159, 165, 166], use of alternative pathways to pass by the step inhibited by Amp or increase in target metabolite production [166], modification of Amps targets through ribosomal mutations [166]. Here the focus is more on the mechanisms that result in cell surface alteration, which could lead to Amp resistance. The peptidoglycan and teichoic acids in the outer membrane and the cytoplasmic membrane of several microorganisms have a net negative charge.

Mutants of *Staphylococcus aureus* resist Amps defensin hNP-1, protegrin, thrombocidin and gallidermin by modifying their teichoic acid through esterification by adding D-alanine resulting in a decrease in negative charges of the cell wall [167]. D-alanisation of the teichoic acid is encoded by the *dlt* operon [168-170]. According to Shi *et al.* [171], Amp resistance in *Salmonella* is controlled by PhoP-PhoQ regulatory system that regulate the remodelling of the cell surface. This remodelling confer cell resistance to magainin 2 and polymycin B by modification of lipid A in the lipopolysaccharide and adding more positive charges to the membrane [171-174]. The biosynthesis of lipid A is activated by the TmrA-PmrB also controlled by PhoP-PhoQ regulatory system [175] and at low Mg^{2+} concentrations [176].

Thedieck *et al.* [177], reported that resistance to β-defensin in *Listeria* is modulated by *lmo* gene which encode for a membrane protein homologue to multi-peptide resistance factor (MprF). MprF causes membrane secretion of lysylphophatridylglycerol and lysinylation making the membrane more positive thus less susceptible to Amps cathelicidin LL-37 and defensin hNP-1 [177-179]. Starvation and stationary phase can also trigger resistance to polymyxin B by reducing membrane permeabilization [180]. This is due to independent pathways induced by *rpoS* and *phoP* genes in *Salmonella typhimurin* [180].

A second mode of resistance is the shielding or masking the target such as the formation of protective biofilms. Genes such as *rpoS* are involved in stress response induced in biofilm formation [181]. The development of biofilms involve cell-to-cell signalling [182]. Biofilms are composed of aggregates of slow growing bacteria constituting a barrier that stops or limits Amp penetration [141, 183]. Biofilm formation has not only been proven to enhance the impact of *B. subtilis* as bio-control agent in the plant root [184], but also its resistance towards antimicrobial agents [12, 141, 185]. It has been shown that the secretion of Srf also encourages the formation of biofilm in *B. subtilis* strains [5, 142]. However, studies have also shown that Srf can inhibit biofilm formation of the wild type *Salmonella enterica in vitro* causing an inhibition of the swarming motility of the organism [186]. Srf and iturin A absorb to the *B. subtilis* surface and cause a change in hydrophobicity [87, 187] which can lead to cell attachment and aggregation. The absorbed Srf can also shield the membrane target of Amp and because of its own negative charge trap Amp, conferring resistance. This aspect of shielding and antagonistic action toward Amp activity will be addressed in this study (refer to Chapters 2, 3 and 5)

The third mode includes mechanisms that involve the destruction/deactivation of antibiotics through enzyme hydrolysis, group transfer or redox mechanism [188]. The most important mechanism of bacteria to resist β-lactam antibiotics such as penicillin and cephalosporin is the production of hydrolysing enzymes, the β-lactamases which is particularly prevalent in Gram-negative bacilli, (reviewed in [189]). These enzymes deactivate β-lactam antibiotics through the hydrolysis of the β-lactam ring resulting in an opened ring (reviewed in [84, 189]). Aminoglycosides are deactivated by aminoglycoside resistance enzymes that add a substituent onto the antibiotic and stop it from interacting with its RNA target (reviewed in [84]). There are several types of aminoglycoside resistance enzymes that can add groups such as AMP by adenylyl transferases, phosphate groups by phosphoryl transferase or acetyl amino acid groups by acetyl transferases (reviewed in [84]). Although this enzymatic modification or hydrolysis of antibiotics is the most prevalent resistance mechanism, no evidence of Amp resistance by direct modification or hydrolysis has been reported.

The fourth mode of resistance relies on the modification of the transport of the antibiotic to its target. The chloroamphenicol resistance in Gram-negative bacteria, causing numerous resistant hospital infections, is due to the loss of porins through which chloroamphinicol gained entry, from the cell wall [190]. A prevalent transport-based resistance mechanism to small amphipathic antibiotics is the non-specific plasma membrane multi-drug resistance efflux pump (MDR-pumps) to expulse the antibiotic, including some Amps [159, 166, 191, 192]. It has been reported that some Amps may have alternative intracellular targets [193] and therefore interrupted transport may lessen the effect of the Amp. A multidrug efflux mechanism composed of MtrC-MtrD-MtrE protein confer Amp resistance to polymyxin B,

cathelicin LL-37 and PG-1 in *Menigococci* [194]. MtrC-MtrD-MtrE protein is encoded by the mtrCDE operon [195]. According to Bengoechea [196], *Yersinia* resistance to polymyxin B is achieved by an efflux pumps/K^+ antiport system composed of RosA and RosB proteins and activated by temperature shift and the presence of Amp.

In certain *B. subtilis* strains, the exposure to various Amps can activate a stress response system involving three peptide sensing and detoxification (PSD) modules such as BceRS-AB (PSD1), YxdJK-LM (PSD2) and PsdRS-AB (PSD3) [197]. Each PDS consist of a two components system (TCS) linked to an ABC transporter (TCS-ABC system). These TCS can detect the presence of undesired Amp and induce the expression of the ABC transporter, which in turn remove it from its site of action [197]. The first PSD, BceRS-AB, confers resistance to bactracin; YxdJK-LM determines resistance to human Amps such as LL-37 while PsdRS-AB gives resistance to cationic lantibiotics, namely, nisin, subtilin and gallidermin [197].

Problem identification

Our research group have shown that antagonism between bacterially produced antimicrobial peptides similar to the antagonism of vacomycin by penicillin [198], may affect the soil microbial ecosystems. This occurred between two Amps from cohabiting bacteria, namely GS from *A. migulanus* and Srf from *B. subtilis*. Vlok [88] showed that GS and Srf antagonise each other's activity, causing the loss of antimicrobial activity. This antagonism appeared to be target specific. With regard to non–producer Gram-positive targets, a degree of synergism was observed between the two peptides at low Srf

concentration, while antagonism only occurred above the "critical" Srf concentration [88]. Electrospray mass spectrometry of a mixture of the two peptide indicated that Srf interacts with GS in a 1:1 and 2:1 ratio forming stable inactive complexes [88]. These complexes were not influenced by the presence of alkali or earth metal ions or organics solvent [88]. It has been hypothesised that similar antagonistic behaviour may also occur among other peptides from the *B. aneurinolyticus* such as the Trcs and linear Grcs. Therefore, this study aims to elucidate the influence of Srf from *B. subtilis* on different peptides from the soil bacteria, *B. aneurinolyticus* and *A. migulanus* to establish if Srf antagonism of Amp activity leads to improved survival and to clarify its underlying molecular mechanism and specificity.

References

1 Kloepper, J. W., Lifshitz, R. and Zablotowicz, M. (1989) Freeliving bacterial inocula for enhancing crop productivity. Trends Biotechnol. **7**, 39-44

2 Katz, E. and Demain, A. L. (1977) The peptide antibiotics of *Bacillus*: Chemistry, biogenesis, and possible functions. Bacteriol. Rev. **41**, 449-474

3 Marahiel, M. A., Nakano, M. M. and Zuber, P. (1993) Regulation of peptide antibiotic production in *Bacillus*. Mol. Microbiol. **7**, 631-636

4 Mannanov, R. N. and Sattarova, R. K. (2001) Antibiotics produced by *Bacillus* bacteria. Chem. Nat. Compd. **37**, 117-123

5 Stein, T. (2005) *Bacillus subtilis* antibiotics: structures, syntheses and specific functions. Mol. Microbiol. **56**, 845-857

6 Schallmey, M., Singh, A. and Ward, O. P. (2004) Developments in the use of *Bacillus* species for industrial production. J. Microbiol. **50**, 1-17

7 Montesinos, E. (2007) Antimicrobial peptides and plant disease control. FEMS Microbiol. Lett. **270**, 1–11

8 Hamoen, L. W., Venema, G. and Kuipers, O. P. (2003) Controlling competence in *Bacillus subtilis*: shared use of regulators. Microbiology. **149**, 9-17

9 Hamon, M. A. and Lazazzera, B. A. (2001) The sporulation transcription factor Spo0A is required for biofilm development in *Bacillus subtilis*. Mol. Microbiol. **42**, 1199-1209

10 Kearns, D. B. and Losick, R. (2003) Swarming motility in undomesticated *Bacillus subtilis*. Mol. Microbiol. **49**, 581-590

11 Yount, N. Y. and Yeaman, M. R. (2005) Immunocontinuum: Perspectives in antimicrobial peptides mechanism of action and resistance. Protein Pept. Lett. **12**, 49-67

12 O'Connell, H. A., Koltkamp, G. S., Eppelbaum, J. L., Stubblefield, B. A., Gilbert, S. E. and Gilbert, E. S. (2006) Influence of biofilm structure and antibiotic resistance mechanisms on indirect pathogenicity in a model polymicrobial biofilm. Appl. Environ. Microbiol. **72**, 5013-5019

13 Marikawa, M. (2006) Beneficial biofilm formation by industrial bacteria *Bacillus subtilis* and related species. J. Biosci. Bioeng. **101**, 1-8

14 Shida, O., Takagi, H., Kadowaki, K. and Komagata, K. (1996) Proposal for two new genera, Brevibacillus gen. nov. and Aneurinibacillus gen. nov. Int. J. Syst. Bacteriol. **48**, 939-946

15 OKuda, K., Edwards, G. C. and Winnick, T. (1963) Biosynthesis of gramicidin and tyrocidine in the Dubos strain of *Bacillus brevis*. J. Bacteriol. **85**, 329-338

16 Frangou-Lazaridis, M. and Seddon, B. (1985) Effect of gramicidin S on the transcription system of the producer *Bacillus brevis* Nagano. J. Gen. Microbiol. **131**, 437-449

17 Kanda, M., Ohgishi, K., Hanawa, T. and Saito, Y. (1997) Arginase of bacillus brevis nagano: purification, properties, and implication in gramicidin S biosynthesis. Arch. Biochem. Biophys. **344**, 37-42

18 Tang, X.-J., Thibault, P. and Boyd, R. K. (1992) Characterisation of the tyrocidine and gramicidin fractions of the tyrothricin complex from *Bacillus brevis* using liquid chromatography and mass spectrometry. Int. J. Mass Spectrom. Ion Processes. **122**, 153-179

19 Arima, K., Kakinuma, A. and Tamura, G. (1968) Surfactin, a crystalline peptide lipid surfactant produced by *Bacillus subtilis*: isolation, characterization and its inhibition of fibrin clot formation. Biochem. Biophys. Res. commun. **31**, 488-494

20 Sandrin, C., Peypoux, F. and Michel, G. (1990) Coproduction of surfactin and iturin A, lipopeptides with surfactant and antifungal properties, by *Bacillus subtilis*. Biotechnol. Appl. Biochem. **12**, 370-375

21 Hancock, R. E. W. and Chapple, D. S. (1999) Peptide antibiotics. Antimicrob. Agents Chemother. **43**, 1317-1323

22 Chitta, R., K and Gross, M. L. (2004) Electrospray ionisation-mass spectrometry and tandem mass spectrometry reveal self-association and metal-ion binding of hydrophobic peptides: A study of the gramicidin dimer. Biophys. J. **86**, 473-479

23 Orwa, J. A., Govaets, C., Roets, E., Van Schepdael, A. and Hoogmartens, J. (2001) Liquid chromatography of gramicidin. Chromatography. **53**, 17-21

24 Wallace, B. A. (1986) Structure of gramicidin A. Biophys. J. **49**, 295-306

25 Arsen'ev, A. S., Lomize, A. L., Barsukov, I. L. and Bystrov, V. F. (1986) Gramicidin A transmembrane ion channel. Three-dimensional structure reconstruction based on NMR spectroscopy and energy refinement. Biol. Membr. **3**, 1077-1104

26 Arseniev, A. S., Barsukov, I. L., Bystrov, V. F., Lomize, A. L. and Ovchinnikov, Y. A. (1985) 1H-NMR study of gramicidin A transmembrane ion channel: Head-to-head right-handed, single-stranded helices. FEBS Lett. **186**, 168-174

27 Ketchem, R. R., Hu, W. and Cross, T. A. (1993) High-resolution of gramicidin A in a lipid bilayer by solid state NMR. Science. **261**, 1457-1460

28 Mattice, G. L., Koeppe, R. E., Providence, L. L. and Andersen, O. S. (1995) Stabilizing effect of D-alamine-2 in gramicidin channel. Biochemistry. **34**, 6827-6837

29 Koeppe, R. E. and Andersen, O. S. (1996) Engineering the gramicidin channel. Ann. Rev. Biophys. Biomol. Struct. **25**, 231-258

30 Roux, B., Brueschweiler, R. and Ernst, R. R. (1990) The structure of gramicidin A in dimethylsulfoxide/acetone. Eur. J. Biochem. **194**, 57-60

31 Arseniev, A. S., Lomize, A. L., Barsukov, I. L. and Bystrov, V. F. (1986) Gramicidin A transmembrane ion channel. Three-dimensional structure reconstruction based on NMR spectroscopy and energy refinement. Biol. Membr. **3**, 1077-1104

32 Cox, K. J., Ho, C., Lombardi, J. V. and Studds, C. D. (1992) Gramicidin conformational studies with mixed-chain unsaturated phospholipid bilayer systems. Biochemistry. **31**, 1112-1117

33 Glowka, M. L., Olczak, A., Bojarska, J., Szczesio, M., Duax, W. L., Burhart, B. M., Pangborn, W. A., Langs, D. A. and Wawrzak, Z. (2005) Structure of gramicidin D-

RbCl complex at atomic resolution from low-temperature synchroton data: Interactions of double-stranded gramicidin channel contents and cations with channel wall. Acta Cryst. **D61**, 433-441

34 Townsley, L. E., Tucker, A. W., Sham, S. and Hinton, J. F. (2001) Structures of gramicidins A, B, and C incorporated into sodium dodecyl sulfate micelles. Biochemistry. **40**, 11676-11686

35 Kriegger, E., Koraimann, G. and Vriend, G. (2002) Increasing the prescision of comparative models with YASSARA NOVA: A self parameterizing force field. Proteins. **47**, 393-402

36 Hooft, R. W. W., Vriend, G. and Abola, E. E. (1996) Errors in protein structures. Nature. **381**, 272

37 Mihailescou, D. and Smith, J. C. (1999) Molecular dynamics simulation of the cyclic decapeptide antiotic, gramicidin S, in dimetyl sulfoxide solution. J. Phys. Chem. B. **9**, 1586-1594

38 Grotenbreg, G. M., Timmer, M. S. M., Llamas-Saiz, A. L., Verdoes, M., Van der Marel, G. A., Va Raaij, M. J., Overkleeft, H. S. and Overhand, M. (2004) An unusual reverse turn structure adopted by a furanoid sugar acid incorporated in gramicidin S. J. Am. Chem. Soc. **126**, 3444-3446

39 Mihailescou, D. and Smith, J. C. (2000) Atomic detail peptide-membrane interactions: Molecular dynamics simulation of gramicidin S in a DMPC bilayer. Biophys. J. **79**, 1718-1730

40 Kawai, M., Yamamura, H., Tanaka, R., Umemoto, H., Ohmizo, C., Higuchi, S. and Katsu, T. (2005) Proline residue-modified polycationic analogs of gramicidin S with high antibacterial activity against both Gram-positive and Gram-negative bacteria and low hemolytic activity. J. Pept. Res. **65**, 98-104

41 Prenner, E. J., Lewis, R. N. A. H. and McElhaney, R. N. (1999) The interaction of the antimicrobial peptide gramicidin S with lipid bilayer model and biological membranes. Biochem. Biophy. Acta. **1462**, 201-221

42 Masunov, A. (2001) ACD/I-Lab 4.5: An Internet Service Review. J. Chem. Inf. Comput. Sci. **41**, 1093-1095

43 Spessard, G. O. (1998) ACD Labs/LogP dB 3.5 and ChemSketch 3.5. J. Chem. Inf. Comput. Sci. **38**, 1-4

44 Qin, C., Zhong, X., Bu, X., joyce Ng, N. L. and Guo, Z. (2003) Dissociation of antibacterial and hemolytic activity of amphipathic peptide antibiotic. J. Med. Chem. **46**, 4830-4833

45 Bonmatin, J. M., Laprevote, O. and Peypoux, F. (2003) Diversity among microbial cyclic lipopeptides: iturins and surfactins. Activity-structure relationships to design new bioactive agents. Comb. Chem. High Throughput Screening. **6**, 541-556

46 Gallet, X., Deleu, M., Razafindralambo, H., Jacques, P., Thomart, P., Paquot, M. and Brasseur, R. (1999) Computer simulation of surfactin conformation at a hydrophobic/hydrophilic interface. Langmuir. **15**, 2409-2414

47 Bonmatin, J. M., Genest, M., Labbe, H. and Ptak, M. (1994) Solution three dimensional structure of surfactin: A cyclic lipopeptide studies by 1H-NMR, distance geometry, and molecular dynamics. Biopolymers. **34**, 975-986

48 Tsan, P., Volpon, L., Besson, F. and Lancelin, J. M. (2007) Structure and dynamics of surfactin studied by NMR in micellar media. J. Am. Chem. Soc. **129**, 1968-1977

49 Deleu, M., Bouffioux, O., Razafindralambo, H., Paquot, M., Hbid, C., Thonard, P., Jacques, P. and Brasseur, R. (2003) Interaction of surfactin with membranes: A computational approach. Langmuir. **19**, 3377-3385

50 Kondejewski, L. H., Farmer, S. W., Wishart, D. S., Hancock, R. E. W. and Hodges, R. S. (1996) Gramicidin S is active against both Gram-positive and Gram-negative bacteria. Int. J. Pept. Protein Res. **47**, 460-466

51 Dubos, R. J. (1939) Studies on a bactericidal agent extracted from a soil bacillus. I. Preparation of the agent. Its activity *in vitro*. J. Exp. Med. **70**, 1-11

52 Dubos, R. J. and Hotchkiss, R. D. (1941) The production of bactericidal substances by aerobic sporulating *Bacilli*. J. Exp. Med., 629-640

53 Moll, G. N., Van den Eertwegh, V., Tournois, H., Roelofsen, B., Op den Kamp, J. A. F. and Van Deenen, L. L. M. (1991) Growth inhibition of *Plasmodium falciparum* in *in vitro* cultures by selective action of tryptophan-N-formylated gramicidin incorporated in lipid vesicles. Biochim. Biophys. Acta. **1062**, 206-210

54 Rautenbach, M., Vlok, M., Stander, M. and Hoppe, H. (2007) Inhibition of malaria blood stages by tyrocidines, membrane-active cyclic peptide antibiotics from *Bacillus brevis*. Biochim. Biophys. Acta. **1768**, 1488-1497

55 Dufour, S., Deleu, M., Nott, K., Wathelet, B., Thonart, P. and Paquot, M. (2005) Hemolytic activity of new linear surfactin analogs in relation to their physico-chemical properties. Biochim. Biophys. Acta. **1726**, 87-95

56 Separovic, F., Barker, S., Delahunty, M. and Smith, R. (1999) NMR structure of C-terminally tagged gramicidin channels. Biochim. Biophys. Acta. **1416**, 48-56

57 Wallace, B. A. (1998) Recent advances in the high resolution structures of bacterial channels: Gramicidin A. J. Struct. Biol. **212**, 5249-5256

58 Onda, M., Hayashi, H. and Mita, T. (2001) Interaction of gramicidin with lysophosphatidylcholine as revealed by calorimetry and fluorescence spectroscopy. J. Biochem. **130**, 613-620

59 Harold, F. M. and Baarda, J. R. (1967) Gramicidin, valinomcin, and cation permeability of *Streptococcus faecalis*. J. Bacteriol. **94**, 53-60

60 Bourinbaiar, A. S. and Coleman, C. F. (1997) The effect of gramicidin, a topical contraceptive and antimicrobial agent with anti-HIV activity, against herpes simplex virus type 1 and 2 *in vitro*. Arch. Virol. **142**, 2225-2235

61 Bourinbaiar, A. S., Kraisinski, K. and Borkowsky, W. (1993) Anti-HIV effect of gramicidin in vitro: Potential for permicide use. Life Sci. **54**, 5-9

62 Hansen, J., Pschorn, W. and Ristow, H. (1982) Function of the peptide antibiotics tyrocidine and gramicidin: Induction of conformational and structural changes of superhelical DNA. Eur. J. Biochem. **126**, 279-280

63 Ristow, H., Scharzschneider, B., Vater, J. and Kleinkauf, H. (1975) Some charateristics of the DNA tyrocidine complex and a possible mechanism of the gramicidin action. Biochim. Biophys. Acta. **414**, 1-8

64 Hirano, T., Oka, K. and Tamaki, T. (1994) Gramicidin as a petential immunausuppressant for organ transplantation: Suppression of human lyphocyte blastogenesis in vitro and prolongation of heart allograft survival in the rat. J. Pharm. Exp. Ther. **273**, 223-229

65 Divo, A. A., Geary, T. G. and Jensen, J. B. (1985) Oxygen and time-dependent effects of antibiotics and selected mitochondria inhibitors on *Plasmodium falciparum* in culture. Antimicrob. Agents Chemoter. **27**, 21-27

66 Otten-Kuipers, M. A., Beumer, T. L., Kronenburg, N. A., Roelofsen, B. and Op den Kamp, J. A. (1996) Effects of gramicidin on the sodium and potassium content of human erythrocytes. Mol. Membr. Biol. **13**, 225-235

67 Otten-Kuipers, M. A., Coppens-Burkunk, G. W., Kronenburg, N. A., Vis Mde, A., Roelofsen, B. and Op den Kamp, J. A. (1997) Tryptophan-N-formylated gramicidin causes growth inhibition of *Plasmodium falciparum* by inducing potassium efflux from infected erythrocytes. Parasitol. Res. **83**, 185-192

68 Gumila, C., Ancelin, M. L., Jeminet, G., Delort, A. M., Miquel, G. and Vial, H. J. (1996) Differential *in vitro* activities of ionophore compounds against *Plasmodium falciparum* and mammalian cells. Antimicrob. Agents Chemoter. **40**, 602-608

69 Kelkar, D. A. and Chattopadhyay, A. (2007) The gramicidin ion channel: A model membrane protein. Biochim. Biophys. Acta

70 Jordan, J. B., Shobana, S., Andersen, O. S. and Hinton, J. F. (2006) Effects of glycine substitutions on the structure and function of gramicidin A channels. Biochemistry. **45** 14012-14020

71 Seoh, S. A. and Busath, D. (1995) Gramicidin tryptophans mediate formamidinium-induced channel stabilization. Biophys. J. **68**, 2271-2279

72 Salom, D., Bano, M. C., Braco, L. and Abad, C. (1995) HPLC demonstration that an all Trp to Phe replacement in gramicidin A results in a conformational rearrangement from beta-helical monomer to double stranded dimer in model membranes. Biochem. Biophys. Res. commun. **209**, 466-473

73 Durkin, J. T., Providence, L. L., Koeppe, R. E. and Andersen, O. S. (1983) Energy of heterodimer formation among gramicidin analogues with an NH2-terminal addition or deletion: Consequence of missing the residue at the join in the channel. J. Mol. Biol. **231**, 1102-1121

74 Danders, W., Marahiel, A. M., Krause, M. I., Kosui, N., Kato, T., Izumiya, N. and Kleinkauf, H. (1982) Antibacterial action of gramicidin S and tyrocidines in relation to active transport, *in vitro* transcription, and spore outgrowth. Antimicrob. Agents Chemother. **22**, 785-790

75 Jelokhani-Niaraki, M., Kondejewski, L. H., Farmer, S. W., Hancock, R. E. W., Kay, C. M. and Hodges, R. S. (2000) Diasteroisomeric analogues of gramicidin S: Structure, biological activity and interaction with lipid bilayers. Biochem. J. **349**, 747-755

76 Kondejewski, L. H., Jelokhani-Niaraki, M., Farmer, S. W., Lix, B., Kay, C. M., Sykes, B. D., Hancock, R. E. W. and Hodges, R. S. (1999) Dissociation of antimicrobial and hemolytic activitities in cyclic peptide diasteeomers by systematic alteration in amphipathicity. J. Biol. Chem. **274**, 13181-13192

77 Kondejewski, L. H., Farmer, S. W., Wishart, D. S., Kay, C. M., Hancock, R. E. W. and Hodges, R. S. (1996) Modulation of structure and antibacterial and hemolytic activity by ring size in cyclic gramicidin S analogs. J. Biol. Chem. **271**, 256261-256268

78 Nagamurthi, G. and Rambhav, S. (1985) Gramicidin-S: Structure-activity relationship. J. Biosci. **7**, 323-329

79 Kiricsi, J. M., Prenner, E., Jelokhani-Niaraki, M., Lewis, R. N. A. H., Hodges, R. S. and McElhaney, R. N. (2002) The effects of ring-size analogs of the antimicrobial

peptide gramicidin S on phospholipid bilayer model membranes and on the growth of Acholeplasma laidlawii B. Eur. J. Biochem. **269**, 5911-5920

80 Dubos, R. J. (1939) Studies on a bacterial agent extracted from a soil bacillus. I. Preparation of the agent. Its activity *in vitro*. J. Exp. Med. **70**, 1488-1497

81 Spathelf, B. M. and Rautenbach, M. (2009) Anti-listerial activity and structure activity relationships of the six major tyrocidines, cyclic decapeptides from *Bacillus aneurinolyticus*. Bioorg. Med. Chem. **17**, 5541-5548

82 Bohg, A. and Ristow, H. (1987) Tyrocidine-induced modulation of the DNA conformation in *Bacillus brevis*. Eur. J. Biochem. **170**, 253-258

83 Kuo, M.-C. and Gibbons, W. A. (1979) Determination of individual side chain configurations, tertiary configurations, and molecular topography of tyrocidine A from scalar coupling constants and chemical shifts. Biochemistry. **18**, 5855-5867

84 Walsh, C. T., Gehring, A. M., Weinreb, P. H., Quadri, L. E. and Flugal, R. S. (1997) Post-translational modification of polyketide and nonribosomal peptide synthases. Curr. Opin. Struct. Biol. **1**, 309-315

85 Ohno, A., Ano, T. and Shoda, M. (1995) Effect of temperature on production of lipopeptide antibiotics, iturin A and surfactin by a dual producer, *Bacillus subtilis* RB14, in solid-state fermentation. J. Ferment. Bioeng. **80**, 517-519

86 Thimon, L., Peypoux, F., Maget-Dana, R., Roux, B. and Michel, G. (1992) Interactions of bioactive lipopeptides, iturin A and surfactin from *Bacillus subtilis*. Biotechnol. Appl. Biochem. **16**, 1799-1904

87 Ahimou, F., Jacques, P. and Deleu, M. (2000) Surfactin and iturin A effects on *B. subtilis* hydrophobicity. Enzyme Microbiol. Technol. **27**, 749-754

88 Vlok, N. M. (2005) Investigation of complexation and antimicrobial activity of gramicidin S in the presence of lipopeptides from *Bacillus subtlis*. PhD thesis, University of Stellenbosch, Stellenbosch

89 Kim, K. (1998) Suppression of inflammatory responses by surfactin, a selective inhibitor of platelet cytosolic phospholipase A2. Biochem. Pharmacol. **55**, 975-985

90 Vollenbroich, D. (1997) Antimycoplasma properties and applications in cell culture of surfactin, a lipopeptide antibiotic from *Bacillus subtilis*. Appl. Environ. Microbiol. **63**, 44-49

91 Vollenbroich, D., Ozel, M., Vater, J., Kamp, R. M. and Pauli, G. (1997) Mechanism of inactivation of enveloped viruses, by the biosurfactant surfactin from *Bacillus subtilis*. Biologicals. **25**, 289-297

92 Hosono, K. and Suzuki, H. (1983) Acylpeptides, the inhibitors of cyclic adenosine 3',5'-monophosphate phosphatase III. Inhibition of cyclic-AMP phosphodiesterase. J. Antibiot. **36**, 679-683

93 Singh, P. and Singh Caeotra, S. (2004) Potential application of microbial surfactants in biomedical sciences. Trends Biotechnol. **22**, 142-146

94 Bortolato, M., Besson, F. and Roux, B. (1997) Inhibition of alkaline phosphatase by surfactin as natural chelating lipopeptide from *B. subtilis*. Biotechnol. Lett. **19**, 433-435

95 Eaman, M., Berquand, A., Dufrene, Y. F., Paquot, M., Dufour, S. and Deleu, M. (2006) Penetration of surfactin into phospholipid monolayers: Nanoscale interfacial organization. Langmuir. **22**, 11337-11345

96 Lee, D. L. and Hodges, R. S. (2003) Structure-activity relationships of the *novo* designed cyclic antimicrobial peptides based on gremicidin S. Pept. Sci. **71**, 28-48

97 Andersen, O. S. (1984) Gramicidin channels. Annu. rev. Physiol. **46**, 531-548

98 Meyers, V. B. and Haydon, D. A. (1972) Ion transfer across lipid membranes in the presence of gramicidin A. II. The ion selectivity. Biochim. Biophys. Acta. **274**, 313-320

99 Miloshevsky, G. V. and Jordan, P. C. (2004) Gating gramicidin channels in lipid bilayers: reaction coordinates and mechanism of dissociation. Biophys. J. **86**, 92-104

100 O'Connell, A. M., Koeppe, D. E. and Andersen, O. S. (1990) Kinetics of gramicidin channel formation in lipid bilayers: transmembrane monomer association. Science. **250**, 1256-1259

101 Elliott, J. R., Needham, D., Dilger, J. P. and Haydon, D. A. (1983) The effects of bilayer thickness and tension on gramicidin single-channel lifetime. Biochim. Biophys. Acta. **735**, 95-103

102 Nezil, F. A. and Bloom, M. (1992) Combined influence of cholesterol and synthetic amphiphilic peptides upon bilayer thickness in model membranes. Biophys. J. **61**, 1176-1182

103 Simon, S. A., McIntosh, T. J. and Latorre, R. (1982) Influence of cholesterol on water penetration into bilayers. Science. **216**, 65-67

104 Elliott, J. R., Needham, D., Dilger, J. P., Brandt, O. and Haydon, D. A. (1985) A quantitative explanation of the effects of some alcohols on gramicidin single-channel lifetime. Biochim. Biophys. Acta. **814**, 401-404

105 Shagina, L. V., Blasko, K., Grinfield, A. E., Krorchev, Y. E. and Lev, A. A. (1989) Cholesterol-dependent gramicidin A channel inactivation in red blood cell membranes and lipid bilayer membranes. Biochim. Biophys. Acta. **978**, 145-150

106 Bamberg, E., Noda, K., Gross, E. and Lauger, P. (1976) Single-channel parameters of gramicidin A, B, and C. Biochim. Biophys. Acta. **419**, 223-228

107 Eisenman, G. and Horn, R. (1983) Ionic selectivity revisited: the role of kinetic and equilibrium processes in ion permeation through channels. J. Membr. Biol. **76**, 197-225

108 Roux, B. and Karplus, M. (1991) Ion transport in a model gramicidin channel: structure and thermodynamics. Biophys. J. **59**, 961-981

109 Killian, B., de Kruijff, C. J., van Echteld, A. J., Verkleij, J., Leunissen-Bijvelt, J. and de Gier. (1983) Mixtures of gramicidin and lysophosphatidylcholine form lamellar structure. Biochim. Biophys. Acta. **728**, 141-144

110 Rochetti, P., Spisni, A., Casali, E., Masotti, L. and Urry, D. W. (1983) Gramicidin A induces lysolecithin to form bilayers. Biosci. Rep. **3**, 127-133

111 Tournois, H., Henseleit, U., de Gier, J., de Kruijff, B. and Haest, C. W. (1988) Relationship between gramicidin conformation and dependent induction of phospholipid transbilayer movement and hexagonal H_{II} phase formation in erythrocyte membranes. Biochim. Biophys. Acta. **946**, 173-177

112 Tournois, H., Leunissen-Bijvelt, J., Haest, C. W., de Gier, J. and de Kruijff, B. (1987) Gramicidin-induced hexagonal H_{II} phase formation in erythrocyte membranes. Biochemistry. **26**, 6613-6621

113 Cornell, B. A., Weir, L. E. and Separovic, F. (1988) The effect of gramicidin A on phospholipid bilayers. Eur. Biophys. J. **16**, 113-119

114 Watnick, P. I., Chan, S. I. and Dea, P. (1990) Hydrophobic mismatch in gramicidin A'/lecithin systems. Biochemistry. **29**, 6215-6221

115 Aranda, F. J. and de Kruijff, B. (1988) Interrelationships between tyrocidine and gramicidin A' in their interaction with phospholipids in model membranes. Biochim. Biophys. Acta. **937**, 195-203

116 Ristow, H. (1977) The peptide antibiotic gramicidin D: A specific reactivator of tyrocidine-inhibited transcription. Biochim. Biophys. Acta. **477**, 177-184

117 Katsu, T., Kobayashi, H. and Fujita, Y. (1986) Mode of action of gramicidin S on *Escherichia Coli* membrane. Biochim. Biophys. Acta. **860**, 608-619

118 Katsu, T., Ninomiya, C., Kuroko, M., Kobayashi, H., Hirota, T. and Fujita, Y. (1988) Action mechanism of amphipathic peptides gramicidin S and melittin on erythrocyte membrane. Biochim. Biophys. Acta. **939**, 57-63

119 Staudegger, E., Prenner, E., Kriechbaum, M., Degovics, G., Lewis, R. N. A. H., McElhaney, R. N. and Lohner, K. (2000) X-ray studies on the interaction of the antimicrobial peptide gramicidin S with microbial lipid extracts: evidence for cubic phase formation. Biochim. Biophys. Acta. **1468**, 213-230

120 Beven, L. and Wrobleswski, H. (1997) Effect of natural amphipathic peptides on viability, membrane potential, cell shape and motility of mollicutes. Res. Microbiol. **148**, 163-175

121 Katsu, T., Kuroko, M., Morikawa, T., Sanchika, K., Fujita, Y., Yamamura, H. and Uda, M. (1989) Mechanism of membrane damage induced by the amphipatic peptides gramicidin S and melittin. Biochim. Biophys. Acta. **983**, 135-141

122 Rautenbach, M., Gerstner, G. D., Vlok, M., Kulenkampff, J. and Westerhoff, H. V. (2006) Analyses dose-response curves, to compare the antimicrobial activity of model cationic α-helical peptides, highlights the necessity for a minimum of two active parameters. Anal. Biochem. **350**, 81-90

123 Prenner, E., Lewis, R. N. A. H., Jelokhani-Niaraki, M., Hodges, R. S. and McElhaney, R. N. (2001) Cholesterol attenuates the interaction of the antimicrobial peptide gramicidin S with phospholipid bilayer membranes. BioChim. Biophys. Acta. **1510**, 83-92

124 Lazaridis, I., Frangou-Lazaridis, M., Maccuish, F., Nandi, S. and Seddon, B. (1980) Gramicidin S content and germination and outgrowth of *Bacillus brevis* Nagano spores. FEMS Microbiol. Lett. **7**, 229-232

125 Nandi, S. and Seddon, B. (1978) Evidence for gramicidin S functioning as a bacterial hormone specifically regulating spore outrowth in *Bacillus brevis* Nagano. Biochem. Soc. Trans. **6**, 409-411

126 Bentzen, G. and Demain, A. L. (1990) Studies on gramicidin S-mediated suicide during germination outgrowth of *Bacillus brevis* spores. Curr. Microbiol. **20**, 165-169

127 Gale, E. F. and Taylor, E. S. (1947) Assimilation of amino acids by bacteria. II. Action of tyrocidine and some detergent substances in releasing amino acids from the internal environment of *Streptococcus faecalis*. j. Gen. Microbiol. **1**, 77-84

128 Hotchkiss, R. D. (1944) Gramicidin, tyrocidine and tyrothricin. Adv. Enzymol. **4**, 153-199

129 Goodall, M. C. (1970) Structural effects in the action of antibiotics on the ion permeability of lipid bilayers. II. Kinetics of tyrocidine B. Biochim. Biophys. Acta. **219**, 28-36

130 Goodall, M. C. (1970) Structural effects in the action of antibiotics on the permeability of lipid bilayers. I. Tyrocidine B. Biochim. Biophys. Acta. **203**, 28-33

131 Goodall, M. C. (1970) Structural affects in the action of antibiotics on the ion permeability of lipid bilayers. III. Gramicidins "A" and "S" and lipid specificity. Biochim. Biophys. Acta. **219**, 471-478

132 Spathelf, B. M. (2009) The structure-activity/toxicity relationships of the tyrocidines, a group of cyclic decapeptides from *Bacillus brevis*. PhD thesis, University of Stellenbosch, Stellenbosch

133 Mach, B. and Slayman, C. W. (1966) Mode of action of tyrocidine on neurospora. Biochim. Biophys. Acta. **124**, 351-361

134 Changeux, J.-P., Ryter, A., Leuzinger, W., Barrand, P. and Podleski, T. (1968) On the association of tyrocidine with acetylcholinesterase. Biochemistry. **62**, 986-993

135 Woodward, G. E. and Hudson, M. (1957) Effect of tyrocidine on the carbohydrate metabolism of yeast ant tumor tissue, and on the growth of tumor in mice. J. Fran. Inst. **264**, 147-152

136 Liu, X., Huang, W. and Wang, E. (2005) An electrochimical study on the interaction of surfactin with a supported bilayer lipid on a glassy carbon electrode. J. Electroanal. Chem. **577**, 349-354

137 Maget-Dana, R. and Ptak, M. (1995) Interaction of surfactin with membrane models. Biophys. J. **68**, 1937-1943

138 Heerklotz, H., Wieprecht, T. and Seelig, J. (2004) Membrane pertubation by the lipopeptide surfactin and detergents as studied by deuterium NMR. J. Phys. Chem. **108**, 4909-4015

139 Carrillo, C., Teruel, J. A., Aranda, F. J. and Ortiz, A. (2003) Molecular mechanism of membrane permeabilization by the peptide antibiotic surfactin. Biochim. Biophys. Acta. **1611**, 91-97

140 Kinsinger, R., Shirk, M. C. and Fall, R. (2003) Rapid surface motilitycin *Bacillus subtilis* is dependent on extracellular surfactin and potassium ion. J. Bacteriol. **185**, 5627-5631

141 Stewart, P. S. and Costerton, J. W. (2001) Antibiotic resistance of bacteria in biofilms. The Lancet. **358**, 135-138

142 Bais, H. P., Fall, R. and Vivanco, J. M. (2004) Biocontrol of *Bacillus subtilis* against infection of arabidopsis roots by *Pseudomonas syringae* is facilitated by biofilm formation and surfactin production. Plant Physiol. **134**, 307-319

143 Borchert, S., Stacherlhaus, T. and Mahariel, M. A. (1994) Induction of surfactin production in *Bacillus subtilis* by gsp, a gene located upstream of the gramicidin S operon in *Bacillus brevis*. J. Bacteriol. **176**, 2458-2462

144 Gerers, W., Kleinkauf, H. and Lipmann, F. (1968) The activation of amino acids for biosynthesis of gramicidin S. Biochemistry. **60**, 269-276

145 Finking, R. and Mahariel, M. A. (2004) Biosynthesis of nonribosomal peptides 1. Annu. Rev. Microbiol. **58**, 453-488

146 Stein, T., Vater, J. V., Kruft, A., Otto, B., Wittmann-Liebold, P., Franke, M., Panico, R., McDowell and Morris, H. R. (1996) The multiple carrier model of nonribosomal peptide biosynthesis at modular multienzymatic templates. J. Biol. Chem. **271**, 15428-15435

147 Schneider, A. T., Stachelhaus and Mahariel, M. A. (1998) Targeted alteration of the substrate specificity of peptide synthetases by rational module swapping. Mol. Gen. Genet. **257**, 308-318

148 Mootz, H. D. and Marahiel, M. A. (1997) The tyrocidine biosynthesis operon of Bacillus brevis: complete nucleotide sequence and biochemical characterization of functional internal adenylation domains. J. Bacteriol. **179**, 6843-6850

149 Kessler, N., Schuhmann, H., Morneweg, S., Linne, U. and Marahiel, A. m. (2003) The linear pentadecapeptide gramicidin is assembled by four multimodular nonribosomal peptide synthetases that comprise 16 modules with 56 catalytic domains. J. Biol. Chem. **279**, 7413-7419

150 Schracke, N., Linne, U., Mahlert, C. and Mahariel, M. A. (2005) Synthesis of linear gramicidin required the cooperation of two independent reductases. Biochemistry. **44**, 8507-8513

151 Kratzschmar, J., Krause, M. and Mahariel, M. A. (1989) Gramicidin S biosynthesis operon containing the structural genes grsA and grsB has an open reading frame encoding a protein homologous to fatty acid thioterases. J. Bacteriol. **170**, 5422-5429

152 Krause, M. and Mahariel, M. A. (1988) Organisation of the biosynthesis genes for the peptide antibiotic gramicidin S. J. Bacteriol. **170**, 4669-4674

153 Stein, T., Vater, J., Kruft, A., Wittemann-Liebold, B., Franke, P., Panico, M., McDowell, R. and Morris, H. R. (1994) Detection of 4'-phosphopantetheine at the

thioester binding site for L-valine of gramicidin S synthetase 2. FEBS Lett. **340**, 39-44

154 Martin and Liras. (1989) Organization and expression of genes involved in the biosynthesis of antibiotics and other secondary metabolites. Annu. Rev. Microbiol. **43**, 173-206

155 Hoyer, K. M., Mahlert, C. and Marahiel, M. A. (2007) The interative gramicidin S thioesterase catalyzes peptide ligation and cyclization. Chem. Biol. **14**, 13-22

156 Vollenbroich, D., Mehta, N., Zuber, P., Vater, J. and Kamp, R. M. (1994) Analysis of surfactin synthetase subunits in srfA mutants of *Bacillus subtilis* OKB105. J. Bacteriol. **176**, 395-400

157 Kira, J. W. and Rolf, M. (2008) Crystal structure of a molecular assembly line. Angew. Chem. Int. Ed. **47**, 8344-8346

158 Steller, S., Sokoll, A., Wilde, C., Bernhard, F., Franke, P. and Vater, J. (2004) Initiation of surfactin biosynthesis and the role of the SrfD-Thioesterase protein. Biochemistry. **43**, 11331-11343

159 Nizet, V. (2004) Antimicrobial peptides resistance mechanisms of human bacterial pathogens. Curr. Issues Mol. Biol. **8**, 223-238

160 Wu, M. and Hancock, R. E. W. (1999) Interaction of the cyclic antimicrobial cationic peptide bactenecin with the outer and cytoplasmic membrane. J. Biol. Chem. **274**, 29-35

161 Shai, Y. (1999) Mechanism of the binding, insertion and destabilization of phospholipid bilayer membranes by alpha-helical antimicrobial and cell non-selective membrane-lytic peptides. Biochim. Biophy. Acta. **1462**, 55-70

162 Straus, S. K. and Hancock, R. E. W. (2006) Mode of action of the new antibiotic for Gram-positive pathogens daptomycin: Comparison with cationic antimicrobial peptides and lipopeptides. Biochim. Biophy. Acta. **1758**, 1215-1223

163 Yeaman, M. L. and Yount, N. (2003) Mechanism of antimicrobial peptide action and resistance. Pharmacol. Res. **55**, 27-55

164 Henriques, S. T., Melo, M. N. and Castanho, M. A. R. B. (2006) Cell-penetrating peptides and antimicrobial peptides: how different are they? Biochem. J. **399**, 1-7

165 Harris, M., Mora-Montes, H. M., Gow, N. A. R. and Coote, P. J. (2009) Loss of mannosylphosphate from *Candida albicans* cell wall proteins results in enhanced resistance to the inhibitory effect of a cationic antimicrobial peptide via reduced peptide binding to the cell surface. Microbiology. **155**, 1058-1070

166 Prescott, L. M., Harley, J. P. and Klein, D. A. (2005) Microbiology. McGraw-Hill, New York, pp. 792

167 Peschel, A. and Collins, L. V. (2001) Staphylococcal resistance to antimicrobial peptides of mammalian and bacterial origin. Review. Peptides. **22**, 1651-1659

168 Khattar, A., Rejasse, A., Destoumieux-Garzon, D., Escoubas, J. M., Sanchis, V., Lereclus, D., Givaudan, A., Kallassy, M., Nielsen-Leroux, C. and Gaudriault, S. (2009) The dlt operon of *Bacillus cereus* is required for resistance to cationic antimicrobial peptides and for virulence in insects. J. Bacteriol. **191**, 7063-7073

169 Kovacs, M., Halfmann, A., Fedtke, I., Heintz, M., Peschel, A., Vollmer, W., Hakenbeck, R. and Bruckner, R. (2006) A functional dlt operon, encoding proteins required for Incorporation of D-alanine in teichoic acids in Gram-positive bacteria, confers resistance to cationic antimicrobial peptides in *Streptococcus pneumoniae*. J. Bacteriol. **188**, 5797-5805

170 Kristian, S. A., Datta, V., Weidenmaier, C., Kansal, R., Fedtke, I., Peschel, A., Gallo, R. L. and Nizet, V. (2005) D-alanylation of teichoic acids promotes group A *Streptococcus* antimicrobial peptide resistance, neutrophil survival, and epithelial cell invasion. J. Bacteriol. **187**, 6719-6725

171 Shi, Y., Cromie, M. J., Hsu, F.-F., Turk, J. and Groisman, E. A. (2004) PhoP-regulated *Salmonella* resistance to the antimicrobial peptides magainin 2 and polymyxin B. Mol. Microbiol. **53**, 229-241

172 Guina, T., E.C., Y., Wang, E., Hackett, M. and Miller, S. I. (2000) A PhoP-regulated outer membrane protease of *Salmonella enterica* serovar Tyyphimurium promotes resistance to Alpha-helical antimicrobial peptides. J. Bacteriol. **183**, 4077-4086

173 Gunn, J. S. and Miller, S. I. (1996) PhoP-PhoQ activates transcription of pmrAB, encoding a two-component regulatory system involved in *Salmonella typhimurium* antimicrobial peptide resistance. J. Bacteriol. **178**, 6857-6864

174 Tran, A. X., Whittimore, J. D., Wyrick, P. B., McGrath, S. C., Cotter, R. J. and Tren, M. S. (2006) The lipid A 1-phosphatase of Helicobacter pylori Is required for resistance to the antimicrobial peptide polymyxin J. Bacteriol. **188**, 4531-4541

175 Gunn, J. S., Ryan, S. S., Van Velkinburgh, J. C., Ernst, R. R. and Miller, S. I. (2000) Genetic and functional analysis of a PmrA-PmrB-regulated locus necessary for lipopolysaccharide modification, antimicrobial peptide resistance, and oral virulence of *Salmonella enterica* Serovar Typhimurium. Infect. Immun. **68**, 6139-6146

176 McPhee, J. B., Lewenza, S. and Hancock, R. E. W. (2003) Cationic antimicrobial peptides activate a twocomponent regulatory system, PmrA-PmrB, that regulates

resistance to polymyxin B and cationic antimicrobial peptides in *Pseudomonas aeruginosa*. Mol. Microbiol. **50**, 205-217

177 Thedieck, K., Hain, T., Mohamed, W., Tindall, B. J., Nimtz, M., Chakraborty, T., Wehland, J. and Jänsch, L. (2006) The MprF protein is required for lysinylation of phospholipids in listerial membranes and confers resistance to cationic antimicrobial peptides (CAMPs) on Listeria monocytogenes. Mol. Microbiol. **62**, 1325-1339

178 Ernst, C. M., Staubitz, P., Mishra, N. N., Yang, S.-J., Hornig, G., Kalbacher, H., Bayer, A. S., Kraus, D. and Peschel, A. (2009) The bacterial defensin resistance protein MprF consists of separable domains for lipid lysinylation and antimicrobial peptide repulsion. Pathogens. **5**, 1-9

179 Samant, S., Hsu, F.-F., Neyfakh, A. A. and Lee, H. (2009) The *Bacillus anthracis* protein MprF Is required for synthesis of lysylphosphatidylglycerols and for resistance to cationic antimicrobial peptides. J. Bacteriol. **191**, 1311-1319

180 McLeod, G. I. and Spector, M. P. (1996) Starvation- and stationary-phase-induced resistance to the antimicrobial peptide Polymyxin B in *Salmonella typhimurium* is RpoS (sS) independent and occurs through both phoP-dependent and -independent pathways. J. Bacteriol. **178**, 3683-3688

181 Mah, T.-F. C. and O'Toole, G. A. (2001) Mechanisms of biofilm resistance to antimicrobial agents. TRENDS Microbiol. **9**, 34-39

182 Davies, D. G., Parsek, M. R., Pearson, J. P., Iglewski, B. H., Costerton, J. W. and Greenberg, E. P. (1998) The involvement of cell-to-cell signals in the development of a bacterial biofilm. Science. **280**, 295-298

183 Davies, D. G. (2003) Understanding bioflim resistance to antimicrobial agents. Nat. Rev. Drug Discovery. **2**, 114-123

184 Morikawa, M. (2006) Beneficial biofilm formation by industrial bacteria *Bacillus subtilis* and related species. J. Biosci. Bioeng. **101**, 1-8

185 Xu, K. D., McFeters, G. A. and Stewart, P. S. (2000) Biofilm resistance to antimicrobial agents. Microbiology. **146**, 547-549

186 Mirelles II, J. R., toguchi, A. and Harshey, R. M. (2001) *Salmonella enterca* serova typhimurium swarming mutants with altered biofilm-forming abilities: Surfactin inhibits biofilm formation. J. Bacteriol. **183**, 5848-5854

187 Ishigami, Y., Osman, M., Nakahara, H., Sano, Y., Ishiguro, R. and Matsumoto, M. (1995) Significance of β-sheet formation for micellization and surface absorption of surfactin. Coillois Surf., B. **4**, 341-348

188 Wright, G. D. (2005) Bacterial resistance to antibiotics: Enzymatic degradation and modification. Adv. Drug Deliv. Rev. **57**, 1451-1470

189 Gold, O. H. and Moellering, R. C. (1996) Antimicrobial drug resistance. New Eng. J. Med. **335**, 1445-1457

190 Burns, J. L., Rubens, C. E., Mendelman, P. M. and Smith, A. L. (1986) Cloning and expression in *Escherichia coli* of a gene encoding nonenzymatic chloramphenicol resistance from *Pseudomonas aeruginosa*. Antimicrob. Agents Chemoter. **29**, 445-450

191 Levy, S. B. (1992) Active efflux mechanisms for antimicrobial resistance. Antimicrob. Agents Chemoter. **36**, 695-703

192 Paulsen, I. T., Brown, M. H. and Skurray, R. A. (1996) Proton-dependant multi-drug efflux systems. Antimicrob. Agents Chemoter. **60**, 575-608

193 Cudic, M. and Otvos, J. L. (2002) Intracellular targets of antibacterial peptides. Curr. Drug Targ. **3**, 101-106

194 Tzeng, Y.-L., Ambrose, K. D., Zughaier, S., Zhou, X., Miller, Y. K., Shafer, W. M. and Stephens, D. S. (2005) Cationic antimicrobial peptide resistance in *Neisseria meningitidis*. J. Bacteriol. **187**, 5387-5396

195 Shafer, W. M., Veal, W. L., Lee, E.-H., Leticia Zarantonelli3, Balthazar, J. T. and Rouquette, C. (2001) Genetic organization and regulation of Antimicrobial efflux systems possessed by *Neisseria gonorrhoeae* and *Neisseria meningitidis*. J. Mol. Microbiol. Biotechnol. **3**, 219-224

196 Bengoechea, J. A. and Skurnik, M. (2000) Temperature-regulated efflux pump/potassium antiporter system mediates resistance to cationic antimicrobial peptides in *Yersinia*. Mol. Microbiol. **37**, 67-80

197 Staron, A., Finkeisen, D. E. and Mascher, T. (2011) Peptide antibiotic sensing and detoxification modules of *Bacillus subtilis*. Antimicrob. Agents Chemoter. **55**, 515-525

198 Forrer, C. B., Blahy, D. M., Mariatico, A. L., Campos, J. M. and Freeman, H. M. (1982) Comparison of vancomycin and penicillin for viral isolation. J. Clin. Microbiol. **16**, 295-298

Chapter 2

A microbiological investigation of the antagonism between surfactin from *Bacillus subtilis* and gramicidin S from *Aneurinibacillus migulanus*

Introduction

Pathogenic microorganisms are responsible for major diseases or illnesses that affect animal, plant and human species. Several antimicrobial therapeutic drugs have been developed over the past century to combat most pathogens. These drugs generally act by inhibiting the pathogen's metabolic pathways, interfering with the synthesis of its cell wall or by inhibiting its protein or nucleic acid synthesis [1]. Unfortunately, disease-causing microorganisms have also evolved in turn different resistance mechanisms and have become defiant to most classical antibiotics [2, 3]. This resistance has arisen in different ways and may differ in terms of either the type of antibiotic or the microorganism involved. Today, bacterial resistance has developed into a serious problem, which threatens human societies and urges for a global increase in the search for new antibiotics [4].

There are at least five main resistance mechanisms that pathogens use to resist most antibiotics. The first resistance mechanism is used by Gram-negative bacteria and mycoplasma: they generally change their outer-membrane composition to prevent drug binding or entrance [5]. The second mechanism is used by a variety of microorganisms: they express non-specific multi-drug resistance efflux pumps in their plasma membranes to expulse drugs [3, 6-8]. The third mechanism is utilized by certain Gram-

negative bacteria that chemically modify antibiotics by adding groups that render the drug inactive [9], or use trapping proteins that bind the drug to neutralise it (reviewed in [10]). In the fourth mechanism alternative pathways are utilised to avoid the step inhibited by the drug or the production of target metabolites is increased [4]. The fifth resistance mechanism arises from the ability of certain bacteria such as *Mycobacterium tuberculosis* to modify drug targets through ribosomal mutations [4].

A sixth resistance mechanism, mainly biofilm formation, has also been described [11-16]. It is developed by certain Gram-positive soil bacteria, such as *Bacillus subtilis* and it consists of sessile bacterial community close together in a glycocalyx matrix to resist drugs [16]. It has been demonstrated by Bais *et al.* [12] that biofilm formation was related to the production of the antibiotic peptide surfactin (Srf) in *B. subtilis* strains. However, the mechanism by which Srf encourages biofilm formation and hence confers resistance to *B. subtilis* is not well understood. According to Vlok [17], Srf acts by antagonising the antimicrobial activity of other antibiotic peptides either via complex formation or an unknown mechanism.

Antagonistic activity, a putative resistance mechanism, can occur between two antibiotics when they associate or cause a change in the target to neutralise the actions of one another. An example of this resistance mechanism was reported between vancomycin and penicillin [18]. Vlok [17] showed that the activity of the antimicrobial peptide gramicidin S (GS) from *Aneurinibacillus migulanus* (previously known as the Nagano strain of *B. brevis* [19-21]) is antagonised by the *B. subtilis* peptide Srf [22, 23]. This antagonism was proposed to be due to inactive complexes that formed in solution phase between GS and Srf. It was hypothesised that when these two soil organisms are

present together they produce peptides that antagonise the effects of one another as a mechanism of survival [17]. Similar antagonistic behaviour was also hypothesised to occur between different peptides from the *Bacillus* species.

GS is a basic/cationic and amphipathic cyclic decapeptide consisting of two pentapeptide (Val-Orn-Leu-D-Phe-Pro) repeats in an antiparallel β-sheet structure (Table 2.1) [24]. The ring structure is linked between Val and Pro residues [25] and is reinforced by four hydrogen bond [26]. This conformation is adopted in various solutions of differing polarities, as well as in the crystalline form [25]. GS has a broad activity spectrum against Gram-negative and Gram-positive bacteria [27], erythrocytes and malarial infected erythrocytes [28, 29]. GS also has inhibitory actions on active transport [30] and on the DNA transcription in its producer during germination and outgrowth [20, 31, 32]. GS first absorbs into the membrane of the bacterium and then interacts with the lipid membrane or other GS molecules, causing changes in the morphology and leading to deterioration in the membrane structure [33]. According to Staudegger *et al.* [34], GS disrupts lipid membranes by increasing the negative curvature stress, causing the formation of bi-continuous inverted cubic phases.

Table 2.1. Primary structures of the cyclic peptides used in this study.

Peptides	Abbreviation	Peptide primary structure	monoisotopic Mr	Net charge (pH7)
Gramicidin S	GS	Cyclo-(VOLfP)$_2$ [24]	1140.68	+2
Surfactin 1	Srf$_1$	Cyclo-(ELlVDlV-C$_{15}$) [35]	993.27	-2
Surfactin 2	Srf$_2$	Cyclo-(ELlVDlI-C$_{13}$) [35]	1007.30	-2
Surfactin 3	Srf$_3$	Cyclo-(ELlVDlL-C$_{14}$) [35]	1021.33	-2
Surfactin 4	Srf$_4$	Cyclo-(ELlADlL-C$_{15}$) [35]	1035.36	-2

Standard one letter abbreviations are used for the amino acid residues, apart for O for Orn. D-amino acids are given in lower case. C$_{13}$-C$_{15}$ are the possible variants in the lipid moiety.

Srf is an acidic/anionic and amphipathic cyclic lipopeptide with seven amino acids interlinked with an alkyl chain *via* a lactone bond (Table 2.1) [35]. Srf has a limited solubility and aggregates in solution due to its very strong surface active character that results from its tendency to absorb at hydrophilic/hydrophobic interfaces [36]. Srf is an antifungal agent with moderate antibacterial activity [37]. Srf has also been shown to have antitumoral, antiviral as well as antimycoplasma activity [38-40]. However, it also exhibits haemolytic activity [41], that makes it an unsuitable compound for medical applications. The primary step in Srf's mechanism of membrane disturbance is the insertion of the peptide into the lipid bilayers [42]. Srf spontaneously interacts with the lipid membrane by means of hydrophobic interactions [43]. Once inserted, Srf molecules aggregate and cause the formation of pores that break down the underlying structure of the lipid bilayers [42].

The present study was a continuation of the study by Vlok [17] on the antagonism between GS and Srf. *Micrococcus luteus* and two *B. subtilis* strains, OKB120, which produces Srf only under certain culturing conditions, and the continuous Srf producer ATCC21332 [44-46], as well as erythrocytes were included as test organisms. We aimed to further elucidate the influence of Srf on the antibacterial and haemolytic activity of GS by using standard dose-response assays and to investigate the possible site of interaction using liquid chromatography mass spectrometry (LC-MS).

Materials

Gramicidin S from *A. migulanus* was purchased from Sigma-Aldrich (Steinheim, Germany). The lipopeptide Srf from *B. Subtilis,* was supplied by Fluka Chemie (St Louis, USA).

Micrococcus luteus (NCTC 8340), *B. subtilis* strains (ATCC21332 and OKB 120) were from the BIOPEP culture collection, while *A. migulanus* (ATCC9999) were supplied by ATCC. Reagents for TGYM media namely the skim milk powder was supplied by Clover (Roodepoort, SA). Romil Ltd (Cambridge, UK) supplied the acetonitrile (CH_3CN, HPLC-grade, far UV cut-off) and the methanol (>99.9%). The ethanol (GR grade) was supplied by United Scientific (Durban, RSA). D-glucose, the components for the Luria Bertani (LB); sodium chloride (NaCl), tryptone and yeast extract, the tryptone soy broth (TSB), the peptone, agar as well as NaH_2PO_4 and Na_2HPO_4 were supplied by Merck (Darmstadt, Germany). The trifluoroacetic acid (TFA, > 98%) was provided by Sigma-Aldrich (St. Louis, USA). Non sterile, standard non-treated polystyrene microtiter plates (96 well flat bottom) and culture dishes were supplied by Greiner bio-one (Frickenhausen, Germany) and Lasec (Cape Town, SA). A Millipore Milli Q® water system (Milford, USA) was used to prepare analytical quality water by filtering it from a reverse osmosis plant.

Methods

Antibacterial assays

Cell preparation for antimicrobial assays

Bacterial freezer stocks were cultured on LB agar (1% (*w/v*) tryptone, 0.5% (*w/v*) yeast extract, 1 % NaCl, 1.5% (*w/v)* agar) for *M. luteus* NCTC 8340, or TGYM agar (0.5% (*w/v*) peptone, 0.25% (*w/v*) yeast extract, 0.1 % (*w/v*) glucose, 0.1% (*w/v*) skim milk powder, 1.5% (w/v) agar) for *B. subtilis* strains ATCC21332 and OKB120 and *A. migulanus* ATCC9999 and incubated at 37°C for 48 h. Selected colonies of *M. luteus*

and *B. subtilis* strains were grown overnight for 16 h in LB and TSB, respectively. The organisms were then sub-cultured in TSB (15 % (*w/v*) agar) at 37°C for 6 h to an optical density (OD) of 0.60 ± 0.01 at 620 nm.

Micro-broth dilution assays

Sub-cultured cells were diluted to an OD of 0.20 ± 0.01 before adding to the plates. Micro-broth dilution assays were performed with the diluted culture suspensions and growth was measured after 16 h incubation, at 620 nm on a Titertek Multiscan Plus Mk II (Flow Laboratories, USA) microtitre plate reader (adapted from Rautenbach *et al*. [47]). The microtiter plates were previously blocked with 0.5% casein in Dulbecco's phosphate buffered saline (PBS) and sterilized under UV light before use.

Gel diffusion assays

Sub-cultured *M. luteus* and *B. subtili*s strains (1 mL cell culture; OD = 0.60) were mixed with 2% TGYM agar (10 mL; 45°C). A laboratory vortex was then used to mix the agar with the cells by dispersion for 10 s. The mixed cultured were poured into a culture dish and let to set for 30 minutes. Selected colonies of *B. subtilis* and *A. migulanus* were then spotted either on normal or on top of the *M. luteus* seeded gel at close proximity (< 1 mm) to allow interaction between the products of the two producer strains (adapted from the radial diffusion assay by Du Toit and Rautenbach [48]). Alternatively, *A. migulanus* was spotted on either *B. subtilis* ATCC21332 or OKB120 seeded TGYM agar. Cell colonies on the culture dishes were processed and photographed after 2 days of incubation at 37^{o}C using a Nikon SMZ 10A trinocular sterozoom microscope mounted with a Nikon Coolpix 990 camera.

Haemolysis assays

Human A+ erythrocytes (2% hematocrit or 2.0 x 10^5 cells/mL) in RPMI-1640 medium supplemented with 0.65 mM hypoxanthine, 25 mM HEPES, 0.2% (*w/v*) $NaHCO_3$, 50 mM glucose, 0.048 mg/mL gentamicin and 0.5% (*w/v*) albumax II (serum substitute), was distributed in microtiter plates at 90 µL per well. Serial dilutions of test peptides and combinations were added at 10 µL to erythrocytes to a final volume of 100 µL. Haemolytic activity of the peptides was determined after incubation for 48 h at 37°C. Microtiter plates with assay mixtures were centrifuged at 200 x g for 3 minutes after incubation to sediment intact erythrocytes in wells. The haemoglobin content of a 1:8 dilution of the supernatant in water was measured at 405 nm for each well. The addition of 200 µM GS to the control wells was used to determine the total haemolysis in the haemolysis assays.

Supernatant cell assay

M. luteus were first cultured in LB and sub-cultured in TSB to an OD of 0.60 at 630 nm. The cultures were centrifuged at 900 x g for 8 minutes and washed with a 0.9% NaCl solution. The cells were then re-suspended in 0.9% NaCl and diluted to an OD of 0.20 and then distributed (180 µL) into the microtitre plates. After incubation for 30 minutes at 37ºC with the peptide combinations (20 µL), the plates with cultures centrifuged for 8 minutes at 900 x g and the supernatants transferred into glass tubes (160 µL in triplicate) for LC-MS analysis. The remaining cell pellets were washed with TSB by centrifugation, and the cells re-suspended in TSB (160 µL) and left to incubate for 16 h at 37ºC and growth measured a before.

Liquid chromatography mass spectrometry

LC-MS analysis of supernatants from the supernatant cells assay was analysed on a Waters Acquity autosampler attached to a Waters QTOF Ultima mass spectrometer. A Waters UPLC BEH C_{18} column (2.1 x 50 mm, 1.7 µm spherical particles) was used with a 0.1% TFA (solvent A) to CH_3CN (solvent B) gradient to separate peptides contained in the samples. This was done as follows: 100% A for the first 30 seconds, 0 to 30% B from 0.5 to 1 min, 70% to 40% A from 1 to 10 min, 60% to 100% B from 10 to 11 min, then 0% to 100% A from 11.10 to 14 min, at a flow rate of 300 µL/min. The peak areas of all GS species (triplicate analyses), were integrated for analysis using a Lynex® software package.

Data processing for the biological dose-response analysis

The relative growth was calculated from the dose-response data obtained from the antimicrobial assays. This was done by dividing the light dispersion (after blank correction) per well by the mean light dispersion of the wells containing the growth medium, the bacterial culture and peptide solvent (considered as 100% growth). The percentage inhibition in all assays was calculated by subtracting the relative growth from 100. GraphPad Prism 4.0 (GraphPad Software Incorporated) was used to analyse all data for curve fits and statistical analyses. Sigmoidal dose response curves were fitted for all assay results. Only the mean was considered to fit the curve. The 50% inhibitory concentrations (IC_{50}) towards *M. luteus* and *B. subtilis,* as well as the 50% haemolysis concentration (HC_{50}) were calculated according to the method described by Rautenbach *et al.* [47].

For the determination of antagonism, synergism or sum of activities for two active peptides the fractional haemolytic concentration (FHC) and FHC index were calculated for each of the two peptides in the assay using the following equations [49]:

FHC(A) = HC_{50} (peptide [A] in A+B mixture)/ HC_{50} (peptide A alone) (2.1)

FHC(B) = HC_{50} (peptide [B] in A+B mixture)/ HC_{50} (peptide B alone) (2.2)

From the FHC values the FHC index is calculated according to equation 2.3;

FHC index = FHC (A) + FHC (B) (2.3)

with FHC index =1 indicating that the resultant HC_{50} is due to the sum of the activity of peptides A and B; FHC index >1 indicating that the resultant HC_{50} is due to antagonistic activity between peptides A and B; FHC index <1 indicating that the resultant HC_{50} is due to synergistic activity between peptides A and B.

Results

Influence of surfactin on the antibacterial activity of gramicidin S

The antagonism of GS by Srf was investigated towards both *M. luteus* (NCTC8340) and *B. subtilis* (ATCC21322 and OKB120) using dose-response assays. GS was found to be active against all tested organisms in the low μM range, whereas Srf did not show any activity towards the target organisms (Table 2.2). Srf was found to antagonise the activity of GS in a dose-dependent manner, regardless of the bacterial targets, as shown by the dose-response curves in Figure 2.1. In these dose-response curves four independent experiments, each in quadruplicate were used to obtain the results for the addition of 30 μM Srf plus GS and GS alone.

An IC_{50} of 7.8 μM of GS towards *M. luteus* was observed, similar to the results of Vlok [47]. Pre-incubation of the bacteria with 30 and 60 μM Srf caused the inhibition curve of GS against *M. luteus* to shift to the right (significant IC_{50} increase, $P>0.001$), meaning that more GS was required to cause the same level of inhibition (Figure 2.1). Srf had no inhibitory effects against the test organism at any concentration used. We also found, similar to the results of Vlok [17], that the sensitivity of *M. luteus* depended on the order of addition of the two peptides. Addition of GS to the target cells first without pre-incubation with 30 μM Srf leads to only slight antagonism at high Srf concentrations and synergism at low concentrations (results not shown). Pre-incubating of the target organism with 30 μM (or 60 μM) Srf 10 minutes before adding GS had a protective effect and the presence of Srf therefore antagonised GS activity (Figure 2.1A and Table 2.2).

In order to verify whether this antagonism resulted from a true resistance mechanism, the "protection" experiments were repeated on two *B. subtilis* strains, namely *B. subtilis* OKB120 which does not produce Srf under experimental conditions and *B. subtilis* ATCC21332 which is a strict aerobic and anaerobic Srf producer [17]. The IC_{50} of GS towards *B. subtilis* OKB120 was significantly lower ($P<0.05$) than towards *B. subtilis* ATCC21332 and was determined as 1.9 μM and 3.5 μM respectively. In order to simulate conditions with a high Srf concentration, the bacterial cultures were pre-incubated with 30 μM Srf. This protected the Srf producers against GS as evidenced by the increased IC_{50} towards *B. subtilis* ATCC21332 with a significant change (> 175%; $P>0.001$) to 10.7 μM as compared to the IC_{50} towards the non-producer *B. subtilis* OKB120 of 3.8 μM (>75%, $P>0.05$) (Figure 2.1B and C, Table 2.2). Pre-incubation of *B. subtilis* OKB120 with 60 μM Srf also significantly ($P<0.001$) increased the GS IC_{50}

with >250% to 6.1 μM. Table 2.2 summarises the effect of Srf on the antimicrobial activity of GS against the three test organisms.

Table 2.2. Influence of Srf on the antimicrobial activity of GS as measured by changes in IC_{50} of GS toward *M. luteus* NCTC8340 and *B. subtilis* ATCC21332 and OKB120

	***M. luteus* NCTC8340**		***B. subtilis* ATCC21332**		***B. subtilis* OKB120**	
Peptides or combinations	**IC50 (μM)**	**% Δ IC_{50}**	**IC_{50} (μM)**	**% Δ IC_{50}**	**IC_{50} (μM)**	**% Δ IC_{50}**
Srf	inactive	-	inactive	-	inactive	-
GS	7.8 ± 0.8	-	3.5 ± 0.7	-	1.9 ± 0.2	-
30 μM Srf + GS	13.8 ± 1.1[#]	77	10.7 ± 3.7[#]	205	3.8 ± 0.1*	101
60 μM Srf + GS	29.2 ± 0.1[#]	274	-	-	6.2 ± 0.5[#]	226

[#] $P<0.001$ and [*] $P<0.05$ as compared to GS

Next, the dose-dependent antagonism of GS activity by Srf was investigated across a broader concentration range in order to assess the change in the IC_{50} and activity of GS towards the two Srf non-producers, *M. luteus* and *B. subtillis* OKB120, in response to Srf concentration (Figure 2.2). A direct linear trend was observed between the % change in GS IC_{50} and the concentration of Srf for the two Gram-positive target cells (Figure 2.2). However, for *M. luteus* as target organism, synergism between Srf and GS was observed below 8 μM Srf, while *B. subtilis* OKB120 was protected over the whole concentration range. This indicated that a critical concentration, above the critical micelle concentration (CMC) of Srf (9.4 μM in 200 mM $NaHCO_3$ at pH 8.7 [50]) is needed to protect organisms other than the Srf producer. Srf alone did not show any activity against its producer *B. subtilis* at any of the concentrations used and at 60 μM of pre-incubation of the bacteria with Srf, the IC_{50} of GS toward *B. subtilis* and *M. luteus* shifted with > 200%.

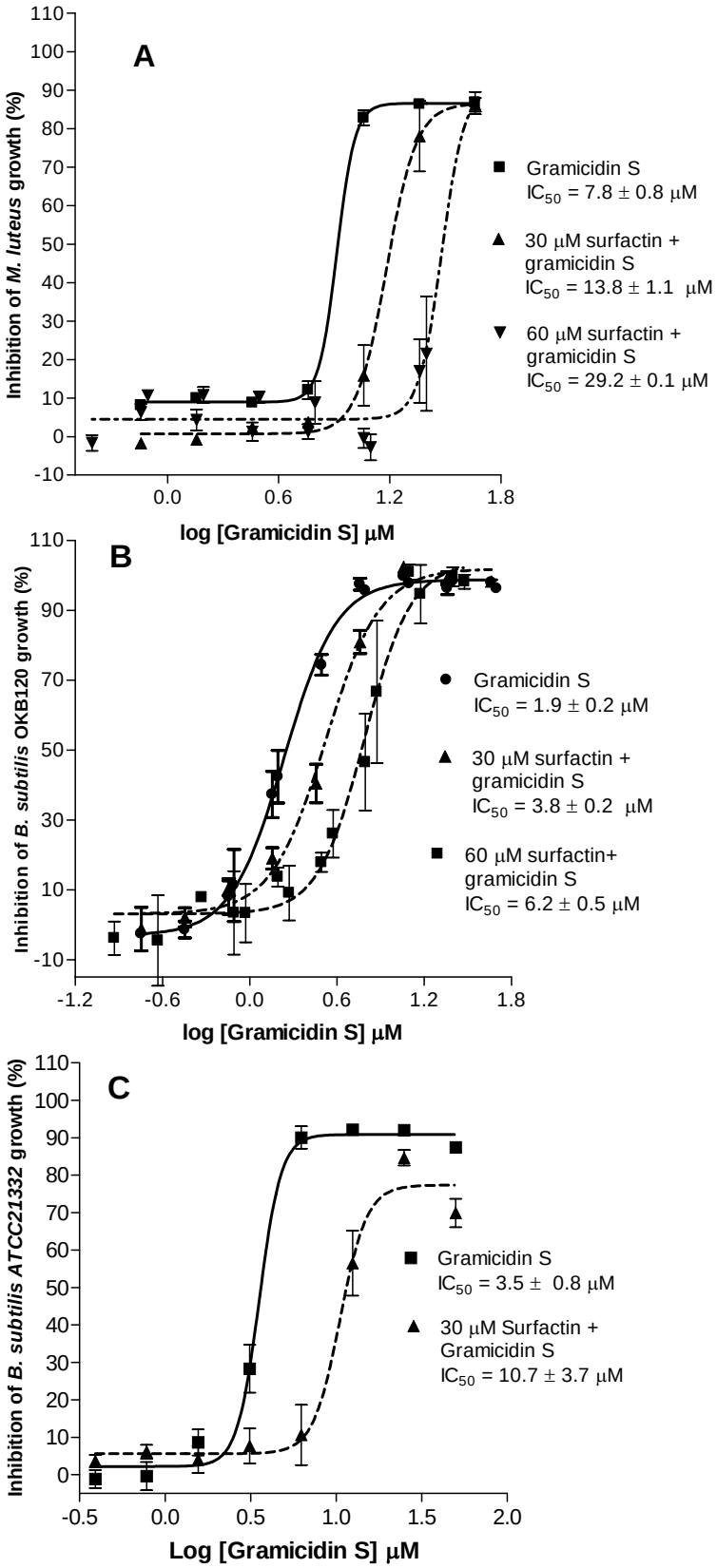

Figure 2.1 Representative results showing dose-response antagonism of the antimicrobial activity of GS toward **A** *M. luteus,* **B** *B. subtilis* OKB120 and **C** *B. subtilis* ATCC21332 by Srf. Standard error of each data point (the average of at least 2 determinations) is shown with $R^2 > 0.99$ for all curves.

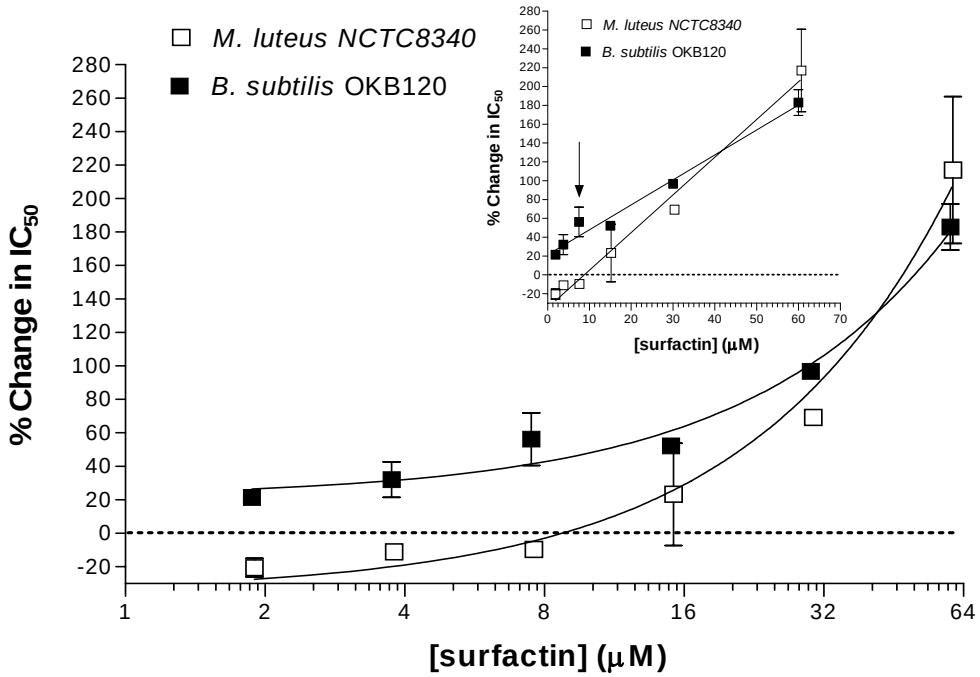

Figure 2.2 Change in IC_{50} and activity of GS toward *B. subtilis* and *M. luteus* in response to Srf concentration. The X-axis is given in log2 scale in order to show more detail on the data points below 8 μM (see arrow in insert). The linear regression lines were fitted with $R^2>0.98$ (see linear line fits in insert). The IC_{50} results were obtained from two independent dose response experiments, each done in quadruplicate.

The influence of Srf, GS and combinations of GS and Srf on the growth rate of the non-Srf producers, *M. luteus* and *B. subtilis* OKB120, was also recorded over 13 hours (Figure 2.3 A, C). It was again observed that Srf protected a number of the cells from lysis by GS, with better survival at about two fold IC_{50} of GS by the Srf producer, *B. subtilis*. However, there was a net decrease in the observed growth rate of both organisms in the presence of Srf (Figure 2.3 B, D) and we observed an unexpected increase in growth rate of the Srf non-producer, *B. subtilis* OKB120 in the presence of 1.6 μM GS (Figure 2.3 D).

In the case of *M. luteus*, Srf showed bacteriostatic activity over the first 8 hours, after which the culture recovered to normal growth rate and biomass (Figure 2.3 A, B). Srf together with 7.5 μM GS also led to recovery and survival of cells, showing similar

growth rate to that with Srf alone (Figure 2.3 B). However, Srf caused visible cell clumping, most probably by encouraging cell aggregation, which led to large variations in OD measurements.

In the presence of Srf the biomass of the *B. subtilis* OKB120 culture in suspension (as measured at 600 nm), were lower in the stationary phase than without Srf (Figure 2.3C). The lower OD at 600 nm is due to biofilm formation, which was visible as films/flakes when the Srf-treated cultures were disturbed. It is known that Srf encourages biofilm formation by increasing the hydrophobicity of its producer [12, 51, 52]. Srf enabled *B. subtilis* to form biofilms by adhering to each other and to the surface of the wells, resulting in a decrease in suspended cells and lower OD at 600 nm. The GS (1.6 μM) + Srf treated cultures recovered within six hours (360 minutes) to the same suspended biomass than the cultures treated with Srf alone (Figure 2. 3 C). This result indicated the role of Srf-dependent biofilm formation [12, 51, 52] in resistance towards GS. Cell viability assays using Cell Titer Blue^{TM} dye [53-55] showed that Srf did not cause any loss in viability of *B. subtilis* (results not shown).

The low concentration GS (1.6 μM) caused a substantial increase in the growth rate of the surviving *B. subtilis* OKB120 from $\mu = 0.34$ to 0.44 (Figure 2.3 B). This could be due to a stress condition caused by the presence of GS, which triggered cell proliferation. In the pre-incubated cultures, Srf protected *B. subtilis* OKB120 against complete killing by GS.

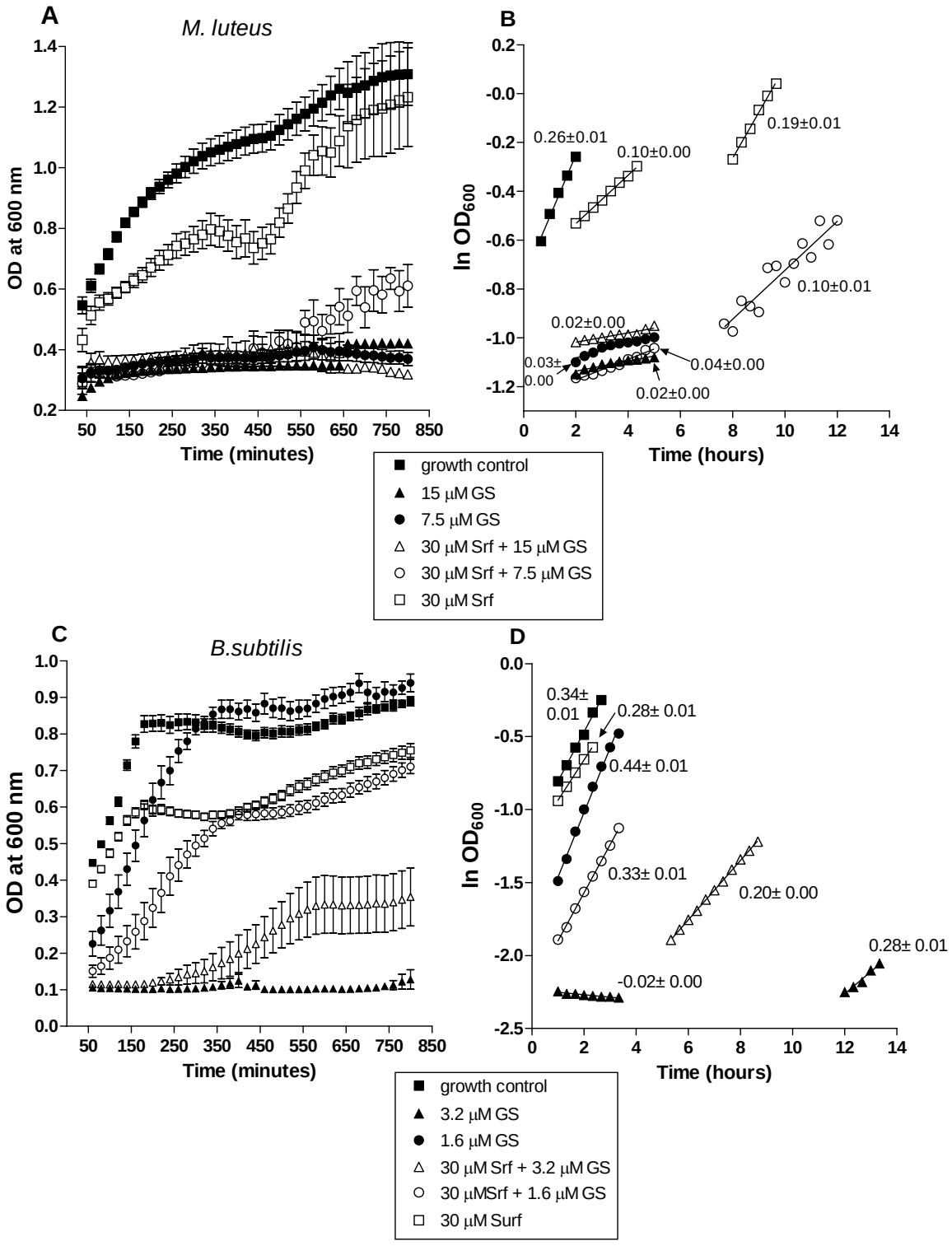

Figure 2.3 Average growth curves over 780 minutes of *M. luteus* (A) and *B. subtilis* OKB120 (C) cultures and the translated growth rate curves of *M. luteus* (B) and *B. subtilis* OKB120 (D) in the presence/absence of Srf, GS and combinations of GS and Srf. The error bars in A and C show the SEM of OD_{600} of at least 15 cultures from three independent experiments. The numbers in B and C are the calculated μ (growth rate in $\Delta \ln OD_{600}$/hour).

At high GS concentration (3.1 μM) most of the cells were lysed before they had time to adapt, as in the OD_{600} decreased without visible biofilm formation. However, in certain wells incubated with 3.1 μM GS, where no growth was expected, persistent cells were observed to survive. These particular experiments represented a 4/21 (±20%) survival (cultures with OD_{600} >0.20 indicating survival and growth) of *B. subtilis* cultures incubated with 3.1 μM GS ($2\times IC_{50}$) for 780 min, while cultures pre-incubated with 30 μM Srf and 3.1 μM GS presented a 9/22 (±40%) survival. A similar survival pattern of >35% survival of *B. subtilis* ATCC21322 in the presence of $2\times IC_{50}$ GS was found, but without the addition of Srf. This survival pattern was not observed for *M. luteus*.

LCMS investigation of M. luteus *treated with gramicidin S and surfactin*

Our results strongly indicated that Srf dependent biofilm formation of *B. subtilis* plays a role in the observed GS resistance. However, Srf also protected other types of microorganisms, such as *M. luteus*, *Penicillium* cf. *corylophilum* [17] and *Escherichia coli* HB 101 against GS activity [17], therefore the role of Srf in GS antagonism may be broader than inducing biofilm formation. *M. luteus* was used as target cell to assess the role of solution phase complexation with GS and cell wall trapping of GS in the presence of Srf. Previously Vlok [17] observed complex formation in an 1:1 mixture of the Srf and GS under ESMS conditions. A more detailed biophysical characterisation of the GS and Srf complex and possible conformational changes in GS structure due to Srf presence is discussed in Chapter 3. The influence of Srf on the recovery of GS from a bacterial culture was investigated utilising ultra-performance liquid chromatography linked to electrospray mass spectrometry (UPLC-MS). The present chapter describes a study of the site of these interactions using the "supernatant cell" assay. *M. luteus* in

saline (0.9% NaCl) was incubated with the two peptides in a 1:1 combination for 30 minutes. Cells and debris were then removed by centrifugation, and the supernatant analysed by LC-ESMS (Figures 2.4 and 2.5).

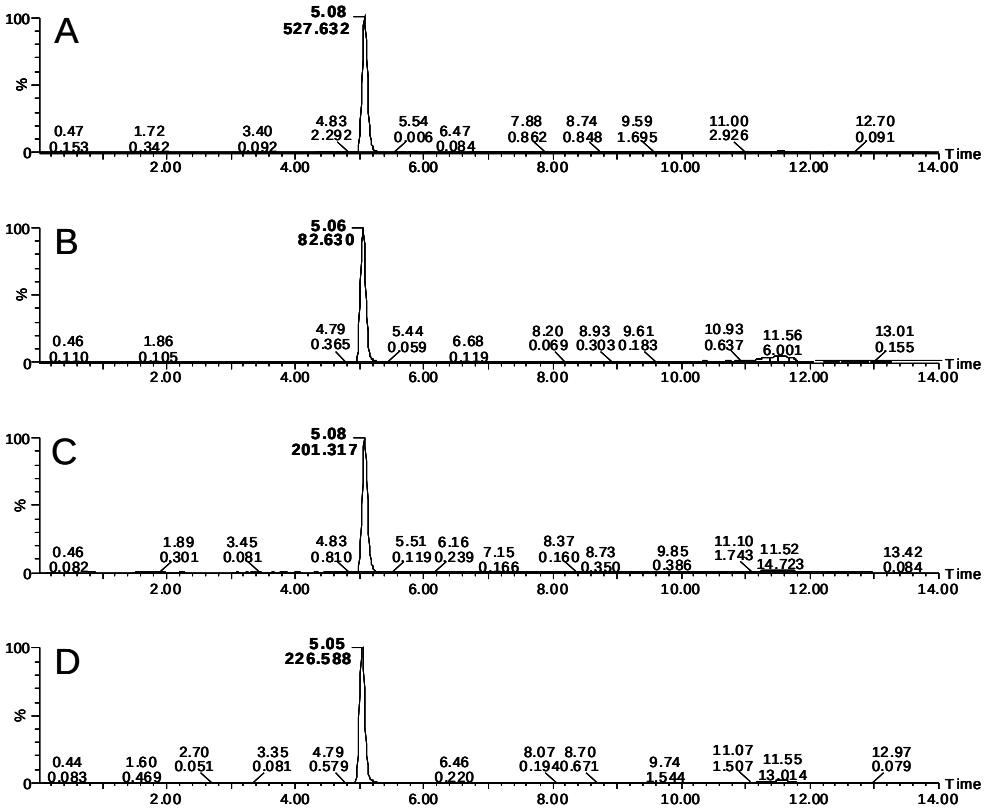

Figure 2.4 Representative UPLC-MS chromatograms of the recovery of $[M+2H]^{2+}$ (*m/z* 572) molecular ion of GS from different reaction mixtures after 30 minute incubation: A 5.0 μM GS alone; B 5.0 μM GS + 30 μM Srf; C. *M. luteus* + 5.0 μM GS; D. *M. luteus* + 5.0 μM GS + 30 μM Srf. The Y-axis shows % signal intensity; the X-axis the run time in minutes; the top value with each peak denotes the retention time and the bottom value, the peak area.

From the UPLC-MS analysis of the supernatants, the peak areas of all GS molecular species were recorded (Figure 2.4) and the percentage recovery of GS was calculated for the samples of GS alone (GS) and for samples of GS in combination with cells (GS + cells), Srf (GS + Srf) and GS plus Srf plus cells (GS + Srf + cells) (Figure 2.5A). The results showed a similar percentage recovery of GS between samples of GS + cells, GS

+ Srf, and GS + Srf + cells (28-41%). There was a lower GS recovery when both Srf and cells were present (about 24%). Results indicated that Srf at 30 μM removed similar amounts of GS (related to detected peak area) than *M. luteus* (OD of 0.20 at 600 nm).

Determination of *M. luteus* survival in the isolated bacterial pellets after 16 hours incubations again showed an improved cell survival in the presence of Srf (Figure 2.5B). About 50% of cells survived after exposure to 5 μM GS over the incubation period. Srf caused the cells to aggregate and also led to lower growth due to bacteriostatic action, which may explain the fact that only 75% of the expected growth was observed in the presence of Srf. This may also be an underestimation due to the protocol (centrifugation and re-suspension) since the micro-broth assays have shown that at 5 μM GS and/or 30 μM Srf, more than 90% of cells survived. However, in the absence of Srf an inverse correlation was found between growth and the GS detected via UPLC-MS (Figure 2.5). This correlation was mimicked in the presence of Srf when no cells were present (Figure 2.5).

The UPLC-MS results indicated that both the cell wall and solution phase are sites of GS antagonism by Srf which explains why Srf shifted the dose-response curves of GS toward antagonism with both *B. subtilis* and *M. luteus* as target cells. However, there was some selectivity between the two target cells with regard to the action of Srf towards GS. Below the "critical" Srf concentration (below the CMC of Srf) the combination with GS resulted in synergetic action. This may indicate the antagonistic role of micellar Srf, trapping GS (solution phase interaction) at higher concentrations. In *B. subtilis* Srf caused significant antagonism of the antimicrobial activity of GS over the entire concentration range used, indicating the role of cell wall associated Srf in

antagonism, albeit as an integral factor of biofilm formation or acting as a shield-like trapping agent of GS.

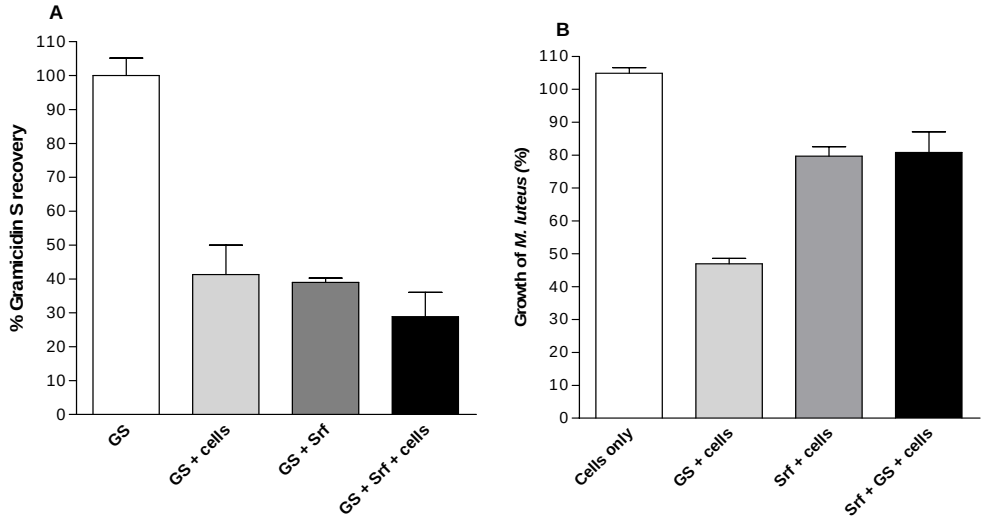

Figure 2.5 Bar-graph representation of the **A.** LC-ESMS detection of GS ion species for samples of GS, GS and cells, GS and Srf) and the combination of GS, Srf and cells) GS recovery differed significantly ($P>0.001$) between the GS control sample (first bar) and other three samples; SEM are shown for 6-12 determinations each. B. *M. luteus* growth after exposure to GS (GS + cells), Srf (Srf+Cells) and GS-Srf mixture (Srf + GS + cells). GS treated cell growth were significantly lower than cells alone ($P<0.001$) and cells pre-incubated with Srf ($P<0.01$). No significant difference between cells growth after treatment with Srf and treatment with Srf and GS.

Surfactin assisted survival in mixed cultures

The question remained if there is a real survival benefit for the Srf producer in mixed cultures challenged with GS. In mixed cultures of *M. luteus* and *B. subtilis* OKB120 the addition of 30 μM Srf caused an increase in *B. subtilis* OKB120 colony spreading on agar, but about 30% decrease of the *M. luteus* CFUs (results not shown). *B. subtilis* colonies also out-competed nearby colonies of *M. luteus,* which was assisted by the Srf induced spreading. The 5 μM GS killed >90% of *B. subtilis* OKB120 and ±50% of *M.*

luteus. When the mixed cultures were challenged with 5 μM GS, in the presence of 30 μM Srf, survival of *B. subtilis* increased dramatically to 80%, but only marginally to 58% for *M. luteus* (results not shown).

To further investigate if Srf protects its producers in mixed culture, the GS producer *A. migulanus* ATCC9999 was co-cultured on TGYM agar gel in close proximity with each of the two *B. subtilis* strains; the Srf producer *B. Subtilis* ATCC21332 and the Srf non-producer *B. subtilis* OKB120 (Figure 2.6).

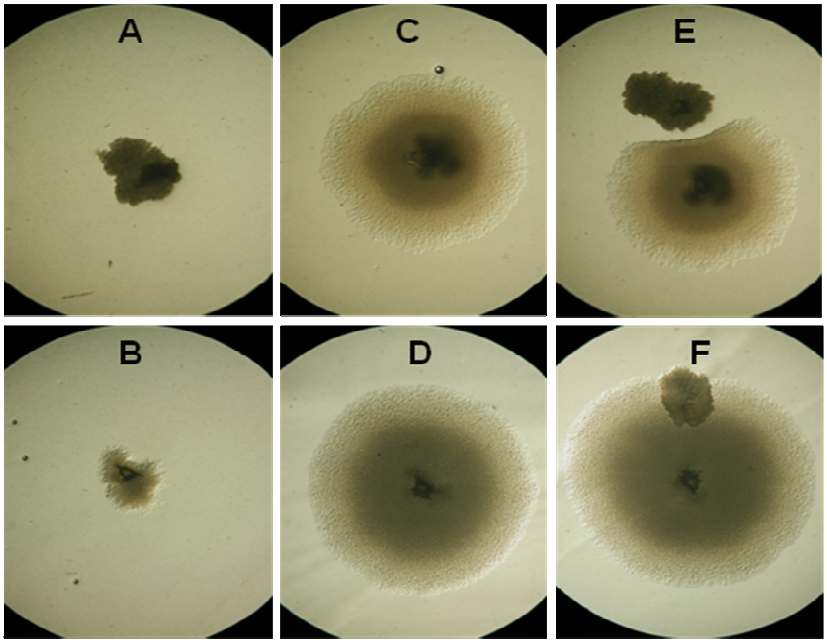

Figure 2.6 Evidence of the co-survival between colonies of *Bacillus* strains grown in TGYM agar for 24h at 37°C. Each of the plates depicts a 15× enlarged image of an individual colony or two bacterial colonies placed in close proximity. **A** and **B** show the GS producer *A. migulanus* ATCC9999, **C** the Srf non-producer *B. subtilis* OKB120 and **D** the Srf producer *B. subtilis* ATCC21332. Close proximity colonies of the GS producer *A. migulanus* ATCC9999, with **E** the Srf non-producer *B. subtilis* OKB120 and **F** the Srf producer *B. subtilis* ATCC21332, respectively.

B. subtilis ATCC21332 grew and survived in the presence of *A. migulanus* ATCC9999, with the colonies of the GS producer actually being surrounded by the Srf producer in

the absence of inhibition zones (Figure 2.6 F). However, *A. migulanus* ATCC9999 out-competed the non-Srf producer *B. subtilis* OKB120 causing a decrease in its colony growth showing an inhibition zone at the interphase between the colonies (Figure 2.6 E). Colonies of the GS producer *A. migulanus* ATCC9999 and the Srf producer *B. subtilis* ATCC21332 were able to cohabit on solid media, while the growth of the Srf non-producer *B. subtilis* OKB120 was out-competed by *A. migulanus* ATCC9999.

Similar results were also found when the colonies were cultured in close proximity on TGYM agar gel seeded with *M. luteus* (results not shown). *A. migulanus* ATCC9999 and *B. subtilis* ATCC21332 caused inhibition zones in *M. luteus* seeded gel around both the organisms, with a smaller zone for *B. subtilis* ATCC21332 which survived within the inhibition zone of *A. migulanus* ATCC9999. *A. migulanus* ATCC9999 also caused a decrease in *B. subtilis* OKB120 colony size on TGYM agar gel seeded with *M. luteus*. *B. subtilis* OKB120 did not cause any *M. luteu*s inhibition zones, indicating low or no Srf production.

In an alternative mixed culture assay, the *B. subtilis* strains was seeded in TGYM agar and challenged when GS producing *A. migulanus* colonies were placed on the agar. After two days visible inhibition zones formed around the GS producer in the *B. subtilis* OKB120 seeded gel, which became larger, but more diffuse around the edges after eight days (result not shown). *A. migulanus* showed no inhibition towards *B. subtilis* ATCC21332 after two or eight days and the two organisms seem to survive in the same culture. No clear inhibition zone was noticeable in the *B. subtilis* ATCC21332 seeded gel around *A. migulanus* colonies, possibly because it produced Srf which protected it against GS from *A. migulanus*. These results indicate that direct antagonism of GS by

Srf is part of the *B. subtilis* resistance mechanism and that the presence of Srf can protect its producer.

ESMS analyses of extracts from the producer cultures confirmed that both *A. migulanus* ATCC9999 and *B. subtilis* ATCC21332 were able to produce GS and Srf respectively (results not shown), while *B. subtilis* OKB120 do not produce Srf under our experimental conditions.

Influence of surfactin on gramicidin S on erythrocytes

In order to assess the role of the target cell and target cell membrane in the influence of Srf on GS we also investigated the activity of GS and Srf on erythrocytes as GS and Srf have known haemolytic activity [29, 41].

The HC_{50} of GS was found to be 6.8 µM and 19.5 µM for Srf. The peptide mixture had an HC_{50} value of 6.3 µM each (Table 2.3). The fractional haemolytic concentration (FHC) for the haemolytic activity was 1.25. If the FHC index is >1 it is assumed that the combination is antagonistic while if FHC index is <1 it is assumed that the combination is synergistic [49]. The FHC of 1.25 indicate only slight antagonism of haemolytic activity by the combination of GS and Srf (Table 2.3). This suggested that for normal erythrocytes the solution phase interaction of the two peptides may not lead to totally inactive complexes.

Table 2.3. Summary of the haemolytic activity parameters of GS and Srf. Values are the average of two determinations (each in quadruplicate) ± SEM.

Peptides	HC_{50} (μM)	HC_{50} in 1:1 combination (FHC)
Srf	19.5 ± 1.0	6.3 ± 0.4 (0.32)
GS	6.8 ± 0.7	6.3 ± 0.4 (0.93)
FHC index	-	1.25

Discussion

Results from this study corroborated the findings of Vlok [17], as we again observed that the activity of the amphipathic antimicrobial peptide GS was antagonised by the lipopeptide Srf. For *M. luteus,* antagonism of GS occurred at high Srf concentrations (above 8 μM which is above the CMC of Srf [50]) while synergism with GS was observed at low Srf concentrations, lowering the IC_{50} of GS toward *M. luteus*. The synergism may result from additive actions since both peptides have antimicrobial activities against Gram-positive bacteria [27, 37]. Srf has the potential to cause positive curvature stress in a biological membrane resulting in membrane fluidisation [56]. This fluidisation could facilitate GS action on a *M. luteus* membrane. However, GS antagonism took place at high Srf concentrations, above the CMC of Srf, when target cells were pre-incubated with Srf [50]. When the bacteria were pre-incubated with Srf, it is possible that the pre-absorbed Srf [50], as well as Srf micelles interacted with GS prevented it from reaching the membrane target. Our UPLC-MS determination of GS recovery from the GS-Srf mixtures and/or *M. luteus* mixtures indicated that both cell wall and solution phase interaction may be important in the GS antagonism by Srf. It was previously found that the two peptides formed complexes in solution phase, as

revealed by ESMS [17]. These complexes may be inactive and result in the observed antagonism. A more detailed study on the molecular aspect of the GS-Srf complexes is described in Chapter 3.

Srf was shown to also antagonise the antimicrobial activity of GS towards *B. subtilis* OKB120 and *B. subtilis* ATCC21332, with the latter strain being significantly less sensitive than the former towards GS. We demonstrated that *B. subtilis* OKB120 did not produce Srf under the culture conditions, hence the effects observed resulted only due to Srf addition, while *B. subtilis* ATCC21332 did produce Srf under our culture conditions. When *B. subtilis* OKB120 was pre-incubated with different concentrations of Srf, dose-dependent antagonism of GS activity was observed even at the lowest concentration of 0.9 μM Srf.

It was also found that *B. subtilis* OKB120 had better survival in a mixed culture with *M. luteus* and the addition of Srf protected *B. subtilis* OKB120 cells against GS better than it protected *M. luteus* cells. In a co-culture assay the Srf producer *B. subtilis* ATCC21332 grew in the inhibition zone of the colonies from the GS producer *A. migulanus* ATCC9999, while *B. subtilis* OKB120 growth was inhibited.

A decrease in the overall observed growth rate of both *M. luteus* and *B. subtilis* OKB120 was observed when they were grown in the presence of Srf, which is probably due to cell clumping/bacteriostatic Srf activity and biofilm formation [12, 50, 51], respectively. Srf and iturin A have the potential to absorb to the *B. subtilis* surface and modify its hydrophobicity [50, 51]. Srf arranges itself so that its acidic groups interact with the membrane head groups while its fatty acid tail is exposed to the environment, making the membrane more hydrophobic, in hydrophilic *B subtilis* strains [50]. Srf may have enabled cells, in particular *B. subtilis* to adhere to each other and the surface of the

microtiter plate wells forming biofilms [50] reducing the number of suspended cells. Cell viability assays showed that Srf did not cause significant growth inhibition of *B. subtilis*. The antagonism of GS activity may be the consequence of increased hydrophobicity caused by Srf on the surface of its producer and masking of cell wall targets of GS. The Srf induced formation of *B. subtilis* biofilms [12, 50, 51] will further protect the inner cells against GS. GS could also be trapped by complexation with membrane-absorbed Srf molecules [12, 50, 51], by micellar Srf or by direct complexation with Srf to form inactive complexes. Any or all of these interactions could result in antagonism of GS activity and protection of the target cell.

The results from the haemolysis assays showed that the effect of the combination of GS with Srf on human erythrocytes was only slightly antagonistic. The complexation between GS and Srf may cause a shielding of the cationic hydrophilic side of GS which is important for its binding to the negative bacterial targets [27, 57], but not neutral eukaryotic cells. On normal erythrocytes these electrostatic interactions may not play such a crucial role in the lytic mode of action of GS and therefore little effect was observed. According to Ketsu *et al.* [28, 29], GS molecules embed in the lipid membrane of erythrocytes from its hydrophobic side with the two cationic Orn residues protruding into the hydrophilic interface. The accumulation of GS in the erythrocyte membrane leads to a deformation and release of phospholipids which leads to lysis through small lesions [28, 29]. This indicates that the antagonism of GS activity by Srf may be target membrane specific.

Conclusions

This study showed that peptides from *Bacillus* species, such as Srf, may have an alternative protective function for improving the survival of its producer strains and allowing it to cohabit with other bacilli. This peptide may shield important groups of GS and/or GS targets that are essential for its membrane interaction and lytic action, as well as induce protective biofilm formation in *B. subtilis* and cell clumping in *M. luteus*. However, the group(s) in GS may not be absolutely essential for the lysis of normal erythrocyte membranes and therefore little change in effect was observed for the combination. Our results indicated that the antagonism is target membrane specific and that antagonism may take place both in the solution and on the cell wall.

The antagonism of GS by Srf may be a unique phenomenon as previous studies by Vlok [17] indicated that complex formation between GS and Srf may lead to antagonism. In Chapter 3 we report a biophysical investigation of the influence of Srf and GS on each other's structure. It is possible that similar antagonistic actions may also occur among and towards other *B. aneurinolyticus* peptides such as the linear Grcs and the Trcs. The pure peptides from the tyrothricin complex are not commercially available. Chapter 4 describes the development and optimisation of two C_{18} reverse phase HPLC methods for the purification and analysis of the Trcs and Grcs from the tyrothricin complex of *B. aneurinolyticus*. Chapter 5 describes the testing of the purified Trcs and Grcs for antagonistic and synergistic actions with Srf and each other.

References

1 Sande, A. M. and Mandell, L. G. (1985) Section XII: Chemotherapy of microbial diseases: Antimicrobial agents, general consideration, In: The pharmacological basis of therapeutics, 7th ed. Eds. A.G. Gilima, L. S. Goodman, T. W. Rall and F. Murad. Macmilan Publishing Company, New York, pp.1066-1094

2 Rice, L. (2001) Evolution and clinical importance of extended-spectrum β-Lactamases. Chest. **19**, 391-396

3 Walsh, C. T. (2000) Molecular mechanisms that confer antibacterial drug resistance. Nature. **406**, 775-781

4 Alpuche, C., Garau, J. and Lim, V. (2007) Global and local variation in antimicrobial susceptibilities and resistance development in major respiratory pathogens. Int. J. Antimicrob. Agents. **30**, 135-138

5 Harris, M., Mora-Montes, H. M., Gow, N. A. R. and Coote, P. J. (2009) Loss of mannosylphosphate from *Candida albicans* cell wall proteins results in enhanced resistance to the inhibitory effect of a cationic antimicrobial peptide via reduced peptide binding to the cell surface. Microbiology. **155**, 1058-1070

6 Paulsen, I. T., Brown, M. H. and Skurray, R. A. (1996) Proton-dependant multi-drug efflux systems. Antimicrob. Agents Chemoter. **60**, 575-608

7 Levy, S. B. (1992) Active efflux mechanisms for antimicrobial resistance. Antimicrob. Agents Chemoter. **36**, 695-703

8 Bengoechea, J. A. and Skurnik, M. (2000) Temperature-regulated efflux pump/potassium antiporter system mediates resistance to cationic antimicrobial peptides in *Yersinia*. Mol. Microbiol. **37**, 67-80

9 Davis, J. (1994) Inactivation of antibiotics and the desamination of resistant genes. Science. **264**, 375-382

10 Nezil, F. A. and Bloom, M. (1992) Combined influence of cholesterol and synthetic amphiphilic peptides upon bilayer thickness in model membranes. Biophys. J. **61**, 1176-1182

11 O'Connell, H. A., Koltkamp, G. S., Eppelbaum, J. L., Stubblefield, B. A., Gilbert, S. E. and Gilbert, E. S. (2006) Influence of biofilm structure and antibiotic resistance mechanisms on indirect pathogenicity in a model polymicrobial biofilm. Appl. Environ. Microbiol. **72**, 5013-5019

12 Bais, H. P., Fall, R. and Vivanco, J. M. (2004) Biocontrol of *Bacillus subtilis* against infection of arabidopsis roots by *Pseudomonas syringae* is facilitated by biofilm formation and surfactin production. Plant Physiol. **134**, 307-319

13 Davies, D. G., Parsek, M. R., Pearson, J. P., Iglewski, B. H., Costerton, J. W. and Greenberg, E. P. (1998) The involvement of cell-to-cell signals in the development of a bacterial biofilm. Science. **280**, 295-298

14 Xu, K. D., McFeters, G. A. and Stewart, P. S. (2000) Biofilm resistance to antimicrobial agents. Microbiology. **146**, 547-549

15 Stewart, P. S. and Costerton, J. W. (2001) Antibiotic resistance of bacteria in biofilms. The Lancet. **358**, 135-138

16 Morikawa, M. (2006) Beneficial biofilm formation by industrial bacteria *Bacillus subtilis* and related species. J. Biosci. Bioeng. **101**, 1-8

17 Vlok, N. M. (2005) Investigation of complexation and antimicrobial activity of gramicidin S in the presence of lipopeptides from *Bacillus subtlis*. PhD thesis, University of Stellenbosch, Stellenbosch

18 Forrer, C. B., Blahy, D. M., Mariatico, A. L., Campos, J. M. and Freeman, H. M. (1982) Comparison of vancomycin and penicillin for viral isolation. J. Clin. Microbiol. **16**, 295-298

19 Shida, O., Takagi, H., Kadowaki, K. and Komagata, K. (1996) Proposal for two new genera, Brevibacillus gen. nov. and Aneurinibacillus gen. nov. Int. J. Syst. Bacteriol. **48**, 939-946

20 Frangou-Lazaridis, M. and Seddon, B. (1985) Effect of gramicidin S on the transcription system of the producer *Bacillus brevis* Nagano. J. Gen. Microbiol. **131**, 437-449

21 Kanda, M., Ohgishi, K., Hanawa, T. and Saito, Y. (1997) Arginase of bacillus brevis nagano: purification, properties, and implication in gramicidin S biosynthesis. Arch. Biochem. Biophys. **344**, 37-42

22 Arima, K., Kakinuma, A. and Tamura, G. (1968) Surfactin, a crystalline peptide lipid surfactant produced by *Bacillus subtilis*: isolation, characterization and its inhibition of fibrin clot formation. Biochem. Biophys. Res. commun. **31**, 488-494

23 Sandrin, C., Peypoux, F. and Michel, G. (1990) Coproduction of surfactin and iturin A, lipopeptides with surfactant and antifungal properties, by *Bacillus subtilis*. Biotechnol. Appl. Biochem. **12**, 370-375

24 Mihailescou, D. and Smith, J. C. (2000) Atomic detail peptide-membrane interactions: Molecular dynamics simulation of gramicidin S in a DMPC bilayer. Biophys. J. **79**, 1718-1730

25 Mihailescou, D. and Smith, J. C. (1999) Molecular dynamics simulation of the cyclic decapeptide antiotic, gramicidin S, in dimetyl sulfoxide solution. J. Phys. Chem. B. **9**, 1586-1594

26 Grotenbreg, G. M., Timmer, M. S. M., Llamas-Saiz, A. L., Verdoes, M., Van der Marel, G. A., Va Raaij, M. J., Overkleeft, H. S. and Overhand, M. (2004) An unusual reverse turn structure adopted by a furanoid sugar acid incorporated in gramicidin S. J. Am. Chem. Soc. **126**, 3444-3446

27 Kondejewski, L. H., Farmer, S. W., Wishart, D. S., Hancock, R. E. W. and Hodges, R. S. (1996) Gramicidin S is active against both Gram-positive and Gram-negative bacteria. Int. J. Pept. Protein Res. **47**, 460-466

28 Katsu, T., Kuroko, M., Morikawa, T., Sanchika, K., Fujita, Y., Yamamura, H. and Uda, M. (1989) Mechanism of membrane damage induced by the amphipatic peptides gramicidin S and melittin. Biochim. Biophys. Acta. **983**, 135-141

29 Katsu, T., Ninomiya, C., Kuroko, M., Kobayashi, H., Hirota, T. and Fujita, Y. (1988) Action mechanism of amphipathic peptides gramicidin S and melittin on erythrocyte membrane. Biochim. Biophys. Acta. **939**, 57-63

30 Danders, W., Marahiel, A. M., Krause, M. I., Kosui, N., Kato, T., Izumiya, N. and Kleinkauf, H. (1982) Antibacterial action of gramicidin S and tyrocidines in relation to active transport, *in vitro* transcription, and spore outgrowth. Antimicrob. Agents Chemother. **22**, 785-790

31 Lazaridis, I., Frangou-Lazaridis, M., Maccuish, F., Nandi, S. and Seddon, B. (1980) Gramicidin S content and germination and outgrowth of *Bacillus brevis* Nagano spores. FEMS Microbiol. Lett. **7**, 229-232

32 Nandi, S. and Seddon, B. (1978) Evidence for gramicidin S functioning as a bacterial hormone specifically regulating spore outrowth in *Bacillus brevis* Nagano. Biochem. Soc. Trans. **6**, 409-411

33 Jelokhani-Niaraki, M., Kondejewski, L. H., Farmer, S. W., Hancock, R. E. W., Kay, C. M. and Hodges, R. S. (2000) Diasteroisomeric analogues of gramicidin S: Structure, biological activity and interaction with lipid bilayers. Biochem. J. **349**, 747-755

34 Staudegger, E., Prenner, E., Kriechbaum, M., Degovics, G., Lewis, R. N. A. H., McElhaney, R. N. and Lohner, K. (2000) X-ray studies on the interaction of the antimicrobial peptide gramicidin S with microbial lipid extracts: evidence for cubic phase formation. Biochim. Biophys. Acta. **1468**, 213-230

35 Bonmatin, J. M., Laprevote, O. and Peypoux, F. (2003) Diversity among microbial cyclic lipopeptides: iturins and surfactins. Activity-structure relationships to design new bioactive agents. Comb. Chem. High Throughput Screening. **6**, 541-556

36 Gallet, X., Deleu, M., Razafindralambo, H., Jacques, P., Thomart, P., Paquot, M. and Brasseur, R. (1999) Computer simulation of surfactin conformation at a hydrophobic/hydrophilic interface. Langmuir. **15**, 2409-2414

37 Rodrigues, L., Banat, I. M., Teixeira, J. and Oliveira, R. (2006) Biosurfactants: potential applications in medicine. J. Antimicro. Chemother. **57**, 609-618

38 Kim, K. (1998) Suppression of inflammatory responses by surfactin, a selective inhibitor of platelet cytosolic phospholipase A2. Biochem. Pharmacol. **55**, 975-985

39 Vollenbroich, D. (1997) Antimycoplasma properties and applications in cell culture of surfactin, a lipopeptide antibiotic from *Bacillus subtilis*. Appl. Environ. Microbiol. **63**, 44-49

40 Vollenbroich, D., Ozel, M., Vater, J., Kamp, R. M. and Pauli, G. (1997) Mechanism of inactivation of enveloped viruses, by the biosurfactant surfactin from *Bacillus subtilis*. Biologicals. **25**, 289-297

41 Dufour, S., Deleu, M., Nott, K., Wathelet, B., Thonart, P. and Paquot, M. (2005) Hemolytic activity of new linear surfactin analogs in relation to their physico-chemical properties. Biochim. Biophys. Acta. **1726**, 87-95

42 Liu, X., Huang, W. and Wang, E. (2005) An electrochimical study on the interaction of surfactin with a supported bilayer lipid on a glassy carbon electrode. J. Electroanal. Chem. **577**, 349-354

43 Maget-Dana, R. and Ptak, M. (1995) Interaction of surfactin with membrane models. Biophys. J. **68**, 1937-1943

44 Chen, H.-L. and Juang, R.-S. (2008) Recovery and separation of surfactin from pretreated fermentation broths by physical and chemical extraction. Biochem. Eng. J. . **38**, 39-46

45 Symmank, H., Franke, P., Saenger, W. and Bernhard, F. (2002) Modification of biologically active peptides: production of a novel lipohexapeptide after engineering of *Bacillus subtilis* surfactin synthetase. Prot. Eng. **15**, 913-921

46 Davis, D. A., Lynch, H. C. and J., V. (1999) The production of surfactin in batch culture by *Bacillus subtilis* ATCC21332 is strongly influenced by the conditions of nitrogen metabolism. Enz. Microb. Technol. **25**, 322–329

47 Rautenbach, M., Gerstner, G. D., Vlok, M., Kulenkampff, J. and Westerhoff, H. V. (2006) Analyses dose-response curves, to compare the antimicrobial activity of model cationic α-helical peptides, highlights the necessity for a minimum of two active parameters. Anal. Biochem. **350**, 81-90

48 Du Toit, E. A. and Rautenbach, M. (2000) A sensitive standardised micro-gel well diffusion assay for the determination of antimicrobial activity. J. Microbiol. Methods. **1**, 159-165

49 Hall, M. J., Middleton, R. F. and Westmacott, D. (1982) The fractional inhibitory concentration (FIC) index as a measure of synergy. J. Antimicro. Chemother. **11**, 427-433

50 Ishigami, Y., Osman, M., Nakahara, H., Sano, Y., Ishiguro, R. and Matsumoto, M. (1995) Significance of β-sheet formation for micellization and surface absorption of surfactin. Coillois Surf., B. **4**, 341-348

51 Ahimou, F., Jacques, P. and Deleu, M. (2000) Surfactin and iturin A effects on *B. subtilis* hydrophobicity. Enzyme Microbiol. Technol. **27**, 749-754

52 Hamon, M. A. and Lazazzera, B. A. (2001) The sporulation transcription factor Spo0A is required for biofilm development in *Bacillus subtilis*. Mol. Microbiol. **42**, 1199-1209

53 O'Brien, J., Wilson, I., Orton, T. and Pognan, F. (2000) Investigation of the Alamar Blue (resazurin) fluorescent dye for the assessment of mammalian cell cytotoxicity. Eur. J. Biochem. **267**, 5421-5426

54 Anon. (2002) CellTiter-Blue™ cell viability assay, Promega™ technical bulletin. p. 317, Madison

55 Niles, A. L., Moravec, R. A. and Riss, T. L. (2009) In vitro viability and cytotoxicity testing and same-well multi-parametric combinations for high throughput screening. Curr. Chem. Genomics. **3**, 33-41

56 Heerklotz, H., Wieprecht, T. and Seelig, J. (2004) Membrane pertubation by the lipopeptide surfactin and detergents as studied by deuterium NMR. J. Phys. Chem. **108**, 4909-4015

57 Nagamurthi, G. and Rambhav, S. (1985) Gramicidin-S: Structure-activity relationship. J. Biosci. **7**, 323-329

Chapter 3

Biophysical characterisation of the intermolecular interaction between the antagonistic antimicrobial peptides, surfactin and gramicidin S

Introduction

Vlok [1] observed non-covalent complexes between the *Bacillus subtilis* peptide surfactin (Srf) and gramicidin S (GS) from *Aneurinibacillus migulanus,* by using electrospray mass spectrometry (ESMS). If these complexes form in solution phase, this complexation is possibly related to the antagonism of the antimicrobial activity of GS by Srf toward *Micrococcus luteus* and *Bacillus subtilis* strains (OKB120 and ATCC21332) discussed in Chapter 2. Complex formation between these two peptides may be a general defence mechanism, which also extends to other related peptides such as the cyclic tyrotricines (Trcs) and linear gramicidins (Grcs) from *Bacillus aneurinolyticus* (refer to Chapter 5). Therefore, characterising possible non-covalent complex formation and/or structural influence of GS by Srf would enhance our understanding of this protective and putative resistance mechanism.

GS has two free amino groups (basic groups) from the two ornityl (Orn) residues [2] while Srf has two free acidic groups from both the Asp and Glu residues [3]. Non-specific complexation between GS and Srf could involve electrostatic interactions between these two basic groups of GS and the two acidic groups of Srf, but if there is specific recognition between the two peptides, hydrogen bonding would be important. The techniques used in this study, among the variety of physical and analytical techniques utilised for structural analysis and for probing non-covalent

interactions in molecules, were ESMS, circular dichroism (CD) and nuclear magnetic resonance spectroscopy (NMR).

ESMS is a chemical analysis technique used, for example, to determine the mass and primary structure of peptides [4]. First, ionised peptides in solution are transferred to gas phase via the electrospray source where further ionisation can take place. Second, the ionised peptides pass through a mass analyser where they are detected according to their mass-to-charge ratio (*m/z*). Electrospray ionisation can generate either singly or multiple charged ions [5]. Ions are formed in solution either from complexation with metal ions ($[M+Na]^+$, $[M+K]^+$) or from an acid-base reaction ($[M+H]^+$, $[M-H]^-$). Since ionisation in ESMS is carried out in solution, it is regarded as a suitable technique for probing non-covalent interactions between molecules [4, 6-8]. Likewise, tandem mass spectrometry, also denoted as MS-MS [9, 10], allows the *de novo* sequence determination of a compound and can in theory be used to determine the site of interactions between molecules in a non-covalent complex.

MS-MS makes use of collision induced dissociation (CID) to fragment peptides and is generally used to deduce information regarding their amino acid sequence. One of the prerequisites in the fragmentation of cyclic peptides is the controlled opening of the backbone ring. For GS, the ring opening mostly occurs at one of the Pro residues. However, for Srf the opening of the ring occurs at the lactone bond. This technique can be used to obtain information regarding the residues involved in the interaction of fragmented GS-Srf complexes as the peptide bonds of the residues involved in the interaction may be more protected from CID.

CD is based on the interaction of optically active molecules with polarized light which gives information of chirality and organized hydrogen bonded structures. Biological molecules, such

as peptides, are able to absorb polarized light and will give a distinct characteristic UV-CD absorption spectrum based on their secondary structure, comprising for example of α-helixes and β-sheets, with β-turn and/or random coil regions. In a CD spectrum the occurrence of two minima (negative Cotton effects) at 222 and 208 nm at a ratio of $\theta_{222}/\theta_{208} = 0.4$ and a maximum (positive Cotton effect) at 192 nm is indicative of α-helical structures [11, 12]. In contrast, β-sheets structure have a minimum around 217 nm and a maximum around 198 nm [11, 12]. β-turns in peptides have been mapped to a minimum between 202 to 208 nm [13-16]. These peptide structures absorb in far-UV CD due to hydrogen bonding with/between peptide backbone amide bonds [15, 16] and the existence and changes in such ordered structures can therefore be studied using CD. However, in small peptides the far UV-CD spectral character is complicated when there are aromatic side chains in the peptide sequence [15, 16], such as is found in GS (and the Trcs).

The CD spectra of GS and Srf have been determined by a number of investigators [15-20]. The CD spectrum of GS in Tris-buffer is characterised by a double minimum at 206 and 222 nm reminiscent of an α-helix [19]. However, the ratio of $\theta_{222}/\theta_{206}$ at 0.94 in Tris-buffer and a double minima at 207 and 215 nm in water [15] does not correlate with the spectra of α-helical peptides. The GS CD spectrum changes according to the type of solvent. In TFE, which stabilises the H-bonds in solution, GS exhibits increased ellipticity [16, 19]. According to Ruotolo *et al.* [20] the β-sheet content of GS increases from a 50% in methanol/water solution to a 100% in TFE solution which indicate more structural stability. The GS structure has been shown to consist of a combination of a short β-sheet and two β-turn motifs [15, 16, 21, 22]. Srf is also regarded as a β-sheet peptide with β-turn motifs [17], but has also shown uncharacteristic CD spectra. The structure of Srf is characterised by β-sheet and/or β-turn conformations in trifluoroethanol (TFE)

and in aqueous media and the presence of Ca^{2+} causes structural change in Srf structure [17, 18]. Therefore the CD spectra of the cyclic peptides, Srf and GS, with a mixture of L- and D-amino acids, as well as aromatic amino acids (only GS) cannot be fully assessed using only protein models of CD spectra.

One of the most powerful techniques to elucidate secondary (and tertiary) structures and molecular interactions is NMR. These interactions can be indentified in three ways: 1) the change in chemical shift of residues which take part in the interaction between the peptides; 2) the observation through-space dipole coupling nuclear Overhauser effects (NOEs) between interacting residues and; 3) the change in the diffusion coefficient of single and mixture peptides with diffusion ordered 2D-NMR spectroscopy (DOSY). DOSY NMR facilitates the assessment of possible interaction and/or aggregation phenomena in a mixture [23].

Previous NMR and X-ray study results show that the amide protons L-Val[1], L-Orn[2], L-Leu[3] and D-Phe[4] of GS are involved in intramolecular hydrogen bonding [24-27]. The backbone $J_{HNH\alpha}$ coupling constants for L-Val[1], L-Orn[2] L-Leu[3] and D-Phe[4] that were observed are typical for the presence of β-turn/β-sheet structures [24, 27]. The ^{1}H-NMR of Srf shows two distinct conformations for Srf (S1 and S2), characterized by a "horse saddle" ring atom and having one and three hydrogen bonds respectively [3]. In S1 the two acidic Glu[1] and Asp[5] are close together, whereas in S2 they are separated in space [3].

This chapter describes a comprehensive investigation of the cyclic peptide structures of both the acidic lipopeptide Srf and the cyclic cationic peptide GS to assess the structures in selected solvents. The determined baseline structural parameters of GS is compared with mixtures of GS and Srf to characterise the possible conformational changes of GS structure arising from binding

or influence of Srf to ultimately elucidate the molecular parameters of the antagonistic peptide interactions.

Materials

Purified GS from *Aneurinibacillus migulanus* was purchased from Sigma-Aldrich and Fluka (Steinheim, Germany). The Srf complex from *B. subtilis* was supplied by Fluka Chemie (St Louis, USA). Acetic anhydride (98.0%) was supplied by BDH Chemicals Ltd (Poole, England). Acetonitrile (CH_3CN, HPLC grade, UV cut-off 190 nm) and methanol (CH_3OH, HPLC grade, UV cut-off 205 nm) were supplied by Romil Ltd (Cambridge, UK). Ethanol (GR grade) and ninhydrin were purchased from Merck Chemicals (Darmstadt, Germany). The deuterated acetonitrile (CD_3CN, deuteration degree >99% for NMR spectrometry) was supplied by Merck (Darmstadt, Germany). N,N-dimethylformamide (DMF) was supplied by Merck Chemicals (Pty) Ltd (Wadeville, RSA). N-ethyldiisopropylamine (DIPEA) and 2,2,2-trifluoroethanol (TFE) were supplied by Sigma Chemicals Co (St Louis, USA). A Milli Q® water purification system was used to filter water from a reverse osmosis plant to prepare analytical grade water.

Methods

Gramicidin S acetylation

All glassware was prepared to facilitate an anhydrous environment. Freeze-dried GS (1.5 mg) was first dissolved in 43 µL dry distilled DIPEA and 50 µL freshly distilled amine and water free DMF, then diluted in 130 µL of the freshly distilled anhydrous acetic anhydride (acetic anhydride was distilled immediately before use in an anhydrous environment). The mixture in a tightly closed vessel was shaken on a mechanical shaker for one hour to allow the reaction to take place. After incubation, 5 µL of the mixture was spotted onto a thin layer chromatography

(TLC) plate and the plate was sprayed with a 2% ninhydrin solution in 95% ethanol (note that the plate was not developed). The absence of a purple or pink taint on the TLC spot, after five minutes incubation at 80ºC, indicated that the acetylation reaction was completed. The identity and purity of the acetylated GS was later confirmed with analytical HPLC and ESMS.

Electrospray mass spectrometry

The GS and Srf were prepared by dissolving 0.1 mM each in a CH_3CN/water (1:1, *v/v*). A Waters Q-TOF Ultima mass spectrometer fitted with a Z-spray electrospray ionisation source was used to perform ESMS. A sample solution (5 to 10 μL) was introduced into the spectrometer via a Waters Acquity UPLC^{TM}. For titration, stock solutions of both Srf and GS (1.0 mM) were made in CH_3CN/water (1:1, *v*/*v*). Peptides (10 μL) were then diluted to 50 μM in water and mixed at different molar ratios, before injection. The carrier solvent was CH_3CN/water (1:1, *v/v* in 0.1% formic acid) and the flow rate was 300 μL/min. A capillary voltage of 3.5 kV and cone voltage of 35 V were applied. The source temperature was set at 100^{o}C. Data acquisition was in the positive mode, scanning the second analyzer (MS_2), through *m/z* = 100–1999 (where the *m/z* is defined as the molecular mass to charge ratio). A combination of the scans across the elution peak and subtraction of the background produced representative scans.

CID of selected molecular ions was performed with argon gas at a gas pressure of 11 psi in MS_2 and the collision energy varying from 15 to 75 eV. The second analyzer was scanned from *m/z* = 100 to 100 atomic mass units above the *m/z* value of the parent ions in order to detect daughter ions (fragment ions).

Circular dichroism spectropolarimetry

Analytical stock solutions (2.0 mM) of Srf and GS were prepared in ethanol/water (1:2, *v*/*v*) for CD. Peptides (10 μL) were then diluted to 10 μM in water or TFE (final volume was 2.0 mL, <0.2% ethanol) before measurement. For titration a fixed volume (2.5 μL of 2.0 mM peptide) of the titrating peptide was added each time to the titrated peptide (10.0 μM, 2 mL) until it reached 1:1 molar ratio; then 10 μL was added for a 1:2 ratio (final volume added was 20 μL). For the premixing experiment different ratio of peptide mixtures were made at least 30 min before analysis. A high resolution Chirascan CD spectrometer was used to obtain circular scan with a 1.00 cm quartz cuvette. CD and UV absorption spectra were collected simultaneously from 190 to 250 nm in water and 200 to 250 nm in TFE with a 0.1 nm step in three to five scans.

Nuclear magnetic resonance spectroscopy

Peptides (1-2 mg) were prepared in CD_3CN/water (1:1, *v/v*) solution for NMR experiments. A Varian Unity INOVA 600 MHz and a Bruker Avance 500 MHz NMR spectrometer, operating at variable temperatures and equipped with a 5mm IDPFG ^{1}H [^{15}N-^{31}P] (Varian) or a 5 mm BBI (Bruker) indirect detection pulse field gradient probe, were used for the 1D and 2D NMR measurements. The water solvent signal was suppressed by pre-saturation using the transmitter (Varian) or Watergate-based suppression sequences (Bruker) and a total of 64 scans were used to obtain the ^{1}H-NMR spectra. One dimensional data were processed and analysed using ACD/NMR processor academic edition (ACDLABS 12.0, software [28, 29]). Data acquisition was done using the VnmrJ software for the Varian spectrometer or the Topspin 2.1 software package for the Bruker spectrometer. All chemical shifts were referenced to the CD_3CN peak (1.94 ppm at 25 °C). Diffusion orientated spectroscopy (DOSY), nuclear Overhauser effect spectroscopy (NOESY), rotating-frame Overhauser effect spectroscopy (ROESY) and total

correlation spectroscopy (TOCSY) spectra were collected at 298 K with mixing times of 150 ms for the NOESY/ROESY experiment.

The ^{1}H-NMR titration data were used to calculate the height fraction of the spin coupling of the different NH protons of GS (proton x) in GS alone or the GS+Srf mixture at different titrating temperatures (temp) (Equation 3.1 and 3.2)

$$Height\ fraction\ of\ x\ in\ GS = \frac{height\ of\ NH\ proton\ x\ in\ GS\ at\ temp\ y}{average\ NH\ heights\ in\ GS\ at\ temp\ y} \quad (3.1)$$

$$Height\ fraction\ of\ x\ in\ GS \pm Srf = \frac{height\ of\ NH\ proton\ x\ in\ GS \pm Srf\ at\ temp\ y}{average\ NH\ heights\ in\ GS \pm Srf\ at\ temp\ y} \quad (3.2)$$

The fraction of height was then determined from the ratio of the height in the GS-Srf mixture versus the height in GS alone according to equation 3.3.

$$Fraction\ of\ height\ of\ proton\ x = \frac{Height\ fraction\ of\ x\ in\ GS \pm Srf}{Height\ fraction\ of\ x\ in\ GS} \quad (3.3)$$

Results and discussion

The main aim of this study was to characterise the possible non-covalent complex(es) formed and/or structural influences of Srf on GS, which may be responsible for the antagonism of GS activity described in Chapter 2. This was done by first investigating the structures of GS and Srf and possible change in structures due to GS-Srf interaction utilising UV-CD (Part 1). Then, a more detailed structural analysis was attempted utilising ESMS and NMR (Parts 2 and 3 respectively).

Results and discussion: Part 1

UV-CD analysis of the influence of surfactin on gramicidin structure

Far UV-CD analysis of peptide fractions

The CD spectra of both GS and Srf complex were determined in water and TFE. The CD spectrum of GS in water exhibited characteristic negative ellipticity values with minima at 206 and 216 nm (θ_{206} and θ_{216}) which is related to its predominant antiparallel β-sheet structure with its two type II β-turns (Figure 3.1A) [30, 31]. However, there was a red shift of the ellipticity minimum from 206 nm to 208 nm and a significant increase in the negative ellipticity of GS in a less polar, but hydrogen-bond promoting solvent mixture containing 50% TFE (Figure 3.1 and Table 3.1).

The ratio of the two molar ellipticity minima (216 nm and 208 or 206 nm in 50% TFE and water respectively) decreased in 50% TFE compared to that in water correlating with previous literature reports (Table 3.1) [26]. The increase in the ellipticity (and decrease in $\theta_{216}/\theta_{208}$) observed in 50% TFE were indicative of a more structured GS [32, 33]. This is caused by increased intermolecular hydrogen backbone bonds and thus increasing of the stability, rigidity and self-assembly states of GS [22, 31]. Water, more effectively than TFE, can form hydrogen bonds with the carbonyl groups of the peptide backbone, therefore GS in water will exhibit an overall lower negative molar ellipticity [22, 32, 33].

Srf exhibited much weaker CD spectra in water and in 50% TFE as compared to GS (Figure 3.1B). In water Srf presented two weak minima (197 nm and 226 nm) and a maximum at 212 nm. The spectrum has elements of β-turn and β-sheet structures [17], but also random structures.

The change in CD profile of Srf in a 50% TFE solution was predominantly characterised by the minimum between 195-200 nm that was inverted and blue shifted to a maximum at 193 nm.

Table 3.1 CD spectra parameters of the GS and Srf in water and in 50% TFE (average molar ellipticities (θ) are given in deg.cm^2.μM^{-1} x 10^1; the standard error of the mean (SEM) was calculated for three determinations).

Gramicidin S (*θ_{208} for GS in 50% TFE)			
Solvents	**θ_{206}***	**θ_{216}**	**$\theta_{216}/\theta_{206}$**
H_2O	-21.85 ± 0.20	-21.33 ± 0.10	0.98 ± 0.01
50%TFE	-31.85 ± 0.15	-30.39 ± 0.31	0.95 ± 0.01

Surfactin

Solvents	**$\theta_{220-230}$**	**$\theta_{210-215}$**	**$\theta_{190-200}$**	**$\theta_{220-230}/\theta_{190-200}$**
H_2O	-0.92 ± 0.01	-0.42 ± 0.06	-0.90 ± 0.06	1.02
50% TFE	-2.01 ± o.o3	-2.09 ± 0.10	40.50 ± 0.8	-0.05

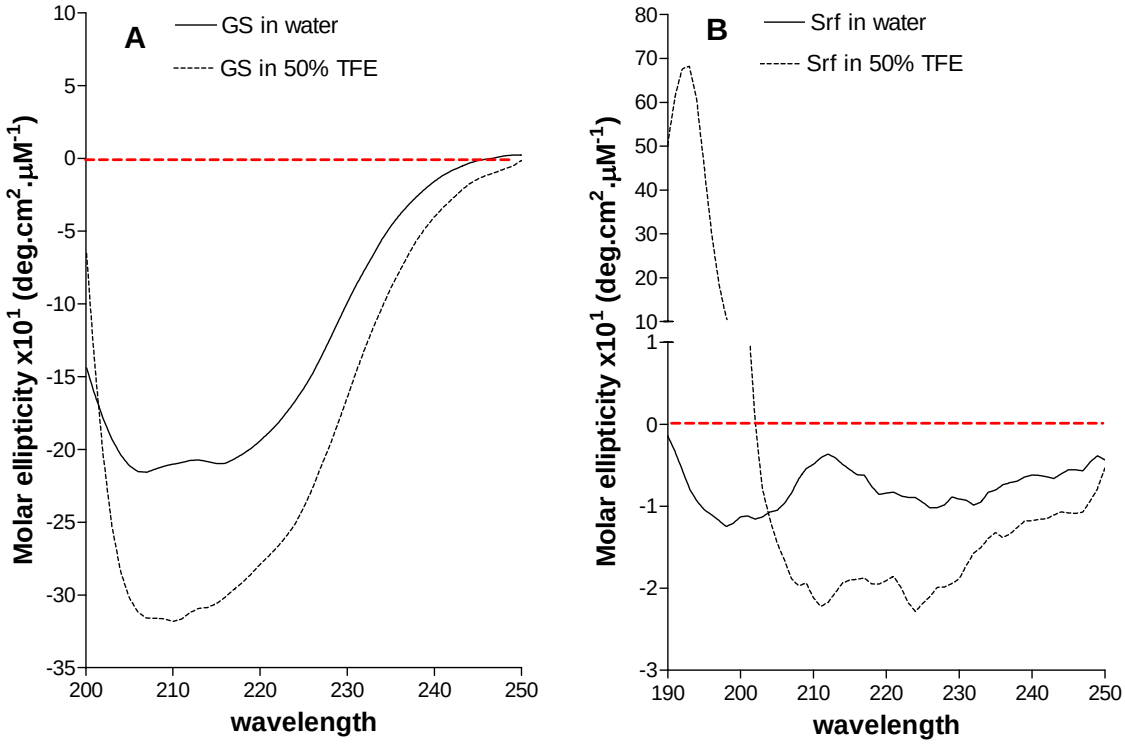

Figure 3.1 CD absorbance spectra of **A** GS and **B** Srf in water and 50% TFE. The average of three determinations was used to fit a Lowess fit line (20 point smoothing windows). Mollar ellipticity is given in term of **A** GS or **B** Srf concentrations.

Also, the negative ellipticity minimum between 220-230 nm increased. The maximum at 212 nm inverted and blue shifted to a minimum at 211 nm. The induced maximum at 193 and the higher

negative ellipticity at between 220-230 nm indicates an increase in β-sheet structures of Srf in the 50% TFE solution (Table 3.1 and Figure 3.1 B) [34]. The ratio of the ellipticity minimum of the longer wavelength to that of the shorter wavelength in depicted in Table 3.1 decreases from water to TFE. This result corroborates with results from Vass *et al.* [17] and points to the formation of sheet-like micelles of Srf.

Far UV-CD characterisation of non-covalent peptide complexes

The CD spectra of a freshly prepared 1:1 molar mixture of GS and Srf (10 μM) showed a predominance of the GS spectrum over the Srf spectrum which was almost absent (Figure 3.2). In water, there was a red shift in the CD spectrum of GS in presence of Srf, with the ellipticity minimum at 216 nm shifted to 220 nm. There was a decrease in the ellipticity minimum at 206 nm which was also red shifted to 208 nm, similar to that in TFE (Figure 3.1A and Table 3.2). The ellipticity ratios of the longer wavelengths to that of the shorter wavelengths [($\theta_{220}/\theta_{206}$), ($\theta_{220}/\theta_{216}$) and ($\theta_{216}/\theta_{206}$)] increased in presence of Srf (Table 3.2).

The overall shape of the CD spectrum of GS in the presence of Srf in 50% TFE solution showed only a minor change in the ellipticity minimum at 206 nm (Figure 3.2B and Table 3.2). The ratio of the ellipticity $\theta_{216}/\theta_{206}$ ratio in the 1:1 GS-Srf in the membrane mimetic TFE were similar to that of GS alone in water (Table 3.2). Compared to the far UV-CD spectra of GS alone in water, the spectra of GS-Srf in water reflected some conformational changes in the structure of GS reminiscent of GS in TFE. These changes may result from GS associating with the negatively charged Srf [31]. Although, Srf may act as a surfactant and cause a decrease in the assembly and structural order of GS, new β-sheet structures may be induced in both peptides. According to Jelokhani-Niaraki *et al* [31], the association of GS with negatively charged phospholipid vesicles

caused similar change in the CD spectrum of GS. These conformational changes increase with increase phospholipids/lipid ratios and are caused by electrostatic interactions between GS and the phospholipids [31].

Table 3.2 Summary of CD parameters determined for GS and Srf and GS-Srf mixture in water and in 50% TFE (average molar ellipticities are given in deg.cm^2.μM^{-1} x 10^1 ± SEM of three determinations).

Solvent	Peptide or mixture	θ_{206}	θ_{216}	θ_{220}	$\theta_{220}/\theta_{206}$	$\theta_{220}/\theta_{216}$	$\theta_{216}/\theta_{206}$
H_2O	GS	-21.8 ± 0.2	-21.3 ± 0.1	-19.5 ± 0.0	0.89 ± 0.0	0.92 ± 0.01	0.95 ± 0.04
	GS-Srf	-14.5 ± 0.2	-22.0 ± 0.2	-23.2 ± 0.9	1.60 ± 0.0	1.06 ± 0.01	1.54 ± 0.04
50% TFE	GS	-31.9 ± 0.2	-30.4 ± 0.3	na	na	na	0.93 ± 0.06
	GS-Srf	-29.5 ± 0.6	-30.0 ± 0.2	na	na	na	0.99 ± 0.06

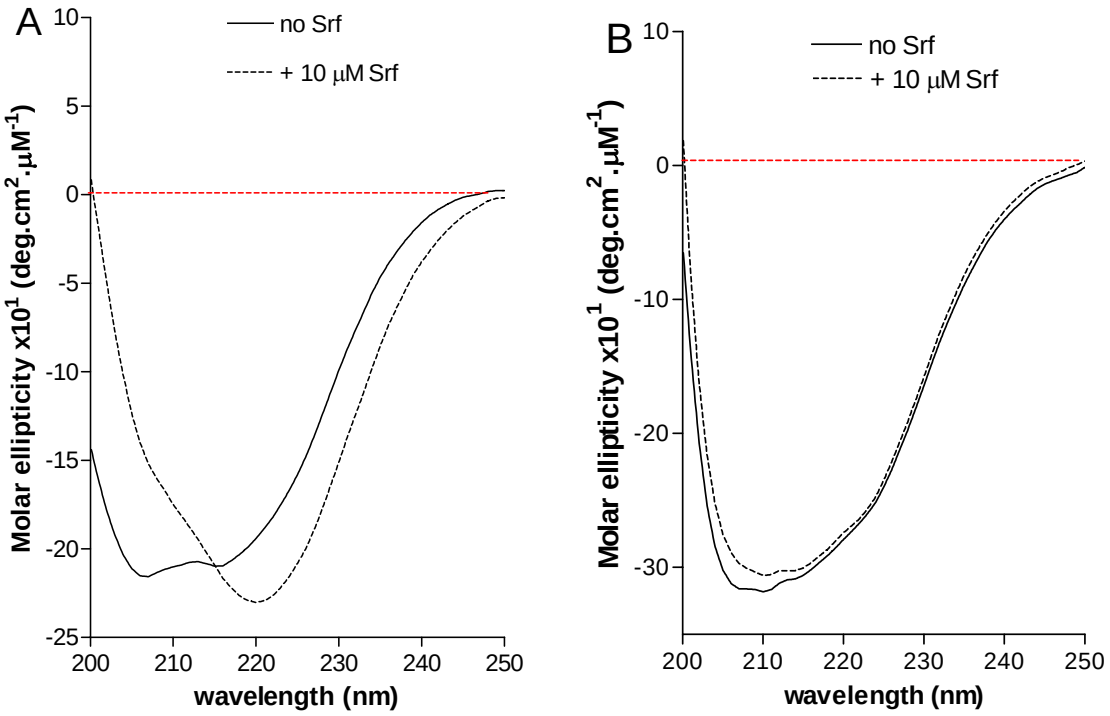

Figure 3.2 CD spectra of GS and the 1:1 molar mixture of GS-Srf in **A** H_2O and **B** 50% TFE. The average of three determinations was used to represent each spectrum by a Lowess fit line (20 point smoothing window). The molar ellipticity is given in terms of the GS concentration.

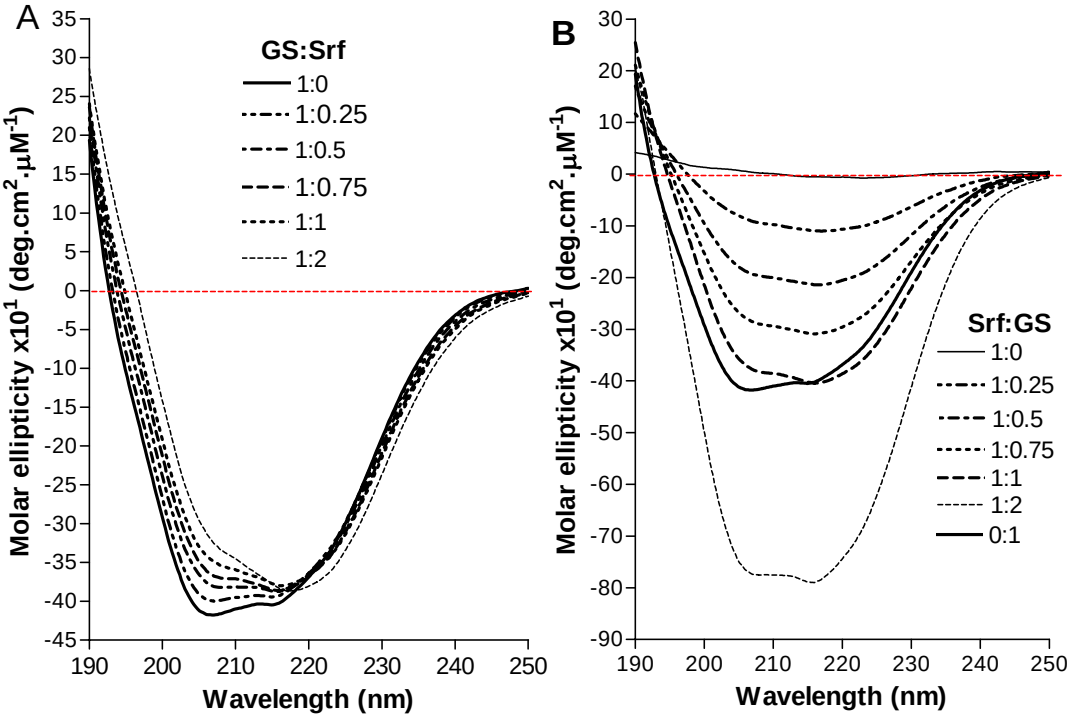

Figure 3.3 CD spectra of the titration of **A** GS by Srf and **B** Srf by GS in water. An average of five determinations was used to represent each CD spectrum by a Lowess fit line (20 point smoothing window). The molar ellipticities are given in terms of the GS concentration for **A** and Srf for **B**.

The change in the orientation of the positively charged Lys residue in GS analogues by chemical isomeration can also cause a decrease in the negative ellipticity values of GS [35]. Srf may interact or shield the positive Orn[2] or the Phe[4] side-chain groups of GS reducing their CD absorption. This may affect the structural stability, hydrophobicity and propensity for self-assembly of GS in water (Figure 3.3) [35]. However, the addition of Srf caused only slight changes in the CD spectrum of GS in 50% TFE solution. This is possibly due to greater conformational stability of GS in the membrane mimetic media. This also suggested that the interaction between the two molecules may not occur in the membrane, however, it does not rule out interaction at the membrane interphase. The decrease in ellipticity of GS as function of Srf concentration was investigated by titrating GS with Srf and vice-versa.

Table 3.3 Summary of CD parameters determined during GS-Srf titration in water (average molar ellipticities (θ) are given in $deg.cm^2.\mu M^{-1}$ x 10^1 and SEM of five determinations are given).

	Titration of 10 µM GS by Srf		Titration of 10 µM Srf by GS	
Peptide ratio	**$A_{230-210}$**	**$\theta_{216}/\theta_{206}$**	**$A_{230-210}$**	**$\theta_{216}/\theta_{206}$**
1:0	0.15 ± 0.14	0.96 ± 0.01	0.07 ± 0.03	-
1:0.25	0.18 ± 0.12	0.98 ± 0.01	0.15 ± 0.07	1.28 ± 0.02
1:0.5	0.23 ± 0.13	1.02 ± 0.01	0.22 ± 0.10	1.13 ± 0.01
1:0.75	0.28 ± 0.14	1.05 ± 0.01	0.28 ± 0.14	1.10 ± 0.01
1:1	0.32 ± 0.15	1.08 ± 0.01	0.36 ± 0.17	1.08 ± 0.01
1:2	0.48 ± 0.20	1.19 ± 0.02	0.55 ± 0.17	1.03 ± 0.01

The CD spectra of the titration of GS by Srf and Srf by GS in water also showed a gradual decrease and red shift of the negative ellipticity minimum at 206 to 208 nm, as well as a gradual increase and red shift of the negative ellipticity minimum at 216 to 222 nm (Figure 3.3 and Table 3.3). The ellipticity ratios ($\theta_{216}/\theta_{204}$) increased with increase in Srf concentrations and decreased with increase GS concentrations (Table 3.3 and Figures 3.3 and 3.4). As expected, the average absorbance between 230 and 210 nm ($A_{230-210}$) values of GS also increased with increased Srf and GS concentrations (results not shown).

The titration of GS by the diluting solvent was compared to the titration of GS by Srf (Figure 3.4A). The results show an exponential decrease of the ellipticity ratio ($\theta_{216}/\theta_{206}$) with increased GS concentrations, while it reciprocally increased with increased Srf concentrations. However, this ratio did not change significantly when GS was titrated with the diluting solvent and *vice versa*. This data indicated that the change in the ellipticity ratios was Srf-dependent. Srf may decrease the high-order self-assembly homo-oligomeric structure of GS leading to the loss of GS activity as observed in Chapter 2 (also refer to discussion on DOSY NMR below).

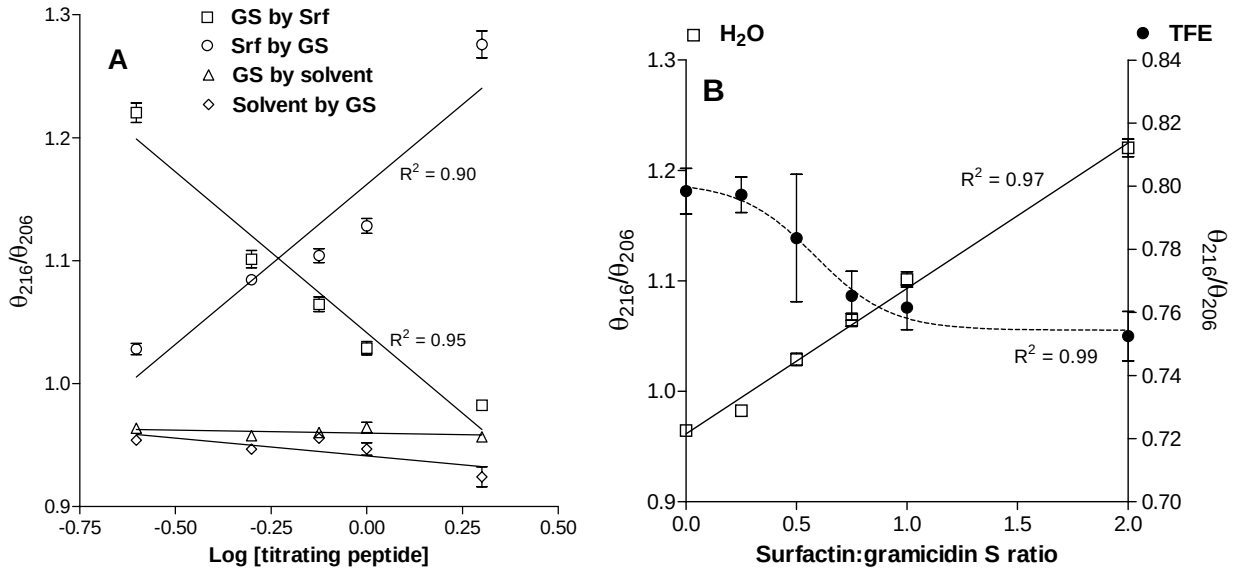

Figure 3.4 Comparison of the change in the molar ellipticity ratios ($\theta_{216}/\theta_{206}$) as function of **A** GS titrated by Srf, Srf titrated by GS and GS-solvent (75% ethanol) titration in water, and **B** Srf titration of to 10 μM GS in different solvent systems, H_2O and 100% TFE. The average of five spectra (except for TFE where three spectra were recorded) and SEM is represented for each data point.

A similar titration of GS by Srf was done in TFE as a membrane mimicking environment. Figure 3.4B compares the change in the molar ellipticity ratios of GS as function of Srf:GS ratio between water and TFE. The ellipticity ratio in TFE did not show the same linear increase as in water with the increase in Srf, but decreased up to 1:1 molar ratio (sigmoidal trend). The trend observed in TFE may indicate a concentration dependent conformational change, different from that in water which is maximal from about 1:1 molar ratio for the two peptides.

Because the titration process of the peptides may not allow the system to reach equilibrium, the CD experiments were repeated by premixing the peptides and allowing the solutions to incubate for at least 15 minutes. Srf showed a similar, but much more pronounced influence, on the spectra of GS (Figure 3.5). The average of the molar ellipticity was calculated from 204-208 nm ($\theta_{204\text{-}208}$) and from 216-222 nm ($\theta_{216\text{-}222}$) to probe the change in the secondary structure of the mixture of GS and Srf (Table 3.4). The change in the $\theta_{204\text{-}208}$ part of GS spectrum is more sensitive to modification in β-turn structure of GS [16] and Srf [34], which is related to the

observed red shift of the ellipticity minimum at 206 nm to 208 nm. Whereas, the red shift of the ellipticity minimum at 216 nm to 222 nm was related to the change in $\theta_{216\text{-}222}$ part of GS spectrum which is more sensitive to change in β-sheet structure of GS [16] and Srf (Figure 3.5 and Table 3.4).

Table 3.4 Summary of CD parameters determined analyzing premixed GS-Srf mixtures in water (average molar ellipticities (θ) are given in deg.cm^2. μM^{-1} x 10^1 and SEM of three determinations are given).

Peptide ratio Srf:GS	**$\theta_{216\text{-}222}$**	**$\theta_{204\text{-}218}$**	**$\theta_{216\text{-}222}$/ $\theta_{204\text{-}208}$**
0.00	-19.89 ± 0.05	-21.50 ± 0.14	0.93 ± 0.01
0.25	-17.67 ± 0.04	-17.71 ± 0.01	0.99 ± 0.01
0.50	-18.68 ± 0.05	-15.05 ± 0.13	1.24 ± 0.01
0.60	-18.41 ± 0.09	-13.93 ± 0.07	1.32 ± 0.01
0.70	-21.82 ± 0.04	-16.25 ± 0.15	1.34 ± 0.01
0.75	-21.24 ± 0.13	-15.54 ± 0.14	1.37 ± 0.01
0.90	-20.03 ± 0.07	-10.11 ± 0.15	1.98 ± 0.03
1.00	-22.76 ± 0.09	-13.98 ± 0.15	1.63 ± 0.02
2.00	-27.35 ± 0.16	-14.06 ± 0.17	1.95 ± 0.03

A plot of the molar ellipticity changes (Figure 3.6) shows that addition of Srf caused a nonlinear decrease in the β-turn component at 204-208 nm which levels off at about 0.5:1 Srf:GS ratio (Table 3.4 and Figure 3.5). In the folded GS, Pro^{5,10} and D-Phe^{4,9} are part of the β-turn structure of GS [36, 37]. The decrease in β-turn structure of GS also points to a change in the orientation/exposure/location of the D-Phe^{4,9} residues of GS in presence of Srf. The increase of the β-sheet structure component of GS-Srf mixture [16, 31, 38] seem to follow a linear trend (R^2=0.80) with the increase in Srf, although it may tend to level off according to the sigmoidal fit parameters (R^2=0.89) (Figure 3.6), correlating with the spectral change in TFE (compare with Fig 3.4B). These results may indicate that the interaction of the two peptides cause an increase in the β-sheet structures of both GS and Srf.

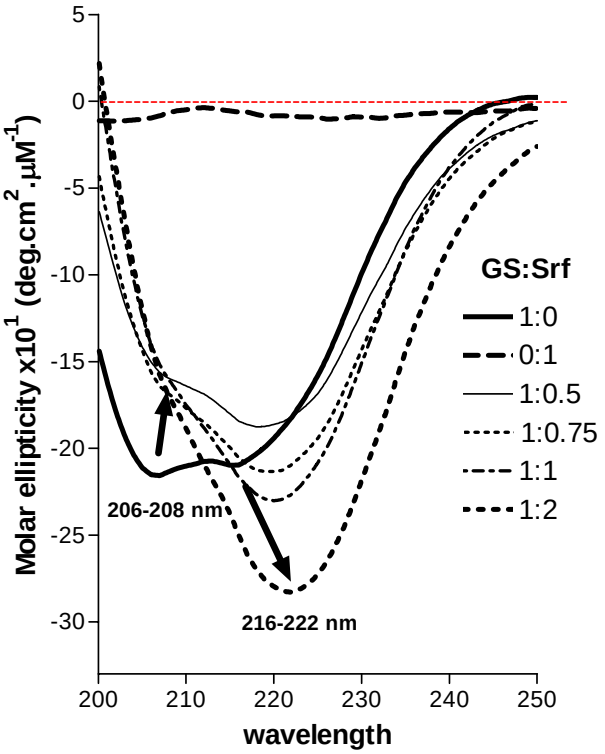

Figure 3.5 CD spectrum of the titration of GS by Srf in water after pre-incubation of the two peptides. Each spectrum is a representation of a Srf;GS mixture (Srf:GS ratios are given in the legend). An average of three determinations was used to represent each CD spectrum by a Lowess fit line (20 point smoothing window). The molar ellipticity is given in terms of the GS concentration except that of Srf.

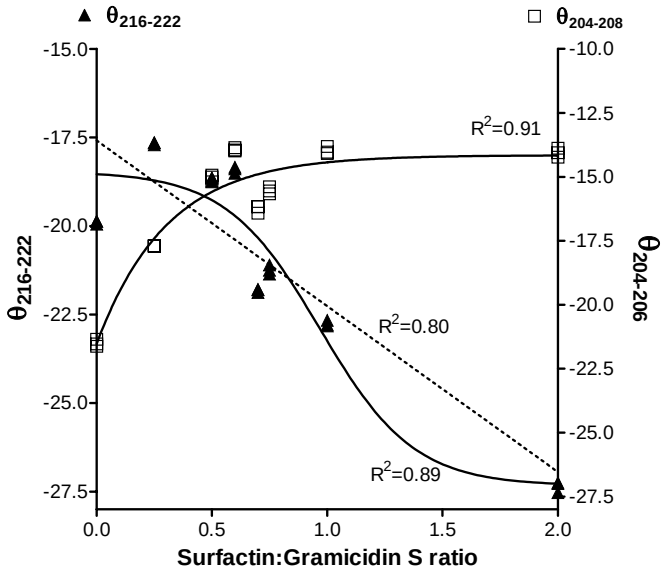

Figure 3.6 Change in the molar ellipticity minima between 204-208 nm and 216-222 nm of GS as function of Srf;GS molar ratio. Each data point represents spectrum and the line fits were done on the average of the triplicate data points.

Summary and conclusions: Part 1

The far UV-CD results indicated that Srf causes a change in the secondary structure of GS in water and possibly *visa versa*. The decrease and red shift of the ellipticity minimum from 206 nm to 208 nm indicates a decrease in the prominent β-turn structures of GS. Whereas, the increase and red shift of the negative ellipticity minimum at 216 nm to 222 nm of the CD spectra of the GS-Srf mixture is related to an increase in β-sheet structures. These changes were most probably due to interactions of the cationic GS with the negatively charged Srf, stabilizing or inducing hetero-oligomeric β-sheet structures, or structures resembling those in membranes. These interactions may have caused a change in the orientation/exposure/location of D-Phe^{4,9} or Orn^{2,7} residues of GS reducing the aggregation and/or self-assembly properties of GS in aqueous media. These complexes were further investigated with ESMS and NMR.

Results and discussion: Part 2

ESMS investigation of gramicidin S and surfactin mixture

ESMS analysis of the commercial GS showed that the extract contained high purity GS. Results showed mono-isotopic molecular ions with *m/z* = 1141.7 and *m/z* = 571.3, correspond to the singly and doubly charged molecular ions of GS with expected *m/z* values of 1141.6 and 570.8 respectively (Table 3.5 and Figure 3.7A). Other species with *m/z* of 1163.7 corresponding to the sodium adduct species of GS (*m/z* = 1163.7).

The ESMS results of the commercial lipopeptide Srf extract showed four singly charged Srfs $[M+H]^+$ ions with the *m/z* values of 994.87, 1008.89, 1022.68 and 1036.71 (Table 3.5). These ions corresponded to the Srf species with the molecular masses of 993.27, 1007.30, 1021.33 and

1035.36 respectively (Srf_1-Srf_4). Their respective Na^+ adduct molecular ions and isotopes at *m/z* of 1016.65, 1030.66, 1044.67 and 1058.68, in this order, were also observed (Figure 3.7B).

Table 3.5 Summary of the different ion species in the commercial GS and Srf complex and the synthesized acetylated-GS as detected by ESMS.

Peptides	Mr	Abbr	species	Expected m/z	Detected m/z
GS	1140.6	GS	$[M_{GS}+H]^+$	1141.6	1141.7
			$[M_{GS}+Na+H]^+$	1163.6	1163.7
			$[M_{GS}+2H]^{2+}$	571.8	571.3
Srf	993.7	Srf_1	$[M_{Srf1}+H]^+$	994.7	994.67
	1007.7	Srf_2	$[M_{Srf2}+H]^+$	1008.7	1008.69
	1021.6	Srf_3	$[M_{Srf3}+H]^+$	1022.7	1022.68
	1035.7	Srf_4	$[M_{Srf4}+H]^+$	1036.7	1036.71
Acetylated-GS	1224.9	ac-GS	$[M_{ac\text{-}GS}+H]^+$	1225.82	1225.7
			$[M_{ac\text{-}GS}+Na+H]^+$	1247.82	1247.7
			$[M_{ac\text{-}GS}+2H]^{2+}$	613.41	613.43
			$[M_{ac\text{-}GS}+3H]^{3+}$	409.60	409.21

The 1:1 molar mixture of GS and Srf showed that the two peptides formed cationic complexes stable enough to be observed under ESMS conditions (Table 3.6). Apart from detection of the different singly and doubly charged ion species of the individual peptides in the GS-Srf mixture, ESMS detected both 1:1 and 1:2 doubly charged GS-Srf complexes (Table 3.6 and Figure 3.8).

The titration study of Srf by GS in water (Figure 3.9) lead to a decrease in signal intensity of the Srf ions and the ion signals for GS and GS-Srf complexes increased, as expected. However, consistently in repeated analysis (including different solvents), all three molecular ions unexpectedly reached a minimum at 1:1 molar ratio of the two peptides, indicating the formation of neutral complexes.

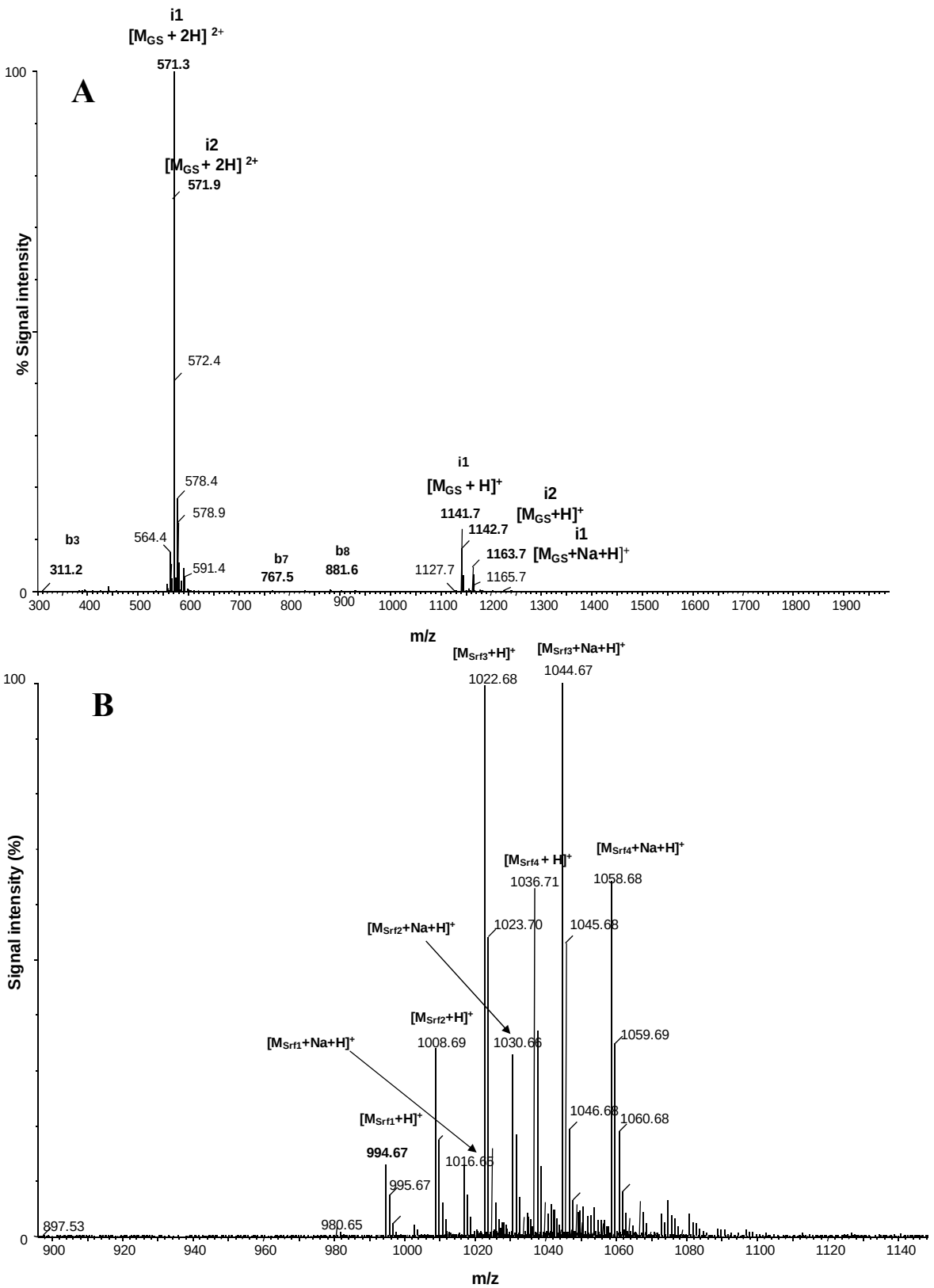

Figure 3.7 Positive mode ESMS spectra with **A** GS, GS ions denoted as M_{GS}, and **B** Srf with its ions denoted as M_{Srf1}-M_{Srf4}.

The two positive charges of GS are possibly neutralized by the two negative charges of Srf in a stable 1:1 neutral complex. However, at ratios higher than 2:1, the intensity of molecular ions of Srf and GS-Srf increased again (Figure 3.9). The signal intensity of the complexes was maximal at 4:1 GS:Srf ratio. This may indicate that larger complexes formed (GS>Srf in oligomeric complexes) and that these complexes dissociated into charged 1:1 complexes which was detected, explaining both the re-appearance of GS-Srf and Srf molecular ions. The increase in the GS molecular ion signal is expected as GS is the titrating peptide.

Table 3.6 Summary of the different doubly charged 1:1 and 1:2 complex ion species in mixture between the commercial GS and Srf as detected by ESMS.

GS-Srf (1:1)	**Mr**	**Species**	**calculated *m/z***	**observed *m/z***
C1	2134.29	$[M_{GS}+M_{Srf1}+2H]^{2+}$	1068.145	-
C2	2148.32	$[M_{GS}+M_{Srf2}+2H]^{2+}$	1075.16	1075.68
C3	2162.34	$[M_{GS}+M_{Srf3}+2H]^{2+}$	1082.17	1082.68
C4	2176.37	$[M_{GS}+M_{Srf4}+2H]^{2+}$	1089.185	1089.68
GS-$(Srf)_2$ (1:2)	**Mr**	**species**	**calculated *m/z***	**observed *m/z***
C5	3141.94	$[M_{GS}+M_{Srf1}+M_{Srf2}+2H]^{2+}$	1571.97	-
C6	3155.96	$[M_{GS}+M_{Srf1}+M_{Srf3}+2H]^{2+}$	1578.98	-
C7	3169.99	$[M_{GS}+M_{Srf1}+M_{Srf4}+2H]^{2+}$	1585.95	1586.51
C8	3169.99	$[M_{GS}+M_{Srf2}+M_{Srf3}+2H]^{2+}$	1585.99	1586.51
C9	3184.02	$[M_{GS}+M_{Srf2}+M_{Srf4}+2H]^{2+}$	1593.01	1593.51
C10	3198.04	$[M_{GS}+M_{Srf3}+M_{Srf4}+2H]^{2+}$	1600.02	1600.52

These complexes that formed between GS and Srf may result from electrostatic interactions between the two amino side chains of GS and the two acidic side chains of Srf. To investigate the role of these amino groups (two Orn residue side chains) of GS in formation of the complexes with Srf, GS's Orn δ-amino groups were acetylated using acetic anhydride in pyridine. The acetylated GS was then mixed with Srf and analysed by ESMS. The expected molecular ions corresponding to the acetylated GS ($[M+2H]^{2+}$, *m/z* = 613.43; $[M+H]^{+}$, *m/z* =

1225.7) as well as the respective ion species of Srf ($[M+H]^+$, *m/z* = 994.7, 1008.7, 1022.7, 1036.7) were detected from the 1:1 molar mixture of the two peptides (Figure 3.10 and Table 3.5). The acetylated GS, however, did not show any complexes with Srf and indicated that at least one of the amino groups of GS (one of the two δ-amino groups) is necessary for interaction with Srf or to form stable ESMS detectable complexes. Previous studies by Danders *et al.* [39] and Nagamurthi and Raubhan [40] also showed that more than 98% of GS activity is lost when these two Orn residues are blocked with different groups.

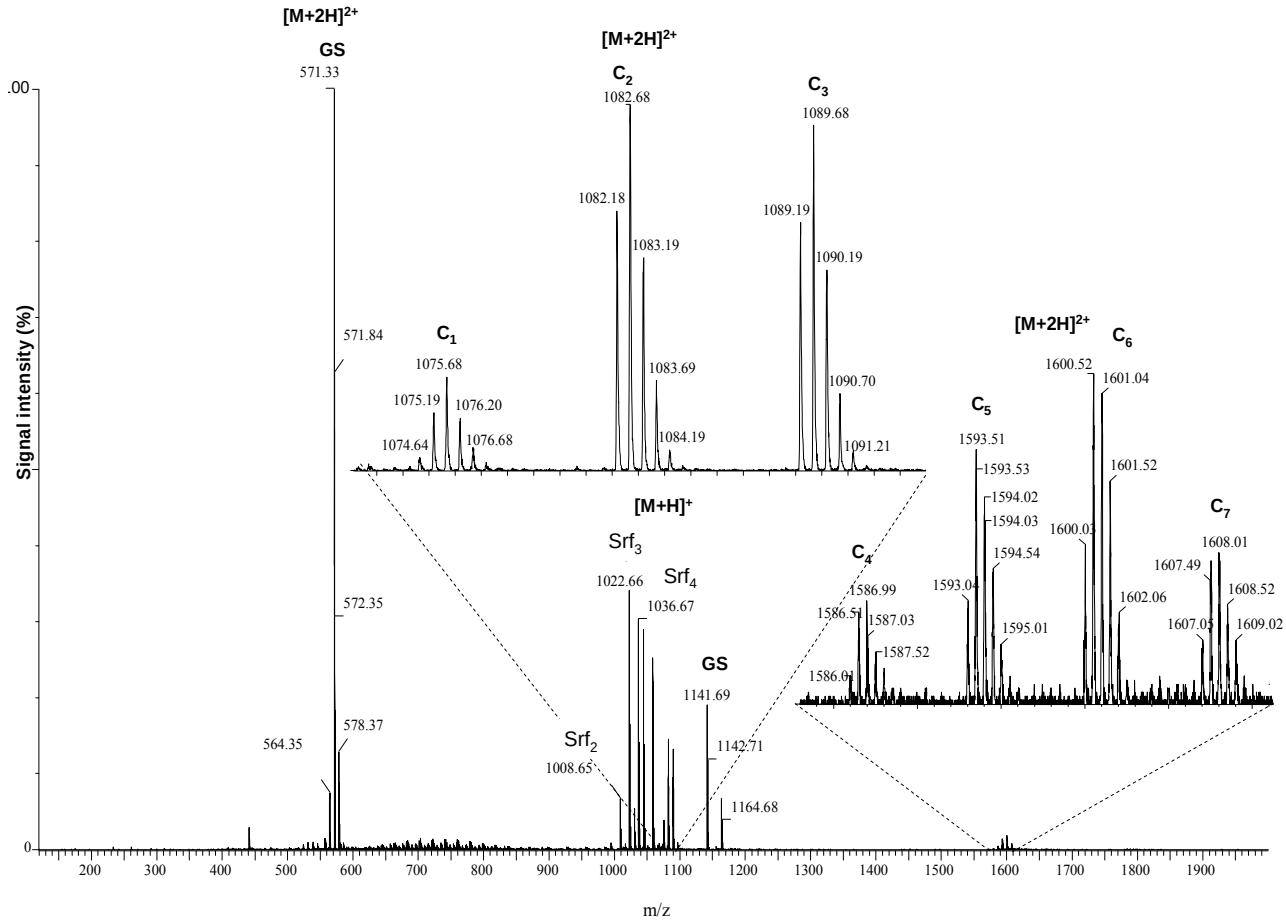

Figure 3.8 Positive mode ESMS spectrum of the GS-Srf mixture showing the different 1:1 and 1:2 doubly charged complex ions.

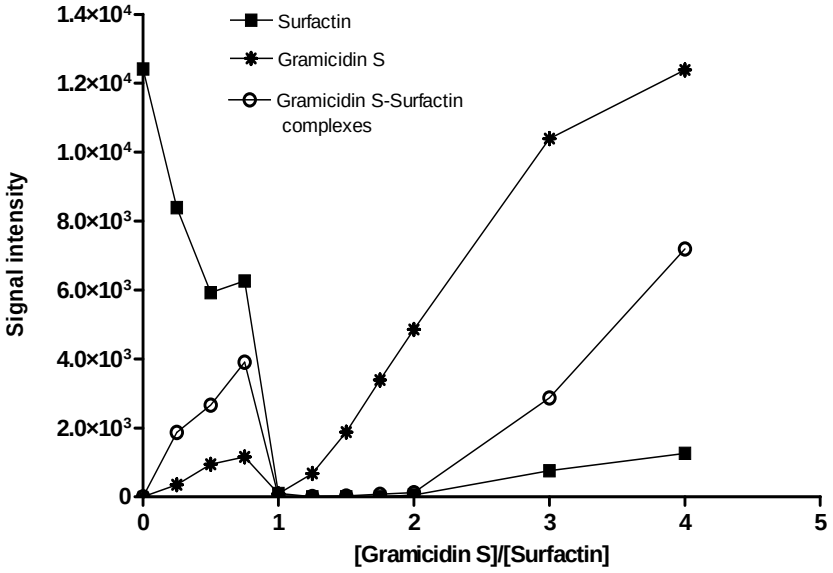

Figure 3.9 A representative titration result showing the positive mode detection of ESMS stable GS-Srf ions, GS and Srf during the titration of Srf in water with GS. The data depicted in the graph represents the sum of the intensity of all the ion species for GS, Srf and GS-Srf complexes indicated in Table 3.6 and Figure 3.8.

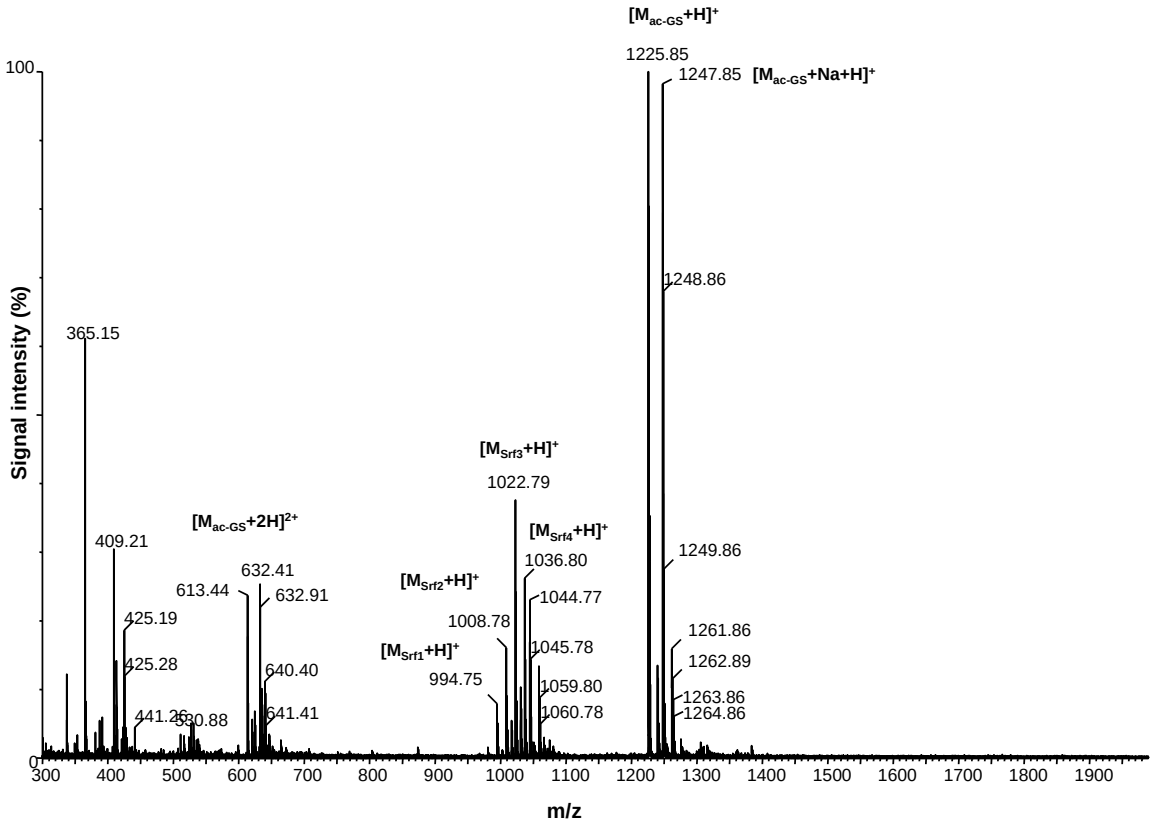

Figure 3.10 Positive mode ESMS spectrum of the acetylated GS-Srf mixture with the acetylated GS ion denoted as $M_{ac\text{-}GS}$ and Srf ions are denoted as M_{Srf1}-M_{Srf4}. No complexes were observed in the peptide mixture.

To further explore non-covalent interaction, the complex formation between GS and Srf were invesitigated with ESMS-MS-MS. According to CID performed on the GS (*m/z* = 1141.7) the major fragment ions found were from the b series and their analogous y-ions arising from the ring-opening acylium of GS at a Pro residue (Table 3.7). Product ions were detected at 197.2, 311.4, 424.6, 571.8 668.9 and 882.2, corresponding to the fragments b_2, b_3, b_4, b_5, b_6 and $b_{8,}$ in accordance with the Roepstorff and Fohlman nomenclature [41] as revised by Biemann [42].

A CID analysis of the Srf (*m/z* = 1022.89) showed product ions with *m/z* = 227.17, 469.2, 681.5 and 910.6 corresponding to fragments $b_{1,}$ b_3, b_5 and b_7 of the ring opening acylium of Srf at C_{14}. Ions with *m/z* = 328.2, 441.3 and 554.4, corresponding to fragments a_2, a_3 and a_4 were also found (results not shown). The b'+ OH ions the b_2 (*m/z* = 328.2), b_5 (*m/z* = 663.3), b_6 (*m/z* = 778.5), b_7 (*m/z* = 891.6) and b_8 (*m/z* = 1004.7) product ions were also identified (Table 3.7). A fragment that may be a water adduct of y_4 (*m/z* = 423.3) was also observed.

A CID analysis of the doubly charged ion of the GS-Srf complex with molecular weight 2177.67 (refer to Table 3.6) produced product ions with *m/z* 169.14, 197.14, 261.17, 311.21, 406.30, 553.36, 572.39 and 666.47 (a to g), corresponding to fragments a_2, b_2, y_2, b_3, b_4-OH, b_5-OH, b_5 and b_6 of GS ($[M+H]^+$ *m/z* = 1141.09) (Figure 3.11 and Table 3.7). Other fragment ions with *m/z* values of 227.14, 338.24, 356.25, 469.34, 582.43 and 684.49 (1 to 6), corresponding to fragments b_1, b_2-OH, b_2, b_3, b_4 and b_5 of Srf ($[M+H]^+$ m/z = 1022.47) were also found (Figure 3.11). The absence of certain fragments indicates that the Srf sequence L-Val^4–L-Asp^5–D-Leu^6–L-Leu^7 may have some interaction with the L-Orn–L-Leu–D-Phe sequence of GS (Table 3.7). According to these results, one possible way in which these two peptides could interact was between Orn^{2,7} of GS and Asp^5 of Srf.

Table 3.7 Summary of the b fragment ion series from the CID of Srf, GS and the 1:1 molar GS-Srf mixture.

	Srf				**GS**			
Frag-ment ions	**Sequence**	**cal *m/z***	**obs *m/z***	**GS-Srf frag**	**sequence**	**cal *m/z***	**obs *m/z***	**GS-Srf frag**
b_1	H-C_{14}	227.28	226.17	227.18	**H-Pro**[1]	98.05	-	-
b_2	C_{14}**E**	356.04	356.24	356.25	P**V**	197.5	197.13	197.14
b_3	C_{14}E**L**	469.12	469.33	*469.34*	PV**O**	311.32	311.21	331.21
b_4	C_{14}EL**I**	582.21	582.34	*582.43*	PVO**L**	424.48	424.3	*424.3*
b_5	C_{14}ELI**V**	681.3	681.5	-	PVOL**f**	571.54	571.38	*572.39*
b_6	C_{14}ELIV**D**	796.3	-	-	PVOLf**P**	668.68	667.46	666.47
b_7	C_{14}ELLVD**I**	910.4	910.6	-	PVOLfP**V**	765.3	-	-
b_8	C_{14}ELIVDI**L**	1022.7	1022.47	-	PVOLfPV**O**	881.87	882.6	-
b_9					PVOLfPVO**L**	995.2	997.65	-
b_{10}					PVOLfPVOL**f**	1141.7	1141.46	-

The fragments in italic font were observed at signal intensity <10%. Standard one letter abbreviations are used for the amino acid residues, except O =Orn. D-amino acids are given in lower case.

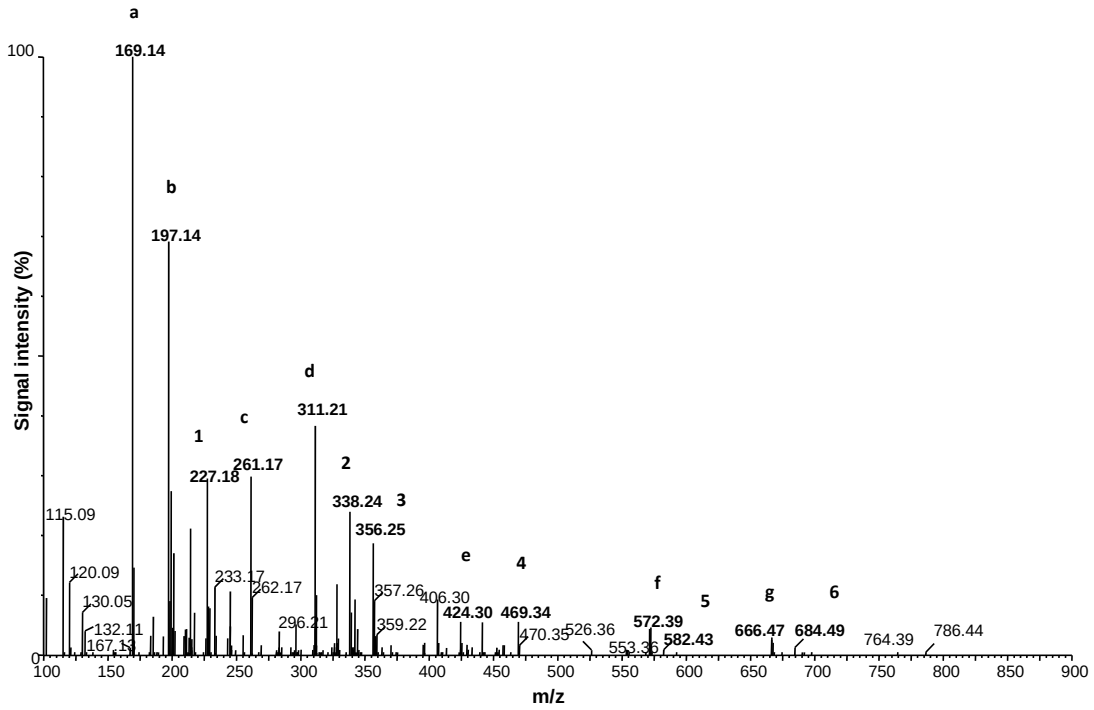

Figure 3.11 CID spectrum of the doubly charged product ion species of the GS-Srf complex with the molecular weight of 2177.64 ($[M+2H]^{2+}$; *m/z* = 1082.7). Fragment ions of GS ($[M+H]^+$; *m/z* = 1141.7) are denoted from a to g while the Srf fragment ions ($[M+H]^+$; *m/z* = 1022.43) are denoted from 1 to 6.

Summary and conclusion: Part 2.

ESMS of the 1:1 GS:Srf mixture revealed the presence of non-covalent complexes which were not observed in the 1:1 mixture of the acetylated GS and Srf. This indicated that one or both of the two δ-amino groups of GS are probably essential for ESMS detection and formation of complexes between the two peptides. Fragments generated during CID of a GS-Srf complex indicated that the Srf sequence, L-Val^{4}–L-Asp^{5}–D-Leu^{6}–L-Leu^{7}, may have some interaction with the L-Orn–L-Leu–D-Phe sequence of GS. Srf may bind to the Orn side chain groups of GS with its acidic Asp groups via electrostatic interactions, while the hydrophobic side chains may stabilise this interaction in an aqueous environment. This interaction could result in inactive complexes and antagonism of the antimicrobial activity of GS as discussed in Chapter 2. An NMR investigation on the molecular interaction between GS and Srf is reported in Part 3.

Results and discussion: Part 3

NMR analysis of the influence of surfactin on gramicidin S structure

NMR of gramicidin S and surfactin

The ^{1}H NMR of GS and Srf in CD_3CN/H_2O solvent mixture was assessed prior to investigating possible interaction between the two peptides. The signal assignments were done using sequence-specific resonance assignments based on 2D NMR TOCSY, NOESY and/or ROESY spectra of the peptides according to Wüthrich [43] and performed in collaboration with Dr Katalin Kövér (University of Debrecen, Hungary). For these assignments, the 1D experiment provided useful information on the chemical shift and spin-spin coupling for fine structures which were observed in the 2D NMR. The TOSCY provided the through-bond scalar spin-spin connectivities to indentify the different amino acid residues in each peptide by their unique spin

systems [43]. The through-space dipole spin-spin connectivities provided with ROESY and/or NOESY experiments together with data from TOSCY and the 1D NMR allowed the connection of these residues in sequence [43]. By matching the amino acid sequence obtained in the 2D NMR with the sequences determined by ES-MS-MS (refer to Table 3.7), the sequence specific assignment was then verified (Figure 3.12).

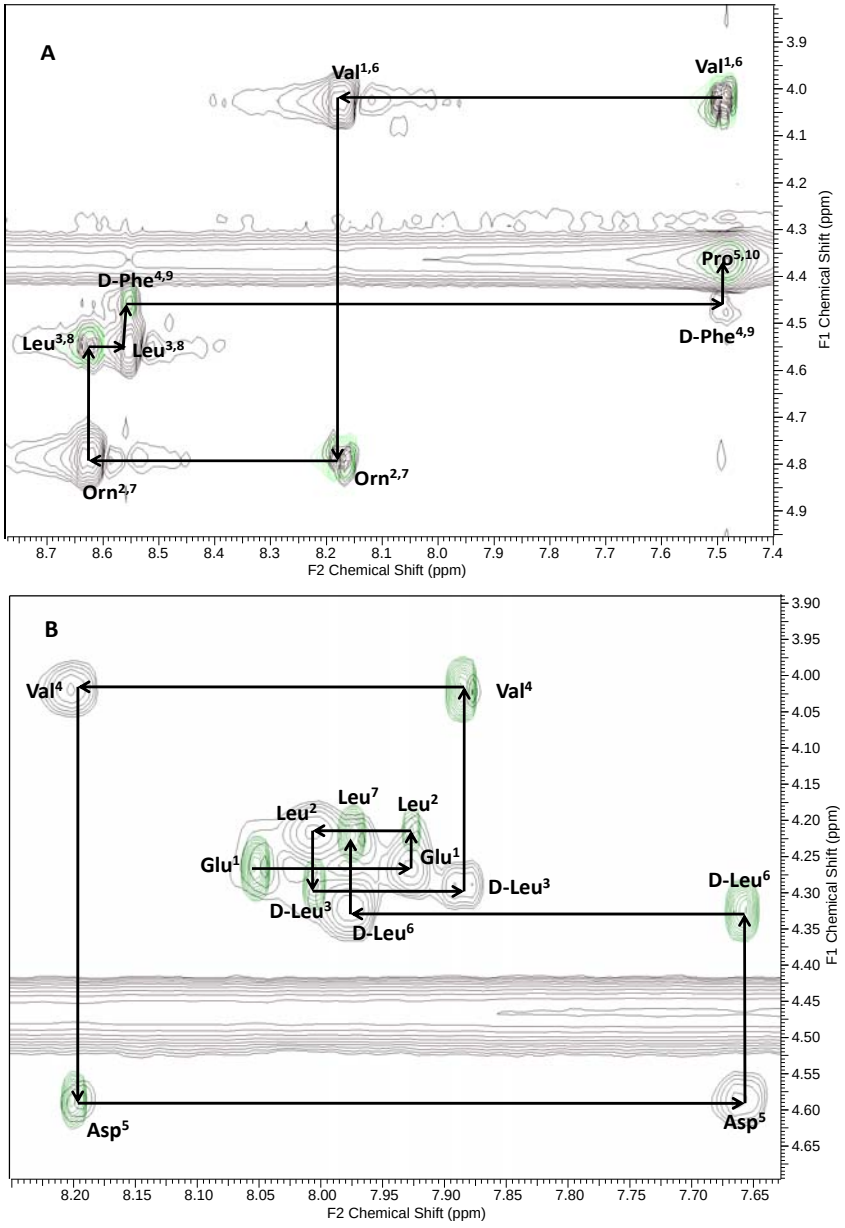

Figure 3.12 ^{1}H-NMR of the NH-Hα region of the TOCSY-ROESY spectra of **A** GS and **B** Srf in CD_3CN:H_2O (5:8, *v/v*) at 270 K and 290 K, respectively. The sequential signal assignment of the peptides is shown by connecting arrows. The NOEs NH-Hα cross peak for each residues is labeled by the standard three letter abbreviations.

For these assignments, the optimal conditions where all the spin coupling of the NH protons are visible and separated from one another had to be found for each peptide. This was achieved by changing either the solvent composition and/or the temperature. The optimal conditions for the assignment of both GS and Srf were a CD_3CN/H_2O (5:8 v/v) mixture at 298K and 290K respectively (Table 3.8 and 3.9 and Figures 3.12 and 3.13). All the different amino acid residues of both GS and Srf were identified by their spin systems from TOSCY experiments combined with ROESY experiments. These led to the complete ^1H assignment of GS and Srf (Tables 3.8 and 3.9 and Figures 3.12 and 3.13). The region containing the NH-Hα of the overlay TOCSY-ROESY data, used to obtain the sequential connectivity between amino acids of both GS and Srf, is shown in Figure 3.12.

Table 3.8 ^1H chemical shifts of GS in CD_3CN/H_2O (5:8, *v/v*) at 298K

Amino acid residue	Chemical shift (ppm)			
	NH	**αH**	**ββ'H**	**other**
L-Val[1,6]	7.49	4.03	2.13	0.79; 0.86
L-Orn[2,7]	8.18	4.78	1.88	2.90; 1.62; 7.36 br (δNH)
L-Leu[3,8]	8.63	4.55	1.44[#]; 1.52;	1.35; 0.80
D-Phe[4,9]	8.56	4.46	3.00; 2.92	7.21(2.6); 7.29 (3,4,5)
L-Pro[5,10]	--	4.34	2.92	1.89; 2.00; 1.62; 1.54

Table 3.9 ^1H chemical shifts of Srf in CD_3CN/H_2O (5:8, *v/v*) at 290K

Amino acid residue	Chemical shift (ppm)			
	NH	**αH**	**ββ'H**	**other**
L-Glu[1]	8.05	4.26	1.80; 1.95	1.95
L-leu[2]	7.92	4.21	1.55; 158	0.77
D-Leu[3]	8.00	4.28	1.55	-
L-Val[4]	7.88	4.01	2.05	0.76; 0.77
L-Asp[5]	8.19	4.58	2.69; 2.80	-
D-Leu[6]	7.66	4.31	1.45; 1.60	0.76; 0.77
L-Leu[7]	7.97	4.21	1.58	0.77

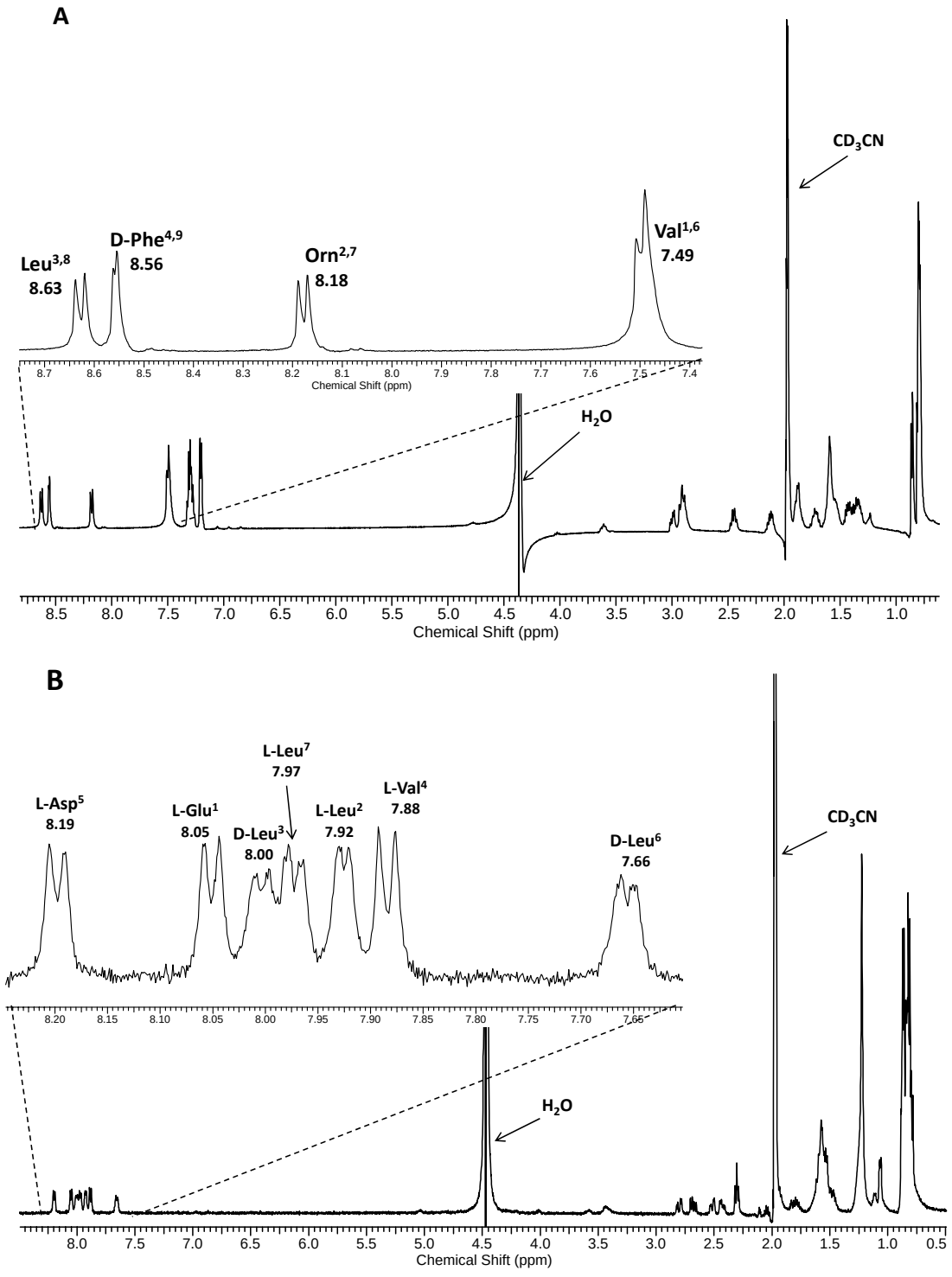

Figure 3.13 ^{1}H-NMR spectra of **A** GS and **B** Srf in CD_3CN/H_2O (5:8, *v/v*) at 298 K and 290K, respectively. Amide protons are annotated with their respective chemical shift and amino acid residue assignment.

Backbone $^{3}J_{HNH\alpha}$ coupling constants were also determined from the ^{1}H-NMR spectra for the resonances with fine structure in both peptides (Table 3.10 and 3.11). For GS, these coupling constants were greater than 8.0 Hz for all amino acid residues except for D-Phe[4,9] which gave a $^{3}J_{HNH\alpha}$ = 3.4 Hz. These, together with the NOE data indicates the presence of a β-sheet and β-turn in the GS structure [21, 27, 30] (Table 3.10), correlating with the CD data of GS in this study. Non-sequential NOEs recorded between Orn-γ and Phe-NH, Leu-NH and Val-NH, and between Leu-H_β and Val-H_β were in agreement with Staudegger *et al.* [44] and these intramolecular hydrogen bonds also suggest that GS adopted a β-sheet and β-turn conformation in this solvent system [26].

Table 3.10 $^{3}J_{HNH\alpha}$ coupling constants for GS in CD_3CN/H_2O (5:8, *v/v*) at 298K.

Amino acid residues	$^{3}J_{NH\alpha H}$ (Hz)
L-Val[1,6]	8.5
L-Orn[2,7]	9.8
L-Leu[3,8]	9.1
D-Phe[4,9]	3.7

In contrast with GS, the $^{3}J_{HNH\alpha}$ coupling constants for Srf were ranging from 4.4 to 8.2 Hz. These $^{3}J_{HNH\alpha}$ coupling constants indicated, in accordance with the CD data, that Srf adopts a β-sheet and β-turn conformation (Table 3.11) [45].

Table 3.11 $^{3}J_{HNH\alpha}$ coupling constants for Srf in 5:8 CD_3CN /H_2O (5:8, *v/v*) at 280K.

Amino acid residues	$^{3}J_{NH\alpha H}$ (Hz)
L-Glu[1]	7.6
L-Leu[2]	4.4
D-Leu[3]	5.5
L-Val[4]	8.2
L-Asp[5]	6.6
D-Leu[6]	5.5
L-Leu[7]	7.1

^{1}H-NMR analysis of the solvent and temperature influence of the NH signals of gramicidin S and surfactin

The one-dimensional plots of the HN region of GS in CD_3CN/H_2O (1:1, *v/v*) recorded from 286 K to 315 K showed that the HN resonance signals for L-Orn[2,7] and D-Phe[4,9] were highly temperature dependent (Figure 3.14 and Table 3.12). The intensity of these signals decreased with increase in temperature with almost a complete disappearance of the D-Phe signal above 300 K. This suggests that L-Orn[2,7] and D-Phe[4,9] residues of GS may be involved in some form of solvent and/or conformational exchange, which would also explain their lack of fine structure (Figure 3.14 and Table 3.12). The amide proton chemical shifts of L-Val[1] and L-Leu[3] were observed to be temperature insensitive suggesting possible solvent shielding or involvement in intramolecular hydrogen bonding [46]. The temperature dependence coefficients for the HN resonances of GS were determined for each amino acid residue from the slopes of the chemical shift change against temperature (Table 3.12). The temperature dependent coefficients of Orn L-Orn[2,7] and D-Phe[4,9] showed absolute values larger than −3 ppb/K. These indicate, in agreement with studies by Ono *et al*. [46], that these two amino acids are not participating in intramolecular hydrogen bonding in GS and they are involved in solvent exchange. The temperature dependent coefficient alone cannot be used to probe the solvent exposure or sequestration of the NH group, particularly if multiple conformations exist [47]. However, in the light of the CD results and rigid backbone structure of GS, these results may indeed indicate solvent exposure of Orn L-Orn[2,7] and D-Phe[4,9] and are consistent with previous findings that only the amide bonds of L-Val[1] and L-Leu[3] are involved in intramolecular hydrogen bonding [44] (Table 3.12).

Table 3.12 ^{1}H NMR amino acid NH chemical shifts at different temperatures (from 286 K to 315 K) and amino acid temperature dependent coefficients of the NH chemical shift for GS in CD_3CN/H_2O (1:1, *v/v*).

Amino acid residues	**NH chemical shift Temperatures (K)**						**Temp. coefficient**
	286.3	292.8	299.4	306.0	312.5	315.1	ppb/K
L-Val$^{1/6}$	7.53	7.5	7.49	7.48	7.46	7.46	-.2.3
L-Orn$^{2/7}$	8.19	8.17	8.13	8.1	8.07	8.06	**-4.7**
L-Leu$^{3/8}$	8.65	8.63	8.61	8.6	8.58	8.57	-2.7
D-Phe$^{4/9}$	8.61	8.57	8.52	8.47	8.42	8.41	**-7.2**

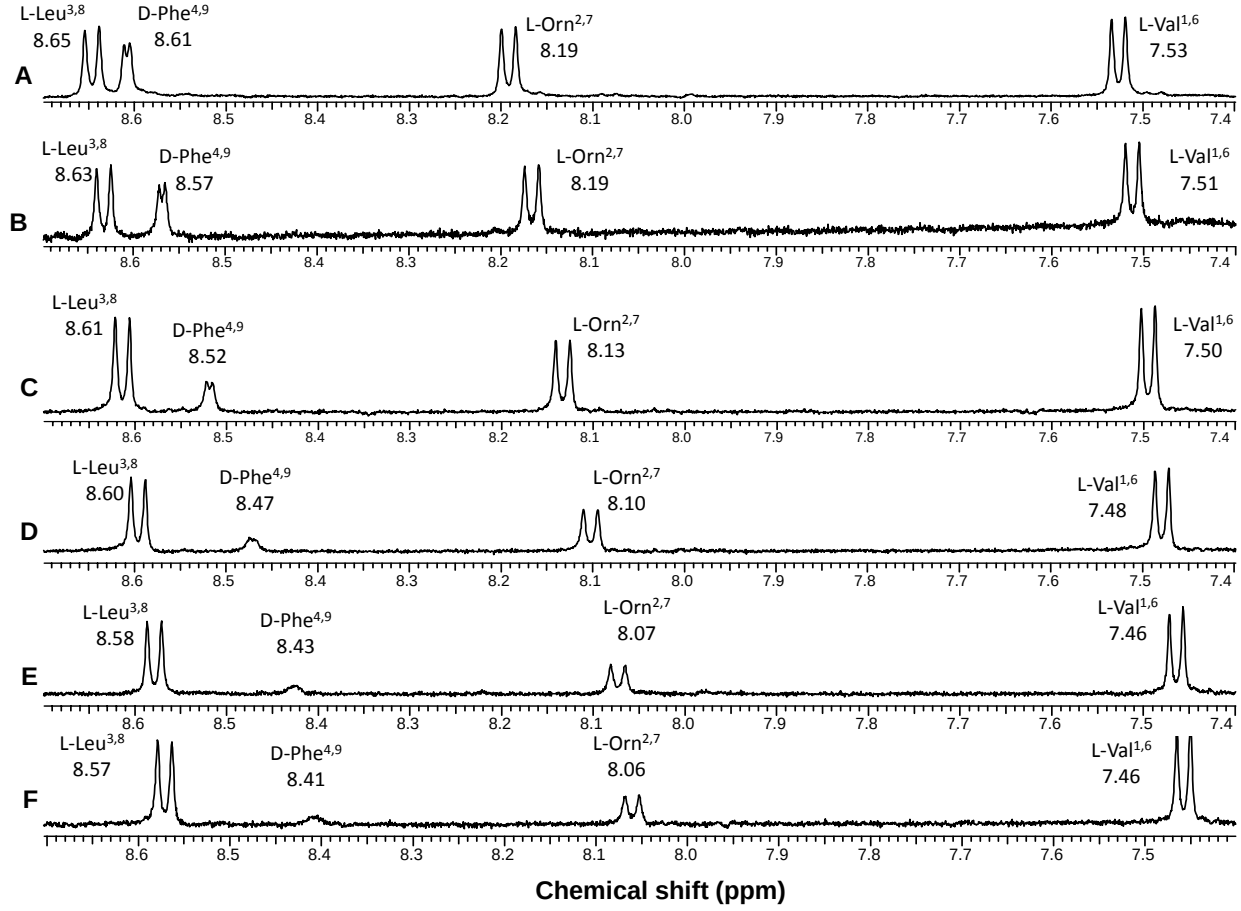

Figure 3.14 Backbone amide protons NMR traces for the temperature titration of GS in CD_3CN/H_2O (1:1, *v/v*). The spectra showing the NH chemical shifts of GS were aquired at **A** 286.3 K; **B** 292.8 K; **C** 299.4 K; **D** 306.0 K; **E** 312.5 K and **F** 315.1 K.

Lastly, increase in the water concentration of the solvent mixture (from 1:1 to 5:8, *v/v* CD_3CN/H_2O for example) improved the resolution, intensity and peak shape of the amide proton of L-Orn[2,7] and D-Phe[4,9] of GS at room temperature (results not shown). In a more aqueous environment GS may form aggregates that protect the NH proton of these residues from solvent exchange resulting in increased resolution and peak intensity.

The one dimensional ^{1}H NMR spectra of Srf recorded in CD_3CN/H_2O (1:1, *v/v*) at different temperatures also showed that the HN proton resonance signals of Srf were influenced by the temperature (Figure 3.15 and Table 3.13). Decreasing the temperature improved the resolution and peak broadening of Srf. It was found that increasing the water content of the solvent mixtures although affecting the solubility of Srf, improved the peak broadening of Srf (results not shown). Again, in an aqueous environment, Srf is forced to self-assemble/aggregate, protecting the NH groups from solvent exchange and therefore improving the peak resolution and intensity.

Table 3.13 ^{1}H NMR amino acid NH chemical shift at different temperatures (from 286 K to 315 K) and amino acid temperature dependent coefficients of the NH chemical shift for Srf in CD_3CN/H_2O (1:1, *v/v*).

Amino acid residues	**NH chemical shift Temperatures (K)**						**Temp. coefficient**
	286.3	292.8	299.4	306.0	312.5	315.1	**ppb/K**
L-Glu[1]	8.02	7.99	7.95	7.91	7.88	7.86	-5.6
L-Leu[2]	7.93	7.90	7.87	7.84	7.81	7.80	-4.5
D-Leu[3]	7.96	7.93	7.87	7.84	7.81	7.80	-5.7
L-Val[4]	7.87	7.86	7.84	7.81	7.79	7.77	-3.5
L-Asp[5]	8.14	8.11	8.07	8.04	8.01	7.99	-5.1
D-Leu[6]	7.61	7.58	7.55	7.52	7.50	7.49	-4.2
L-Leu[7]	7.90	7.88	7.84	7.81	7.79	7.77	-4.5

The temperature dependent coefficients of the HN proton chemical shift of Srf are given in Table 3.13. The lower absolute value of the temperature coefficient for Leu[2,6,7] and especially Val[4] indicates a possible involvement of these residues in intramolecular H-bonds, but this involvement may be "diluted" in the bulk because of the two reported extreme conformations (S1 and S2) of Srf [49].

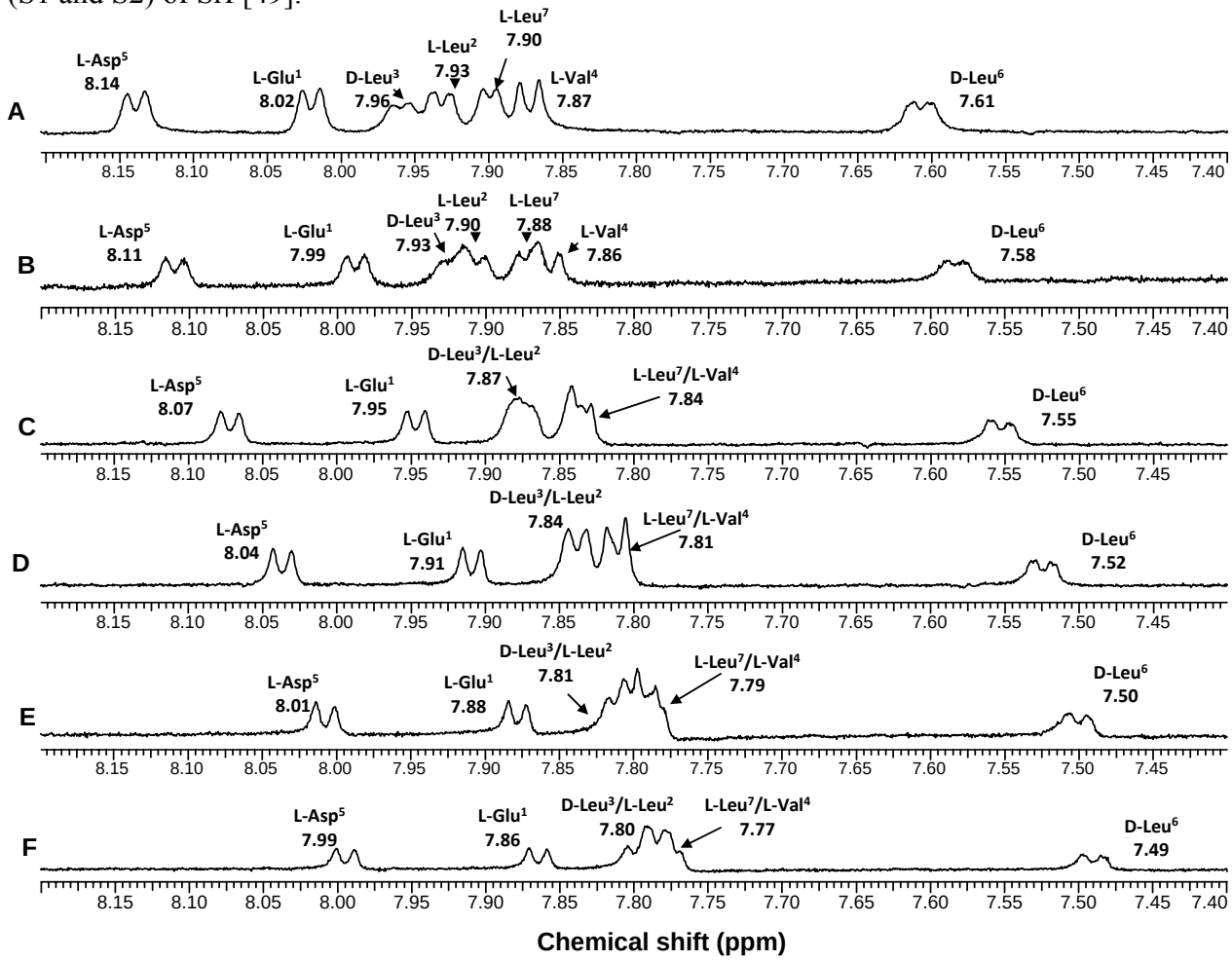

Figure 3.15 Backbone amide protons NMR traces of the temperature titration of Srf in CD_3CN/H_2O (1:1, *v/v).* The spectra showing the NH chemical shifts of Srf were aquired at **A** 286.3 K; **B** 292.8 K; **C** 299.4 K; **D** 306.0 K; **E** 312.5 K and **F** 315.1 K.

^{1}H-NMR analysis of surfactin-gramicidin S mixtures

For the ^{1}H-NMR analysis of peptide mixtures, 1-2 mg of each peptide were mixed in equimolar concentration and diluted in CD_3CN/H_2O (1:1, *v/v*) solvent mixture. This solvent mixture was

used because both peptides are relatively soluble in it. At this concentration, the two peptides were expected to form small solution phase aggregate/higher order structures or micelles as CD studies indicated (also refer to the NMR-DOSY discussion below).

The ^{1}H-NMR spectra recorded at different temperatures of the GS-Srf mixture showed a consistent detection and high intensity of the amide proton signals of the D-Phe^{4,9} and L-Orn^{2,7} residues of GS in the presence of Srf (Figure 3.16 and Table 3.14). These amide proton signals of GS were virtually absent for GS in a CD_3CN/H_2O (1:1, *v/v*) solution above 300 K, probably due to fast exchange with the solvent (refer to Figure 3.14). The addition of Srf caused these two proton signals to become shielded from solvent exchange and/or trapped in a Srf induced conformation, leading to sharper and more intense signals over a broad temperature range (Figure 3.16). Increasing the temperature did not significantly affect the signal enhancement effect caused by the addition of Srf. These results indicated that the amide proton of L-Orn^{2,7} and D-Phe^{4,9}, may have been involved in exchanging with the solvent and/or formed part of a conformational exchange in the absence of Srf. There was >4% decrease in temperature dependent coefficient of the NH chemical shift of L-Orn^{2,7} and D-Phe^{4,9} in the GS-Srf mixture (Table 3.15).

Table 3.14 NH amino acid chemical shift (ppm) of GS in the GS-Srf mixture in CD_3CN/H_2O (1:1, *v/v*) at different temperatures (K).

Amino acid residues	**NH chemical shift**					
	Temperatures (K)					
	286.3	292.8	299.4	306.0	312.5	315.1
L-Val$^{1/6}$	7.53	7.5	7.49	7.48	7.46	7.46
L-Orn$^{2/7}$	**8.2**	**8.17**	**8.14**	**8.11**	**8.08**	**8.07**
L-Leu$^{3/8}$	8.65	8.63	8.61	8.60	8.58	8.57
D-Phe$^{4/9}$	**8.61**	**8.57**	**8.52**	**8.48**	**8.43**	**8.41**

These changes, although small, indicated that these residues may be involved in some form of hydrogen bonding in the GS-Srf mixture [45, 46]. The result correlated well with the CD results showing a Srf induced increase in β-sheet structure, as well as with the CID results of the GS-Srf complex indicating that the L-Orn-L-Leu-D-Phe sequence may be protected from fragmentation (refer to Table 3.7).

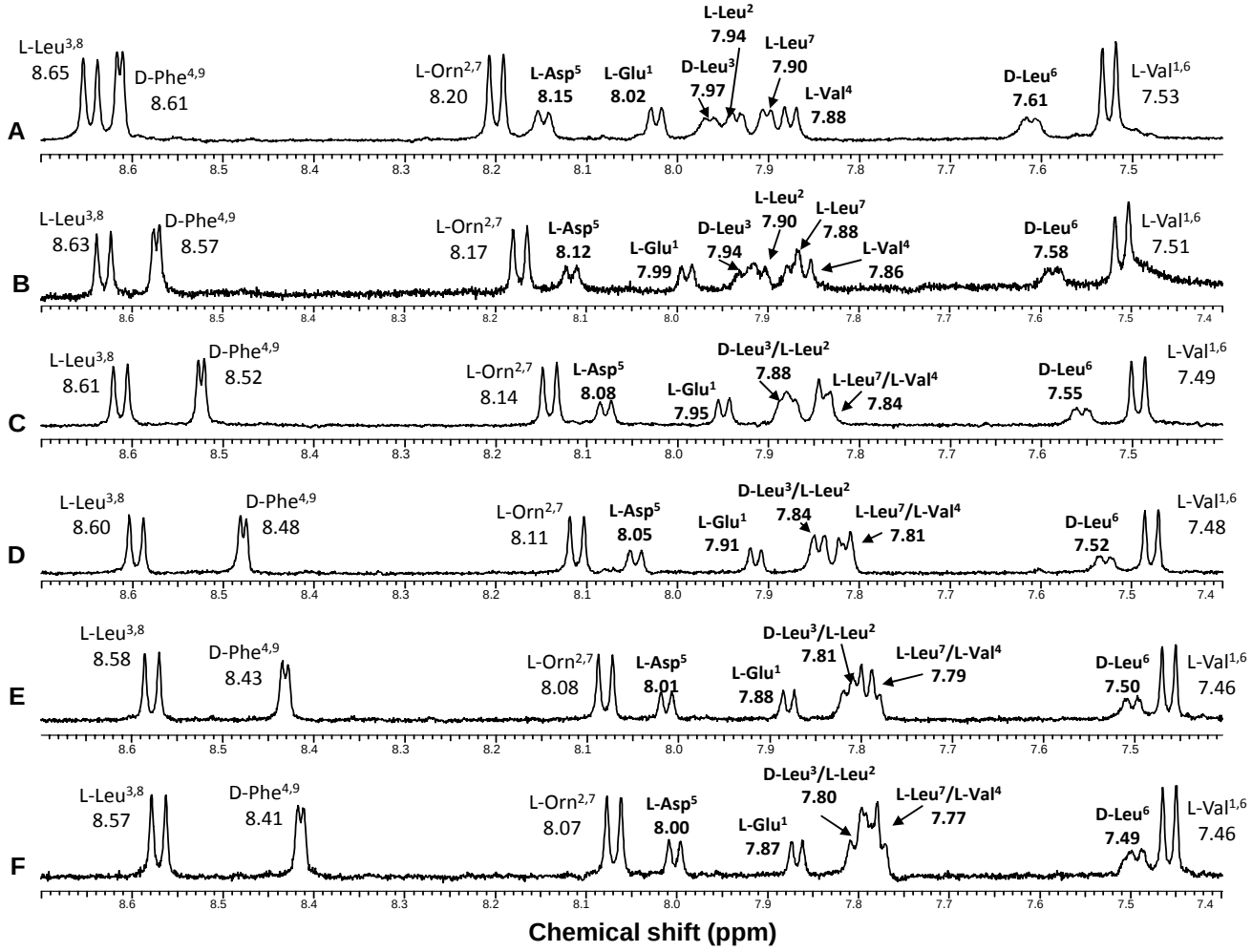

Figure 3.16 Backbone amide proton NMR traces for the temperature titration of the mixture of GS and Srf in CD_3CN/H_2O (1:1, *v/v*). The spectra showing the NH chemical shifts of the peptides mixture were aquired at **A**286.3 K; **B** 292.8 K; **C** 299.4 K; **D** 306.0 K; **E** 312.5 K and **F** 315.1 K.

The effect of Srf on the peak height of the spin coupling of the GS NH protons was also analysed by monitoring the change in the fraction of height (calculations explained in method section,

Figure 3.17). The fraction of the peak heights of Orn[2,7] and Phe[4,9] in GS alone *versus* the height of GS in the GS-Srf mixture significantly increased with increase in temperature, while it stayed constant or sightly decreased for the other amino acids. This result is evidential that both Orn[2,7] and Phe[4,9] of GS in the GS-Srf mixture are protected from solvent/conformational exchange and supports the hypothesis that GS-Srf complexes form in solution.

Table 3.15 Amino acid backbone temperature dependent coefficients of the NH chemical shift for GS alone and in an equimolar mixture with Srf (GS-Srf) in CD_3CN/H_2O (1:1, *v/v*).

Amino acid residues	**Coefficient (ppb/K)**		
	GS	**GS-Srf**	**% Change**
L-Val[1/6]	-2.3	-2.3	0
L-Orn[2/7]	-4.7	**-4.5**	-4.3
L-Leu[3/8]	-2.7	-2.7	0
D-Phe[4/9]	-7,2	**-6.9**	-4.2

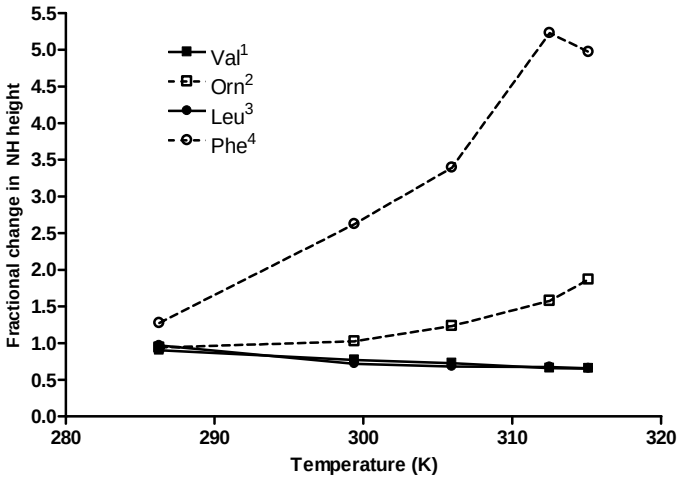

Figure 3.17 Fractional height change of the spin coupling of the NH proton of GS in the GS-Srf mixture over a temperature range from 286.3 K to 315.1 K.

Analysis of the GS-Srf mixture showed that the NH region of Srf is also affected by GS addition (refer to Figure 3.16). The chemical shift change and temperature coefficient change between Srf

alone and in a mixture with GS, showed that all residues were affected, except for L-Leu^7 (Table 3.16). In particular, L-Leu^2, D-Leu^3 and L-Val^4 showed the largest increase in temperature dependent coefficient (albeit modest) indicating increased solvent exposure.

Table 3.16 ^{1}H NMR amino acid backbone temperature dependent coefficient of the NH chemical shift for Srf alone and Srf in GS-Srf mixture in CD_3CN/H_2O (1:1, *v/v*).

	Coefficient (ppb/K)		
Amino acid residues	**Srf**	**GS-Srf**	**% Change**
L-Glu^1	-5.6	-5.4	-3.8
L-Leu^2	-4.5	-4.8	6.0
D-Leu^3	-5.7	-6.2	7.1
L-Val^4	-3.5	-3.7	6.6
L-Asp^5	-5.1	-5.3	3.1
D-Leu^6	-4.2	-4.1	-1.5
L-Leu^7	-4.5	-4.5	0.00

This correlated to the high propensity of CID fragmentation of the peptide bonds in the L-Glu^1–L-Leu^2–D-Leu^3–L-Val^4 sequence during MS/MS analysis (refer to Table 3.7). The Asp^5 signal (peak shape) was the most improved by GS addition at high temperatures, although it only showed only small change in the temperature coefficient. In the Srf micelles, Asp^5 would probably be located on the surface making it susceptible for interacting with other molecules [21]. Srf interaction with groups such as D-Phe^{4,9} and L-Orn^{2,7} of GS may cause a reorientation of the Srf molecule and protect Asp^5 from solvent exchange. The interaction between GS and Srf were further probed using NOESY/ROESY NMR to analyse possible non-sequential NOE cross peaks.

ROESY-NMR analysis of gramicidin S-surfactin mixture

The GS-Srf mixture was examined with NOESY/ROESY to find intermolecular NOEs between interacting residues, which may also provide data to determine the conformation of the GS-Srf complex. NOEs between two small molecules are difficult to observe because of weak signals and the interproton distance for NOE cross peak should be shorter than 5 Å [43]. In this study ROESY was used to partially overcome the problem of spin diffusion related to small molecules, such as peptides while demonstrating internuclear connectivities.

As expected the ROESY spectra were complex and no overt cross peaks were immediately apparent (Figure 3.18). However, we did observe a weak intermolecular ROE cross peak between the one H_γ and two H_β protons of $Orn^{2,7}$ (1.58 ppm) and Asp^5 (2.60 and 2.72 ppm, respectively) for GS and Srf respectively in the peptide mixture (Figure 3.18).These non-sequential ROE cross peaks confirmed the above results and showed that the two peptides may interact through intermolecular bonds. As stated before, intermolecular cross peaks are generally difficult to observe and only interaction of <5 Å can readily be detected [43]. Therefore, the NOE cross peaks identified from NMR ROESY experiments indicated that in the intermolecular distance between certain protons in the side chains of GS $Orn^{2,7}$ and Srf Asp^5 is <5 Å.

DOSY-NMR analysis of peptide influence

The evidence of intermolecular interaction between GS and Srf is also supported by the change observed in the 1D NMR experiment together with the ESMS and CD results. Therefore, the mixture was further investigated with DOSY NMR in order to assess the size of the complex(es) by means of diffusion measurement. The diffusion constant of both GS and Srf were measured

separately and in a 1:1 mixture of GS and Srf. DMF was used as reference compound and diffusion of the peptides and mixture was measured under identical conditions (Table 3.17).

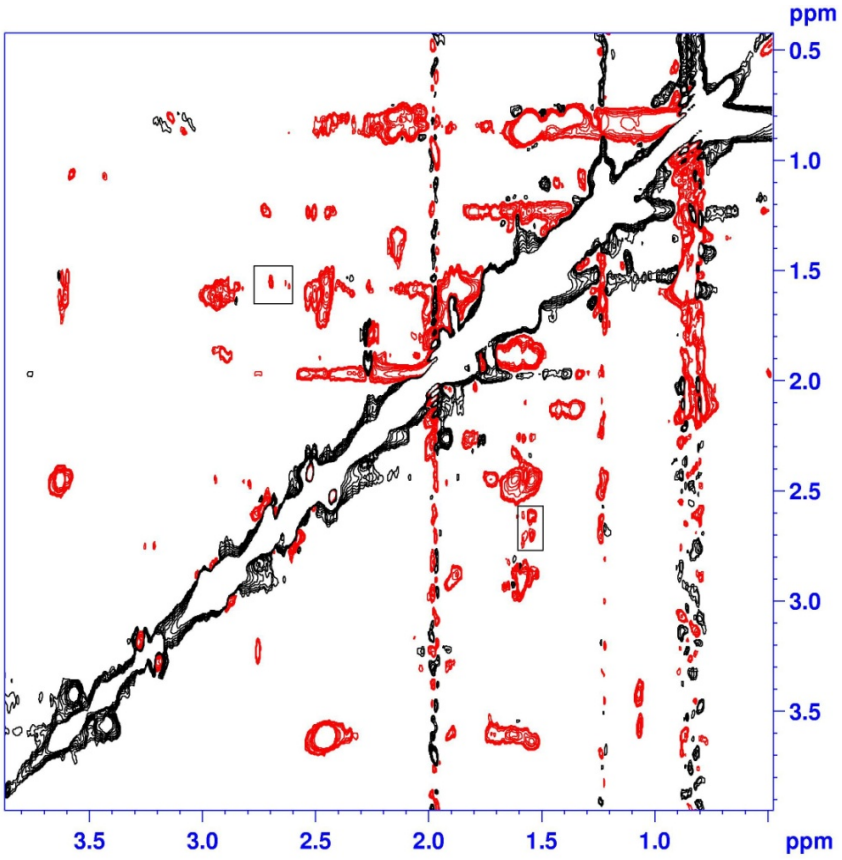

Figure 3.18 Representation of the expansion of the ROESY NMR proton spectrum of the 1:1 mixture of GS and Srf in CD_3CN/H_2O (1:1, *v/v*) at 298 K. The intermolecular ROESY peaks between GS and Srf are indicated by black boxes. The contour plot region were for w_1 = 0.5-3.5 ppm; w_2 = 0.5-4.0 ppm.

The diffusion values of GS and Srf were found to be 3.80 $x10^{-10}$ $m^2.s^{-1}$ and 3.64 $x10^{-10}$ $m^2.s^{-1}$. in CD_3CN/H_2O (1:1, *v/v*) . The diffusion of these peptides in the mixture increased to 3.92 $x10^{-10}$ $m^2.s^{-1}$. This increase in diffusion can only be related to decrease in size, as all NMR conditions were kept constant. Also, the measured diffusion may be underestimated due to the doubling of peptide concentration which may change both the viscosity and density of the medium. This result indicates that Srf and GS were rearranged in the GS-Srf mixture to form smaller homo-

oligomers and/or more compact GS-Srf hetero-oligomers. (Figure 3.19 and Table 3.17). The formation of hetero-oligomers is in accordance with the 2D-NMR, ESMS and CD results.

Table 3.17 Diffusion coefficient (D), of Srf and the GS-Srf mixture in CD_3CN/H_2O (1:1, *v/v*) at 25°C.

Peptide or complex	LogD	D ($x10^{-10}$ $m^2.s^{-1}$)
GS	-9.42	3.80
Srf	-9.44	3.63
GS-Srf	-9.407	3.92

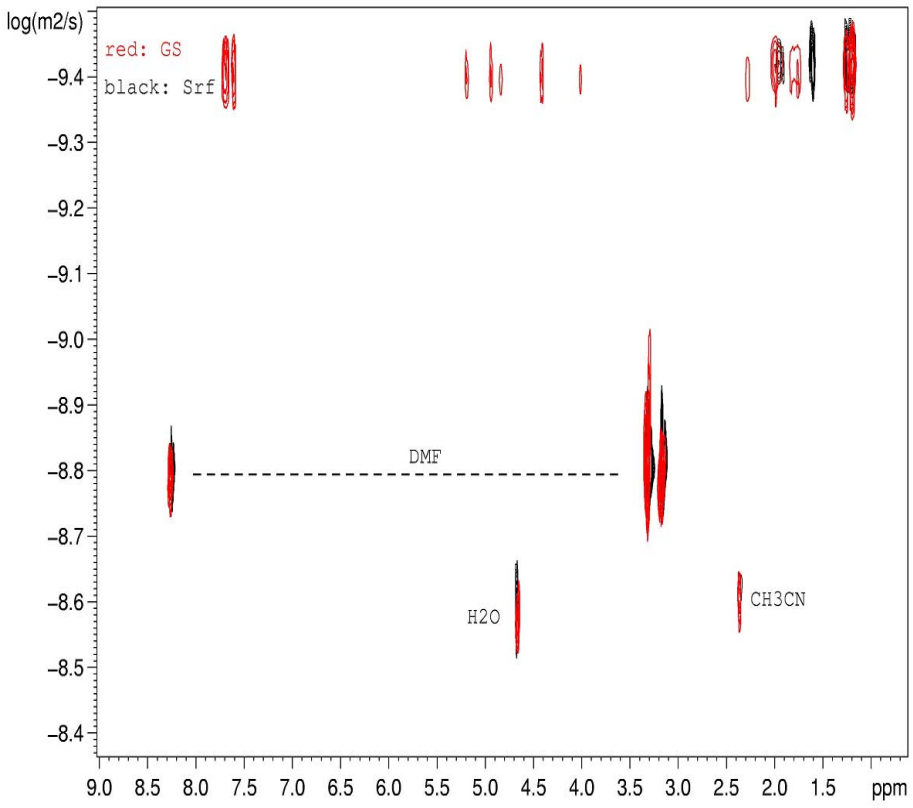

Figure 3.19 A representative 2D DOSY NMR spectrum of the 1:1 mixture of GS and Srf in CD_3CN/H_2O (1:1, *v/v*) at 25°C. Dotted line represents the average diffusion coefficient of DMF which is added as an internal reference to the sample.

Summary and conclusion: Part 3

Utilising advanced 2D NMR we were able to confirm the proton assignments of both GS and Srf in CD_3CN/H_2O. For both GS and Srf the NOEs measurements and proposed structures were in accordance with literature [21, 27, 30]. According to the ^{1}H-NMR temperature titration of GS-Srf mixture, Srf protected the amide protons of D-Phe^{4,9} and L-Orn^{2,7} in GS from exchanging with the solvent. This suggested that the two molecules may be involved in intermolecular interactions. The chemical shift change of Srf in the GS-Srf mixture was minimal, but there is some indication that L-Glu^1–L-Leu^2–D-Leu^3–L-Val^4 is more exposed to solvent exchange in the GS-Srf mixture, indicating a conformational change of Srf in the GS-Srf mixture. The amide signal of Asp^5 in Srf improved in the GS-Srf mixture, particularly at higher temperatures because of shielding of this group from solvent exchange in the mixture. The results indicated that the molecular interaction of Srf and GS possibly involves the residues D-Phe^{4,9} and Orn^{2,7} of GS and Asp^5 of Srf. According to ROESY, intermolecular NOE cross peaks were observed between the H^{β} of Asp from Srf and the H^{γ} of Orn from GS in the GS-Srf mixture. DOSY-NMR indicated that Srf and GS formed homo-oligomers. However, the addition of Srf to GS increased the diffusion coefficient of the GS-Srf mixtures indicating the formation of slightly smaller homo-oligomers or more compact hetero-oligomers.

General conclusions

In this study, the conformational influence of Srf on GS structure was indicated with CD and NMR. CD showed that Srf affects the aggregation and/or high order self-assembly states of GS in solution by possibly influencing the exposure/orientation of the D-Phe and Orn residues. This result was substantiated by the increased diffusion coefficient of GS in the GS-Srf mixture

determined by DOSY, indicating the formation of slightly smaller homo-oligomers or more compact hetero-oligomers. Fragmentation of a GS-Srf complex in ESMS indicated the role of the Srf sequence L-Val^{4}–L-Asp^{5}–D-Leu^{6}–L-Leu^{7} in the interaction with the L-Orn–L-Leu–D-Phe sequence of GS. The fragmentation results correlated well with ROESY NMR data showing intermolecular ROE cross peaks due to the <5Å interaction distance between Orn^{2,7} residues of GS and Asp^{5} residue of Srf in the complexes, ^{1}H-NMR corroborated that D-Phe^{4,9} of GS are involved or affected in intermolecular interactions with Srf. Although the formation of a non-covalent complex is not the only mode of Srf antagonism towards GS, this study showed that non-covalent complexes between GS and Srf may lead to significant changes in the GS and Srf structures. However, the role of inactive complex formation as part of a general resistance mechanism still needs to be further investigated.

References

1 Vlok, N. M. (2005) Investigation of complexation and antimicrobial activity of gramicidin S in the presence of lipopeptides from *Bacillus subtilis*. PhD thesis, University of Stellenbosch, Stellenbosch

2 Mihailescou, D. and Smith, J. C. (2000) Atomic detail peptide-membrane interactions: Molecular dynamics simulation of gramicidin S in a DMPC bilayer. Biophys. J. **79**, 1718-1730

3 Bonmatin, J. M., Genest, M., Labbe, H. and Ptak, M. (1994) Solution three dimensional structure of surfactin: A cyclic lipopeptide studies by 1H-NMR, distance geometry, and molecular dynamics. Biopolymers. **34**, 975-986

4 Light-Wahl, K., Schwartz, B. L. and Smith, R. D. (1994) Observation of noncovalent quaternary associations of proteins by electrospray ionization mass spectrometry. J. Am. Chem. Soc. **116**, 5271-5278

5 Sheehan, D. (2000) Physical Biochemistry: Principles and Applications. Wiley and Sons, Baffins, Chichester, pp. 121-150

6 Ganem, B., Li, T. T. and Henion, J. D. (1991) Detection of noncovalent receptor-ligand complexes by mass spectrometry. J. Am. Chem. Soc. **113**, 6294-6296

7 Li, Y.-T., Hsieh, Y.-L., Henion, J. D., Senko, M. W., McLafferty, F. W. and Ganem, B. (1993) Mass spectrometric studies on noncavalent dimers of leucine zipper peptides. J. Am. Chem. Soc. **115**, 8409-8413

8 Baca, M. and Kent, S. (1992) Direct observation of a ternary complex between the dimeric enzyme HIV-1 protease and a substrate based inhibitor. J. Am. Chem. Soc. **114**, 3992-3993

9 Standing, K. G. (2003) Peptide and protein *de novo* sequencing by mass spectrometry. Curr. Opin. Struct. Biol. **13**, 595-601

10 Tomer, K. B., Crow, F. W., Gross, M. L. and Kopple, K. D. (1984) Fast atom bombardment combined with tandem mass spectrometry for the determination of cyclic peptides. Anal. Chem. **56**, 880-886

11 Grenfield, N. and Fasman, G. D. (1969) Computed circular dichroism spectra for the evaluation of protein conformation. Biochem. **8**, 4108-4116

12 Toniolo, C. and Polese, A. (1996) Circular dichroism of a peptide 310-helix. J. Am. Chem. Sos. **118**, 2744-2745

13 Ishizaki, H., McKay, R. H., Norton, T. R. and Yasunobu, K. T. (1979) Conformational studies of peptide heart stimulant anthopleurin A. J. Biol. Chem. **254**, 9651-9656

14 Green, N. M., Wrigley, N. G., Russell, W. C., Martin, S. R. and McLachlant, A. D. (1983) Evidence for a repeating cross-f sheet structure in the adenovirus fibre. EMBO Journal. **2**, 1357-1365

15 Laiken, S., Printx, M. and Craig, L. C. (1969) Circular dichroism of tyrocidines and Gramicidin S-A. J. Biol. Chem. **244**, 4454-4457

16 Jelokhani-Niaraki, M., Kondejewski, L. H., Farmer, S. W., Hancock, R. E. W., Kay, C. M. and Hodges, R. S. (2000) Diasteroisomeric analogues of gramicidin S: Structure, biological activity and interaction with lipid bilayers. Biochem. J. **349**, 747-755

17 Vass, E., Besson, F., Majer, Z., Volpon, L. and Hollosi, M. (2001) Ca2+-induced changes of Surfactin Conformation: A FTIR and circular dichroism study. Biochem. Biophys. Research Commun. **282**, 361-367

18 Maget-Dana, R. and Ptak, M. (1995) Interaction of surfactin with membrane models. Biophys. J. **68**, 1937-1943

19 Perczel, A. and Hollosi, M. (1996) Turns in circular dichroism and conformational analysis of biomolecules, Plenum, New York

20 Ruotolo, B. T., Tate, C. C. and Russell, D. H. (2004) Ion mobility-mass spectrometry applied to cyclic peptide analysis: conformational preferences of gramicidin S and linear analogs in the gas phase. Am. Soc. Mass Spectrom. **15**, 870-878

21 Kawai, M., Ohya, M., Fukuta, N., Butsugan, Y. and Saito, K. (1991) Preparation, stereochemistry, and antibacterial activity of gramicidin S analogs containing N-methyl groups. Bull. Chem. Soc. Jpn. **64**, 35-41

22 Prenner, E., Lewis, R. N. A. H., Jelokhani-Niaraki, M., Hodges, R. S. and McElhaney, R. N. (2001) Cholesterol attenuates the interaction of the antimicrobial peptide gramicidin S with phospholipid bilayer membranes. BioChim. Biophys. Acta. **1510**, 83-92

23 Šmejkalová, D. and Piccolo, A. (2008) Aggregation and disaggregation of humic supramolecular assemblies by NMR diffusion ordered spectroscopy (DOSY-NMR). Environ. Sci. Technol. **42**, 699-706

24 Krauss, E. M. and Chan, S. I. (1982) intramolecular hydrogen bonding in gramicidin S. 2 Ornithine. J. Am. Chem. Soc. **104**, 6953-6961

25 Krauss, E. M. and Chan, S. I. (1982) Spectroscopic studies of intramolecular hydrogen bonding in gramicidin S. J. Am. Chem. Soc. **104**, 1824-1830

26 Rackrovsky, S. and Scheraga, H. A. (1980) Intermolecular anti-parallel β-sheet: Comparison of predicted and observed conformations of gramicidin S. Proc. Natl. Acad. Sci. USA. **77**, 6965-6967

27 Jones, C. R., Sikakana, C. T., Hehir, S., Kuo, M.-C. and Gibbons, W. A. (1978) The quantitation of nuclear Overhauser effect methods for total conformational analysis of peptide in solution: Application to gramicidin S. Biophys. J. **24**, 815-832

28 Masunov, A. (2001) ACD/I-Lab 4.5: An Internet Service Review. J. Chem. Inf. Comput. Sci. **41**, 1093-1095

29 Spessard, G. O. (1998) ACD Labs/LogP dB 3.5 and ChemSketch 3.5. J. Chem. Inf. Comput. Sci. **38**, 1-4

30 Gibbs, A. G., Kondejewsky, L. H., Gronwalk, W., Nip, A. M., Hodges, R. S. and Wishart, D. S. (1998) Unusual bold β-sheet periodicity in small cyclic peptides. Nat. Struct. Biol. **5**, 284-288

31 Jelokhani-Niaraki, M., Hodges, R. S., Meissner, J. E., Hassenstein, U. E. and Wheaton, L. (2008) Interaction of gramicidin S and its aromatic amino-acid analog with phospholipid membranes. Biophys. J. **95**, 3306-3321

32 Rajan, R. and Balaram, P. (1996) A model for the interaction of trifluoroethanol with peptides and proteins. Int. J. Pept. Protein Res. **48**, 328-336

33 Hirato, N., Mizuno, K. and Goto, Y. (1998) Group additive contribution to the alcohol-induced a-helix formation of mellitin: implication of the mechanism of the alcohol effects on proteins. J. Mol. Biol. **275**, 365-378

34 Han, Y., Huang, X. and Cao, M. (2008) Micellization of surfactin and its effects on the aggregation conformation of amyloid β-(1-40). J. Phys. Chem. **112**, 15195-15201

35 Prenner, E., Miricsi, M., Jelokhani-Niaraki, M., Lewis, R. N. A. H., Hodges, R. S. and McElhaney, R. N. (2002) Structure-activity relationship of diastereomeric lysine ring size analogs of the antimicrobial peptide gramicidin S. J. Biol. Chem. **280**, 2002-2011

36 Yamada, K., Unno, M., Kobayashi, K., Oku, H., Yamamura, H., Araki, S., Matsumoto, H., Katakai, R. and Kawai, M. (2002) Stereochemistry of protected ornithine side chains of gramicidin S derivatives: X-ray crystal structure of the bis-boc-tetra-N-methyl derivative of gramicidin S. J. Am. Chem. Soc. **124**, 12684-12688

37 Salgado, J., Grage, S. L., Kondejewski, L., Hodges, R. S., McElhaney, R. N. and Ulrich, A. S. (2001) Membrane-bound structure and alignment of the antimicrobial β-sheet peptide gramicidin S derived from angular and distance constraints by solid state ^{19}F-NMR. J. Biomol. NMR. **21**, 191-208

38 Hu, H.-Y., Li, Q., Cheng, H.-C. and Du, H.-N. (2001) β-sheet structure formation of proteins in solid state as revealed by circular dichroism spectroscopy. Biopol. Biospect. **62**, 15-21

39 Danders, W., Marahiel, A. M., Krause, M. I., Kosui, N., Kato, T., Izumiya, N. and Kleinkauf, H. (1982) Antibacterial action of gramicidin S and tyrocidines in relation to active transport, *in vitro* transcription, and spore outgrowth. Antimicrob. Agents Chemother. **22**, 785-790

40 Nagamurthi, G. and Rambhav, S. (1985) Gramicidin-S: Structure-activity relationship. J. Biosci. **7**, 323-329

41 Roepstorff, P. and Fohlman, J. J. (1988) Proposal for a common nomenclature for sequence ions in mass spectra of peptides. Biomed. Env. Mass Spectrom. **11**, 601-601

42 Biemann, K. (1988) Contributions of mass spectrometry to peptide and protein structure. Biomed. Env. Mass Spectrom. **16**, 99-111

43 Wuthrich, K. (1986) NMR of proteins and nucleic acids. John Wiley & Sons, Zurich, Switzerland

44 Staudegger, E., Prenner, E., Kriechbaum, M., Degovics, G., Lewis, R. N. A. H., McElhaney, R. N. and Lohner, K. (2000) X-ray studies on the interaction of the antimicrobial peptide gramicidin S with microbial lipid extracts: evidence for cubic phase formation. Biochim. Biophys. Acta. **1468**, 213-230

45 Baumgart, F., Kluge, B., Ullrich, C., Vater, J. and Ziessow, D. (1991) Identification of amino acid substitutions in the lipopeptide surfactin using 2D NMR spectroscopy. Biochem. Biophys. Res. Commun. **177**, 998-1005

46 Ono, S., Lee, S., Kodera, Y., Aoyagi, H., Waki, M., Kato, T. and Izumiya, N. (1987) Environment-dependent conformation and antimicrobial activity of a gramicidin S analog containing leucine and lysine residues. FEBS Letters. **220**, 332-336

47 Andersen, N. H., Neidigh, J. W., Harris, S. M., Lee, G. M., Liu, Z. and Tong, H. (1997) Extracting information from the temperature gradients of polypeptide NH chemical shifts. 1. The importance of conformational averaging. J. Am. Chem. Soc. **119**, 8547-8561

48 Rothemund, S., WeiBhoff, H., Beyermann, M., Krause, E., Bienert, M., Miigge, C., Sykes, B. D. and Sonnichsen, F. D. (1996) Temperature coefficients of amide proton NMR resonance frequencies in trifluoroethanol: A monitor of intramolecular hydrogen bonds in helical peptides. J. Biomol. NMR. **8**, 93-97

49 Tsan, P., Volpon, L., Besson, F. and Lancelin, J. M. (2007) Structure and dynamics of surfactin studied by NMR in micellar media. J. Am. Chem. Soc. **129**, 1968-1977

Chapter 4

Development of two C_{18} HPLC methods for the purification and analysis of the tyrocidines and gramicidins from *Bacillus aneurinolyticus*

Introduction

The Dubos strain of *Bacillus brevis* (reclassified as *Bacillus aneurinolyticus* [1]) is a Gram-positive soil bacterium that produces various types of secondary metabolites, including the antimicrobial peptide complex tyrothricin [2, 3]. The tyrothricin peptide complex contains two groups of non-ribosomally produced peptides, namely the linear and neutral pentadecapeptide gramicidins (Grcs) and the cyclic and basic decapeptide tyrocidines (Trcs) (Table 4.1). Tyrothricin was one of the first antibiotics used for clinical applications and it is still used as a topical antibiotic [4]. These antibiotic peptides have potential as bio-control agents in the agricultural industry [5] and as potential antibiotics [4, 6-8]. The membrane active Grcs can potentially be used as antimalarial drugs [8] and as antibiotic treatment for sexually transmitted diseases [6, 7]. The Trcs have a broad spectrum antimicrobial activity [9, 10], and recently *in vitro* activity against *Plasmodium falciparum* was demonstrated [11].

Only a few studies have been carried out on the purification and analysis of naturally produced peptides from the tyrothricin complex [12, 13]. The purification and characterisation of the different Grcs and Trcs from their commercially available extracts are challenging because there are only minor differences between the different Trcs and different Grcs, they have low solubility in water or pure organic solvents and tend to form aggregates and higher order structures in solutions containing water [14, 15].

There are two known variants of each of the three Grcs (gramicidin A (GA), B (GB) and C (GC)) (Table 4.1, [12]). The two variants differ only at their N-terminal amino acid residue,

which is either a Val or Ile residue (Table 3.1) [12]. The three Grcs (GA, GB and GC) vary in the nature of their eleventh residue, which can be a Trp, Phe or Tyr residue, respectively (Table 1). The Trcs (A (TrcA), B (TrcB) and C (TrcC) groups) are all closely related basic peptides that differ from one another in their aromatic dipeptide unit (Phe-D-Phe, Trp-D-Phe, Phe-D-Trp or Trp-D-Trp, respectively) (see Table 4.1) [16]. In addition, each of the Trc groups contain two variants differing only in one residue, namely the basic residue which could either be an ornithyl (Orn) or Lys residue (see Table 4.1) [16].

General techniques used for the purification of amphipathic peptides include gel permeation chromatography, ion-exchange chromatography, partition chromatography, absorption and reverse phase high performance liquid chromatography (RP-HPLC) [17-20]. The characterisation of peptides is generally done by HPLC and mass spectrometry (MS) techniques [18, 19]. Tang *et al.* [12] used C_{18} HPLC coupled to tandem electrospray mass spectrometry (ESMS) to study the cyclic Trc and linear Grc fractions contained in the tyrothricin peptide complex and identified 28 different Trcs or Trc analogues and nine different linear Grcs. Researchers have resolved the purification problem and developed methods to isolate >95% pure Grcs by RP-HPLC, thin layer chromatography and counter courant distribution methods using methanol (CH_3OH) alone or mixtures of CH_3OH with several other solvents [21-24]. Orwa *et al.* [24] described a separation method to selectively separate 10 linear Grcs on a C_{18} matrix with a CH_3OH/H_2O mobile phase. More recently, Thurbide and Zhang [25], achieved separation of microgram quantities of a Grc mixture on a polystyrene-divinyl-benzene column using a packed column supercritical fluid chromatography method with mobile phase modified with carbon dioxide.

The major difficulty in purifying the peptides from tyrothricin, apart from their limited solubility in water, are their propensity to aggregate at concentrations as low as 30-50 μg/mL,

and strong interaction with the C_{18} matrix, possibly in a similar way that they will interact with their membrane target. No reports (other than from our own group) were found on the semi-preparative purification and characterisation of the Trc and Grc fractions by conventional C_{18}-HPLC using a mobile phase compatible with freeze-drying. One of the aims of this study was to optimise two HPLC separation methods to purify the Trc and Grc fractions from *B. aneurinolyticus* using a C_{18} RP-HPLC column with acetonitrile (CH_3CN) as mobile phase. The choice of CH_3CN as organic modifier in the mobile phase was due to the fact that it freeze-dries easily and most of the tyrothricin peptides used have relatively good solubility in water-acetonitrile mixtures.

Table 4.1 Primary structures of the major peptides extracted from the tyrothricin complex [12].

Peptides	Abbreviation	Peptide primary structure	Monoisotopic Mr	Net charge (pH7)
GA	VGA/IGA	X-(V/I)GAlAvVvWlWlWlW-Z	1880.1/1894.1	0
GB	VGB/IGA	X-(V/I)GAlAvVvWlFlWlW-Z	1842.3/1856.1	0
GC	VGC/IGA	X-(V/I)GAlAvVvWlYlWlW-Z	1859.1/1872.1	0
TrcA/A_1	TrcA/TrcA_1	Cyclo-[V(O/K)LfPFfNQY]	1269.7/1283.7	+1
TrcB/B_1	TrcB/TrcB_1	Cyclo-[V(O/K)LfPWfNQY]	1308.7/1322.7	+1
TrcC/C_1	TrcC/TrcC_1	Cyclo-[V(O/K)LfPWwNQY]	1347.7/1361.7	+1

Standard one letter abbreviations are used for the amino acid residues, apart for O for Orn. D-amino acids are given in lower case. X = CHO- (formyl); Z = -$NHCH_2CH_2OH$.

The optimised HPLC methods will be used to analyse and purify selected peptides from commercial tyrothricin and gramicidin D (GD, is a mixture of all linear gramicidins) mixtures for use in biological activity assays and ESMS studies (see Chapter 5). Although linear GA and GC are commercially available these peptide preparations are expensive and contain VGA/IGA and VGC/IGC mixtures, respectively. It was thus decided to also isolate selected Grcs from the commercial GD. The basic Trcs were extracted from the commercial tyrothricin complex prior to their purification and analysis. This chapter describes the optimisation of two analytical HPLC methods on a C_{18} matrix with CH_3CN as mobile phase and adaptation of the methods for semi-preparative separation of Trcs and Grcs.

Characterisation of the purified fractions was done with analytical HPLC, ESMS and ultra performance liquid chromatography linked to mass spectrometry (UPLC-MS).

Materials

The tyrothricin complex from *B. aneurinolyticus* and trifluoroacetic acid (TFA >98% and 99.5%) were obtained from Sigma-Aldrich (St. Louis, USA). GA, GC and GD were obtained from Fluka (Steinheim, Germany). Crude synthetic TrcA was donated by Prof Samuel Gellman, University of Wisconsin (USA). Acetonitrile (HPLC grade, UV cut-off 190 nm) and methanol (99.9%) were supplied by Romil Ltd (Cambridge, UK). Ethanol (GR grade) was purchased from Merck Chemicals (Darmstadt, Germany). Saarchem (Krugerdorp, RSA) supplied the diethyl ether and acetone. Merck Chemical (Wadeville, Gauteng, RSA) supplied the N,N-dimethylformamide (DMF, 99.0% min). The 0.45 µ HVLP membrane filters, NovaPak® C_{18} HPLC analytical column (5 µm particle size, 60 Å pore size, 150 mm x 3.9 mm), NovaPak HR C_{18} HPLC semi-preparative column (6 µm spherical particles, 300 mm x 7.8 mm) and UPLC BEH C_{18} column (2.1 x 50 mm, 1.7 µm spherical particles) were obtained from Waters-Millipore (Milford, USA). A Milli Q® water purification system was used to filter water from a reverse osmosis plant to obtain analytical grade water.

Methods

Peptide extraction using organic solvents

The Trcs were extracted from the commercial tyrothricin peptide complex, prior to purification, by washing 200 mg with 20 mL acetone/ether (1:1, *v/v*) [26]. The non-dissolved fraction containing the basic Trcs was collected by centrifugation, washed twice more with the acetone/ether mixture before drying under a flow of nitrogen gas, re-suspended in

CH_3CN/H_2O (1:1, *v/v*), and freeze-dried. The supernatant containing the neutral GD fraction was also dried under a nitrogen flow, suspended in CH_3CN/H_2O (1:1, *v/v*), and freeze-dried.

Analytical and semi-preparative HPLC

A C_{18} Nova-Pak® column (5 μm particle size, 60 Å pore size, and 150 mm x 3.9 mm), and different solvents and gradient programs were used to develop HPLC protocols to analyze the extracted Trcs and commercial GD (Table 4.2). The chromatographic system consisted of a Waters Model 440 detector, a WISP 702 autosampler, and two Waters 510 pumps. Different gradients (linear or non-linear, Waters gradient 5), using a flow rate of 1.0 mL/min were generated over different times with or without heating the column from 25ºC to 45ºC.

The different solvents used to create the gradients were the following: eluent A (0.1% TFA in water) combined with either eluent B (10% eluent A and 90% CH_3CN), eluant C (10% eluant A and 90% CH_3OH) or eluant D (10% eluant A and 50/50 CH_3CN/CH_3OH). All solvent systems were prepared as *v/v* mixtures. The different gradient types are given in Table 4.2.

Electrospray mass spectrometry

A Waters Q-TOF Ultima mass spectrometer fitted with a Z-spray electrospray ionisation source was used to perform ESMS. The sample solution (50 or 100 ng peptide in CH_3CN/H_2O 1:1, *v/v*) was introduced into the ESMS at a volume of 5 or 10 μL via Waters Acquity UPLC™. CH_3CN/H_2O (1:1, *v/v* in 0.1% formic acid) was the carrier solvent delivered during each analysis at a flow rate of 300 μL/min. A capillary voltage of 3.5 kV and cone voltage of 35 V were applied with the source temperature set at 100°C. Data acquisition was in the positive mode, scanning the second analyser (MS_2), through *m/z* = 100–1999 (*m/z* is defined as the molecular mass to charge ratio). Combination of the scans across the elution peak and subtraction of the background produced representative scans.

Table 4.2 Summary of the different HPLC gradient programs used, displaying the events, time laps and the compositions of the different eluent systems (percentages of different elution solvents) used.

			Solvent composition		
Method	**Events**	**Time (min)**	**%A**	**%B, or C**	**Gradient type**
1	1	0-0.5	50	50	Linear
	2	0.5-16	30	70	Linear
	3	16-17	0	100	Linear
	4	17-18	0	100	Linear
	5	18-22	50	50	Linear
	6	22-25	50	50	Linear
2	1	0-0.5	50	50	Linear
	2	0.5-16	20	80	Linear
	3	16-17	0	100	Linear
	4	17-18	0	100	Linear
	5	18-22	50	50	Linear
	6	22-25	50	50	Linear
3	1	0-0.5	50	50	Linear
	2	0.5-23	20	80	Linear
	3	23-24	0	100	Linear
	4	24-26	0	100	Linear
	5	26-30	50	50	Linear
	6	30-35	50	50	Linear
4	1	0-0.5	50	50	Linear
	2	0.5-23	20	80	Non-linear
	3	23-24	0	100	Linear
	4	24-26	0	100	Linear
	5	26-30	50	50	Linear
	6	30-35	50	50	Linear
5	1	0-0.5	50	50	Linear
	2	0.5-24	0	100	Non-linear
	3	24-26	0	100	linear
	4	26-30	50	50	Linear
	5	30-35	50	50	Linear
6	1	0-0.5	40	60	Linear
	2	0.5-24	0	100	Non-linear
	3	24-26	0	100	linear
	4	26-30	40	60	Linear
	5	30-35	40	60	Linear

Waters gradient 6 was used for linear gradient while gradient 5 is non-linear. The flow rate was 1.0 mL per minute. DMF was injected after every forth run in order to wash or regenerate the column as the Trcs and Grcs tend to stick to the column matrix.

Ultra-performance liquid chromatography mass spectrometry

The development of the UPLC methods and execution of the UPLC-MS runs of the GD and Trc extracts were done by Dr Marietjie Stander, Stellenbosch University, LC-MS Central Analytical Facility. A Waters Acquity UPLC, attached to a Waters QTOF Ultima Mass

Spectrometer, was used in UPLC-MS analysis of the crude and purified Trcs and Grcs. A Waters UPLC BEH C_{18} column (2.1 x 50 mm, 1.7 μm spherical particles) was used. The following eluants were used to create a gradient for separation of peptides: 0.1% TFA in water (eluant I) for the Trcs, 0.1% formic acid in water for linear Grcs (eluant II), and CH_3CN (eluant III).

Separation of the Trcs was achieved using a gradient of eluant I to eluant III as follows: 100% I for 30 seconds, 0 to 30% III from 30 to 60 seconds, 30 to 60% III from 1 to 10 minutes and 60 to 80% III from 10 to 15 min, followed by re-equilibration of the column to initial conditions. The flow rate was 300 μL/min.

Separation of Grcs was achieved using a gradient of eluant II to III, as follows: 0 to 60% III from 0 to 5 seconds, 60 to 72% III from 5 seconds to 5 min, and 72 to 0% III from 5 to 10 min, following by the re-equilibration of the column to its initial conditions. The flow rate was 300 μL/min.

Data analysis for the optimisation of peptide separation protocols

A Graphpad Prism version 3.01 for Windows (Graphpad software, San Diego, California, USA) was used to draw all chromatograms originally processed through Maxima software. Selected HPLC parameters, calculated with the fundamental HPLC equations [27], were used to determine selected HPLC parameters utilised to compare the peak separations using different protocols.

The capacity factor *k*', as a measure of the solute retention, was calculated using equation 4.1, where t_n is the retention time of compound *n* and t_0 is the elution time of an non-retained compound.

$$k'_n = \frac{t_n - t_0}{t_0} \quad (4.1)$$

The selectivity α, as a measure of the separation ability of the column to separate two components *n* and *n+1*, was calculated using equation 4.2.

$$\alpha = \frac{k'_{n+1}}{k'_n} \quad (4.2)$$

The resolution R_s, as a measure of separation between two neighbouring peaks at the base of the peaks, was calculated using equation 4.3, where w_n and w_{n+1} are the peak widths of compounds *n* and *n+1* respectively.

$$R_s = \frac{2(t_{n+1} - t_n)}{(w_{n+1} + w_n)} \quad (4.3)$$

This use of resolution equation 4.3, to compare the resolution (R_s) between two overlapping adjacent bands ($0.4<R_s<1.3$) as described by Sneyder *et al.* [27], is illustrated in Fig. 4.1.

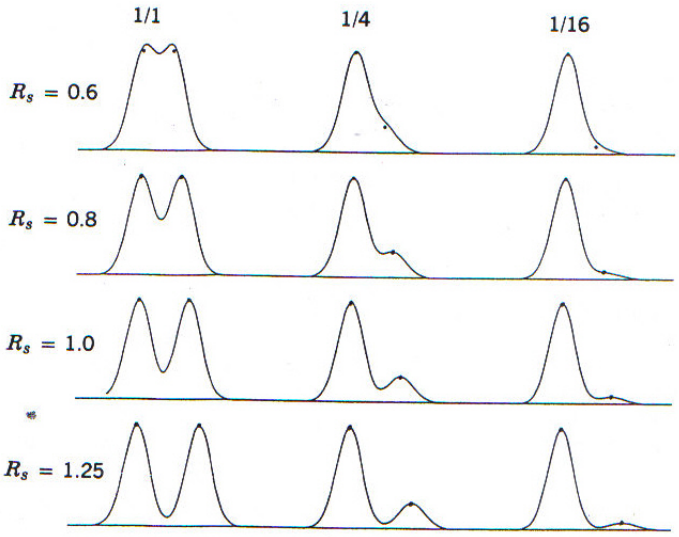

Figure 4.1 Standard resolution curves for the separation of two bands based on their resolution (R_s) and the relative band size (from [27]). At R_s of 1.25 only 0.6% of each peak lies beneath each other and each peak is 99.4% pure.

Results and discussion

The main aim of this study was to utilise conventional C_{18} HPLC to purify the major Trcs and Grcs to homogeneity. RP-HPLC methods were developed and optimised to facilitate the purification and characterisation of the major peptides in the tyrothricin complex and GD. In order for the methods to be useful for semi-preparative purification the optimised protocols entailed short run times and eluants that are compatible with freeze-drying procedures, such as water and CH_3CN.

HPLC purification of peptides using a mobile phase and a solvent modifier, such as TFA has been used by other investigators [17, 28] and therefore, 0.1% TFA the was used in the aqueous eluant A in this study. CH_3CN is the only organic solvent readily compatible with freeze-drying and C_{18} HPLC. The organic eluant B, composed of 90% CH_3CN and 10% eluant A was therefore the organic solvent of choice, however, other organic eluants such as CH_3OH and/or CH_3OH combined with CH_3CN were also tested.

All the peptides in the tyrothricin complex are amphipathic and only soluble in selected organic solvents and aqueous/organic mixtures, such as 40-75% mixture (*v/v*) of water with CH_3OH, ethanol or CH_3CN. A rational choice of CH_3CN for use in the C_{18} HPLC protocols was therefore 40% organic solvent, such as 40% CH_3CN in water, for starting/conditioning eluant composition. The gradients from 40% to 70-90% organic solvent were then optimised over as short a run time as possible. The type of gradient (linear and non-linear) was also considered, as well as the column temperature. The aim was not only to optimise the resolution between the peptide components, but also the chromatographic run time.

The result of the optimization of the peptide purification protocols are discussed in two parts: first the optimization of the tyrocidine purification protocols (Part 1) and second the optimization of the linear gramicidin purification protocols (Part 2).

Results and discussion: Part 1: Optimisation of the tyrocidine purification protocols

UPLC-MS optimization of the tyrocidine purification

The separation of the Trc extract from *B. aneurinolyticus* was first optimised with UPLC-MS in order to determine the elution profile of the different Trcs in the extract, since UPLC-MS is a more powerful and faster technique for peptide separation than HPLC. This elution profile was later used as a guide to optimise the HPLC separation of these peptides. The six major Trcs from the Trc extract were eluted between 7 and 10 min, and identified by their *m/z* values (see Figure 4.2). The identity of each Trc was confirmed in a parallel study by Spathelf [29].

HPLC optimisation of the tyrocidine purification

An HPLC program, developed over 25 minutes on C_{18}-HPLC and using CH_3CN as the organic solvent, was modified (Figure 4.3A). It was found that the gradient developed over 22.5 min was optimal, as shorter runs (gradient over 15.5 min) gave poor resolution (see Table 4.2, methods 1 and 2, Figure 4.3A). Increasing the run time to 35 min, during which solvent B slowly increased from 50% to 80% over 22.5 min (method 3 in Table 4.2), improved separation by improving the peak shape, retention (higher *k'*) and resolution of the six different Trc species (Table 4.3 and Figure 4.3B). The capacity factor increases with the peptide retention on the stationary phase [27], and this retention resulted in the improvement of the resolution of the Trcs. However, from the linear gradient to the non-linear gradient in the 35 min run the capacity factor decreased slightly between the Trc A and B species, but

good resolution was maintained (Table 4.3). Overall the average resolution (R_S) improved by >100%, enabling separation of the six different Trcs.

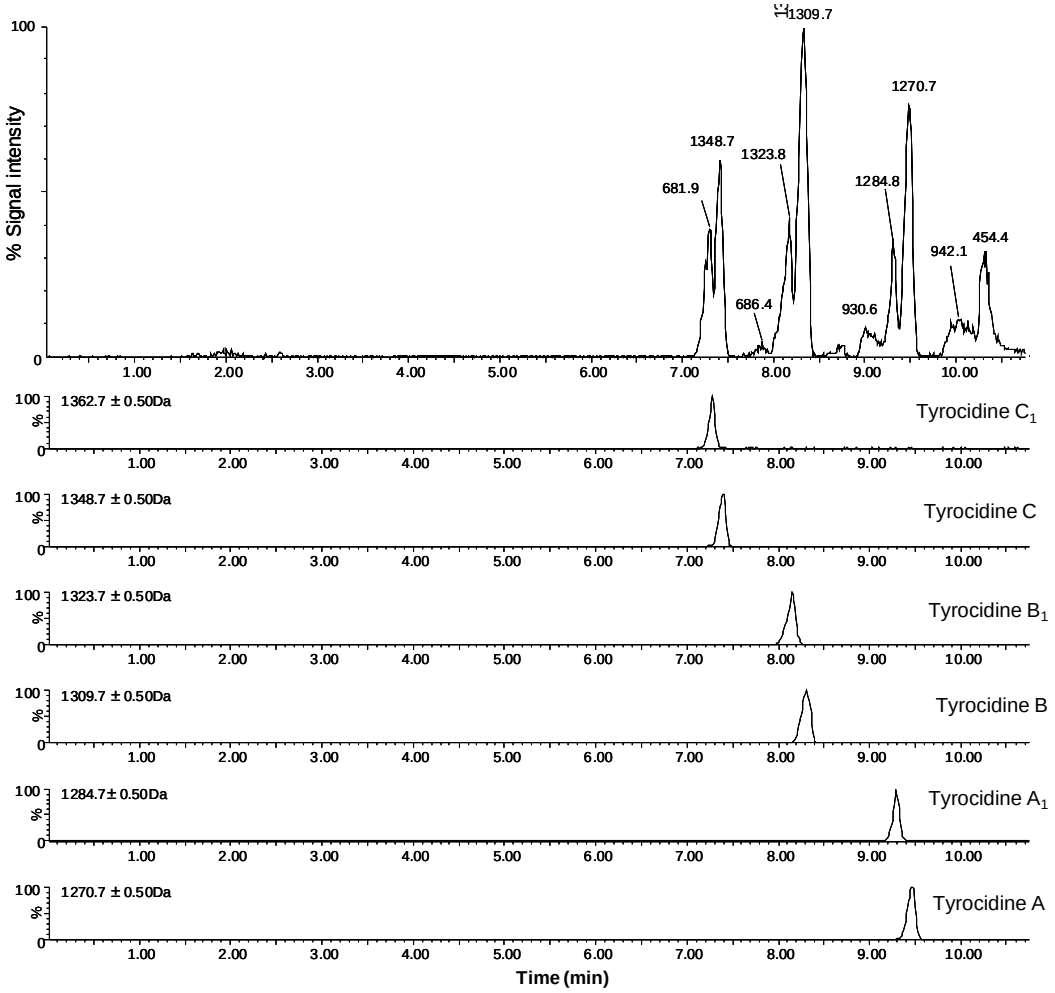

Figure 4.2 UPLC chromatogram of the Trc extract of the tyrothricin complex. The *m/z* values of singly $[M+H]^+$ or doubly $[M+2H]^{2+}$ charged molecular species of the major Trcs are given for each peak. Details on the primary structures of the different Trcs are given in Table 4.1.

Of the two different gradients (linear and non-linear) that were evaluated for their potential to improve the separation of Trc components, it was found that use of a concave non-linear gradient (Waters® gradient 5, method 4) led to better resolution than was obtained with method 3 (Figure 4.3C) by an average of >10%. The non-linear gradient chromatography (Figure 4.3C and 4.3D) provided the best resolution, peak shapes and analyte recovery between the different Trc species (Table 4.3)

Table 4.3 Comparison of the separation of the peptides in the Trc complex using different RP-HPLC purification protocols.

	Parameters	$TrcA_1$	TrcA	$TrcB_1$	TrcB	$TrcC_1$	TrcC
Method 1	R_t (min)	12.25	13.35	6.54	8.48	2.23	3.38
	k'	11.25	12.35	5.54	7.48	1.23	2.38
	α	1.1		1.35		1.93	
	R_S	1.12		0.95		0.64	
Method 2	R_t (min)	11.1	12.57	8.58	9.38	4.41	5.24
	k'	10.1	11.57	7.58	8.38	3.41	4.24
	α	1.15		1.11		1.24	
	R_S	1.39		0.28		0.17	
Method 3	R_t (min)	13.58	14.52	10.34	11.31	7.28	8.18
	k'	12.58	13.52	9.34	10.31	6.28	7.18
	α	1.07		1.1		1.14	
	R_S	0.77		0.75		0.53	
Method 4	R_t (min)	11.19	12.12	9.13	9.48	7.37	8.04
	k'	10.19	11.12	8.13	8.48	6.37	7.04
	α	1.09		1.04		1.11	
	R_S	0.8		0.76		0.73	
Method 4, 35°C	R_t (min)	11.13	12.04	9.17	9.46	7.40	8.06
	k'	10.13	11.04	8.17	8.46	6.40	7.06
	α	1.09		1.04		1.1	
	R_S	1.43		0.89		1.0	

Parameters were calculated as described in the methodology section. Details of the different methods are given in Table 4.2 and methodology section.

Finally, the effect of temperature on resolution was investigated. It was found that 35ºC was optimal for the separation of the TrcA and B species from the Trc peptide complex (Figure 4.3F and table 4.3). Separation at a lower temperature (e.g. 25ºC) led to broader TrcA peaks (Figure 4.3C). At 35ºC, the retention time of the all the Trcs decreased, except that of TrcB. This improved the resolution between the different Trc species (Table 4.3 and Figures 4.3 C-H). The separation between the Trc B and C species also improved with the late elution of TrcB since the volume separating the two group species increased (see Figures 4.3E and F).

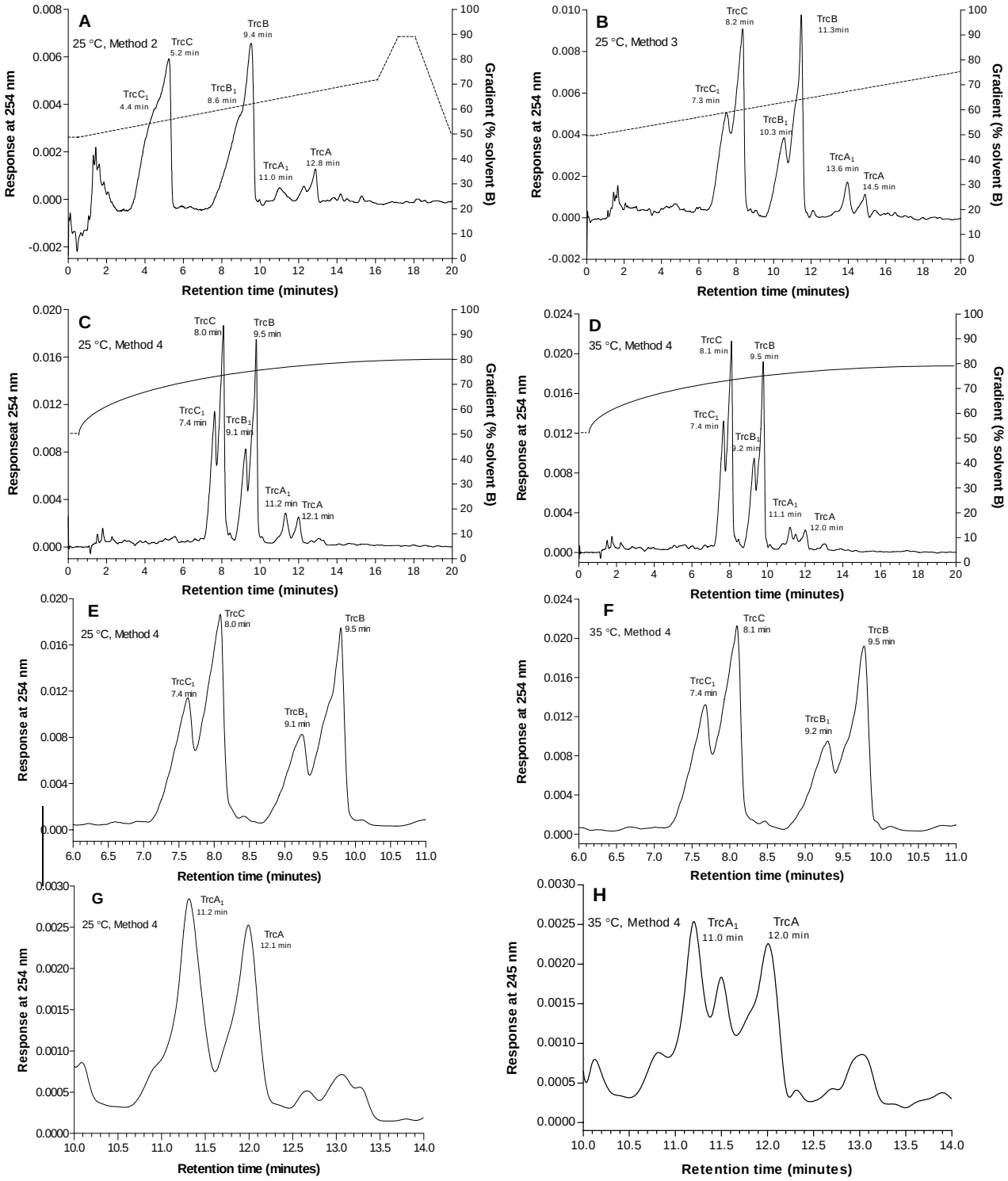

Figure 4.3 Analytical C_{18} HPLC chromatograms showing the influence of gradient time (compare **A, B**); type of gradient (compare **C, D**) and temperature (compare **D, E**; **F, G** and **H, I**) on the separation and resolution of the peptides in the Trc extract. Chromatograms **F, H** and **G, I** shows the detail of the separations in **E** and **F** respectively. 10 µg peptides were injected in each run.

In addition, the resolution that was previously obtained depicted in Figure 4.3A between the TrcA species was regained (see Figures 4.3A, H and I). An increase of the temperature above the melting temperature of the hydrophobic groups of the matrix and the solute leads to an increase in the peptide solubility by increasing the average kinetic energy of the solvent molecules [30]. These factors probably caused a decrease in the capacity factor and a better resolution of the TrcA species. However, high temperature could also increase hydrophobic interactions of solutes with the stationary phase, such as a C_{18} matrix [30], which could be the reason for asymmetrical peak shapes of the Trcs. The higher temperature most probably caused the TrcA aggregation/self-assembly to decrease and the $TrcA_1$ and A eluted earlier with better peak shapes (refer to the discussion on aggregation and analysis of pure Trcs). These results correlated with previous observations, in which the resolution of the Trc A and B species in the 35 min run was dependent on the reducing their retention on the C_{18} matrix. This optimised HPLC separation of the major Trcs also compared well with separation of the Trc extract obtained with UPLC (Figure 4.2).

Purification and analysis of tyrocidine fractions

Eight Trcs were purified to homogeneity (>95%) using semi-preparative HPLC. The isolated peptides were only considered pure if both the analytical HPLC and ESMS data indicated homogeneity (Tables 4.4). Analytical HPLC and ESMS revealed that all the purified Trcs were of high purity and obtained in good yields (Table 4.4). Aggregation, in particular when the Trcs were of high purity presented a major problem during analysis. For example, the HPLC chromatogram of the purified cyclic TrcC presented fronting and tailing characteristic of peptide aggregation at high concentration (results not shown). This problem of aggregation was overcome by reducing the injection amount to 2-20 μg per injection (depending on the Trc), and better chromatographic profiles were obtained (Figure 4.4). Similar aggregation

problems were observed with TrcA (results from previous studies [29]), but were overcome by only injecting 2 μg from a 200 μg/mL solution (Figure 4.4 A).

Table 4.4 Summary of the different Trcs purified under optimal conditions developed in this study* by other researchers in our group.

ID	HPLC Rt (min)	Exp Mr	Theor. Mr	Purity (%)	Yield (mg)	Yield (%)
TrcA**	11.49	1269.70	1269.7	>95	11.6	5.8
$TrcA_1$	11.20	1283.71	1283.7	>95	4.5	2.3
TrcB*	9.29	1308.71	1308.7	>95	18.8	9.4
TrcB'$	9.41	1308.70	1308.7	>94	0.4	0.2
$TrcB_1$	9.14	1322.71	1322.7	>95	9.1	4.6
$TrcB_1$'$	9.05	1322.70	1322.7	>95	0.7	0.4
TrcC*	8.19	1347.71	1347.7	>95	27.1	13.6
$TrcC_1$	7.54	1361.75	1361.7	>95	12.2	6.1

The Trcs were purified from 200 mg commercial tyrothricin (data courtesy BM Spahelf [29]). $ Dipeptide unit in TrcB' and TrcB1' is Phe-D-Trp * Similar R_t, purity and yields were obtained in this study. **Syn-TrcA was purified in this study to >95% and had a similar R_t and identical Mr as determined by ESMS.

Summary and conclusions: Part 1

An optimized HPLC method was developed for the purification and analysis of the Trc fraction from *B. aneurinolyticus* on a C_{18} column with CH_3CN as mobile phase. With the initial development of the HPLC protocol it was found that the resolution of cyclic Trcs increased with an increase in their retention to the stationary phase. Although an increase in temperature led to a decrease in the retention of both the TrcA and TrcB species, it also improved the overall resolution of these groups of Trcs. The separation obtained with HPLC compared well with separation obtained with UPLC. The proposed new analytical HPLC method was easily adapted for semi-preparative HPLC and led to the successful purification of eight tyrocidines from the tyrocidine fraction of the tyrothricin complex (Table 4.4). This is the first study in which milligram amounts of eight natural tyrocidines were successfully purified to >95% from tyrothricin using conventional semi-preparative HPLC. The purified tyrocidines were used in two studies subsequently published by our group [29, 31].

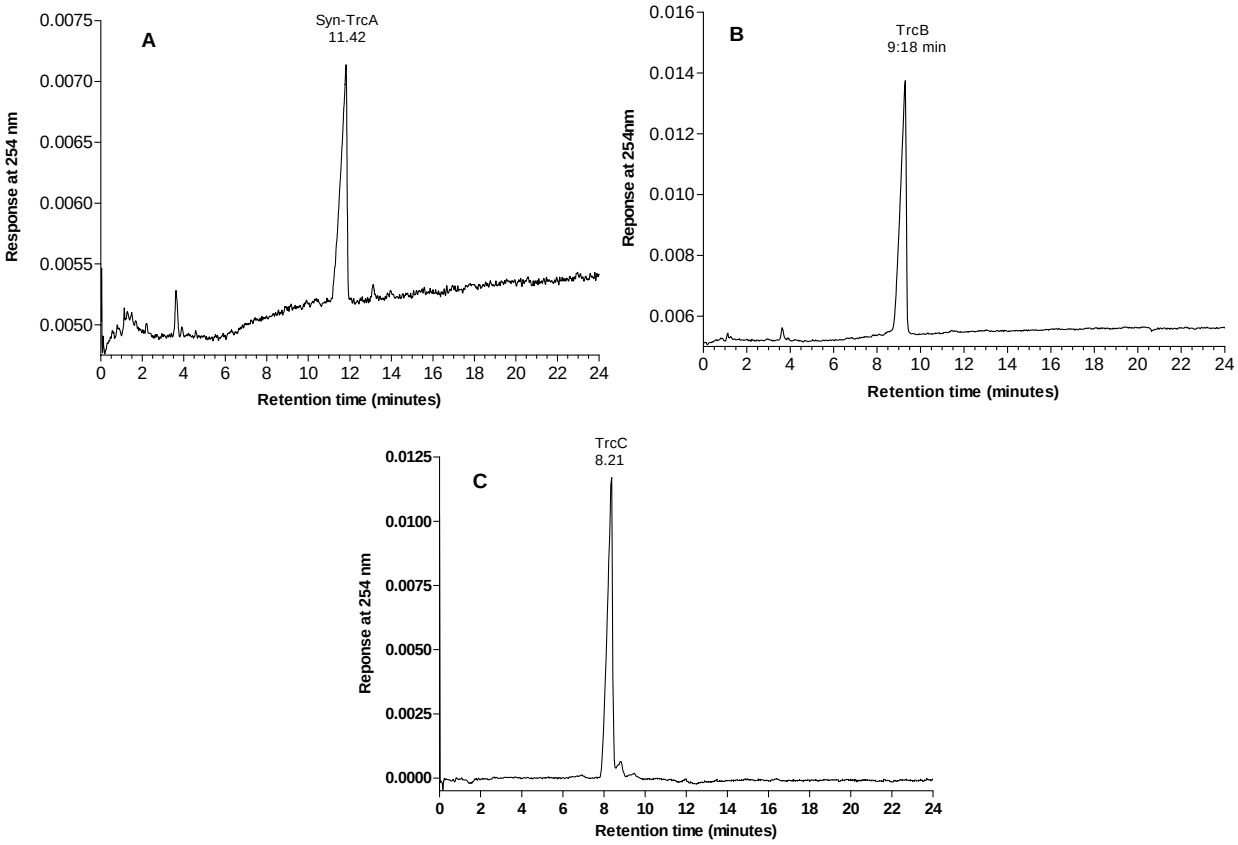

Figure 4.4 Analytical HPLC chromatograms obtained with method 4 at 35°C of the purified Trcs obtained in this study: **A** Syn-TrcA; **B** TrcB and **C** TrcC. The ESMS analyses of TrcB and TrcC are given in Appendix 4.1.

Results and Discussion: Part 2: Optimization of the gramicidin purification protocols

UPLC-MS optimization of the gramicidin D extract

The separation of GD extract from *B. aneurinolyticus* was also optimised with UPLC-MS in order to determine the elution profile of the different Grcs in the extract. This profile was then used as a guide to optimise the HPLC separation of these peptides. Nine Grcs were identified with UPLC-MS in the GD extract by their *m/z* values (see Figure 4.5). The co-elution of the GA analogues with IGA, VGA and IGC fractions was also observed.

HPLC optimization of the gramicidin purification protocol

The linear Grcs are the most hydrophobic fraction of the tyrothricin complex of *B. aneurinolyticus* [12]. A previously optimised Trc RP-HPLC purification protocol (method 4

at 35°C, Table 4.5) was used as a starting point for the development of a HPLC protocol for separating the peptides in the neutral gramicidin fraction.

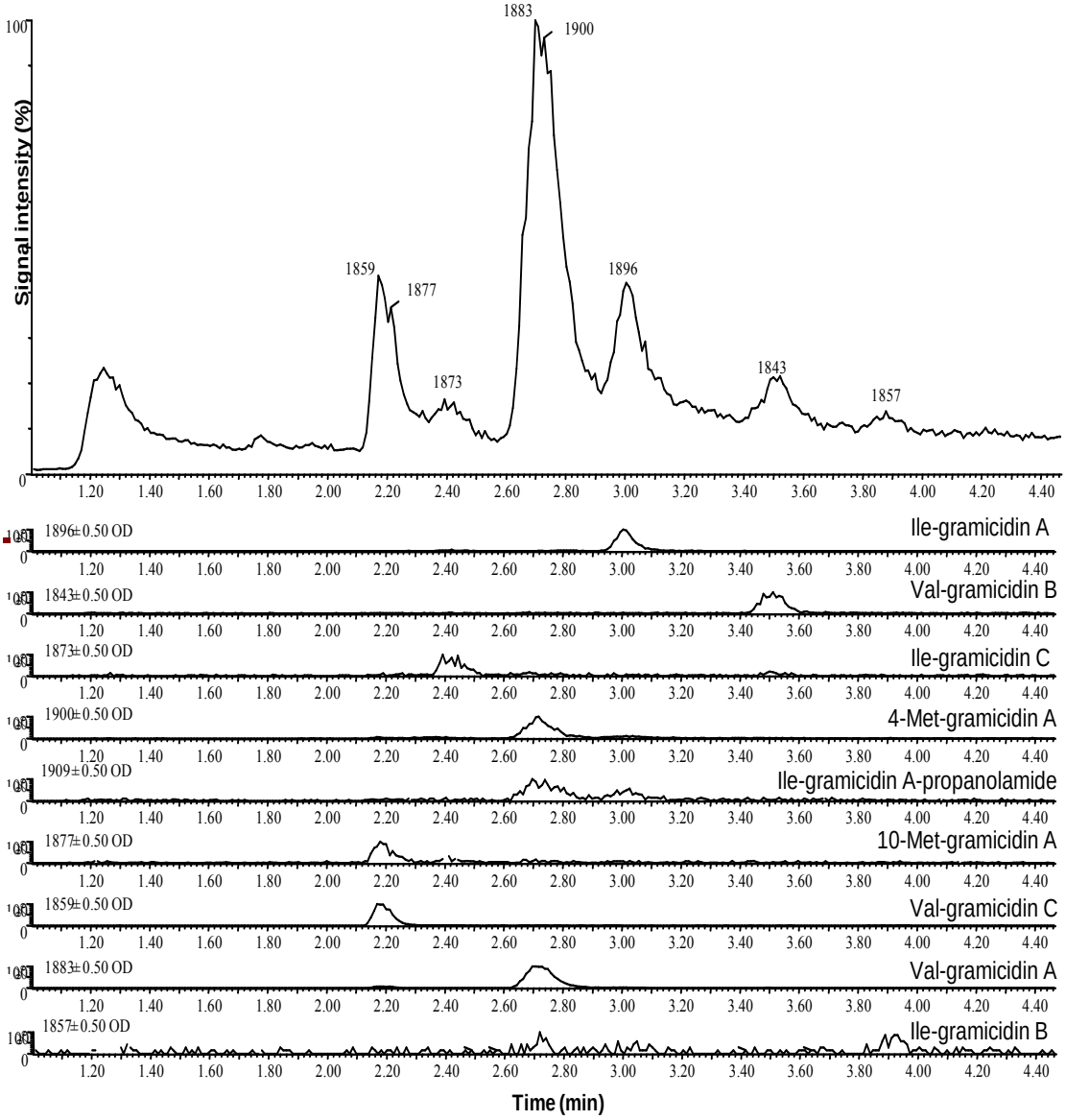

Figure 4.5 UPLC chromatogram of the commercial GD complex. The *m/z* of singly charged molecular species $[M+H]^+$ of the major Grcs are given for each peak. Details on the structure of the different Grcs are tabulated in Table 4.1.

This protocol gave some resolution between the different Grcs, but the peptides eluted in broad peaks only at the end of the gradient program (Figure 4.6A). With overlapping peaks,

the broader the peak, the higher is the percentage of cross-contamination between the different Grc species.

For example, the peak widths of VGC, VGA and VGB were 1.46, 2.22 and 2.17 min, respectively (Figure 4.6 D). In order to improve the resolution, reduce the peak width and decrease the Grc retention on the C_{18} matrix the CH_3CN gradient was changed first from 50→80% to 50→100% over 23.5 min (method 5 in Table 4.2), then from 50→100% to 60→100% over the same time (method 6 in Table 4.2). The latter gradient program led to an improvement in the resolution, retention, peak shape and intensity of all Grc species (Figure 4.6C and Table 4.5). In particular, the peak widths of VGC, VGA and VGB were reduced to 1.25, 1.59 and 1.28 min, respectively (see Figure 4.6 F). This peak width reduction is probably not only due to decrease in association with the C_{18} matrix, but also a decreased aggregation of the Grcs at a higher acetonitrile concentration.

The gradient type was also re-evaluated as early results had shown that an isocratic and linear gradient at 80% CH_3CN gave good resolution for the two GC species (results not shown). However, as for the Trcs, a concave non-linear gradient gave overall the best separation of the different Grcs (Figure 4.6). The effects of temperature on the separation of the linear gramicidins were also investigated in this study. It was found that a 10ºC increase to 45ºC increased the retention of all gramicidin species, but with extensive peak tailing (Figure 4.6 B). The peak tailing may be due to an increase interaction with the C_{18} matrix, a result of the increased hydrophobic effect at higher temperatures.

An attempt to further improve the separation by using CH_3OH (90% CH_3OH, 10% of 0.1% TFA in water) or a CH_3OH/CH_3CN mixture (90% CH_3OH/CH_3CN (*v/v*), 10% of 0.1% TFA in water) resulted in poor chromatographic separations, as was also found by other investigators [25] (results not shown). Alternative solvent modifiers such as formic acid and

triethylamine were also tested, as well as a C_8 stationary phase, but none improved the resolution (results not shown).

Table 4.5 Summary of the calculated parameters from the separation of the Grcs with the different RP-HPLC protocols.

	Parameters	VGA	IGA	VGB	IGB	VGC	IGC
Method 4, 35°C	**Rt (min)**	14.52	15.54	18.38	20.04	11.59	12.22
	k'	13.1	14.09	16.84	18.46	10.25	10.86
	α	1.09		1.07		0.95	
	R_S	0.43		0.27		0.64	
Method 5, 45°C	**Rt (min)**	9.51	10.49	12.4	13.37	6.58	7.29
	k'	6.58	7.39	9.08	9.54	4.34	4.59
	α	1.12		1.05		1.06	
	R_S	0.42		0.47		0.45	
Method 6, 35°C	**Rt (min)**	8.40	9.11	10.37	11.13	6.58	7.04
	k'	7.16	7.84	9.07	9.81	5.39	5.83
	α	1.08		0.91		0.92	
	R_S	0.48		0.26		0.64	
Orwa *et al.* [24] Spherisorb ODS column, 50°C, CH_3OH/H_2O	**Rt (min)**	22.08	26.25	42.51	52.08	15.42	17.51
	R_S'	2		2.8		3.6	
	R_S	1.2		2		2.6	
Thurbide and Zhang [25] pFC column 40°C, CH_3OH	**Rt (min)**	9.19	12.48	18.40	na	6.07	7.28
	R_S'	na		na		na	
	R_S	0.67		na		0.87	

Rs calculated from equation 4.3; Rs' – equations used unknown.

Decreasing the peptide retention on the stationary phase therefore again improved the HPLC resolution between the analogous peptides. The chromatographic separation (elution profile) of the three groups of Grcs achieved here correlated well with results from previous studies [21-25], although the resolution was poorer due to peak broadening. Method 6 gave the best resolution between the GA peptides (see Figure 4.6 and Table 4.5) while method 5 gave the best resolution for the GB peptides. However, method 5 caused extensive peak broadening and tailing, especially for the GA peptides. The best overall results were therefore obtained with method 6 at 35°C, with CH_3CN as mobile phase and with 0.1% TFA as modifier (Table 4.6). This method was selected and used throughout this study for the purification of linear Grcs from GD, A and C and the analysis of the purified peptides.

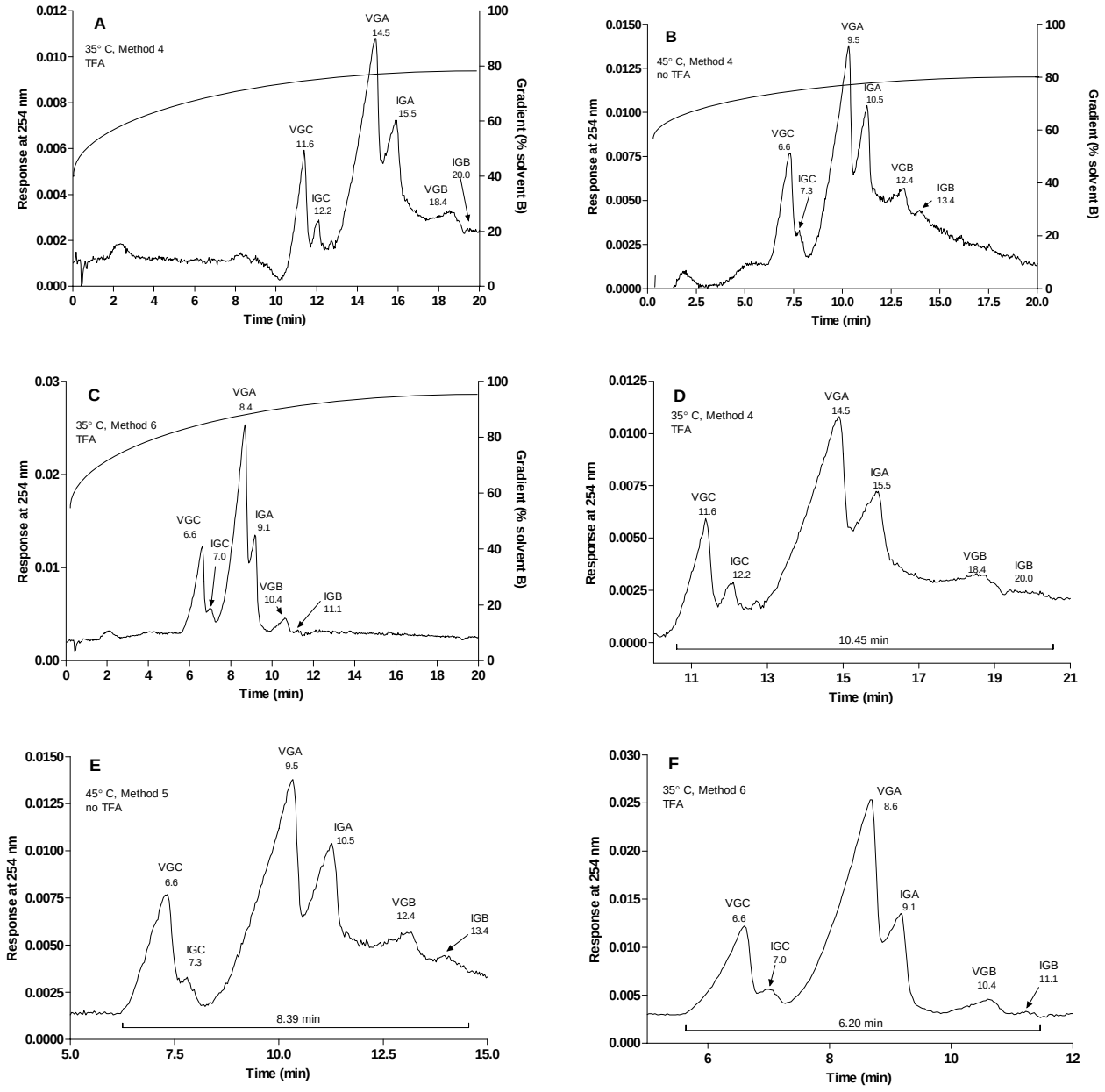

Figure 4.6 Analytical C_{18} HPLC chromatograms of the linear Grcs showing the influence of the temperature and solvent modifier, TFA (compare **A**, **B** and **D**, **E**) and changing the gradient (compare **A**, **C** and **D**, **F**) on the separation and resolution of the peptides in the Grc extract. Chromatograms **D**, **E** and **F** show the detail of the separations in **A**, **B** and **C** respectively. 10 μg peptides were injected in each run.

Purification and characterisation of gramicidin fractions

The optimised analytical protocol was easily adapted to semi-preparative HPLC for the purification of the GD mixture. Up to 400 μg Grc per run could be purified, without compromising the separation of the peptide components. The purification of the different

Grcs to >90% was only successful after two to three sequential purification runs, because of the co-elution of GA analogues (Table 4.6).

Table 4.6 Summary of the different Grcs purified under optimal conditions developed in this study by other researchers in our group. *The results from peptides purified in this study is shown in brackets.

ID	Exp Mr	Theor Mr	Purity (%)	Yield (mg)	Yield (%)
VGA*	1881.1	1881.07	>85 (>95)	0.25 (2.2)	6.2 (11)
IGA	1895.1	1895.06	>85	0.18	4.5
VGB	1842.1	1842.04	>85	0.12	3.1
VGC*	1858.1	1858.13	>85 (>70)	0.16 (0.25)	4.5 (1.3)
IGC	1872.1	1872.07	>85	0.14	4.0
MVGA*	1899.1	1899.33	(>95)	(0.23)	(1.2)

MVGA is 4-Met-VGA. The gramicidins VGA, IGA and VGC and were purified from 20 mg commercial gramicidin D, and VGC and IGC were purified from 10 mg commercial gramicidin C (Data courtesy J Esterhuizen).

The first isolates of the five major Grcs were all contaminated with VGA or analogues. This was to be expected as UPLC showed co-eluting profiles (see Figure 4.5). Similar co-elution problems with RP-HPLC were also reported by Thurbide and Zhang [25] who noticed that small quantities of VGA co-eluted with GC components from a poly(styrene-divinylbenzene) column. This could be due to VGA association with other Grcs, such as the reported hetero-oligomers of VGA and VGC [32]. Repeating the semi-preparative isolation procedure yielded high purity Grcs. The purified peptides were further analysed using analytical HPLC, ESMS and MSMS to confirm their identity and purity (refer to Appendix 4.2 for the analysis of VGA). As for the Trcs, the isolated Grcs were only considered pure if both the analytical HPLC and ESMS data indicated homogeneity (Table 4.6).

The analytical HPLC and ESMS profiles of the three Grcs purified for this study showed that these fractions were of high purity, except for VGC, the purity of which was estimated to be > 70% (see Table 4.6 and Figure 4.8). VGC contained small amount of VGA, because VGA

is capable of forming different dimers with Grc analogues and the hetero-oligomers co-eluted in the same fraction.

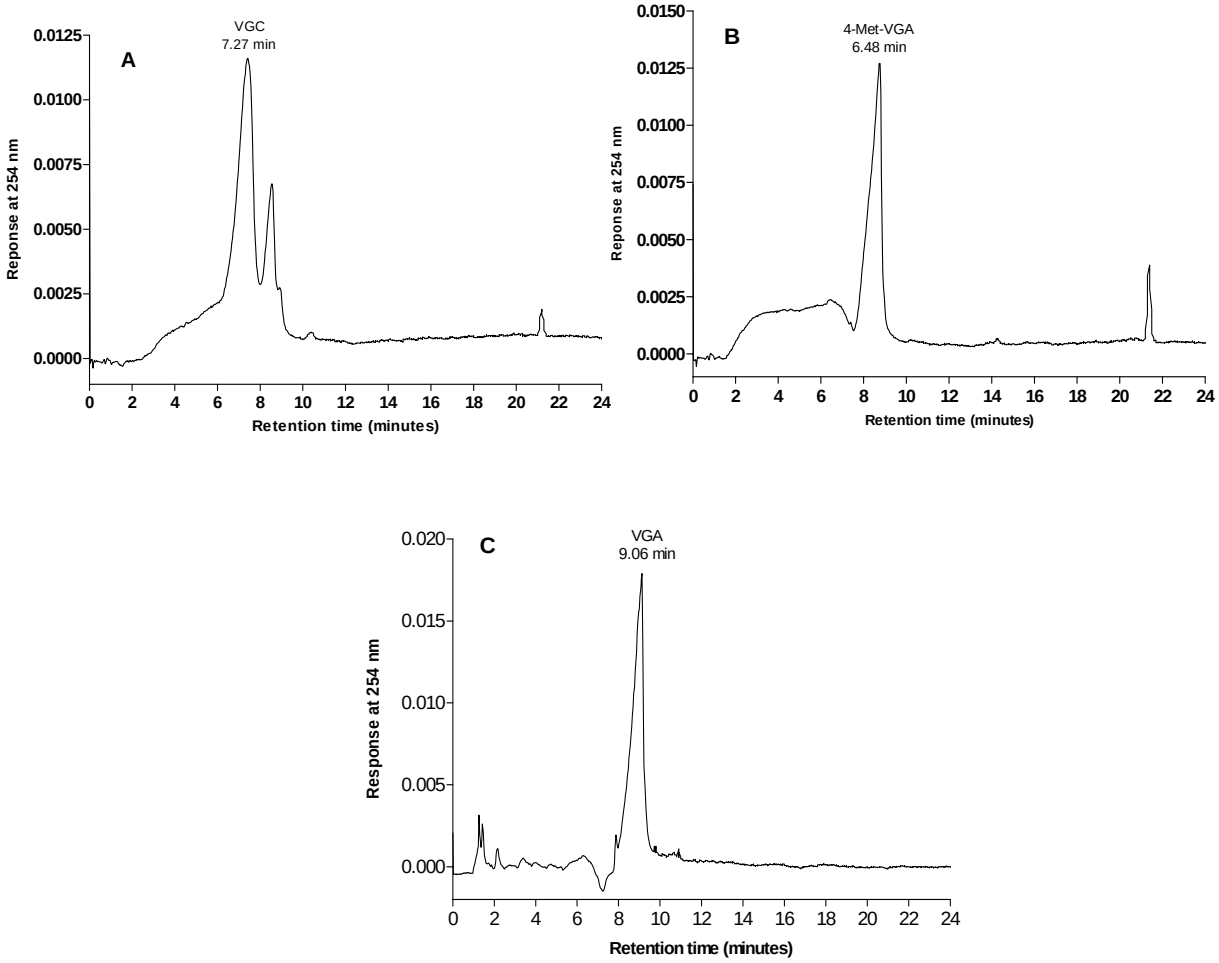

Figure 4.7 Analytical HPLC chromatograms obtained with method 6 at 35°C of the purified Grcs from this study: **A** VGC; **B** 4-Met-VGA and **C** VGA.

In total, six linear Grcs, including the low abundance 4-Met VGA (Table 4.6), were purified from the commercial GD extract in this study and by our group, using the optimised program (Table 4.6**)**.

Summary and conclusions: Part 2

In this second part an optimized HPLC method is presented for the purification and analysis of the linear gramicidin fractions from *B. aneurinolyticus* on a C_{18} column with CH_3CN as mobile phase.

Because of their higher hydrophobicity, linear Grcs could only be separated on a non linear gradient at 35°C starting with a high organic solvent concentration (60%) in the mobile phase. Higher temperature and concentration of CH_3CN caused a decrease in the retention of all Grcs on the stationary phase (early elution), but improved their resolution substantially. The improved Grc HPLC profile obtained with conventional analytical HPLC (method 6 at 35^{o}C) only compared fairly with the better resolved profile achieved with UPLC of the same fraction (compare Figure 4.5 with 4.6C). However, the optimised new analytical HPLC method was easily adaptable to semi-preparative HPLC for the successful purification of six Grcs from the GD extract. This is also the first study in which mg amounts of VGA and four other Grcs were purified with conventional semi-preparative HPLC.

General conclusion

The successful HPLC method optimization was an important step for further investigation as it allowed the purification of the different Trcs and Grcs used in this study. The following chapter (Chapter 5) describes the results of an investigation into the influence of GA and surfactin (Srf) on the antimicrobial activity of the purified Trcs. It also investigates the possible non-covalent complex formation and/or structural change caused by GA and Srf on the purified Trcs and analogues.

References

1 Shida, O., Takagi, H., Kadowaki, K. and Komagata, K. (1996) Proposal for two new genera, *Brevibacillus gen. nov*. and *Aneurinibacillus gen. nov*. Int. J. Syst. Bacteriol. **48**, 939-946

2 Hotchkiss, R. D. (1944) Gramicidin, tyrocidine and tyrothricin. Adv. Enzymol. **4**, 153-199

3 OKuda, K., Edwards, G. C. and Winnick, T. (1963) Biosynthesis of gramicidin and tyrocidine in the Dubos strain of *Bacillus brevis*. J. Bacteriol. **85**, 329-338

4 Dubos, R. J. (1939) Studies on a bactericidal agent extracted from a soil bacillus. II. Protective effect of the bactericidal agent against experimental pneumococcus infections in mice. J. Exp. Med. **70**, 11-17

5 Gutierrez-Manero, F. J., Ramos-Solano, B., Probanza, A., Mehouachi, J., Tadeo, F. R. and Talon, M. (2001) The plant growth promoting rhizobacteria *Bacillus pumilus* and *Bacillus licheniformis* produce high amount of physiologically active gibberellins. Physiol. Plant. **111**, 206-211

6 Bourinbaiar, A. S. and Coleman, C. F. (1997) The effect of gramicidin, a topical contraceptive and antimicrobial agent with anti-HIV activity, against herpes simplex virus type 1 and 2 *in vitro*. Arch. Virol. **142**, 2225-2235

7 Bourinbaiar, A. S., Kraisinski, K. and Borkowsky, W. (1993) Anti-HIV effect of gramicidin in vitro: Potential for permicide use. Life Sci. **54**, 5-9

8 Otten-Kuipers, M. A., Coppens-Burkunk, G. W., Kronenburg, N. A., Vis Mde, A., Roelofsen, B. and Op den Kamp, J. A. (1997) Tryptophan-N-formylated gramicidin causes growth inhibition of *Plasmodium falciparum* by inducing potassium efflux from infected erythrocytes. Parasitol. Res. **83**, 185-192

9 Dubos, R. J. (1939) Studies on a bacterial agent extracted from a soil bacillus. I. Preparation of the agent. Its activity *in vitro*. J. Exp. Med. **70**, 1488-1497

10 Van Epps, H. L. (2006) Rene Dubos: unearthing antibiotics. J. Exp. Med. **203**, 259

11 Rautenbach, M., Vlok, M., Stander, M. and Hoppe, H. (2007) Inhibition of malaria blood stages by tyrocidines, membrane-active cyclic peptide antibiotics from *Bacillus brevis*. Biochim. Biophys. Acta. **1768**, 1488-1497

12 Tang, X.-J., Thibault, P. and Boyd, R. K. (1992) Characterisation of the tyrocidine and gramicidin fractions of the tyrothricin complex from *Bacillus brevis* using liquid chromatography and mass spectrometry. Int. J. Mass Spectrom. Ion Processes. **122**, 153-179

13 Vogt, T. C. B., Schinzel, S. and Bechinger, B. (2003) Biosynthesis of isotopically labeled gramicidins and tyrocidins by *Bacillus brevis*. J. Biomol. NMR. **26**, 1-11

14 Breslow, R. and Chipman, D. (1965) The use of tyrocidines for the study of conformation and aggregation behavior. J. Am. Chem. Soc. **87**, 4196-4198

15 Loundon, G. M., Lukton, D. P. A. and Koshland, D. E. (1969) The effect of association on the nuclear magnetic resonance spectra of tyrocidine B_1. J. Am. Chem. Soc. **91**, 2794-2796

16 Barber, M., Bell, D. J., Morris, M. R., Tetler, L. W., Monaghan, J. J., Morden, W. E., Bycroft, B. W. and Green, B. N. (1992) An investigation of the tyrothricin complex by tandem mass spectrometry. Int. J. Mass Spectrom. Ion Processes. **122**, 143-151

17 Mahoney, W. C. and Hermodson, M. A. (1980) Separation of large denatured peptides by reverse phase high performance liquid chromatography. Trifluoroacetic acid as a peptide solvent. J. Biol. Chem. **255**, 11199-11203

18 Huang, J. X. and Guiochon, G. (1989) Application of preparative high-performance lipuid chromatography to the separation and purification of peptides and proteins. J. Chromatogr. **492**, 431-469

19 Boysen, R. I. and Hearn, M. T. (2001) HPLC of peptides and proteins: Standard operating conditions. Curr. Protoc. Mol. Biol. **10**, 1–10

20 Regnier, F. E. (1983) High performance liquid chromatography of biopolymers. Science. **222**, 245-252

21 Koeppe, R. E. and Weisss, L. B. (1981) Resolution of linear gramicidins by preparative reverse phase high performance liquid chromatography. J. Chromatogr. **208**, 414-418

22 Stankovic, C. J., Delfino, J. M. and Schreiber, S. L. (1990) Purification of gramicidin A. Anal. Biochem. **184**, 100-103

23 Axelsen, K. S. and Vogelsang, S. H. (1977) High performance liquid chromatographic analysis of gramicidin, a polypeptide antibiotic. J. Chromatogr. **140**, 174-178

24 Orwa, J. A., Govaets, C., Roets, E., Van Schepdael, A. and Hoogmartens, J. (2001) Liquid chromatography of gramicidin. Chromatography. **53**, 17-21

25 Thurbide, K. B. and Zhang, J. (2005) Separation of linear gramicidins using carbon dioxide-containing mobile phases. Anal. Bioanal. Chem. **2**, 25-34

26 Hotchkiss, R. D. and Dubos, R. J. (1941) The isolation of bactericidal substances from cultures of *Bacillus brevis*. J. Biol. Chem. **142**, 155-162

27 Sneyder, L. R., Kirkland, J. J. and Glajch, J. L. (1992) Practical HPLC method development. Wiley, New York

28 Guan, K. and Palmer, D. C. (2006) Effects of trifluoroacetic acid concentrations in mobile phases on HPLC retention of zwitterionic and weakly basic triazole derivatives. J. Liquid. Chromatogr. Relat. Technol. **29**, 415-430

29 Spathelf, B. M. (2009) The structure-activity/toxicity relationships of the tyrocidines, a group of cyclic decapeptides from *Bacillus brevis*. PhD thesis, University of Stellenbosch, Stellenbosch

30 Sheehan, D. (2000) Physical Biochemistry: Principles and Applications. Wiley and Sons, Baffins, Chichester

31 Spathelf, B. M. and Rautenbach, M. (2009) Anti-listerial activity and structure activity relationships of the six major tyrocidines, cyclic decapeptides from *Bacillus aneurinolyticus*. Bioorg. Med. Chem. **17**, 5541-5548

32 Bano, M. C., Salom, D. and Abad, C. (2003) Size-exclusion high-performance liquid chromatography in the study of the auto associating antibiotic gramicidin A in micellar milieu. J. Biochem. Biophys. Methods. **56**, 297-309

33 Standing, K. G. (2003) Peptide and protein *de novo* sequencing by mass spectrometry. Curr. Opin. Struct. Biol. **13**, 595-601

34 Tomer, K. B., Crow, F. W., Gross, M. L. and Kopple, K. D. (1984) Fast atom bombardment combined with tandem mass spectrometry for the determination of cyclic peptides. Anal. Chem. **56**, 880-886

APPENDIX 4.1 ESMS analysis of the purified tyrocidine B and tyrocidine C

The positive mode ESMS spectrum of the Trc complex extracted from tyrothricin without further purification showed a complex mixture of Trcs in the range of *m/z* = 1250 to 1400 (results not shown). Other signals arising from *m/z* = 600 to 720 correspond to the doubly charged species of the Trcs. ESMS analysis done on the individual purified peptide fractions showed that these peptides were of high purity. Singly and doubly charged molecular ions were detected for TrcB (*m/z* = 1309.63 singly charged and *m/z* = 655.34 doubly charged ions) and TrcC (*m/z* = 1348.68 singly charged and *m/z* = 674.84 doubly charged ions) with their respective isotopes (Table 4.7 and Figure 4.8). The respective Na^+ adducts molecular ions and isotopes of the purified Trcs were also detected at *m/z* = 1331.66 and 1370.7.

Table 4.7 Summary of the different ion species in the purified TrcB and TrcC fractions as detected by positive ESMS.

Peptide	Mr	Species	Exp *m/z*	Det *m/z*
TrcB	1308.67	$[M_{TrcB}+H]^+$	1309.67	1309.63
		$[M_{TrcB}+Na+H]^+$	1331.67	1331.66
		$[M_{TrcC}+2H]^{2+}$	655.33	655.34
TrcC	1347.70	$[M_{TrcC}+H]^+$	1348.70	1348.62
		$[M_{TrcC}+Na+H]^+$	1370.70	1371.69
		$[M_{TrcC}+2H]^{2+}$	674.85	674.84

Abbreviation: tyrocidine A - Syn-TrcA; tyrocidine B - TrcB; tyrocidine C – TrcC

ESMS-MS analysis of the purified Trcs was done in order to verify the primary structure of these peptides and to assess of their purity [33]. According to collusion induced dissociation (CID) performed on the purified Trcs, the major fragment ions found were from the b and y series occasionally accompanied by their a-ions. These ions arise from the ring-opening acylium of TrcB and TrcC fractions (m/z = 1308.7 and 1348.7) between the D-Phe^4 and Pro^5 residues (see Figure 4.9 and Table 4.8) [34].The entire b_2-b_8 ion series of the corresponding ring-opened acylium ions of the two peptides was found to be in accordance with the studies of Tang *et al.* [12]. Fragments with CO loss (a_2), or water loss (exclusively b_9) were also found in all spectra of the corresponding ring-opened acylium ions.

Table 4.8 Summary of the b fragment ions series obtained from the MSMS fragmentation of the purified TrcB and TrcC fractions.

	TrcB			**TrcC**		
Fragment ions	**amino acid sequence**	**cal *m/z***	**obs *m/z***	**amino acid sequence**	**cal *m/z***	**obs *m/z***
b_1	**H-Pro**	98.5	na	**H-Pro**	98.5	na
b_2	**Trp**	284.13	284.14	**Trp**	284.13	284.14
b_3	**Phe**	431.2	431.21	**Trp**	470.21	470.23
b_4	**Asn**	545.24	545.27	**Asn**	584.25	584.28
b_5	**Gln**	673.55	673.33	**Gln**	712.31	712.33
b_6	**Tyr**	836.3	836.39	**Tyr**	875.37	875.39
b_7	**Val**	935.43	935.48	**Val**	974.44	na
b_8	**Orn**	1049.63	1049.5	**Orn**	1088.64	1088.5
b_9	**Leu-H_2O**	1144.79	1144.6	**Leu-H_2O**	1183.8	1183.6
b_{10}	**Phe**	1309.86	1309.6	**Phe**	1348.87	13348.6

Standard three letter abbreviations are used for the amino acid residues. Abbreviation: tyrocidine B - TrcB; tyrocidine C - TrcC; cal *m/z* – calculated *m/z*; obs *m/z* – observed *m/z*

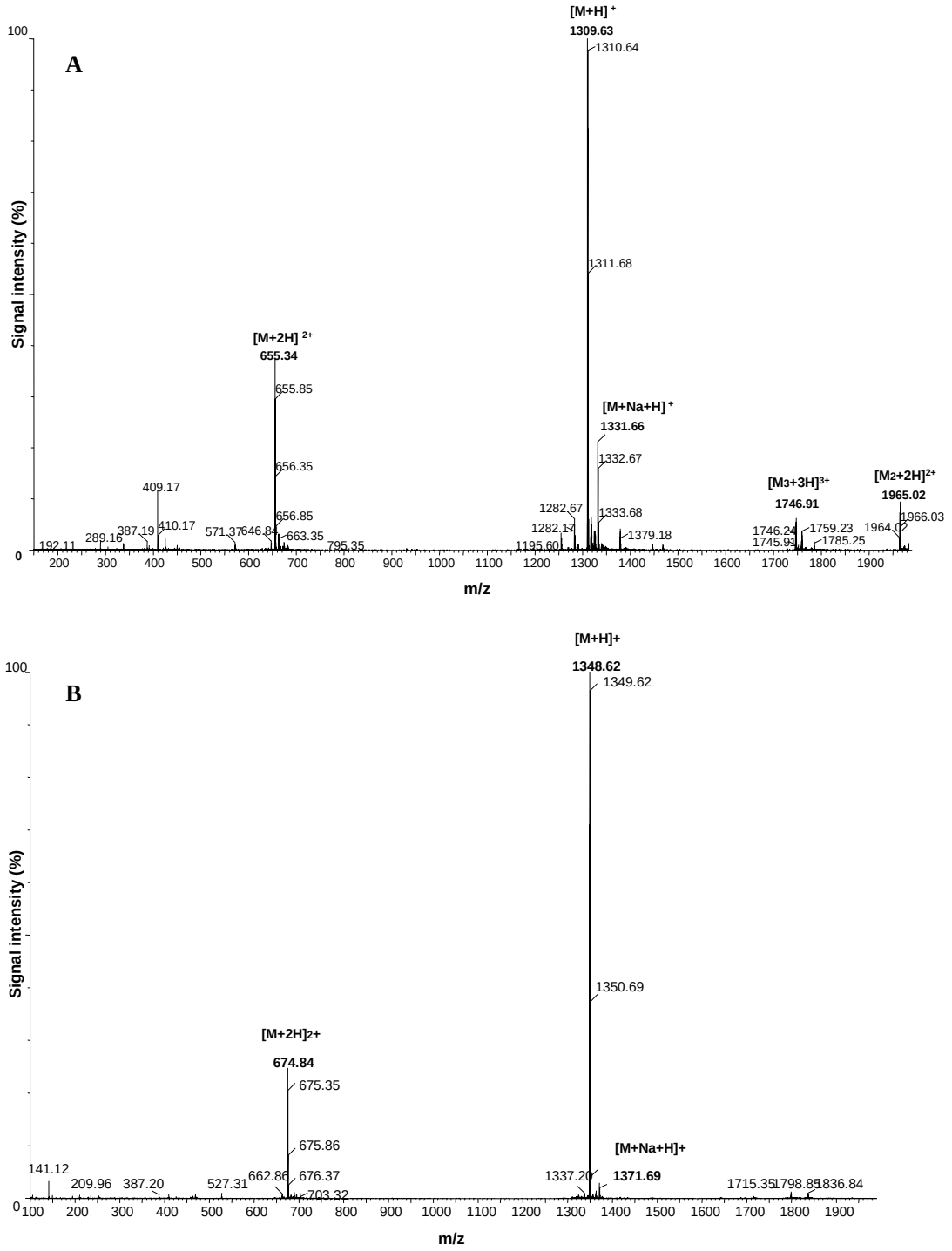

Figure 4.8 Mass spectrum of the purified **A** TrcB and **B** TrcC fractions in the positive mode.

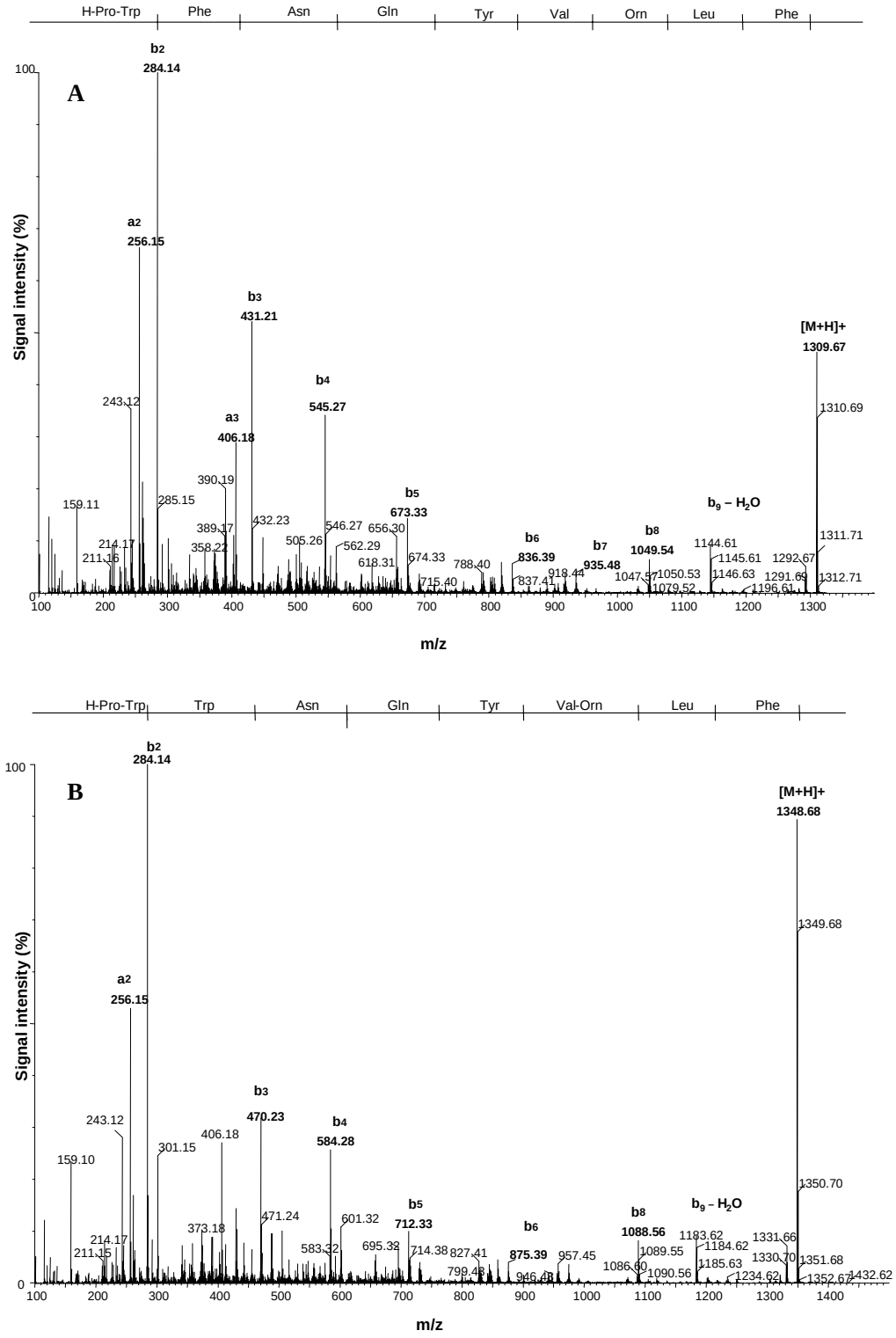

Figure 4.9 CID spectra of the purified tyrocidines with the molecular ions: *m/z* = 1309.7 and 1348.7 corresponding to the ring opened acylium at the Pro residue of the purified **A** TrcB and **B** TrcC respectively.

APPENDIX 4.2 ESMS analysis of the purified valine-gramicidin A

The ESMS spectrum of the purified Grc fractions showed that not more than one peptide was present. Singly charged molecular ions with m/z values of 1882.1 and 1905.1 corresponded to the VGA (molecular weight = 1881.1) and its sodium adduct, respectively (Figure 4.10). Other species with m/z values of 942.0, 953.0 and 964.04 were also found. These corresponded to the doubly charged molecular ion of VGA and its sodium and potassium adducts. Trace quantities of species with *m/z* = 248.14, 539.32, 638.39, 37.47 and 1032.0, which matched with fragments y_1 and b_6-b_8 of VGA ($[M+H]^+$ m/z = 1882.1), were evident.

Table 4.9 Summary of the b fragment ions series from the CID of the singly charger ions of the purified VGA using ESMS-MS.

Fragment ions	**amino acid sequence**	**cal *m/z***	**obs *m/z***
b_0	**HCO**	29.00	-
b_1	HCO-**Val**[1]	128.07	-
b_2	HCO-V**G**	185.12	-
b_3	HCO-VG**A**	256.16	-
b_4	HCO-VGA**L**	369.32	369.21
b_5	HCO-VGAL**A**	440.35	440.26
b_6	HCO-VGALA**V**	539.42	539.33
b_7	HCO-VGALAV**V**	638.49	638.4
b_8	HCO_VGALAVV**V**	737.56	737.47
b_9	HCO-VGALAVVV**W**	923.64	923.56
b_{10}	HCO-VGALAVVVW**L**	1036.80	1037.63
b_{11}	HCO-VGALAVVVWL**W**	1222.88	1223.7
b_{12}	HCO-VGALAVVVWLW**L**	1336.04	1336.8
b_{13}	HCO-VGALAVVVWLWL**W**	1522.12	1522.9
b_{14}	HCO-VGALAVVVWLWLW**L**	1635.28	-
b_{15}	HCO-VGALAVVVWLWLWL**W**	1821.36	-
$[M+H]^+$	HCO-VGALAVVVWLWLWL**W**$\mathbf{NHCH_2CH_2OH}$	1882.10	-

Standard three letter abbreviations are used for the amino acid residues. Abbreviation: cal *m/z* – calculated *m/z*; obs *m/z* – observed *m/z*

Figure 4.11 shows the CID fragmentation spectra of the singly charged ion ($[M+H]^+$) of the purified VGA. The entire b_4-b_{13} ion series of VGA was identified (Table 4.9). Other fragments with *m/z* of 248.41 and 847.48, corresponding to the y_5 and y_1 of the purified peptide, were also found (Figure 4.11). These results confirmed the purity of the purified VGA.

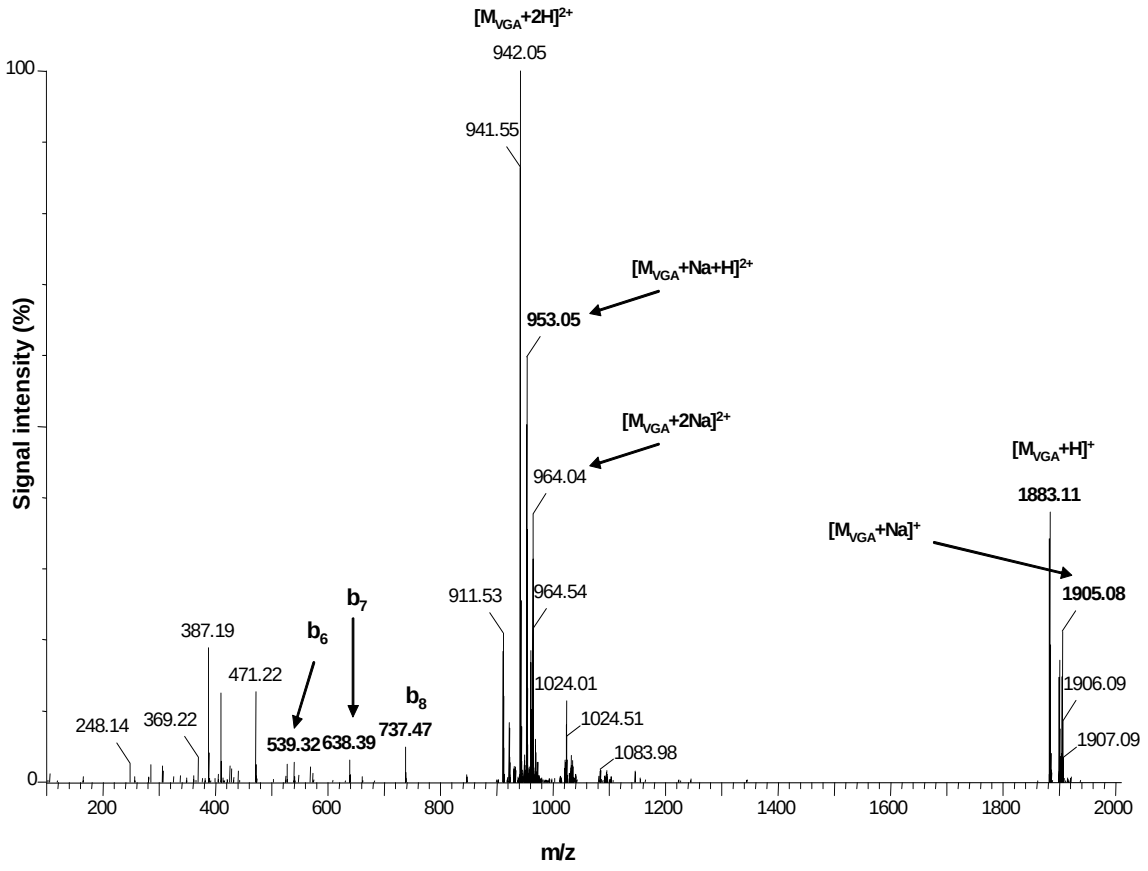

Figure 4.10 Mass spectrum of the purified VGA fraction recorded in the positive mode.

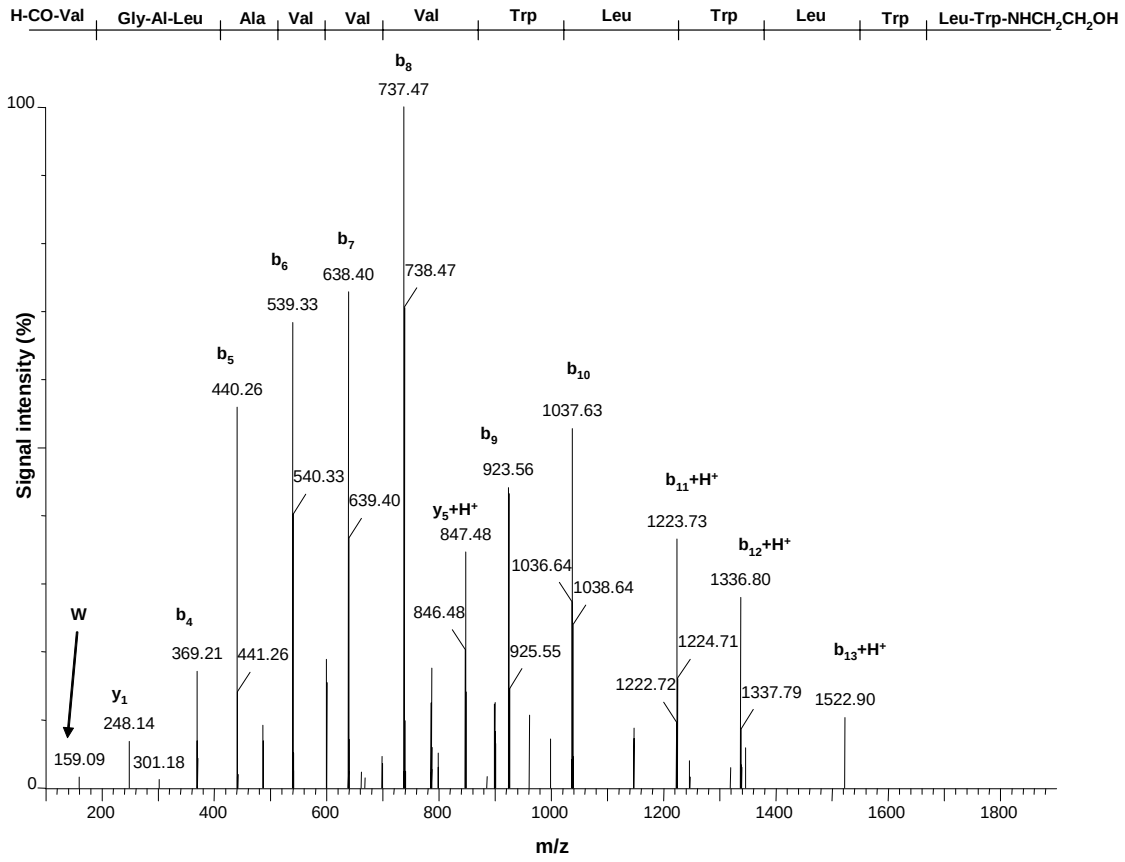

Figure 4.11 CID spectrum of the $[M + H]^+$ ion of the purified VGA (B) fractions recorded in the positive mode.

Chapter 5

The influence of gramicidin A and surfactin on the cyclic tyrocidines from *Bacillus aneurinolyticus*

Introduction

The objective of this part of the study was to test the hypothesis that antagonistic peptide actions, similar to the antagonism of gramicidin S (GS) activity by surfactin (Srf) (described in Chapter 2) [1] also occur between Srf and peptides from the tyrothricin complex, namely the analogous tyrocidines (Trcs) and linear neutral gramicidins (Grcs) from *Bacillus aneurinolyticus* [2, 3]. In Chapter 3 it was demonstrated that the antagonism of GS activity by Srf is partially due to inactive complex formation between GS and Srf. These complexes involve non-covalent interaction between one of the cationic ornithyl (Orn) residues of GS and the anionic Asp residue of Srf, stabilized by the hydrophobic interaction between D-Phe from GS and a number of aliphatic amino acids in Srf. The cyclic and basic decapeptide Trcs share structural similarities with GS, in particular the Val-(Orn/Lys)-Leu-D-Phe-Pro pentapeptide moiety that possess one cationic residue (either Orn or Lys), but vary in the number of Phe residues in the variable neutral pentapeptide unit (Table 5.1) [3].

The Trcs form a rigid antiparallel β-pleated sheet structure [4, 5] and have a broad spectrum of activity towards Gram-positive bacteria such as *B. Subtilis* (this study)*, M. luteus* [6] and *Listeria monocytogenes* [6, 7]. However, the Trcs are less active against Gram-negative bacteria such as *Escherichia coli* [6]. They also exhibit lytic activity against erythrocytes and *Plasmodium*

falciparum infected erythrocytes [8]. Several studies have reported the association of cyclic Trcs in higher order structures. According to Williams *et al*. [9] Trcs can self-associate or aggregate to form either homo or heteropolymers. This association only takes place at higher peptide concentrations and has relatively large activation energy [9]. They can also form non-covalent complexes with the co-produced linear and neutral Grcs. Therefore, studying the influence of Srf on the structure and activity of Trcs would shed light on the role of a single GS pentapeptide (Val-Orn-Leu-D-Phe-Pro or VOLfP) moiety in antagonism, as well as the role of complex formation and/or self assembly/aggregation state of the Trcs in the possible interaction with Srf. The activities of two purified Trcs in the absence and presence of added Srf towards the two *Bacillus subtilis* strains were investigated, one strain which has a high level of basal Srf production, and one strain which does not produced Srf under the culture conditions.

Table 5.1 Amino acid sequence comparison between the purified tyrocidines and the analogous gramicidin S [3]

	Amino acid sequence									
Peptides	**1**	**2**	**3**	**4**	**5**	**6**	**7**	**8**	**9**	**10**
GS	**Pro**	Val	Orn	Leu	D-Phe	Pro	**Val**	**Orn**	**Leu**	**D-Phe**
TrcA	**Pro**	Phe	D-Phe	Asn	Gln	Tyr	**Val**	**Orn**	**Leu**	**D-Phe**
TrcB	**Pro**	Trp	D-Phe	Asn	Gln	Tyr	**Val**	**Orn**	**Leu**	**D-Phe**
TrcC	**Pro**	Trp	D-Trp	Asn	Gln	Tyr	**Val**	**Orn**	**Leu**	**D-Phe**

The second group of peptides from the tyrothricin complex that was included in this study is the Grcs, linear and neutral pentadecapeptides. The Grcs contain several neutral (Leu, Val, Ile) and aromatic amino acids (Phe; Tyr and Trp) in its sequence with the N and C-termini blocked by a formyl and alkanolamide group, respectively [3]. It was observed that linear Grcs, in particular gramicidin A (GA), have antibacterial [10], antiviral [11, 12] as well as antiplasmodial and haemolytic activities [13]. The Grcs were shown to act antagonistically toward the activity of Trcs in the tyrothricin producer strain [14-17]. Grc's association to Trc antagonises the Trc-DNA

complex responsible for the inhibition of RNA synthesis [16] in a similar way that it antagonises the effect of Trcs on membrane permeability in the producer strain [18]. Trc binding to Grcs non-specifically reverse the H_{II} phase induced by high concentrations of Grcs in a dioleoylphosphatidylcholine model membrane [18]. It was therefore decided to re-investigate the influence of GA from *B. aneurinolyticus* on the activity of the Trcs towards a model Gram-positive organism, *Micrococcus luteus*. Because the tyrothricin complex contains both the Trcs and Grcs, the influence of Srf on GA alone and on GA in combination with TrcB was also investigated.

In the biophysical analysis a number of physical analytical techniques were utilised to investigate the structures of the Trcs and the possible structural influences caused by Srf and GA, namely electrospray mass spectrometry (ESMS) [19, 20], circular dichroism (CD), fluorescence spectrometry (FS) and nuclear magnetic resonance (NMR). A brief introduction to ESMS, CD and NMR in the study of peptide structures has already been given in Chapter 3.

According to ESMS and high performance liquid chromatography (HPLC) studies, there are more than 28 Trcs and 10 Grcs which differ from one another in particularly concerning the hydrophobic and aromatic residues [3]. The CD spectra of Trcs exhibit two characteristic minima at about 205 and 215 nm except for tyrocidine C (TrcC) which shows an additional shoulder at 230 nm in water [21]. Linear Grcs exhibit different CD spectra in membrane and in solution [21-25]. This is due to the conformational changes adopted by linear Grcs in these different environments [22, 23, 26]. The CD spectra is influenced by both the aromatic amino acid composition and the aggregation state of the peptides in particular solvent systems [21, 27]. According to NMR the cyclic Trcs form a β-turn type anti-parallel β-sheet structure which is

stabilized by three intramolecular hydrogen bonds [5], while GA has a β-helical structure and forms head to tail a dimer [3].

The other relevant biophysical analytical technique used for probing peptide structure was fluorescence spectroscopy (FS). FS utilizes the intrinsic fluorescence of aromatic amino acids Trp, Tyr and Phe to investigate the conformational state of a peptide and the changes that occur under different conditions [27-29]. Because of their high quantum yields (high fluorescence intensity), only the fluorescence signal of Trp and Tyr are generally used experimentally. Photoselective excitation at 295 nm can be used to obtain the emission from only Trp [28] whereas excitation at 280 nm will excite both Trp and Tyr. Since the fluorescence emission of Trp often obstructs the fluorescence of Tyr and Phe as a consequence of interferences by resonance energy transfer, 295 nm is therefore the preferred excitation frequency for the study of fluorescence of peptides. The cyclic Trcs have a 40% aromatic amino acid residue content and those that contain one or two Trp residues are expected to have fluorescence emission at 295 nm. The changes in self-assembly/aggregation state/folding of the Trp-containing Trcs, due to Srf addition, can be studied by monitoring the change in the quantum yield of Trp. This quantum yield or maximal fluorescence intensity is not only influenced by neighbouring amino acids but also by changes in environmental conditions. If fluorescence intensity decreases or shift to the higher wavelengths (red shift), the peptide is less folded or assembled with exposure of the aromatic residues to the polar solvent leading to quenching of the photo selective excitation at 295 nm. However, if the fluorescence intensity increases or shifts to a lower wave length (blue shift), the peptides are in higher assembly/aggregation/folding state or embedded in a hydrophobic environment [30].

This chapter therefore describes an investigation into the influence of Srf and GA on the antimicrobial activity of purified Trcs (Part 1) and explores the possible molecular mode of these influences using biophysical techniques such as ESMS, CD, FS and basic one dimensional NMR (Part 2).

Materials

The tyrothricin peptide complex, the peptide mixture from which the Trcs and Val-GA were purified and analysed as described in Chapter 4, from *B. aneurinolyticus* was purchased from Sigma-Aldrich (Steinheim, Germany). The lipopeptide Srf from *B. subtilis* was purchased from Fluka Chemie (St Louis, USA). Commercial GA containing Val-GA and Ile-GA was obtained from Sigma-Aldrich (Steinheim, Germany).

B. subtilis (ATCC21332 and OKB120), *B. aneurynolyticus* ATCC10068 and *M. luteus* NCTC8340 were from the BIOPEP culture collection and used as the bacterial targets in the antimicrobial activity experiments. Reagents for TGYM media namely the skim milk powder was supplied by Clover (Rootepoort, SA). Acetonitrile (CH_3CN, HPLC-grade, far UV cut-off) was supplied Romil Ltd (Cambridge, UK). United Scientific (Durban, RSA) supplied ethanol (GR grade). D-glucose, the components for the Luria Bertani (LB); sodium chloride (NaCl), tryptone and yeast extract, tryptone soy broth (TSB), peptone, agar, the NaH_2PO_4 and Na_2HPO_4 as well as deuterated acetonitrile (CD_3CN, min 99% for NMR) were supplied by Merck (Darmstadt, Germany). Non sterile, standard non-treated polystyrene microtiter plates (96 well flat bottom) were supplied by Greiner bio-one (Frickenhausen, Germany) and Lasec (Cape Town, SA)

provided the culture dishes. A Millipore Milli Q® water system (Milford, USA) was used to prepare analytical quality water by filtering it from a reverse osmosis plant.

Methods

Bacterial assays

Freezer stocks of bacteria culture were cultured at 37 °C for 48 h on LB agar (1% (*w/v*) tryptone, 0.5% (*w/v*) yeast extract, 1 % NaCl, 1.5% (*w/v)* agar) for *M. luteus* NCTC8340 or TGYM agar (0.5% (*w/v*) peptone, 0.25% (*w/v*) yeast extract, 0.1 % (*w/v*) glucose, 0.1% (*w/v*) skim milk powder, 1.5% (*w/v*) agar) for *B. subtilis* strains (ATCC21332 and OKB120) and *B. aneurynolyticus* ATCC10068. Selected colonies of *B. subtilis* strains and *M. luteus* were grown overnight for 16 h in TSB and LB respectively and then sub-cultured in TSB at 37 °C for 6 hours to an optical density (OD) of 0.600 at 620 nm.

Microtiter broth dilution assays

Sub-cultured *B. subtilis* was diluted to OD 0.200 ± 0.01 before 90 µL was dispensed into the microtitre plate wells. Ten µL of the serial dilutions of test peptides and/or combinations were added in the plate well (each well contained a final volume of 100 µL) in the broth micro-dilution assays (adapted from Rautenbach *et al*. [31]). The inhibition was measured spectrophotometrically, after 16 h incubation, at 620 nm on a Titertek Multiscan Plus Mk II microtitre plate reader. All microtitre plates were blocked with sterile 0.5% casein in Dulbecco's phosphate buffered saline (PBS), dried and sterilized under UV light for at least 30 minutes prior to use in assays.

Mixed culture assay

Subcultures of *M. luteus* or *B. subtilis* (1 mL; OD = 0.60) were aliquoted into TGYM agar gel (9 mL; <45°C) and then mixed through dispersion for 10 s using a laboratory vortex, where after it was poured into a culture dish and allowed to set for 30 min (adapted from the radial diffusion assay by Du Toit and Rautenbach [32]). Selected colonies of *B. subtilis* and *B. aneurinolyticus* were then toothpick spotted on top of TGYM gel or *M. luteus* seeded TGYM gel in close proximity (< 1 mm) to allow interaction between the diffusible products of the two producer strains. Alternatively, *B. aneurinolyticus* was spotted on either *B. subtilis* ATCC21332 or OKB120 seeded TGYM agar. A Nikon SMZ 10A trinocular sterozoom microscope mounted with a Nikon Coolpix 990 camera was used to process and photograph cell colonies on the culture dishes after 2 days incubation at 37^{o}C.

Data processing for dose-response analysis

The relative growth of *B. subtilis* strains (ATCC21332 and OKB120) was calculated on the dose-response data obtained from antimicrobial assays by dividing the light dispersion per well by the mean light dispersion of the well containing the growth medium, the cells and peptide solvent (considered as 100% growth). The percentage inhibition was calculated by subtracting the relative growth from 100. Control wells with no peptides added were used to determine the total bacterial growth. Curve fits and statistical analyses were done using GraphPad Prism 3.0 (GraphPad Software Incorporated). Sigmoidal dose response curves (variable slope) were fitted for all dose-response data. Only the mean of triplicate/quadruplicate data points was considered for curve fitting. The IC_{50} values of the inhibitory concentration of the *B. subtilis* strains was calculated according to Rautenbach *et al.* [31, 32].

For the determination of antagonism, synergism or sum of activities for two active peptides the fractional inhibition (FIC) and FIC index were calculated for each of the two peptides in the assay using the following equations [33]:

$$FIC(A) = IC_{50} \text{ (peptide [A] in A+B mixture)}/ IC_{50} \text{ (peptide A alone)} \quad (5.1)$$

$$FIC(B) = IC_{50} \text{ (peptide [B] in A+B mixture)}/ IC_{50} \text{ (peptide B alone)} \quad (5.2)$$

$$\text{From the FIC values the FIC index} = FIC(A) + FIC(B) \quad (5.3)$$

with FIC index =1 indicating that the resultant IC_{50} is due to the sum of the activity of peptides A and B; FIC index >1 indicating that the resultant IC_{50} is due to antagonistic activity between peptides A and B; FIC index <1 indicating that the resultant IC_{50} is due to synergistic activity between peptides A and B.

Peptide purification

Natural tyrocidine B (TrcB), tyrocidine C (TrcC) and Val- gramicidin A (VGA) were purified using the optimised semi-preparative HPLC methods described in Chapter 4.

Electrospray mass spectrometry

The peptide samples were prepared by dissolving the respective peptides (0.1-0.05 mM) in a CH_3CN/H_2O (1:1, *v/v*). A Waters Q-Tof Ultima mass spectrometer fitted with a Z-spray electrospray ionisation source was used to perform ESMS analyses. A sample solution (3 to 10 µL) was introduced into spectrometer via a Waters Acquity UPLC^{TM}. The carrier solvent was CH_3CN/H_2O (1:1, *v/v* in 0.1% formic acid) and the flow rate was 300 µL/min. A capillary voltage of 3.5 kV and cone voltage of 35 V were applied. The source temperature was set at

100°C. Data acquisition was in the positive mode, scanning the second analyser (MS_2), through *m/z* 100 to 1999 (where the *m/z* is defined as the molecular mass to charge ratio). A combination of the scans across the elution peak and subtraction of the background produced representative scans.

Circular dichroism and fluorescence experiments

Analytical stock solutions (1.00 mM) of Srf and the purified Trcs and GA were prepared in ethanol/H_2O (2:1, *v*/*v*) for CD and fluorescence studies. Peptides (20.0 μL) were then diluted to 10.0 μM in analytical quality water (final volume was 2.00 mL, < 2% ethanol) before measurement. For the titration experiments a serial dilution of the Trc:Srf was made from 1:0.5 to 1:2 ratios in water and pre-incubated for at least 15 minutes before measurements. A Chirascan CD spectrometer was used to obtain CD spectra of the peptide solutions in a 1.00 cm quartz cuvette. CD and UV absorption spectra were collected simultaneously between 190 and 250 nm in water and 200 and 250 nm in TFE, with a 0.1 nm step in three to five.

For the fluorescence experiments, a model RF-5301PC spectrofluorophotometer (Shimadzu, Japan) was utilised. To acquire the excitation at 295 nm, emission spectra were recorded between 300 and 450 nm in 0.1 nm steps at 3nm slit width.

Nuclear magnetic resonance experiments

NMR analyses were done on a Bruker Avance 500 MHz NMR spectrometer equipped with a 5 mm BBI indirect detection pulse field gradient probe which operated at 298K (25°C). Dried peptide stocks (1-2 mg) were made in CD_3CN/H_2O (1:1, *v*/*v*). ^{1}H-NMR spectra were obtained with 64 scans using Watergate-based suppression sequences. The 2D NMR total correlation

spectroscopy (TOCSY) and rotating-frame Overhauser effect spectroscopy (ROESY) experiments were acquired with a total number 170 ms of mixing times. The ^{1}H NMR data were analysed using the ACD/NMR processor software academic edition (ACDLABS 12.0 software, [34, 35]) while the 2D data were processed on the Topspin 2. 1 package.

Results and discussion

Results and discussion Part 1: Biological activity studies

Influence of surfactin on the antimicrobial activity of the purified tyrocidines

One of the objectives of this chapter was to investigate the biological influence of Srf on the antimicrobial activity of the HPLC purified Trcs, TrcB and TrcC (Table 5.2) to assess whether the antagonism of GS action described in Chapter 2 and 3 is a general resistance mechanism towards peptides with the VOLfP pentapeptide moiety.

Table 5.2 The amino acid sequence, molecular weight (g.mol^{-1}) and retention time (min) of the peptides used in this study.

Peptides	Amino acid sequence	Mr	Retention time (min)	References
Srf	cyclo-(ELlVGlL)- C_{14}*	1021.7	15.50	[36, 37]
TrcB	cyclo-(VOLfPWfNQY)	1308.7	9.29	[3]
TrcC	cyclo-(VOLfPWwNQY)	1346.7	8.19	[3]

Amino acids are denoted using the standard one-letter abbreviations, with O = ornithine. D amino acids are represented with a lower case letter. *The C_{14} group in surfactin is linked via a lactone bond between $L^{7}$and E^{1}[37].

The influence of Srf on the antimicrobial activity of the purified Trcs was analyzed using microtiter broth dilution dose-response assays (Figure 5.1 and Table 5.3) in order to identify possible antagonistic/synergistic pairs. For these, two *B. subtilis* strains were used: *B. subtilis* OKB120 which does not produce Srf under experimental conditions and *B. subtilis* ATCC 21332 which is a strict aerobic and anaerobic Srf producer [38]. All the purified Trcs were active against

these two target organisms in the μM range (Table 5.3). However, Srf was not active against the two test organisms.

In these assays, the IC_{50} values of TrcB and TrcC were found to be 5.2 μM and 3.6 μM against *B. subtilis* OKB120 and 15.6 μM and 12.7 μM against *B. subtilis* ATCC21332 respectively (Table 5.3). Pre-incubation of cells with 30 μM Srf for 10 minutes caused an increase in the IC_{50} values of purified TrcB and TrcC towards both strains (Table 5.3 and Figure 5.1). The increase in the TrcC IC_{50} in the presence of Srf was significant towards the two *B. subtilis* strains and indicated that Srf was antagonistic towards TrcC activity (Figure 5.1). Although a consistent increase in TrcB IC_{50} in the presence of Srf was observed, there was no statistical difference between in the IC_{50} values of TrcB with and without Srf against *B. subtilis* OKB120. There was, however, a significant increase between the IC_{50} of TrcB in presence and in absence of Srf towards *B. subtilis* ATCC21332. As with GS, *B. subtilis* OKB120 was significantly ($P<0.001$) more sensitive towards the Trcs than the Srf producer *B. subtilis* ATCC21332. The change in the IC_{50} values of purified Trcs in addition to Srf towards the two test organisms is shown in Figure 5.1 and summarized in Table 5.3.

Table 5.3 Summary of the activity parameters of TrcB alone and in the presence of Srf towards *B. subtilis* strains OKB 120 and ATCC 21332. IC_{50} ± standard errors of the mean (SEM) and % change in IC_{50} were compiled from n biological repeats, each in triplicate or quadruplicate technical repeats.

	***B. subtilis* OKB120**			***B. subtilis* ATCC21332**		
Peptides	**+0 μM Srf**	**+30 μM Srf**		**+0 μM Srf**	**+30 μM Srf**	
	IC_{50} μM (n)	IC_{50} μM (n)	%Δ IC_{50}	IC_{50} μM (n)	IC_{50} μM (n)	%Δ IC_{50}
TrcB	5.2 ± 0.7 (6)	6.4 ± 0.6 (6)	23	16 ± 3.1 (3)	23 ± 1.6 (3)	48
TrcC	3.6 ± 0.4 (5)	7.4 ± 1.1 (5)	104	13 ± 2.5 (4)	17 ± 1.9 (4)	38

The result also showed that the extent of Srf antagonism may depend on the Trc identity, in particular the aromatic dipeptide unit, as well as the target organism. Srf showed similar protection against the Trc compared to GS (refer to Chapter 2). These results indicate that Srf may improve the survival of its producer toward other *Bacillus* species. The survival in mixed cultures was investigated to test the hypothesis that antagonism of antimicrobials is a survival strategy of to allow soil organisms to cohabit.

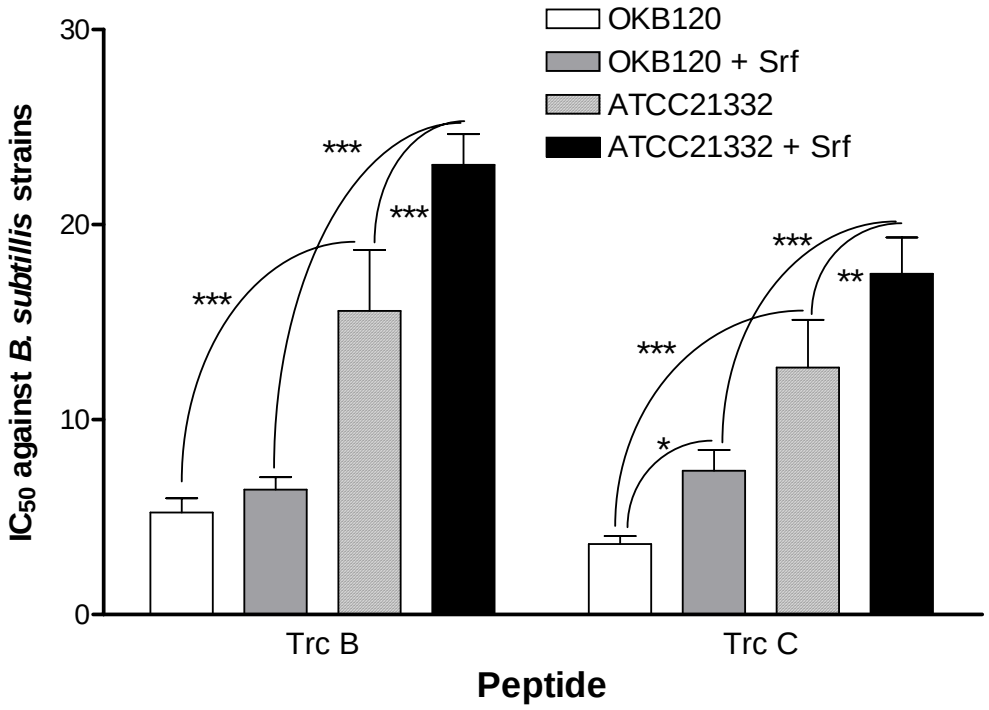

Figure 5.1 Bar graph and statistical comparison of the IC_{50}s of purified Trcs alone and in combination with Srf towards *B. subtilis* OKB120 and ATCC21332 (data from Table 5.3). The statistical analysis were done using Bonferroni's multiple comparison test (One Way ANOVA) with *** P<0.001; **P<0.01; *P<0.05.

Colonies of tyrothricin/Trc producer strain, *B. aneurinolyticus* ATCC10068 were cultured in close proximity with colonies of two *B. subtilis* strains, ATCC21332 which is a Srf producer, or the non-Srf producer OKB120 on TGYM agar gel (Figure 5.2). *B. subtilis* ATCC21332 and *B. aneurinolyticus* ATCC10068 were able to survive and grow together since no inhibition zones

developed around any of the two organisms (Figure 5.2D). However, the non-Srf producer *B. subtilis* OKB120 was out-competed by *B. aneurinolyticus* ATCC10068 causing a decrease in its colony size and spreading (Figure 5.2E).

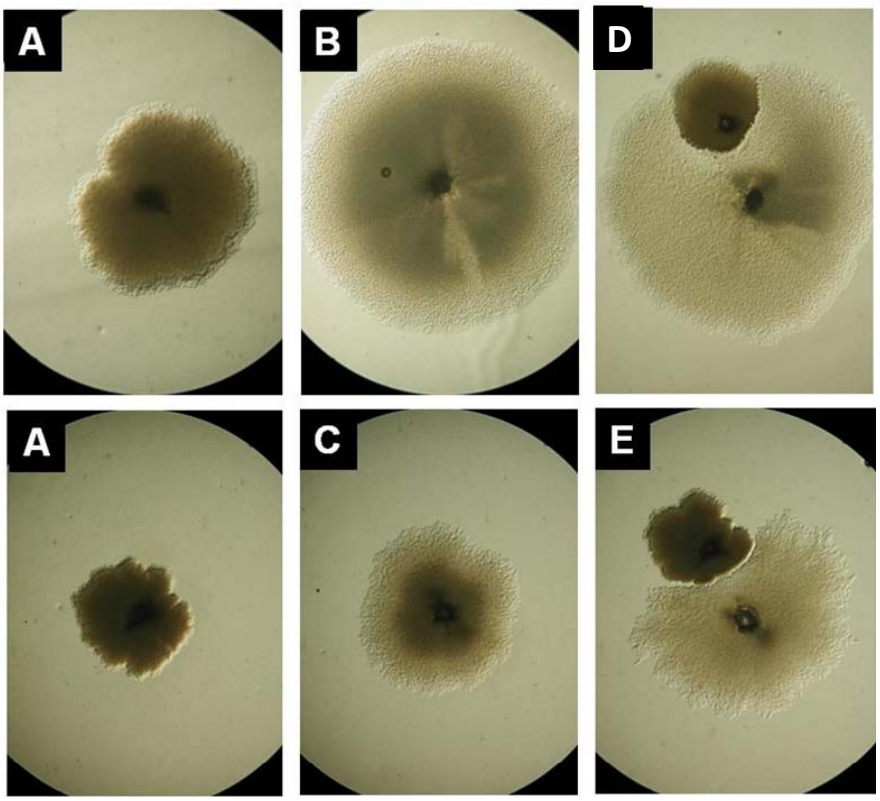

Figure 5.2 Evidence of co-survival between *Bacillus* strains. Colonies (15× enlargement) of the mixed culture assay experiment after two days of incubation with **A** the Trc producer *B. aneurinolyticus* ATCC10068, **B** the Srf producer *B. subtilis* ATCC21332 and **C** the Srf non-producer *B. subtilis* OKB120. **D** and **E** represent the mixed cultures of the tyrothricin/Trc producer *B. aneurinolyticus* ATCC10068, with the Srf producer *B. subtilis* ATCC21332 and the Srf non-producer *B. subtilis* OKB120, respectively.

Similar results were also observed when the colonies were cultured on TGYM agar gel seeded with *M. luteus*. Inhibition zones in the *M. luteus* seeded gel around both the organisms were observed for *B. subtilis* ATCC21332 and *B. aneurinolyticus* ATCC10068, with *B. subtilis* ATCC21332 surviving in the inhibition zone of *B. aneurinolyticus* ATCC10068 (Figure 5.3). The

asymmetric inhibition zone that formed when *B. subtilis* ATCC21332 and *B. aneurinolyticus* ATCC10068 was placed closed together may also indicate improved survival of *M. luteus* (Figure 5.3 C).

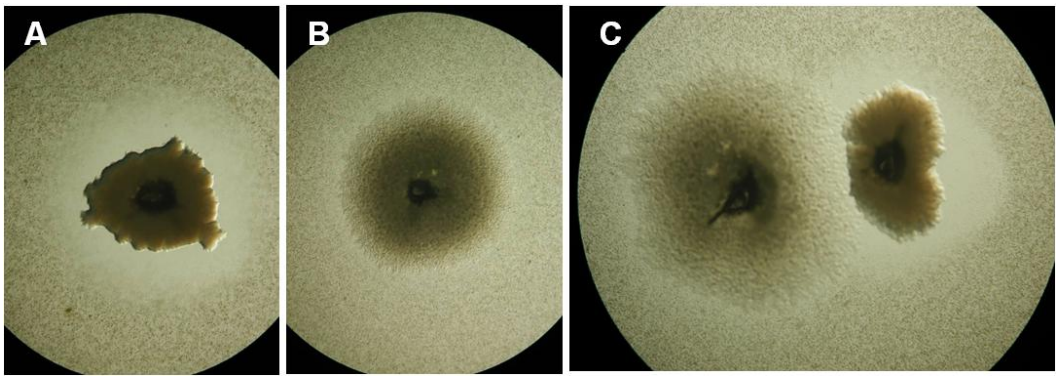

Figure 5.3 Evidence of co-survival between *Bacillus* strains in the presence of *M. luteus*. Colonies (15× enlargement) in the mixed culture assay experiment after two days of incubation with **A** the tyrothricin/Trc producer *B. aneurinolyticus* ATCC10068, **B** Srf producer *B. subtilis* ATCC21332 And **C** the tyrothricin/Trc and Srf producers at 1 mm distance. The gel contained micro-colonies of *M. luteus.*

To summarize, this study demonstrated that Srf also antagonises the antimicrobial activity of Trcs towards Gram-positive targets. Srf protected *B. subtilis* OKB120 towards the Trcs in a similar way as against GS and the antagonism varies according to the type of Trc. The results clearly show that peptides from cohabiting organisms may act antagonistically towards each other's antimicrobial peptides in order to survive in and share the same environment. Srf may improve the survival of its producer towards *Bacillus* species producing Trcs. However, although improved survival of a Srf producer in the presence of purified Trc or a Trc producer was observed, the latter also co-produces linear Grcs which may complicate the mode of survival. The second aim of this study was therefore to investigate the influence of GA alone and in combination with Srf and/or TrcB, against *M. luteus* as the model non-Srf producer.

Influence of gramicidin A on the antimicrobial activity of the tyrocidines and the antagonism by surfactin

Results of an investigation into the influence of GA on the activity of cyclic purified Trcs showed that GA was synergistic towards the *M. luteus* activity of TrcB (Table 5.4, Figure 5.4). In this assay, GA had an IC_{50} of 11.3 μM and the IC_{50} of TrcB was 6.2 μM towards *M. luteus*. The combination of GA and TrcB (1:1 molar ratio) shifted the IC_{50} to 1.6 μM each. The FIC index of 0.40 and significant change in IC_{50} ($P > 0.01$) indicated that the co-produced peptide, TrcB and GA, exhibited synergistic activity towards the growth of a Srf non-producer, *M. luteus* (Table 5.4 and Figure 5.4). This synergistic killing of other organisms will improve the survival ability of the producer strain. Therefore, the influence of Srf on this highly effective synergism between TrcB and GA was investigated.

Table 5.4 Summary of the activity parameters of TrcB and GA alone and in combination of Srf towards *M. luteus.* The IC_{50} ± SEM, % change in IC_{50} and the FIC index were compiled from n biological repeats, each in triplicate or quadruplicate technical repeats.

Peptides	no GA added	+ GA (1:1)		
	IC_{50} (μM) (n)	**IC_{50} (μM) (n)**	**%Δ IC_{50} (FIC)**	***FIC index**
GA	11.3 ± 0.9 (8)	1.6 ± 0.5 (4)	-606 (0.14)	0.40
TrcB	6.2 ± 0.7 (8)	1.6 ± 0.5 (4)	-288 (0.26)	

*FIC index = $IC_{50}^{TrcB\ in\ combination} / IC_{50}^{TrcB} + IC_{50}^{GA\ in\ combination} / IC_{50}^{GA}$ from equations 5.1, 5.2 and 5.3

Srf had an ambiguous influence on the activity of GA towards *M. luteus*. Synergistic action was observed at low concentrations of GA (0.4-12.5 μM) (results not shown), but less inhibition than expected, although not significantly less, at high concentrations of GA (>12.5 μM) (Figure 5.5). The effect of Srf on the synergism between TrcB and GA was further investigated at high concentrations, namely $>2\times IC_{50}$ of GA and $>4\times IC_{50}$ of TrcB, as these bactericidal concentrations

and lethal combination may have relevance in allowing the Srf-producer and the Trc-GA producer to cohabit. TrcB was chosen as representative in these experiments as it showed significant synergism with GA, but was not significantly antagonised by Srf. Also, we showed in our group that the *B. aneurinolyticus* co-produced TrcB and GA [39].

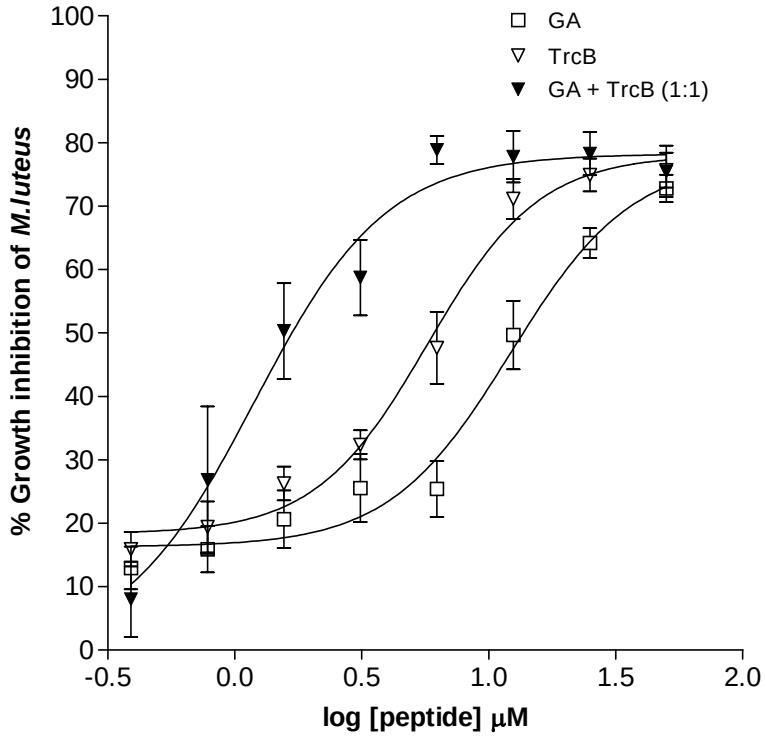

Figure 5.4 Representative dose-response curves showing the antimicrobial synergism between GA and TrcB towards *M. luteus.* SEM of each data point (average of n>15 determinations) is shown with $R^2 > 0.99$ for all curves (average of at least 4 biological repeats).

It was again showed, this time against *M. luteus,* that Srf does not have a statistically significant antagonistic action towards TrcB (Figure 5.5). Similarly, although inhibition caused by 25 μM GA alone was higher than that by the combined 25 μM GA and 30 μM Srf, the difference was also not significant. However, the synergistic and lethal combination of TrcB and GA was significantly antagonised ($P<0.001$) by 30 μM Srf, leading to almost a 40% decrease in inhibition

(Figure 5.5). These results showed that 30 μM Srf significantly antagonise (P<0.001) the synergistic and lethal action of 25 μM GA combined with 25 μM TrcB.

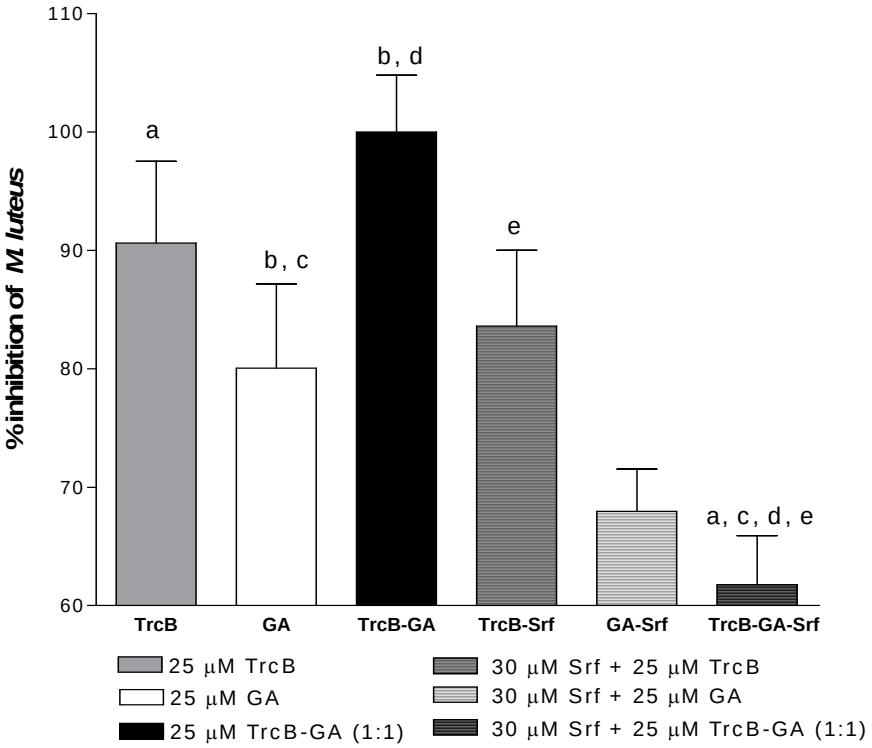

Figure 5.5 Bar graphs and statistical comparison of the influence of 25 μM Srf on the antagonistic action of 25 μM of Trcs alone or in combination with 25 μM GA towards *M. luteus*. Each bar graph represents the average of 8-12 determinations with the the error bar indicating the SEM. The statistical analysis were done using Bonferroni's Multiple comparison test (One Way ANOVA) with $^{a, b, d}$ P<0.001; ^{c} P<0.01; ^{e} P<0.05.

To summarise, the result of the influence of GA on the activity of TrcB demonstrated that GA and TrcB have synergistic activity towards the *M. luteus*. Srf addition (30 μM), antagonised the synergistic and lethal action of GA on TrcB. These results also confirm that Srf may improve the survival of its producer toward other *Bacillus* species producing a mixture of Grcs and Trcs.

Results and discussion Part 2: Biophysical studies

The third objective of this chapter was to investigate possible non-covalent complex formation and/or structural influences among antagonistic/synergistic peptide pairs utilising biophysical methods.

ESMS analysis of purified and mixed peptides

The positive mode ESMS analysis done on the individual purified Trc fractions, as presented in Chapter 4 Appendix 4.1, showed that these peptides were of high purity. Singly and doubly charged mono-isotopic molecular ions were detected for TrcB ($[M+H]^+$; *m/z* = 1309.63 and $[M+2H]^{2+}$; *m/z* = 655.34 doubly charged) and TrcC ($[M+H]^+$; *m/z* = 1348.68 and $[M+2H]^{2+}$;*m/z* = 674.84) with their respective isotopes and sodium adducts (See Appendix 4.1, Chapter 4). The ESMS analysis done on the purified VGA also showed that the peptide was of high purity (refer to Appendix 4.2, Chapter 4). The different molecular ions corresponding to singly and doubly charged mono-isotopic ions of VGA ($[M+H]^+$, *m/z* = 1883.1 and $[M+2H]^{2+}$, *m/z* = 942.0) were observed.

In Chapter 3 it was demonstrated that at least one Orn residue of GS was important for ESMS stable complexes to form with Srf. Since cyclic Trcs, which are analogues to GS, have one free amino group carried by an Orn or Lys residue, it was expected that they would also form complexes with Srf (Table 5.2). However, for the 1:1 molar mixture of Trcs and Srf, no complexes were observed between Srf and the purified Trcs in both the positive and negative ESMS mode. If there is indeed molecular interaction between Srf and the Trcs, as suggested by the CD and fluorescence studies (see below), the absence of complexes in the ESMS may be due to the formation of neutral or ESMS unstable complexes. Although only one Orn residue

participated in ionic interaction between GS and Srf, the two Orn residues may be necessary for ESMS stable and visible (positively charged) complexes.

Linear Grcs and cyclic Trcs are both found in the tyrothricin peptide complex [3] from *B. aneurinolyticus* [2] (previously known as the *B. brevis* [40]). Studies have shown that linear Grcs and cyclic Trcs have antagonistic action in one another's activity in the producer strain [15-17]. Linear Grcs dissociate the Trc-DNA complex and, in a similar way antagonise the effect of Trc on membrane permeability [16]. However, to date, complex formation between Grcs and Trcs has not been found by other investigators. We failed to detect complexes in the 1:1 molar mixture of GA and the Trcs, as well as GA and Srf; in positive and negative mode ESMS (results not shown). However, the failure to detect ESMS stable or visible complexes does not exclude the possibility of complex formation, therefore these Trp-containing peptides were analysed with fluorescence spectroscopy and NMR.

NMR analysis of surfactin influence on tyrocidine structures

The ^{1}H-NMR assignments of the Trcs confirmed the structure and conformation of these peptides in solution (refer to Appendix 5.1). The >7 Hz backbone coupling constants ($J_{NHH\alpha}$) for all the residues, except D-Phe^{4} and Gln^{9}, in both TrcB and TrcC indicated the role of eight of the amino acids in β-sheet and β-turn structures [4, 41], corroborating our CD results discussed below (refer to Appendix 5.1 for NMR data).

The influence of Srf on the structure of Trcs was further investigated by basic ^{1}H-NMR titration experiments. In contrast to the influence that was exerted by Srf on the GS NMR spectra (refer to Chapter 3), Srf caused only a minor chemical shift changes for specific amino acid residues in Trcs and no appreciable improvement on the peak shapes and intensity of the amide protons at

298 K (results not shown). The chemical shift changes at the highest Srf concentration, although small, were consistent (+/-0.1 to +/-0.02) for Orn^2, D-Phe^4, D-Trp^7, L-Trp^6 and Val^1 with Srf addition. Although these basic NMR analyses failed to provide conclusive evidence for complex formation there is some correlation with the CD and fluorescence results discussed below. D-Trp^7 and L-Trp^6 in TrcC and L-Trp^6 in TrcB possibly re-orientate in the presence of Srf, as derived from their fluorescence spectra and the CD spectrum of TrcC.

Fluorescence analysis of peptides and mixtures

A change in the Trp fluorescence (enhancement, quenching or emission wavelength change) could indicate the influence and/or interaction between the antagonistic and synergistic peptide pairs. The application of this technique is widely used to probe the exposure and environment of Trp residues in proteins [28]. The fluorescence emission with excitation at 295 nm (λ_{295}) of the purified Trcs and GA exhibited maximum absorption between 340 and 360 nm which represents the fluorescence emission of Trp residue [28] (Table 5.5 and Figures 5.6 and 5.7). The fluorescence intensity of GA was particularly high as compared to Trcs since it contains four Trp residues in its sequence [3] (Figure 5.7). Srf alone did not present any appreciable fluorescence emission spectrum since it does not contain any aromatic residue in its sequence.

Upon addition of Srf up to 2:1 molar ratio to the Trcs, the fluorescence emission of the TrcB and TrcC decreased and their fluorescence maxima blue-shifted from 355 and 356 nm to 338 and 342 nm, respectively (Table 5.5 and Figure 5.6). Srf induced a decrease in the fluorescence intensity of TrcB at a 1:1 ratio of the two peptides, but it increased at a 1:2 TrcB:Srf molar ratio (Figure 5.6A). This result may be the consequence of different distribution of micellular Srf, monomeric and other oligomeric Srf structures between 0.1 and 0.2 mM Srf. TrcB has L-Trp^6 protruding on

the one side and the D-Phe^7 protruding with the cationic Orn to the other side of the cyclic β-sheet structure [6], which may cause it to interact differently with Srf at higher Srf concentrations. In contrast, there was a constant decrease and blue-shift of the fluorescence intensity and maximum emission of Trp for TrcC with Srf addition (Figure 5.6B). TrcC has L-Trp^6 protruding on the one side and the D-Trp^7 protruding with Orn to the other side of the cyclic β-sheet structure [6]. Any one of the two Trp residues may be interacting with Srf or re-orientating to be exposed to the solvent, leading to either the blue shift or decrease in fluorescence intensity.

Table 5.5 Summary of the fluorescence parameters of TrcB and TrcC alone and in the presence of Srf (fluorescence values are given in arbitrary units from three independent determinations)

	TrcB			TrcC		
Trc:Srf	**λ_{max}**	**Fluorescence**	***% FS change**	**λ_{max}**	**Fluorescence**	***% FS change**
1:0	355	68.95 ± 1.23	-	356	115.5 ± 1.83	-
1:1	339	43.39 ± 1.21	-37	345	85.36 ± 2.48	-26
1:2	338	53.74 ± 1.49	-22	342	73.71 ± 2.54	-36

λ_{max} is the wavelength at the maximum fluorescence intensity.*The % fluorescence change is the ratio of tryptophan maximum fluorescence intensity in the mixture with surfactin against the tryptophan maximum fluorescence intensity in the peptide alone times 100.

These results, in particular the blue shift of the Trp emission maximum, indicated that Srf may interact with the Trcs causing a change in the location/exposure of the Trp residue(s). At least one of the aromatic residues, possibly D-Trp^7 near the cationic Orn of TrcC may be involved in Srf interaction, while the other Trp may be more exposed to the solvent causing a decrease in the fluorescence emission. However, with increase Srf concentrations (1:2 molar ratio), Srf may interact differently with TrcB, possibly due to a shift in Srf oligomeric structures or a more pronounced surfactant action. This also indicated that TrcB may be very sensitive to Srf

concentration, possibly relating to the limited Srf antagonism we observed at 30 μM Srf towards *B. subtilis* OKB120 and *M. luteus*. The Trcs interaction with Srf is summarized in Table 5.5 and spectra are given in Figure 5.6.

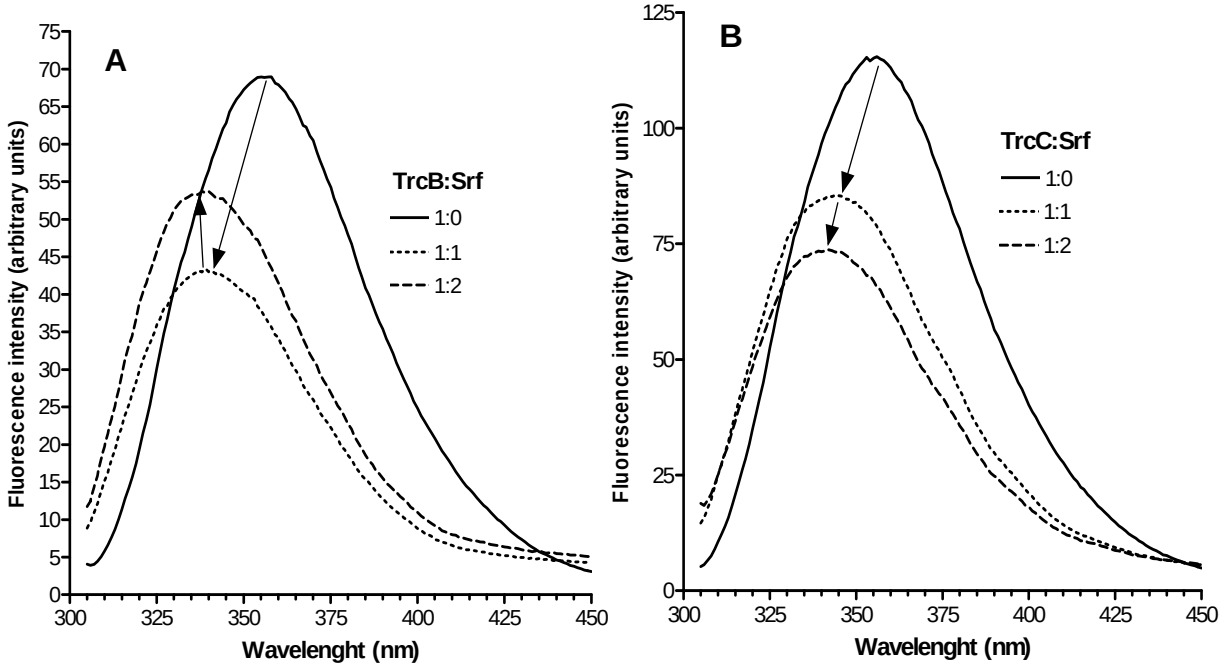

Figure 5.6 Fluorescence emission spectra of **A** TrcB and **B** TrcC in combination with Srf at different peptide ratios in water. Each fluorescence spectrum is represented by a line fit.

The influence of GA on fluorescence spectra of TrcB and Srf (1:1) and *vice-versa*, was also investigated (Figure 5.7). It showed that the addition of TrcB to GA did not affect or cause a significant change in the fluorescence emission spectrum of GA. This corroborated our ESMS data and previous data [18], namely that these two peptides do not interact. However, the addition of Srf did cause a significant increase in the fluorescence spectrum of GA, which may be due to micellular Srf providing a membrane like hydrophobic environment which increases the self-assembly state of GA or due to better solubility of GA in the surfactant environment (Figure 5.7).

This result may also explain the ambiguous activity modulation results we obtained with GA in the presence on Srf.

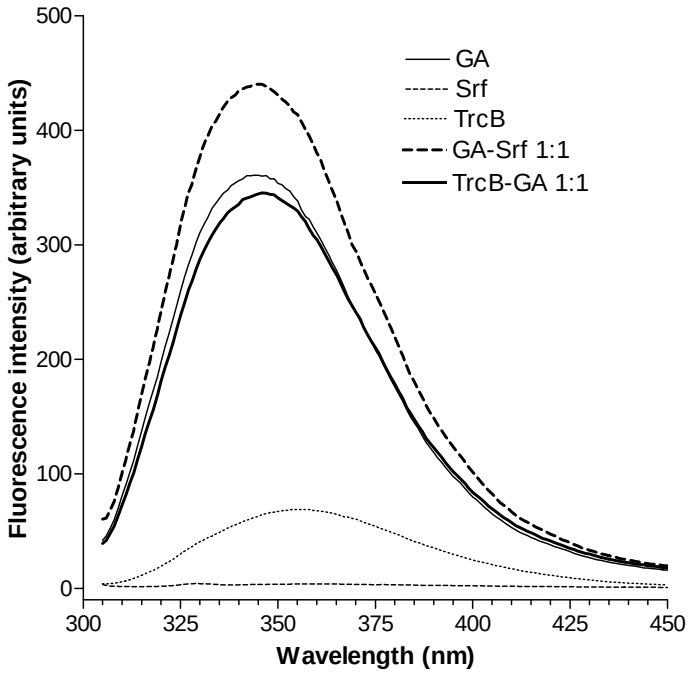

Figure 5.7 Fluorescence emission spectra of GA alone or in combination (1:1 molar ratio) with TrcB or Srf in water.

Far UV-CD secondary structure analysis of tyrocidines and mixtures with surfactin

The UV spectra of the Trcs were characteristic of peptides containing aromatic residues (Figure 5.8A). The CD spectra of the purified Trcs in water exhibited characteristic double minima at 205 nm and 216 nm with an additional shoulder at 230 nm for TrcC (Figure 5.8B) [5]. These minima are characteristic of antiparallel β-sheet and β-turn structure adopted by Trcs in aqueous solution [5]. The difference in the CD spectra of these two peptides is related to the difference in the side chain aromatic dipeptide units L-Trp^6 D-Phe^7 and L-Trp^6-D-Trp^7 of TrcB and TrcC, respectively (Table 5.6 and Figure 5.8B) [21]. The shoulder at 230 nm for TrcC is also related the additional Trp residue as compared to TrcB [21, 42]. Although the two minima are caused by backbone

conformations, the presence of the aromatic dipeptide units, as well as the other two aromatic amino acid residues in the sequence indirectly influence the spectra. It was therefore decided to also look at the ratio between 205 nm and 216 nm in order to obtain more information on the backbone changes.

Table 5.6 Summary of the CD parameters for of TrcB and TrcC as determined from spectra recorded for aqueous solutions of these peptides. Averaged molar ellipticities (θ) are given in $deg.cm^2.\mu M^{-1}$ x 10^1 ± SEM of five determinations. The molar ellipticity is given in terms of the Trc concentrations.

Peptide/ Peptide + Srf	**$A_{210-230}$**	**θ_{216}**	**θ_{205}**	**$\theta_{216}/\theta_{205}$**
TrcB	0.12 ± 0.01	-6.72 ± 0.12	-7.77 ± 0.14	0.87 ± 0.01
TrcB + Srf (1:1)	0.21 ± 0.05	-6.50 ± 0.17	-7.12 ± 0.20	0.92 ± 0.04
TrcB + Srf (1:2)	0.31 ± 0.01	-7.48 ± 0.14	-3.99 ± 0.35	1.89 ± 0.20
TrcC	0.32 ± 0.06	-8.04 ± 0.18	-7.93 ± 0.14	1.01 ± 0.01
TrcC + Srf (1:1)	0.54 ± 0.07	-7.25 ± 0.54	na	na
TrcC + Srf (1:2)	0.76 ± 0.09	-5.79 ± 2.47	3.00 ± 2.62	-1.03 ± 0.47

The far UV-CD spectra of the 1:1 molar mixture of Srf and TrcB showed that the addition of Srf caused a minor decrease of the negative ellipticity minima at 205 and 216 nm in water up to 1:1 ratio (Figure 5.8C). Only at a 1:2 molar ratio, the molar ellipticity at 205 nm decreased significantly and the ellipticity minimum at 216 nm red shifted to 220 nm. However, TrcC was much more sensitive to Srf with the 1:0.5 molar mixture of TrcC:Srf already causing the disappearance of the negative ellipticity minimum at 205 nm and 230, which inverted to a red shifted maximum at 235 nm (Figure 5.8D). There was also a slight decrease in the negative ellipticity at 216 nm (Figure 5.8D).

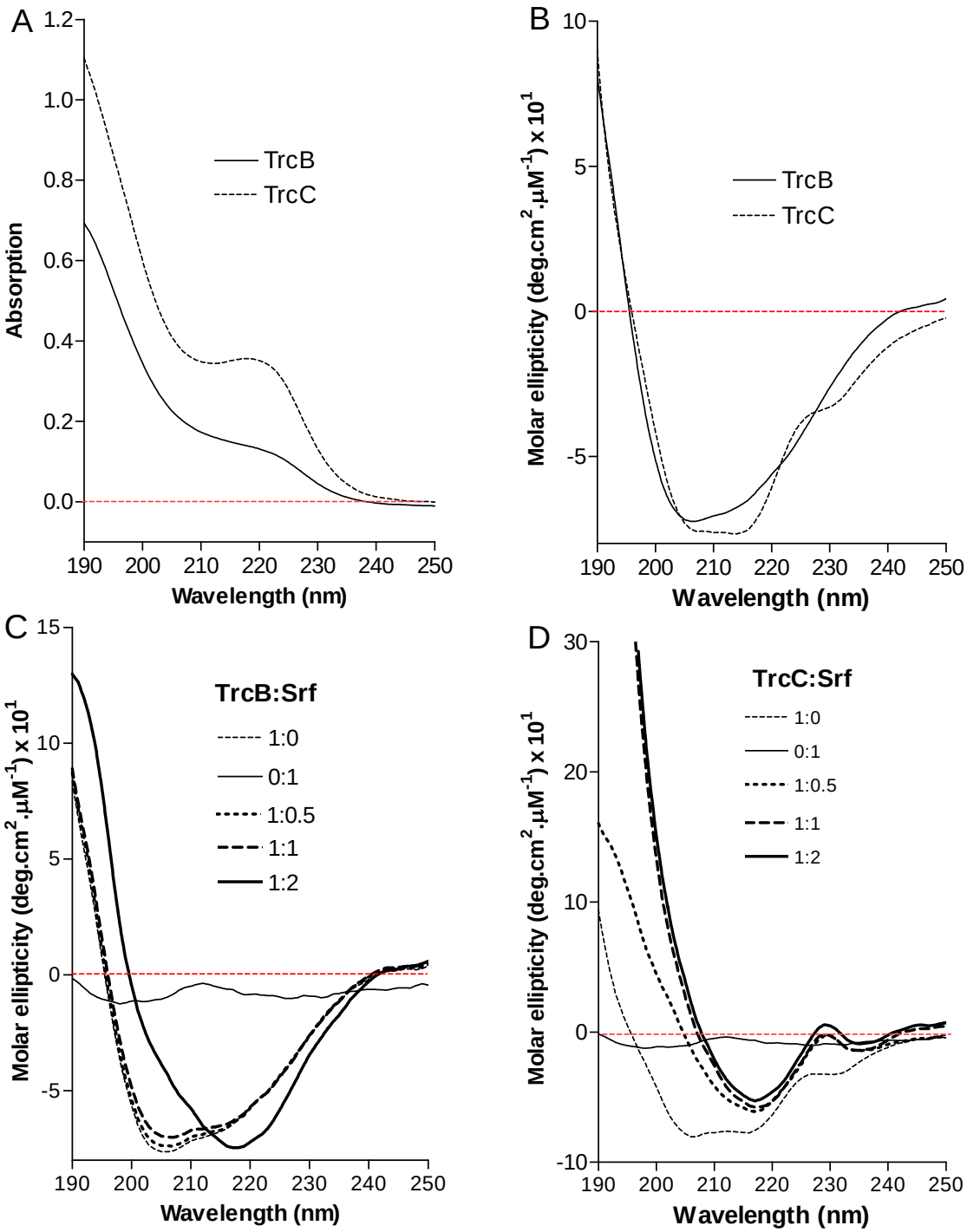

Figure 5.8 Spectrophotometric analyses of Trc and mixtures with Srf with **A** the UV absorption spectrum of Trc B and TrcC, **B** CD absorption spectra of **B** TrcB and TrcC in water; **C** TrcB and **D** TrcC titration with Srf in water. An average of three to ten determinations was used to represent each spectrum by a Lowess fit line (20 point smoothing window). The molar ellipticity is given in terms of the Trc concentrations.

The observed decrease in the negative molar ellipticity minima (decrease in absolute value of ellipticity) and the red shift of the CD profile of the Trcs may be related to decrease in the

aggregation/self assembly state of the Trcs in presence of Srf, indicating that Srf may be acting as a surfactant. However, the spectral changes of both TrcB and TrcC indicated the loss of β-turn structures (as found with GS) and an increase in β-sheet structure, which may be related to both the structures of the Trcs and Srf. These changes in the molar ellipticity of the Trcs may also be due to conformational changes resulting from modifying the orientation/exposure/location of the aromatic dipeptide units of the two Trcs in presence of Srf. These results corroborate well with the fluorescence quenching results as they show that changes in the environment of Trp may affect the aggregation of Trcs in solution. Srf may influence the exposure of the L-Trp[6] in the two Trcs resulting in a change in their CD spectra as observed with the inversion and red shift of the shoulder at 230 nm.

Conclusions

This study indicates that the lipopeptide Srf also antagonizes the antimicrobial activity of Trcs towards Gram-positive targets, possibly with a similar mode of antagonistic action as with GS activity. The mixed culture experiments confirmed that peptides from cohabiting organisms may act antagonistically towards each other to allow their producing organisms to growth and share the same environment. A complicating factor in the argument that Srf antagonises only Trc activity is the co-production of Trcs and Grcs. We observed pronounced synergistic action between the linear GA and TrcB against *M. luteus,* while Srf had a limited effect on TrcB and GA alone, in particular at high concentrations. However, the lipopeptide Srf significantly antagonised the synergistic action of 1:1 molar mixture of GA:TrcB at a lethal concentration to *M. luteus*. These results indicate that Srf has a definite role to protect and improve the survival of its producer toward other *Bacillus* species producing peptide mixtures, such as the tyrothricin.

Although we did not observe Trc-Srf complexes with ESMS and basic NMR studies, spectrophotometric analysis indicated that Srf has an influence on the structures of TrcB and TrcC. Fluorescence quenching indicated that the Trp residue(s) in the two Trcs occur in a different environment when the peptides are in presence of Srf. This change in the environment of Trp coincides with a change in the secondary structure of Trcs resulting in a decrease in their aggregation/self-assembly properties as observed with the far UV-CD. This loss of structure may be due to both interaction with Srf and surfactant action of Srf. Apart from the role of inactive complex formation and previously discussed Srf induced biofilm formation, Srf may also protect sites that are targeted by the Trcs. Membranolytic activity has been demonstrated to be a "secondary" process in the mode of action of the cyclic Trcs and linear Grcs from tyrothricin [43]. The role played by the tyrothricin peptides as gene regulator in *B. aneurinolyticus* [14, 17] suggest that both Grcs and Trcs may also act in a similar manner against other Gram positive bacteria. These actions could include DNA, RNA and protein synthesis inhibition. Srf may inhibit the membrane entry and limit the access to these primary targets.

References

1 Vlok, N. M. (2005) Investigation of complexation and antimicrobial activity of gramicidin S in the presence of lipopeptides from *Bacillus subtlis*. PhD thesis, University of Stellenbosch, Stellenbosch

2 Shida, O., Takagi, H., Kadowaki, K. and Komagata, K. (1996) Proposal for two new genera, Brevibacillus gen. nov. and Aneurinibacillus gen. nov. Int. J. Syst. Bacteriol. **48**, 939-946

3 Tang, X.-J., Thibault, P. and Boyd, R. K. (1992) Characterisation of the tyrocidine and gramicidin fractions of the tyrothricin complex from *Bacillus brevis* using liquid chromatography and mass spectrometry. Int. J. Mass Spectrom. Ion Processes. **122**, 153-179

4 Kuo, M.-C. and Gibbons, W. A. (1978) Total assignments, including four aromatic residues, and sequence confirmation of the decapeptide tyrocidine A using difference double resonance. J. Biol. Chem. **254**, 6278-6287

5 Qin, C., Zhong, X., Bu, X., Joyce Ng, N. L. and Guo, Z. (2003) Dissociation of antibacterial and hemolytic activity of amphipathic peptide antibiotic. J. Med. Chem. **46**, 4830-4833

6 Spathelf, B. M. (2009) The structure-activity/toxicity relationships of the tyrocidines, a group of cyclic decapeptides from *Bacillus brevis*. PhD thesis, University of Stellenbosch, Stellenbosch

7 Spathelf, B. M. and Rautenbach, M. (2009) Anti-listerial activity and structure activity relationships of the six major tyrocidines, cyclic decapeptides from *Bacillus aneurinolyticus*. Bioorg. Med. Chem. **17**, 5541-5548

8 Rautenbach, M., Vlok, M., Stander, M. and Hoppe, H. (2007) Inhibition of malaria blood stages by tyrocidines, membrane-active cyclic peptide antibiotics from *Bacillus brevis*. Biochim. Biophys. Acta. **1768**, 1488-1497

9 Williams, R. C., Yphantis, D. A. and Craig, L. C. (1972) Non covalent association of tyrocidine B. Biochemistry. **11**, 70-77

10 Harold, F. M. and Baarda, J. R. (1967) Gramicidin, valinomcin, and cation permeability of *Streptococcus faecalis*. J. Bacteriol. **94**, 53-60

11 Bourinbaiar, A. S. and Coleman, C. F. (1997) The effect of gramicidin, a topical contraceptive and antimicrobial agent with anti-HIV activity, against herpes simplex virus type 1 and 2 in vitro. Arch. Virol. **142**, 2225-2235

12 Bourinbaiar, A. S., Kraisinski, K. and Borkowsky, W. (1993) Anti-HIV effect of gramicidin *in vitro*: Potential for permicide use. Life Sci. **54**, 5-9

13 Moll, G. N., Van den Eertwegh, V., Tournois, H., Roelofsen, B., Op den Kamp, J. A. F. and Van Deenen, L. L. M. (1991) Growth inhibition of *Plasmodium falciparum* in *in vitro* cultures by selective action of tryptophan-N-formylated gramicidin incorporated in lipid vesicles. Biochim. Biophys. Acta. **1062**, 206-210

14 Bohg, A. and Ristow, H. (1987) Tyrocidine-induced modulation of the DNA conformation in *Bacillus brevis*. Eur. J. Biochem. **170**, 253-258

15 Hansen, J., Pschorn, W. and Ristow, H. (1982) Function of the peptide antibiotics tyrocidine and gramicidin: Induction of conformational and structural changes of superhelical DNA. Eur. J. Biochem. **126**, 279-280

16 Ristow, H. (1977) The peptide antibiotic gramicidin D: A specific reactivator of tyrocidine-inhibited transcription. Biochim. Biophys. Acta. **477**, 177-184

17 Ristow, H., Scharzschneider, B., Vater, J. and Kleinkauf, H. (1975) Some charateristics of the DNA tyrocidine complex and a possible mechanism of the gramicidin action. Biochim. Biophys. Acta. **414**, 1-8

18 Aranda, F. J. and de Kruijff, B. (1988) Interrelationships between tyrocidine and gramicidin A' in their interaction with phospholipids in model membranes. Biochim. Biophys. Acta. **937**, 195-203

19 Light-Wahl, K., Schwartz, B. L. and Smith, R. D. (1994) Observation of noncovalent quaternary associations of proteins by electrospray ionization mass spectrometry. J. Am. Chem. Soc. **116**, 5271-5278

20 Li, S., Dumdei, E. J., Blunt, J. W., Munro, M. H. G., Robinson, W. T. and Panelli, L. K. (1998) Theonellapeptolide IIIe, a new cyclic peptolide from the New Zealand deep water sponge, Lamellomorpha strongylata. J. Nat. Prod. **61**, 724-728

21 Laiken, S., Printx, M. and Craig, L. C. (1969) Circular dichroism of tyrocidines and Gramicidin S-A. J. Biol. Chem. **244**, 4454-4457

22 Salom, D. M., Bano, C., Braco, L. and Adad, C. (1997) HPLC in the characterisation of conformational species of linear gramicidins. Anal. Chim. Acta. **354**, 309-317

23 Wallace, B. A. (1986) Structure of gramicidin A. Biophys. J. **49**, 295-306

24 Arseniev, A. S., Barsukov, I. L., Bystrov, V. F., Lomize, A. L. and Ovchinnikov, Y. A. (1985) 1H-NMR study of gramicidin A transmembrane ion channel: Head-to-head right-handed, single-stranded helices. FEBS Lett. **186**, 168-174

25 Xie, X., Al-Momani, L. A., P., R., Griesinger, C. and Koert, U. (2005) An asymetric ion channek derived from gramicidin A: Synthesis, function and NMR structure. FEBS J. **272**, 975-986

26 Koeppe, R. E. and Andersen, O. S. (1996) Engineering the gramicidin channel. Ann. Rev. Biophys. Biomol. Struct. **25**, 231-258

27 Paradies, H. H. (1979) Aggregation of tyrocidine in aqueous solutions. Biochem. Biophys. Research Commun. **88**, 810-817

28 Chattopadhyay, A. and Raghuraman, H. (2004) Application of fluorescence spectroscopy to membrane protein structure and dynamics. Curr. Sci. **87**, 175-180

29 Shin, H.-C. and McFarlene, E. F. (1995) Conformation studies by circular dichroism and fluorescence spectroscopy of myelin P2 protein and two of its peptides. J. Biochem. Mol. Biol. **28**, 546-551

30 Yanga, X., Lu, R., Zhoua, H., Xuea, P., Wanga, F., Chena, P. and Zhaoa, Y. (2009) Aggregation-induced blue shift of fluorescence emission due to suppression of TICT in a phenothiazine-based organogel. J. Colloid Interface Sci. **339**, 527-532

31 Rautenbach, M., Gerstner, G. D., Vlok, M., Kulenkampff, J. and Westerhoff, H. V. (2006) Analyses dose-response curves, to compare the antimicrobial activity of model cationic α-helical peptides, highlights the necessity for a minimum of two active parameters. Anal. Biochem. **350**, 81-90

32 Du Toit, E. A. and Rautenbach, M. (2000) A sensitive standardised micro-gel well diffusion assay for the determination of antimicrobial activity. J. Microbiol. Methods. **1**, 159-165

33 Hall, M. J., Middleton, R. F. and Westmacott, D. (1982) The fractional inhibitory concentration (FIC) index as a measure of synergy. J. Antimicro. Chemother. **11**, 427-433

34 Spessard, G. O. (1998) ACD Labs/LogP dB 3.5 and ChemSketch 3.5. J. Chem. Inf. Comput. Sci. **38**, 1-4

35 Masunov, A. (2001) ACD/I-Lab 4.5: An Internet Service Review. J. Chem. Inf. Comput. Sci. **41**, 1093-1095

36 Baumgart, F., Kluge, B., Ullrich, C., Vater, J. and Ziessow, D. (1991) Identification of amino acid substitutions in the lipopeptide surfactin using 2D NMR spectroscopy. Biochem. Biophys. Res. Commun. **177**, 998-1005

37 Bonmatin, J. M., Laprevote, O. and Peypoux, F. (2003) Diversity among microbial cyclic lipopeptides: iturins and surfactins. Activity-structure relationships to design new bioactive agents. Comb. Chem. High Throughput Screening. **6**, 541-556

38 Davis, D. A., Lynch, H. C. and J., V. (1999) The production of surfactin in batch culture by *Bacillus subtilis* ATCC21332 is strongly influenced by the conditions of nitrogen metabolism. Enz. Microb. Technol. **25**, 322–329

39 Volsoo, A. and Rautenbach, M. (2010) The production, isolation and activity of cyclic antibiotic peptides produced by *Bacillus aneurinolyticus* (ATCC 10068). ed.)^eds.). pp. 1-15, Stellenbosch University, Stellenbosch

40 OKuda, K., Edwards, G. C. and Winnick, T. (1963) Biosynthesis of gramicidin and tyrocidine in the Dubos strain of *Bacillus brevis*. J. Bacteriol. **85**, 329-338

41 Holtzel, A., Jack, R. W., Nicholson, G. J., G., J., Gebhardt, K., Fieldler, H.-P. and Sussmuth, R. D. (2001) Streptocidins A-D, novel cyclic decapeptide antibiotics produced by *Streptomyces sp.* Tu 6071. II. Structure elucidation. J. Antibiot. **54**, 434-440

42 Fernadez-Escamilla, A. M., Ventura, S., Serrano, L. and Jimenez, A. (2006) Design and NMR conformational study of a β-sheet peptide based on Betanova and WW domains. Prot. Sci. **15**, 2278-2289

43 Dubos, R. J. (1939) Studies on a bactericidal agent extracted from a soil bacillus. I. Preparation of the agent. Its activity *in vitro*. J. Exp. Med. **70**, 1-11

44 Wuthrich, K. (1986) NMR of proteins and nucleic acids. John Wiley & Sons, Zurich, Switzerland

Appendix 5.1: NMR analysis of the TrcB and TrcC

The assignment of the Trcs was investigated in order to confirm the structure and conformation of these peptides in solution. This was done by sequence-specific resonance assignments of the ^{1}H resonance based on 2D NMR TOCSY and ROESY spectra of the peptides [44]. The different amino acid residues of the two Trcs were identified by their spin systems from combining TOCSY and ROESY spectra (Tables 5.7 and 5.8 Figures 5.9; 5.10 and 5.11) and ESMS-MS primary sequence data (see Appendix 4.1, Chapter 4). The backbone $J_{NHH\alpha}$ coupling constants were also calculated for each amino acid. In general, all residues gave coupling constant of greater than 7 Hz except for residues D-Phe^{4} and Gln^{9} which showed smaller values. These features are characteristic of β-sheet and β-turn structure of these peptides [4, 41].

Table 5.7 ^{1}H chemical shifts (ppm) and $J_{NH\text{-}H\alpha}$ (Hz) coupling constants (in brackets) of TrcB I CD_3CN/H_2O (1:1, *v/v*) at 298K.

Amino acid residues	chemical shift (ppm)		
	HN ($J_{NH\text{-}H\alpha}$)	Hα	Hββ'
L-Val[1]	7.82 (8.8)	4.39	2.08
L-Orn[2]	8.34 (8.5)	5.66	2.82
L-Leu[3]	8.26 (9.5)	5.26	1.71, 1.91
D-Phe[4]	8.61 (2.9)	4.26	2.98; 2.88
L-Pro[5]	-- --	4.12	0.93; 0.23
L-Trp[6]	7.45 (8.8)	4.49	2.45; 2.61
D-Phe[7]	8.23 (8.8)	5.5	1.34; 1.54
L-Asn[8]	9.11 (7.3)	4.77	2.98; 3.21
L-Gln[9]	8.56 (2.9)	4.21	3.94
L-Tyr[10]	8.37 (10.25)	4.5	2.90, 3.10

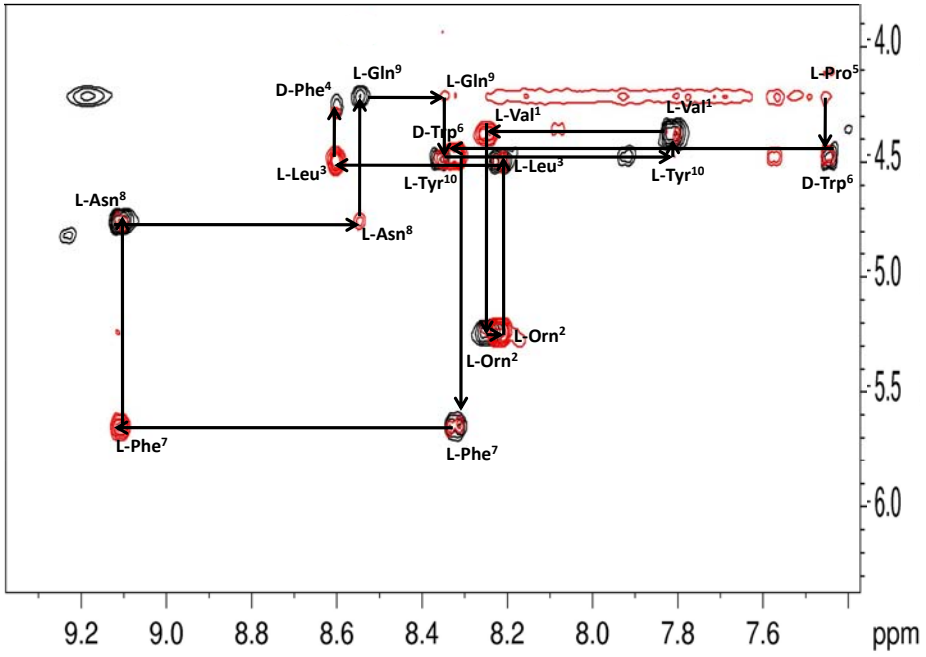

Figure 5.9 ^{1}H-NMR HN-Hα region of the TOCSY-ROESY spectra of TrcB in CD_3CN/H_2O (1:1, *v/v*) at 298 K. The sequential signal assignment of the peptide is shown by connecting arrows. The NOE HN-Hα cross peak for each residues is labelled by the standard three letter abbreviations of amino acids.

Table 5.8 ^{1}H chemical shifts (ppm) and $J_{NH\text{-}H\alpha}$ (Hz) constants (in brackets) of TrcC in CD_3CN/H_2O (1:1, *v/v*) at 298K.

Amino acid residues	Chemical shift (ppm)		
	HN ($J_{NH\text{-}H\alpha}$)	Hα	Hββ'
L-Val[1]	7.84 (8.6)	4.45	2.08
L-Orn[2]	8.30 (8.6)	5.26	2.81
L-Leu[3]	8.14 (9.4)	4.43	1.25, 1.37
D-Phe[4]	8.62 (1.7)	4.34	4.21; 2.87
L-Pro[5]	- -	4.08	0.24, 0.91
L-Trp[6]	7.39 (8.6)	4.38	1.88; 2.33
D-Trp[7]	8.09 (9.4)	5.67	3.03; 3.16
L-Asn[8]	9.21 (7.7)	4.82	2.94; 3.21
L-Gln[9]	8.45 (2.6)	4.34	3.92
L-Tyr[10]	8.39 (9.4)	4.48	2.91, 3.08

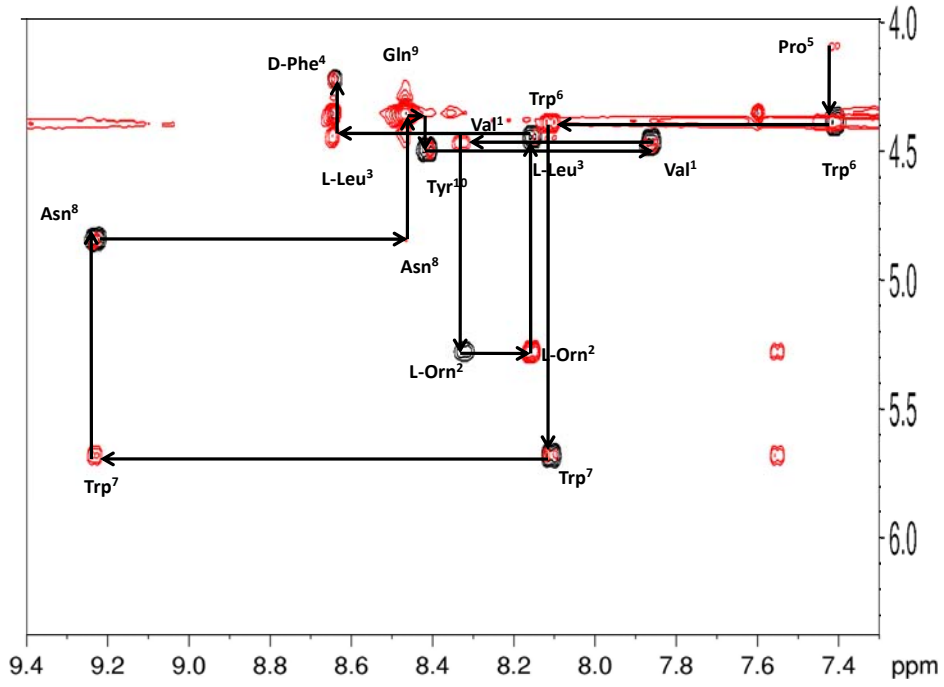

Figure 5.10 ^{1}H-NMR HN-Hα region of the TOCSY-ROESY spectra of TrcC in CD_3CN/H_2O (1:1, *v/v*) at 298 K. The sequential signal assignment of the peptide is shown by connecting arrows. The NOEs HN-Hα cross peak for each residues is labelled by the standard three letter abbreviations of the amino acids.

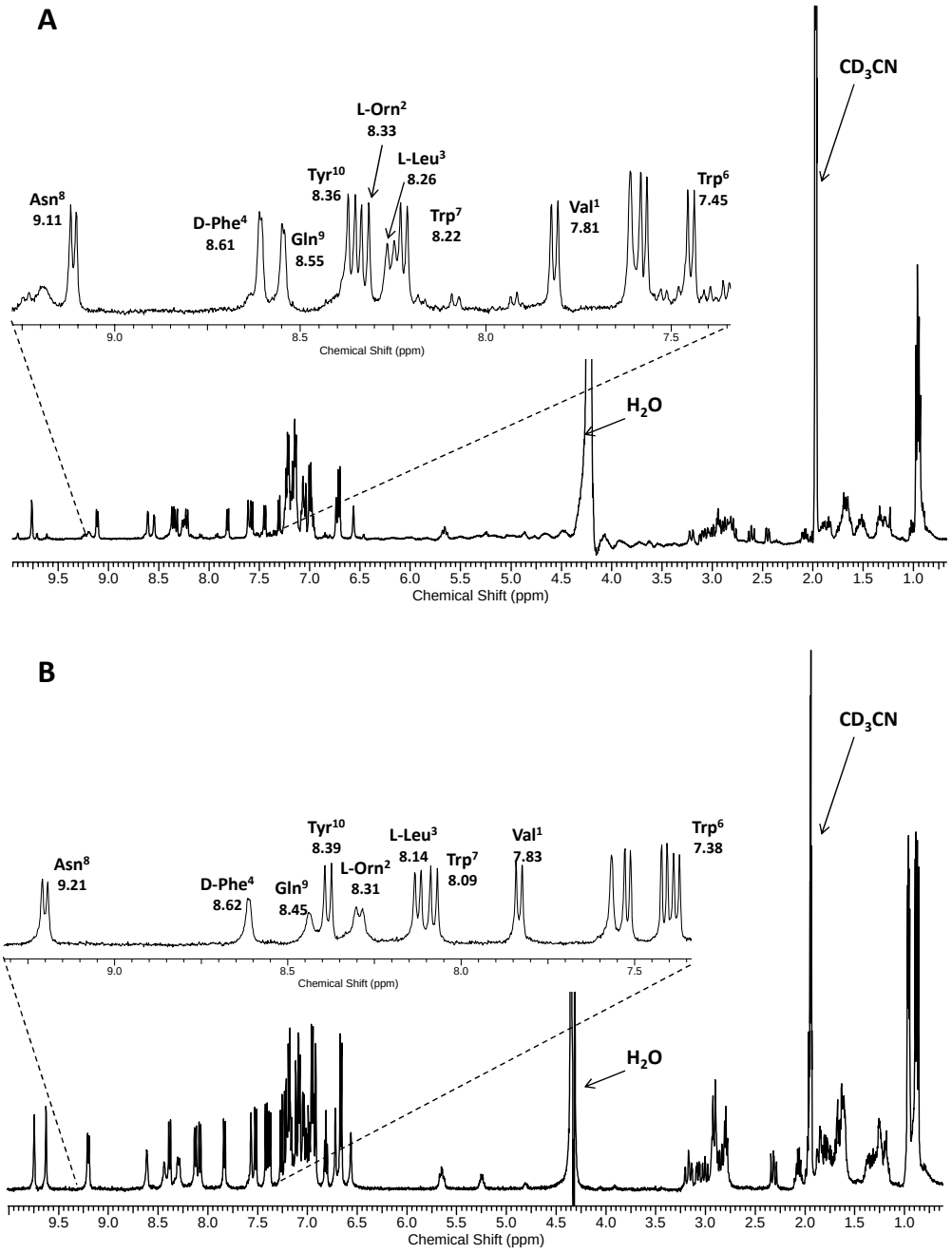

Figure 5.11 ^{1}H-NMR spectra of **A** TrcB and **B** TrcC in CD_3CN/H_2O (1:1, *v/v*) at 298K. Amide protons are annotated with their respective chemical shift and amino acid residue assignment.

Chapter 6

Summary, general conclusions and future prospects

In a natural environment soil bacteria such as the *Bacillus* species generate antimicrobial compounds, including antibiotic peptides responsible for their survival and protection of plants against other microorganisms [1]. Vlok [2] hypothesised that when two species of bacilli, producing peptide antibiotics, cohabit they are able to inactivate or shield the peptide antibiotics of the other as a survival strategy. Vlok [2] proposed that the observed antagonism between the peptide antibiotic surfactin (Srf) and gramicidin S (GS) involved the formation of inactive complexes between antimicrobial peptides [2].

The major goal of this study was to test the hypothesis: "Resistance of the cohabiting bacilli toward each other's antibiotic peptides is the consequence of antagonistic peptide action". In other words, the questions we attempted to answer were: Is antagonistic peptide action, similar to the antagonism of GS activity by Srf, a general resistance mechanism? Will Srf antagonize the activity of other *Bacillus* peptides, such as analogues of GS namely the cyclic tyrocidines (Trcs), as well as the co-produced linear gramicidins (Grcs) from *Bacillus aneurinolyticus*? To reach the study goal, the objectives were: 1) to investigate the biological influence of the *B. subtilis* peptide Srf on the antibacterial and haemolytic activity of GS, 2) to characterise possible intermolecular interactions between the antagonistic peptides GS and Srf 3) to investigate the influence of Srf on the biological activity of peptides from *B. aneurinolyticus* (Trcs and gramicidin A (GA) and combinations of the Trcs and GA) in order to identify possible antagonistic/synergistic pairs and characterize them. An important objective, before testing the peptide pairs, was

the development of two reverse phase high performance liquid chromatography (HPLC) protocols to purify and characterize *B. aneurinolyticus* peptides.

Results summary and conclusions

The study, reported in Chapter 2, corroborates the results of Vlok [2], as it was also shown that Srf has a pronounced antagonistic effect against the antimicrobial activity of GS towards the Gram-positive *Micrococcus luteus*. This antagonistic influence of Srf on the GS bioactivity extended to two Gram-positive organisms, *B. subtilis* ATCC21332 and OKB120, with constant (general producer) and nutrient-induced (general non-producer) Srf production, respectively.

For *M. luteus*, antagonism only occurs above a "critical" Srf concentration (> 8 μM, which is above the critical micelle concentration (CMC) of Srf [3]). Below that concentration the mixture of GS and Srf showed synergistic activity towards *M. luteus*. When the bacterium was pre-incubated with 30 μM Srf, the pre-absorbed Srf or Srf micelles interacted with GS preventing it to reach *M. luteus* membrane. GS recovery from Srf-treated *M. luteus,* using ultra performance liquid chromatography mass spectrometry (UPLC-MS) showed that both cell wall and solution phase were important in GS antagonism by Srf (Chapter 2).

Antagonism of GS activity towards *B. subtilis* was also observed over a broad concentration range, after pre-incubation with 0.9-30 μM Srf. This antagonism may be related to the induction of more resistant biofilms by Srf in *B. subtilis* [4] at the low Srf concentrations. The Srf producer *B. subtilis* ATCC21332 was less sensitive to GS and

presented the highest antagonistic response compared to *B. subtilis* OKB120, possibly due to its natural Srf production. The antagonistic effect of GS activity on the more sensitive *B. subtilis* OKB120 resulted from Srf addition. In a mixed culture, pre-incubation with Srf protected *B. subtilis* OKB120 considerably better than *M. luteus.* However, only the constant Srf producer, *B. subtilis* ATCC21332, grew in the inhibition zone of the colonies from the GS producer *Aneurinibacillus migulanus* ATCC9999, while growth of the non-producer, *B. subtilis* OKB120, was inhibited (Chapter 2).

In order to determine the influence of the type of membrane on GS-Srf antagonism, the combination of GS and Srf on erythrocytes was assessed. Since the cationic hydrophilic side groups of GS are important for it binding to bacteria [5, 6], it was hypothesized that the antagonism of GS activity by Srf may be caused by an ionic shielding of the cationic side chain groups of the Orn residues in GS. Srf had little effect on GS activity toward the erythrocytic target membranes, probably because these groups are not as important for the binding of GS to the neutral cell membranes of eukaryotic cells, such as the erythrocyte membranes [7, 8]. This showed that the antagonism of GS activity by Srf was at least Gram-positive target membrane specific (see Chapter 2).

Srf alone or in a mixture with GS caused a decrease in the detectable growth (light dispersion) of *M. luteus* and *B. subtilis* OKB120 in broth media possibly due to Srf-induced cell clumping/bacteriostatic activity on *M. luteus* and visible biofilm formation by *B. subtilis* [3, 9, 10] (Chapter 2). This indicated the role of biofilm formation in the resistance of *B. subtilis* towards antimicrobial peptides. Srf is known to induce biofilm formation [11-13] and this film may protect the cells in the inner layers from GS.

However, Vlok [2] also found that Srf antagonized the activity of GS against organisms that do not generally form biofilms such as plant fungi, indicating that Srf may directly interfere with the action of GS. The loss of GS activity in presence of Srf was most probably due to non-covalent inactive complexes forming among these peptides that affect the secondary structure aggregation/self-assembly of GS in solution (Chapter 3). According to circular dichroism (CD) Srf caused a decrease in the prominent β-turn structures of GS as observed by the decrease and red shift of the negative ellipticity minimum at 206 nm to 208 nm. The GS-Srf mixture also presented an increase in β-sheet structure as monitored by the increase and red shift of the negative ellipticity minimum at 216 nm to 222 nm. These ellipticity changes can be explained by interaction of the negatively charged Srf with the cationic GS, causing a change in the orientation/exposure/location of D-Phe^{4,9} in the β-turns or Orn^{2,7} residues and changing the aggregation and/or self-assembly GS in aqueous media.

ESMS of the 1:1 molar mixture of GS and Srf showed that GS forms stable complexes with Srf which corroborated the CD data and previous results [2] (Chapter 3). No complexes formed between Srf and the acetylated GS showing the importance of the two amino group side chains in the GS structure on the Srf-GS interaction. Results from collision-induced-dissociation (CID) on Srf-GS complex showed that the interaction between the two peptides involves at least one Orn residue of GS with either Asp or Glu residues of Srf, with the peptide bonds in the Val-Orn-Leu-D-Phe moiety of GS and the Val^4-Asp^5-D-Leu^6-Leu^7 moiety of Srf protected from fragmentation. The ^{1}H-NMR temperature titration of GS-Srf mixture confirmed the CD and ESMS results as it showed that Srf protects the amide protons of D-Phe^{4,9} and L-Orn^{2,7} of GS from exchanging with

the solvent. There was also an increase/improvement in the Asp^5 NH signal in the GS-Srf mixture indicating shielding or solvent exchange/protection. These results suggested that the two molecules may be implicated in intermolecular interactions involving the residues D-$Phe^{4,9}$ and $Orn^{2,7}$ of GS with Asp^5 of Srf. These results were further confirmed with ROESY and DOSY NMR. There were non-sequential NOE cross peaks observed between the H^{β} of Asp from Srf and the H^{γ} of Orn from GS in the ROESY spectrum of the GS-Srf mixture, indicating <5Å interaction distance. DOSY-NMR indicated that Srf and GS formed homo-oligomers. However, the addition of Srf to GS increased the diffusion coefficient of GS pointing to the formation of slightly smaller homo-oligomers possibly due to the surfactant effect of Srf or more compact hetero-oligomers.

Next, to test the hypothesis that the antagonism of GS action by Srf is a general resistance mechanism, the influence of Srf on peptides and peptide combinations from the tyrothricin complex, namely GA, tyrocidine B (TrcB) and tyrocidine C (TrcC) was investigated. This required the extraction and purification of the individual Trcs and Grcs from *B. aneurinolyticus* since they are not commercially available in pure form (Chapter 4). However, the purification and characterisation of these peptides have presented challenges because of minor differences that exist between the different Grcs and Trcs in the tyrothricin complex. Two reverse phase high HPLC methods were developed using a C_{18} column and acetonitrile (CH_3CN) as mobile phase (Chapter 4). These optimized HPLC methods involved the use of a non-linear gradients developed over 22.5 min at 35 °C. Cyclic Trcs separated well using a 50 to 80% non-linear CH_3CN gradient developed over 22.5 min. Linear Grcs separated well over the same run time with a 60 to 100% non-linear CH_3CN gradient. These optimized analytical HPLC protocols methods adapted

well to semi-preparative HPLC and resulted in the purification (>90% purity) of ten Trcs and six linear Grcs and analogues from the tyrothricin extract and the commercial GD extract.

The low μM antimicrobial activity of the purified Trcs (B and C) was confirmed with *B. subtilis* ATCC21332 and OKB120 as target cells (Chapter 5). It was found that Srf also antagonizes the antimicrobial activity of Trcs towards Gram-positive bacterial targets similar to the antagonism of GS activity. However, the extent of the antagonistic action varied depending on the type of Trc; for example TrcC was more sensitive to antagonism than TrcB. In a mixed culture study, we showed that the Srf producer *B. subtilis* ATCC21332 could grow in the presence of the tyrothricin/Trc producer *B. aneurinolyticus* ATCC10068, while the Srf non-producer *B. subtilis* OKB120 was outcompeted. This established that peptides from cohabiting organisms may act antagonistically towards one another in order to allow their producing organisms to share the same environment. Srf may improve the survival of its producer towards other *Bacillus* species producing Trcs. However, *B. aneurinolyticus* ATCC10068 co-produces Grcs, in particular GA with Trcs such as TrcB, which may complicate the protective role of Srf. GA and TrcB have a pronounced synergistic activity towards the *M. luteus,* while Srf had a synergistic effect on GA at low GA concentrations towards the *M. luteus*. However, Srf at 30 μM antagonized the synergistic and lethal action of 25 μM GA on 25 μM TrcB (Chapter 5), indicating that the protective role of Srf extend to synergistic peptide mixtures in the tyrothricin complex.

In contrast to the observed complexes between Srf and GS, no complexes were observed with ESMS between Srf and any of the purified Trcs, and basic 1D NMR studies did not show overt spectral changes when the Trcs were mixed with Srf (Chapter 5). However, fluorescence spectroscopy (FS) and CD presented clear evidence of Srf induced changes in secondary structures and/or higher order self-assembled structures of the Trcs. Srf induces a blue shift of the fluorescence emission of the TrcB and TrcC indicating that Srf may interact with the Trcs causing a change in the location/exposure of the Trp residue(s). At least one Trp in the Trc structure may be located in a more hydrophobic environment causing a blue-shift in the presence of Srf. However, the decrease in the fluorescence emission indicates that a larger concentration of the Trp residues in the Trcs may be exposed to the solvent upon Srf interaction, than without Srf. The observed decrease and red shift in the negative ellipticity minima of the CD spectra of the Trcs corroborate the FS results. It shows that Srf may act as a surfactant towards the Trcs causing a decrease in the aggregation/self assembly states in water related to the loss of β-turn structures (as found with GS) and increase in β-sheet structures. These changes in the molar ellipticity of the Trcs are mostly due to environmental changes in the orientation/exposure/location of the aromatic dipeptide units, Trp^{6}-($DTrp^{7}$/D-Phe^{7}) resulting from Srf interaction.

No detectable stable complexes in the 1:1 molar mixture of GA and the Trcs in positive and negative ESMS mode were observed which indicates that GA does not interact with the Trcs. This result also corroborates the FS results which showed that the addition of TrcB to GA did not affect the fluorescence emission spectrum of GA. The synergism of GA and TrcB is therefore not the consequence of formation of more active heteromeric

complexes. However, the addition of Srf did cause a significant increase in the fluorescence spectrum of GA possibly due to micellar Srf providing a membrane like hydrophobic environment for the Trp-residues or improving the solubility of GA via its surfactant activity (Chapter 5). The fact that both TrcB and GA possibly interact with Srf could explain the antagonistic effect that Srf had on the lethal synergism of GA-TrcB mixtures

Although complexation between Srf and GS or peptide analogous to GS is not the only mode of Srf antagonistic action, these results substantiates that complex formation and/or structural changes play a major part in the mode of peptide antagonism and action. The antagonism of GS activity by Srf conferred in part by inactive complex formation is a resistance mechanism that also extends to other peptides containing the Val-Orn-Leu-D-Phe-Pro moiety such as the Trcs from *B. aneurinolyticus*. Table 6.1 summarizes the microbiological and biophysical results of this study.

Future studies

The microbiological studies, given in Chapter 2 and 5, indicate that the antagonism was target membrane specific, as antagonism only occurred primarily against prokaryotic target cells. On eukaryotic cells, only slight antagonism on the activity of the peptides was observed. An area for future research would involve a more detailed investigation on the specificity of this type of antagonism (or putative resistance mechanism), i.e. whether the antagonism is exclusively dependent on target membrane composition and whether any other non-membrane targets or systems such as ABC transporters are involved.

Table 6.1. Summary of the different peptides in combination with Srf or/and GA showing the antagonism or synergism as well as the detected complex formation of structural changes

	Combined with surfactin				**Combined with gramicidin A**			
	Antagonism/ Synergism	**Detection of complex formation/ structural change**			**Antagonism/ synergism**	**Detection of complex formation/ structural change**		
Peptides	**Target organism**	**ESMS**	**CD/ FS**	**NMR**	**Target organism**	**ESMS**	**CD**	**FS**
GS	Antagonism *M. luteus* *B. subtilis* OKB120/ ATCC21332	yes	yes/ na	yes	Antagonism* *M. luteus* Additive* *B. subtilis* OKB120	yes	nd	nd
GA	Mixed results *M. luteus*	no	nd/ yes	nd				
Trc B	Antagonism *B. subtilis* ATCC21332	no	yes/ yes	no	Synergism *M. luteus*	no	nd	no
TrcB+GA	Antagonism *M. luteus*	nd	nd/ nd	nd				
TrcC	Antagonism *B. subtilis* OKB120/ ATCC21332	no	yes/ yes	no	nd	no	nd	nd

Abbreviations: nd – not determined; na - not applicable; *preliminary results

Most *Bacillus* peptides act by disturbing the permeability barrier of bacteria since they are able to interact with biological membranes. Potential antagonistic or peptide-shielding effects of Srf on the membrane interaction of GS and the Trcs can be studied using model membranes. The amount, time-dependent and dose-dependent release of a trapped fluorescent maker from liposomes using fluorescent spectrometry could be used as indicator for the membrane activity of the peptides and combinations. In order to further the biophysical investigation and better understand the molecular structure(s) of the antagonistic complex between GS and Srf, uniform isotopic enrichment NMR may be conducted. This technique has contributed in improving the analysis of interaction among complex molecules [14, 15]. ^{15}N and/or ^{13}C isotopic enrichment of GS or Srf can be used

to obtain additional information on the existing ^{1}H-NMR data or can be combined in triple resonance NMR experiments [16]. The peptides may be labeled by growing the producer strain using enriched media as nitrogen ($^{15}NH_4Cl$, $^{15}NH_4SO_4$ or N^{15} labeled urea) or as carbon ($^{13}C_6$ glucose) source. Our research group has the facilities and recently optimised methodology to grow both the GS and Srf producer strains (*A. migulanus* ATCC9999 and *B. subtilis* ATCC21332), as well as isolate the peptide products from the media using optimized reverse-phase HPLC protocols. Data from these advanced NMR studies could provide the molecular detail to construct models of the GS-Srf complex(es).

Finally, in order to evaluate the hypothesis of the antagonism of Srf is a resistance mechanism of *B. subtilis* towards other bacilli producing peptides, the biological and biophysical influence of the Srf analogues, for example other lipopeptides such as the neural iturin A and anionic iturin C could be investigated. The lipopeptides Srf and iturin A/C, are co-produced in some *B. subtilis* strains and have been shown to have synergistic activity [17, 18].

Last word

This study provided the first evidence that Srf acts as an "antimicrobial shield" through the antagonism of the antimicrobial activity of several antimicrobial peptides produced by *Bacillus* species. The broader study of this "antimicrobial peptide shield" hypothesis may contribute in future, explaining this putative resistance mechanism. This research may help solving the problem of competition among soil bacteria which generate the peptides responsible for the protection of the plant against other microorganisms in the agricultural industry.

References

1 Marahiel, M. A., Nakano, M. M. and Zuber, P. (1993) Regulation of peptide antibiotic production in *Bacillus*. Mol. Microbiol. **7**, 631-636

2 Vlok, N. M. (2005) Investigation of complexation and antimicrobial activity of gramicidin S in the presence of lipopeptides from *Bacillus subtlis*. PhD thesis, University of Stellenbosch, Stellenbosch

3 Ishigami, Y., Osman, M., Nakahara, H., Sano, Y., Ishiguro, R. and Matsumoto, M. (1995) Significance of β-sheet formation for micellization and surface absorption of surfactin. Coillois Surf., B. **4**, 341-348

4 Bais, H. P., Fall, R. and Vivanco, J. M. (2004) Biocontrol of *Bacillus subtilis* against infection of arabidopsis roots by *Pseudomonas syringae* is facilitated by biofilm formation and surfactin production. Plant Physiol. **134**, 307-319

5 Danders, W., Marahiel, A. M., Krause, M. I., Kosui, N., Kato, T., Izumiya, N. and Kleinkauf, H. (1982) Antibacterial action of gramicidin S and tyrocidines in relation to active transport, *in vitro* transcription, and spore outgrowth. Antimicrob. Agents Chemother. **22**, 785-790

6 Nagamurthi, G. and Rambhav, S. (1985) Gramicidin-S: Structure-activity relationship. J. Biosci. **7**, 323-329

7 Katsu, T., Kuroko, M., Morikawa, T., Sanchika, K., Fujita, Y., Yamamura, H. and Uda, M. (1989) Mechanism of membrane damage induced by the amphipathic peptides gramicidin S and melittin. Biochim. Biophys. Acta. **983**, 135-141

8 Katsu, T., Ninomiya, C., Kuroko, M., Kobayashi, H., Hirota, T. and Fujita, Y. (1988) Action mechanism of amphipathic peptides gramicidin S and melittin on erythrocyte membrane. Biochim. Biophys. Acta. **939**, 57-63

9 Ahimou, F., Jacques, P. and Deleu, M. (2000) Surfactin and iturin A effects on *B. subtilis* hydrophobicity. Enzyme Microbiol. Technol. **27**, 749-754

10 Carrillo, C., Teruel, J. A., Aranda, F. J. and Ortiz, A. (2003) Molecular mechanism of membrane permeabilization by the peptide antibiotic surfactin. Biochim. Biophys. Acta. **1611**, 91-97

11 Stein, T. (2005) *Bacillus subtilis* antibiotics: structures, syntheses and specific functions. Mol. Microbiol. **56**, 845-857

12 Marikawa, M. (2006) Beneficial biofilm formation by industrial bacteria *Bacillus subtilis* and related species. J. Biosci. Bioeng. **101**, 1-8

13 Stewart, P. S. and Costerton, J. W. (2001) Antibiotic resistance of bacteria in biofilms. The Lancet. **358**, 135-138

14 Ikura, M. and Bax, A. (1992) Isotope-filtered 2D NMR of a protein-peptide Complex: Study of a skeletal muscle myosin light chain Kinase fragment bound to calmodulin. J. Am. Chem. Soc. **114**, 2433-2440

15 Majerle, A., Kidri, J. and Jerala, R. (2000) Production of stable isotope enriched antimicrobial peptides in *Escherichia coli*: An application to the production of a ^{15}N-enriched fragment of lactoferrin. J. Biomol. NMR. **18**, 145-151

16 Weisemann, R., Rfiterjans, H. and Bermel, W. (1993) 3D Triple-resonance NMR techniques for the sequential assignment of NH and ^{15}N resonances in ^{15}N- and ^{13}C-labelled proteins. J. Biomol. NMR. **3**, 113-120

17 Ohno, A., Ano, T. and Shoda, M. (1995) Effect of temperature on production of lipopeptide antibiotics, iturin A and surfactin by a dual producer, *Bacillus subtilis* RB14, in solid-state fermentation. J. Ferment. Bioeng. **80**, 517-519

18 Thimon, L., Peypoux, F., Maget-Dana, R., Roux, B. and Michel, G. (1992) Interactions of bioactive lipopeptides, iturin A and surfactin from *Bacillus subtilis*. Biotechnol. Appl. Biochem. **16**, 1799-1904